MRI and MSCT for the Assessment of Myocardial Function and Viability

Timo Baks

ISBN 90-9021082-2
Lay-out: D. Verver
Cover: T. Baks
Illustrations: T. Baks

Printed by Van Werkhovens Drukkerij BV

MRI and MSCT for the Assessment of Myocardial Function and Viability

Het bepalen van myocardviabiliteit en hartspierfunctie met behulp van MRI en MSCT

Proefschrift

ter verkrijging van de graad van doctor aan de
Erasmus Universiteit Rotterdam
op gezag van de
rector magnificus

Prof.dr. S.W.J. Lamberts

en volgens besluit van het College voor Promoties.

De openbare verdediging zal plaatsvinden op
Woensdag 18 oktober 2006 om 9.45 uur

door

Timo Baks

geboren te
's-Gravenzande

Promotiecommissie

Promotoren:	Prof.dr. P. J. de Feyter
	Prof.dr. G. P. Krestin
Overige leden:	Prof.dr. D. Duncker
	Prof.dr. W. van der Giessen
	Prof.dr. D. Poldermans
Copromotor:	Dr. R.J. van Geuns

Financial support by the Netherlands Heart Foundation for the publication of this thesis is gratefully acknowledged.

Financial support by the department of Radiology, Erasmus MC, University Medical Center Rotterdam, for the publication of this thesis is gratefully acknowledged.

voor Else

Part 1: Preface

Part 2: Experimental Application of Magnetic Resonance Imaging

Part 3: Clinical Application of Magnetic Resonance Imaging

Part 4: Innovation in Viability Imaging

Part 5: Summary and Conclusions

Part 1

Preface

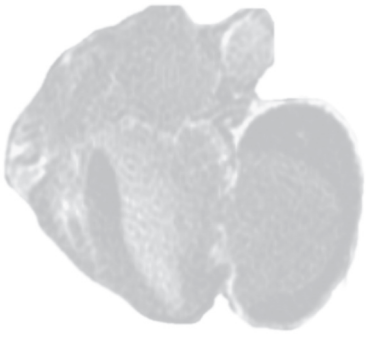

Introduction

Ischemic heart disease as a result of coronary artery disease is currently the leading cause of mortality in the western world (1). The number of patients suffering from acute and chronic ischemic heart disease is expected to increase in the next decades because of ageing populations and patients surviving their first myocardial infarction as a result of improved early revascularization therapy (2). Ischemic heart disease may cause left ventricular systolic and diastolic dysfunction which is clinically relevant since the extent of left ventricular dysfunction is associated with clinical symptoms and cardiovascular mortality (3-5). Importantly, the extent of left ventricular systolic and diastolic dysfunction can be assessed with non-invasive imaging modalities such as echocardiography, single photon emission computed tomography, positron emission tomography and more recently with magnetic resonance imaging (6-8).

In the early 1980s, Magnetic Resonance Imaging (MRI) was introduced as a novel non-invasive imaging tool that allowed imaging of the beating heart. Major technical developments have happened since then and MRI is now considered an excellent non-invasive imaging modality with multiple established and promising clinical applications (9). MRI can assess left ventricular function accurately without making assumptions on 3 dimensional geometry of the left ventricle. The reproducibility for the assessment of left ventricular function with MRI is excellent (10) . Furthermore, MRI can differentiate necrotic from viable myocardium in reperfused and non-reperfused acute myocardial infarction and in the setting of chronic ischemic heart disease (11,12). Experimental studies demonstrated a strong relation between infarct size measured with MRI and infarct size measured ex-vivo (11-13). Infarct size can be assessed accurately after administration of gadolinium-chelates that have T1 shortening characteristics resulting in excellent soft tissue contrast. Recently, a technique was introduced that improved tissue contrast further by applying a non-selective inversion pulse before data-acquisition allowing suppression of the signal of remote myocardium (14). MRI allows assessment of infarct size with superior spatial resolution and permits the detection of small subendocardial myocardial infarctions in patients which are easily missed by nuclear imaging modalities like SPECT and PET (15,16). The reproducibility of MRI for the detection of myocardial infarction is excellent(17,18). No heart rate control is necessary but patients with an arrhythmia are excluded from imaging. MRI is safe, patient friendly and can be repeated multiple times to evaluate therapy without causing harm to the patient. These characteristics make MRI a great imaging tool for assessment of left ventricular function and for the detection of myocardial viability in patients with acute myocardial infarction and patients with chronic ischemic heart disease. Furthermore, the excellent image

quality and reproducibility of MRI allows the refined study of the pathophysiology of ischemic heart disease in an experimental and clinical setting.

Multislice Computed Tomography (MSCT) was introduced more recently and the cardiac application looks promising. It all started with Computed Tomography of the heart that was performed as early as the late seventies and these initial results were encouraging (19). However, practical utilization of this technique was hampered by insufficient image quality mainly caused by cardiac motion. CT technology has developed rapidly during the last decade and with the introduction of spiral and later multislice spiral CT a marked increase in temporal and spatial resolution was obtained. In recent years, Multislice Computed Tomography (MSCT) technology has made great strides and non-invasive assessment of coronary artery stenosis is now feasible with high diagnostic accuracy using a 64-slice scanner (20,21). MSCT has also been proposed as an alternative non-invasive imaging modality for the detection of myocardial infarction and viability. However, different imaging protocols have been proposed at different time points after myocardial infarction and the diagnostic accuracy is currently unclear (22,23).

In part 2, chapter 3 to 6 of this thesis, the novel information provided by MRI is used in experimental models of ischemic heart disease to study the pathophysiology of ischemic heart disease and to monitor novel treatment strategies. In chapter 3, MRI is used to assess diastolic function in swine and patients with acute reperfused myocardial infarction and varying infarct size. The impact of infarct size on the extent of left ventricular diastolic dysfunction is assessed. In chapter 4 and 5, MRI is used to evaluate the effects of stem cell application for left ventricular dysfunction and infarct size in the setting of acute reperfused myocardial infarction in swine. In chapter 6, the MR imaging characteristics of acute reperfused myocardial infarction in swine are studied to assess the consequences for iron labeled stem cell tracking in reperfused myocardial infarction.

Part 3, chapter 7 to 13, is focused on the clinical application of MRI. In chapter 7, we study the recovery of regional and global left ventricular function after acute myocardial infarction in patients who underwent primary stenting with drug-eluting stents. Additionally, we evaluate the value of MRI-based myocardial perfusion and delayed enhancement imaging to predict left ventricular volumes and function. In chapter 8, we study the effects of early successful primary angioplasty for ST-segment elevation acute myocardial infarction (AMI) on early and late infarct size and left ventricular wall characteristics. In chapter 9, MRI is applied in the setting of chronic ischemic heart disease. We study the effect of drug-eluting stent implantation for a

chronic total coronary occlusion on left ventricular volumes and function and assess the predictive value of MRI performed before revascularization. In chapter 10, we assess the accuracy and reproducibility of MRI to measure left ventricular volumes. In chapter 11, we evaluate the relative merits of myocardial contrast echocardiography (MCE) and magnetic resonance imaging (MRI) to predict myocardial functional improvement after percutaneous coronary intervention. In chapter 12, we show a case report of a patient with pseudoaneurysm of the left ventricle diagnosed several years after myocardial infarction. MSCT and MRI provide clinical relevant information. In Chapter 13, we demonstrate a case of iatrogenic myocardial infarction nicely depicted with MRI in a patient with hypertrophic myocardial infarction.

In part 4, chapter 14 and 15, we evaluate MSCT as a novel imaging modality to assess myocardial infarct size. We assess the accuracy of in-vivo delayed enhancement Multislice Computed Tomography (DE-MSCT) and delayed enhancement Magnetic Resonance Imaging (DE-MRI) for the assessment of myocardial infarct size using post-mortem TTC pathology as standard of reference. We discuss the advantages and disadvantages of MSCT versus MRI for the assessment of myocardial infarction and viability.

A full color version of the displayed figures marked with an * can be found in the image color section in part 5 of this book.

References

1. Fox CS, Evans JC, Larson MG, Kannel WB, Levy D. Temporal trends in coronary heart disease mortality and sudden cardiac death from 1950 to 1999: the Framingham Heart Study. Circulation 2004;110:522-7.
2. Stewart S, MacIntyre K, Capewell S, McMurray JJ. Heart failure and the aging population: an increasing burden in the 21st century? Heart 2003;89:49-53.
3. White HD, Norris RM, Brown MA, Brandt PW, Whitlock RM, Wild CJ. Left ventricular end-systolic volume as the major determinant of survival after recovery from myocardial infarction. Circulation 1987;76:44-51.
4. Baks T, van Geuns RJ, Biagini E, et al. Recovery of left ventricular function after primary angioplasty for acute myocardial infarction. Eur Heart J 2005;26:1070-7.
5. Nijland F, Kamp O, Karreman AJ, van Eenige MJ, Visser CA. Prognostic implications of restrictive left ventricular filling in acute myocardial infarction: a serial Doppler echocardiographic study. J Am Coll Cardiol 1997;30:1618-24.
6. Levy WC, Cerqueira MD, Abrass IB, Schwartz RS, Stratton JR. Endurance exercise training augments diastolic filling at rest and during exercise in healthy young and older men. Circulation 1993;88:116-26.

7. Cerisano G, Bolognese L, Carrabba N, et al. Doppler-derived mitral deceleration time: an early strong predictor of left ventricular remodeling after reperfused anterior acute myocardial infarction. Circulation 1999;99:230-6.
8. Tseng WY, Liao TY, Wang JL. Normal systolic and diastolic functions of the left ventricle and left atrium by cine magnetic resonance imaging. J Cardiovasc Magn Reson 2002;4:443-57.
9. The clinical role of magnetic resonance in cardiovascular disease. Task Force of the European Society of Cardiology, in collaboration with the Association of European Paediatric Cardiologists. Eur Heart J 1998;19:19-39.
10. van Geuns RJ, Baks T, Gronenschild EH, et al. Automatic Quantitative Left Ventricular Analysis of Cine MR Images by Using Three-dimensional Information for Contour Detection. Radiology 2006;240:215-21.
11. Kim RJ, Fieno DS, Parrish TB, et al. Relationship of MRI delayed contrast enhancement to irreversible injury, infarct age, and contractile function. Circulation 1999;100:1992-2002.
12. Gerber BL, Rochitte CE, Melin JA, et al. Microvascular obstruction and left ventricular remodeling early after acute myocardial infarction. Circulation 2000;101:2734-41.
13. Baks T, van Geuns RJ, Duncker DJ, et al. Prediction of left ventricular function after drug-eluting stent implantation for chronic total coronary occlusions. J Am Coll Cardiol 2006;47:721-5.
14. Simonetti OP, Kim RJ, Fieno DS, et al. An improved MR imaging technique for the visualization of myocardial infarction. Radiology 2001;218:215-23.
15. Wagner A, Mahrholdt H, Holly TA, et al. Contrast-enhanced MRI and routine single photon emission computed tomography (SPECT) perfusion imaging for detection of subendocardial myocardial infarcts: an imaging study. Lancet 2003;361:374-9.
16. Klein C, Nekolla SG, Bengel FM, et al. Assessment of myocardial viability with contrast-enhanced magnetic resonance imaging: comparison with positron emission tomography. Circulation 2002;105:162-7.
17. Mahrholdt H, Wagner A, Holly TA, et al. Reproducibility of chronic infarct size measurement by contrast-enhanced magnetic resonance imaging. Circulation 2002;106:2322-7.
18. Thiele H, Kappl MJ, Conradi S, Niebauer J, Hambrecht R, Schuler G. Reproducibility of chronic and acute infarct size measurement by delayed enhancement-magnetic resonance imaging. J Am Coll Cardiol 2006;47:1641-5.
19. Gray WR, Buja LM, Hagler HK, Parkey RW, Willerson JT. Computed tomography for localization and sizing of experimental acute myocardial infarcts. Circulation 1978;58:497-504.
20. Raff GL, Gallagher MJ, O'Neill WW, Goldstein JA. Diagnostic accuracy of noninvasive coronary angiography using 64-slice spiral computed tomography. J Am Coll Cardiol 2005;46:552-7.
21. Mollet NR, Cademartiri F, van Mieghem CA, et al. High-resolution spiral computed tomography coronary angiography in patients referred for diagnostic conventional coronary angiography. Circulation 2005;112:2318-23.

22. Hoffmann U, Millea R, Enzweiler C, et al. Acute myocardial infarction: contrast-enhanced multidetector row CT in a porcine model. Radiology 2004;231:697-701.
23. Buecker A, Katoh M, Krombach GA, et al. A feasibility study of contrast enhancement of acute myocardial infarction in multislice computed tomography: comparison with magnetic resonance imaging and gross morphology in pigs. Invest Radiol 2005;40:700-4.

Cardiovascular Magnetic Resonance Imaging for the Assessment of Myocardial Viability

Timo Baks, Robert-Jan van Geuns, Pim de Feyter

Department of Cardiology and Radiology, Erasmus MC, Rotterdam

Adapted from: The Paris course on revascularization chapter 15, pgs 203-213

Abstract

Cardiovascular magnetic resonance imaging (MRI) is becoming an exciting diagnostic tool. Recent technical developments including increase in gradient power and higher magnetic field strengths make it possible to obtain images in less time with higher spatial resolution. MRI is a patient friendly imaging modality and MRI uses low-energy radio frequency waves and safe contrast material. The technique offers excellent soft tissue contrast. Contrast-enhanced MRI combines high temporal resolution with excellent spatial resolution for the assessment of myocardial viability. Myocardial viability is a clinical relevant issue in patients with dysfunctional myocardium due to ischemic heart disease. The extent of myocardial viability assessed with MRI is predictive for functional improvement after revascularization therapy, as shown in several clinical trials.

Cardiovascular Magnetic Resonance Imaging

Cardiovascular magnetic resonance (MRI) imaging is becoming part of the diagnostic armamentarium in cardiology. MR imaging is a technique that offers excellent soft tissue contrast and nowadays MRI is accepted as a reliable diagnostic tool in many clinical situations, as proposed by the European Society of Cardiology [1]. We will provide some basic technical backgrounds of MRI which allow better understanding of contrast-enhanced MRI for the assessment of myocardial viability.

Magnetic Resonance Imaging System

A MRI imaging system requires (1) a static homogeneous magnetic field, (2) a coil to transmit and/or receive radiofrequency (RF) energy, (3) gradient coils and (4) a computer to set up the pulse sequences and process the data into images.

(1) High magnetic field systems use superconducting magnets. Coil windings exposed to the temperature of liquid helium (around 4 degrees Kelvin/ -269 degrees Celsius) become superconducting and produce a spatially homogeneous magnetic field, once an inductive current is applied. The patient is placed within the bore of the magnet.

(2) Radiofrequency (RF) coils produce specific RF waves (**Figure 1**), which are transmitted to the patient to excite atomic nuclei with an odd number of protons or neutrons. Most clinical MRI systems observe the hydrogen (H-1) nucleus because of its relative abundance in the body and its inherent large magnetic momentum. Hydrogen nuclei are excited and will resonate if RF pulses with a resonant frequency are applied (depending on magnetic field strength: 62MHz at 1,5 Tesla). Hydrogen nuclei absorb the transmitted energy. The time for an excited nucleus to return to its former energy state is called relaxation time and can be expressed in two parameters known as T1 and T2. Contrast in an image depends on the differences in relaxation times between different types of tissue. Relaxing nuclei produce an electrical current (signal) with a resonant frequency in a coil (receiver coil), which is positioned near the excited tissue. The coil used for transmitting RF to the patient may also be used for receiving the signal, but dedicated receiver coils with a better signal to noise ratio have been developed for different parts of the body.

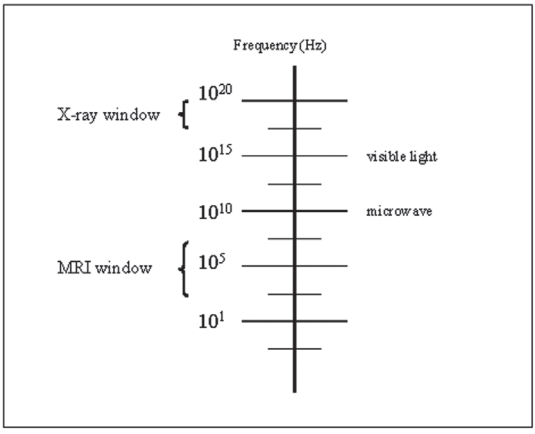

Figure 1: MRI uses low energy radio frequency waves.

(3) Gradient coils are programmed to produce weak linear changes in magnetic field, superimposed on the main magnetic field (**Figure 2**). The increasing magnetic field strength along the imaging plane creates differences in resonant frequencies. These specific frequencies are characteristic for specific locations and provide the spatial information of an image. Gradients can be ap-plied in three dimensions and all desired tomographic planes can be planned, but standardized imaging planes have been proposed [2].

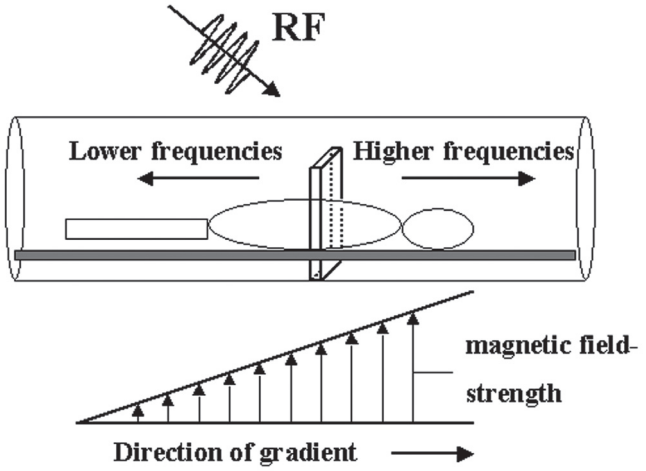

Rapidly switching gradients produce a typical noise, which may be disturbing for the patient.

Figure 2: The application of a gradient varies the magnetic field strength in a controlled manner. Increasing magnetic field strength causes higher resonant frequencies. These specific frequencies are characteristic for specific locations and provide the spatial information of an image.

(4) Several techniques or so-called sequences are applied to obtain different kind of images. The different types of sequences can be subdivided roughly in three major categories;

a. *Spin echo imaging*: "black blood" images where blood appears as black because of signal void due to rapid flow; good for anatomical detail with excellent tissue contrast (**Figure 3a**). These types of sequences are less sensitive for magnetic field inhomogeneities caused by for example coronary stents, sternal wires and surgical clips, but the scan-time is rather long.
b. *Gradient echo imaging*: "bright blood" images where blood appears as bright **(Figure 3b**). This is a fast sequence that can be used for cine-imaging. Wall motion and flow patterns can be evaluated. These sequences are more sensitive for magnetic field inhomogeneities .
c. *Velocity mapping*: quantitative assessment of flow/volume using a specific gradient echo sequence.

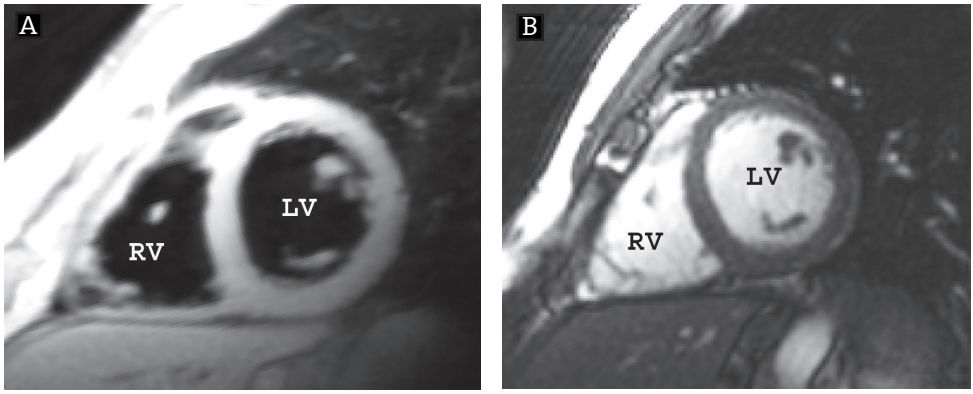

Figure 3: Short axis view in a healthy volunteer: (**A**) Spin echo "black blood" image with the corresponding (**B**) "bright blood" gradient echo image.

Contrast Agents

Gadolinium-chelates are used in MRI to enhance the signal in magnetic resonance angiography, perfusion and/or viability studies. Gadolinium ions (Gd^{3+}) have paramagnetic properties and influence the magnetization characteristics of directly surrounding tissue. The increased regional differences in magnetization are used to enhance the signal. An example is delayed enhancement imaging for myocardial infarction which will be discussed later. Gadolinium itself is toxic but if chelated to other molecules it can be safely administered intravenously. Gadolinium-chelates have the same distributional properties as iodinated x-ray agents but are not nefrotoxic and much safer to use [3]. Adverse reactions to gadolinium-chelates are rarely seen[4].

Safety of MRI

MRI is a safe and patient friendly imaging modality. No ionizing x-rays are used and the contrast agents are not nephro- toxic. Coronary stents are not a contraindication and can be scanned within a few days of placement, because the deflection forces of the heart are much stronger than the displacement forces of the stent by the magnetic field [5,6]. Prosthetic heart valves are not a contraindication to MRI but do cause an image artifact [7]. Contraindications at this moment include patients with a pacemaker, implantable defibrillator, intracranial cerebrovascular aneurysm clips, intra-ocular shards and other implantable electronical devices. Although some studies show that patients with an implanted pacemaker can undergo MRI, imaging have to be performed under close supervision of a cardiologist/electrophysiologist [8]. For any advise on safety in MRI we advise to look on the website www.mrisafety.com.

Clinical Indications

In 1998 a task force of the European Society of Cardiology (ESC) proposed guidelines on the use of MRI in clinical practice [1]. The task force adopted a classification proposed by the American college of Cardiology and American Heart Association (ACC/AHA). Although technical developments are going fast, these guidelines still give an useful overview of the relevant topics. For the purpose of this chapter we mainly focus on ischemic heart disease.

MRI and Myocardial Viability

Atherosclerotic coronary artery disease may cause an acute and/or persistent reduction of blood flow to the myocardium, resulting in the occurrence of (1) stunned myocardium, (2) myocardial hibernation, and/or (3) myocardial necrosis.

(1) Stunned myocardium: reversible contractile dysfunction caused by transient ischemia. A period of 5 to 20 minutes of ischemia followed by complete reperfusion causes prolonged contractile dysfunction of viable myocardium that may remain for hours, days or weeks before contractility recovers [9].

(2) Hibernating myocardium: a state of more persistent myocardial dysfunction at rest due to repetitive transient ischemia or chronically reduced blood flow. Hibernating myocardium will recover function after days to months if coronary blood flow is restored or oxygen demand is decreased [10]. Hibernating myocardium is a clinical relevant issue in patients with chronic ischemic heart disease.

(3) Necrosis: irreversible dysfunction of myocardium due to myocyte cell death.

Acute myocardial infarction

In acute myocardial infarction (AMI), the extent of myocardium salvaged by reperfusion therapy (viable myocardium) may predict left ventricular function and cardiac mortality at long term follow-up. Different parameters can be evaluated with MRI to assess myocardial viability in patients who suffered acute myocardial infarction: (**1**) evaluation of wall motion/thickening/thickness (**2**) assessment of first-pass perfusion and (**3**) performing delayed enhancement imaging.

(**1**) Wall motion/thickening/thickness

Wall motion/thickening and wall thickness can be evaluated with cine-MRI using an ECG-gated gradient-echo imaging technique. These parameters are not well suited for the differentiation between viable and necrotic myocardium. Normal wall motion/thickening indicates the presence of viable myocardium. However, a resting wall motion/thickening disorder does not differentiate between viable or non-viable myocardium, since stunned, hibernating and necrotic myocardium all exhibit contractile dysfunction. End-diastolic wall thickness might be unchanged or increased just after acute myocardial infarction and does not differentiate well between viable or

non-viable myocardium in AMI [11]. In weeks following acute myocardial infarction, the region of infarction will gradually get thinner when scar tissue formation proceeds.

(**2**) First-pass perfusion

The first-pass of an intravenously administered contrast agent can be assessed with MRI and provides information on myocardial perfusion. A breath-holding ECG-triggered sequence is used for the continuous acquisition of images before, during and after administration of a bolus contrast agent. First-pass perfusion provides information about coronary artery patency and/or microvasculature. A hypoperfused region of the myocardium appears as a hypoenhanced zone (dark, no contrast agent) and may represent either a (a) residual stenosis/occlusion of the coronary artery or (b) damage to the microvasculature.

(a) A high grade stenosis or a total occlusion of a coronary artery prevents contrast agents from entering the myocardium. This hypoperfused region appears as a hypoenhanced zone. If damage to the microvasculature is absent and, in the case of a total occlusion, collateral vessels are present the hypoenhanced region will enhance shortly after.

(b) Hypoenhanced regions in the co-existence of a patent coronary artery represent microvascular obstruction, the so called "no reflow zone" (**Figure 4**). These hypoenhanced regions are severely injured and show irreversible dysfunction at follow up [12,13]. The extent of microvascular obstruction predicts left ventricular dilatation on follow up as shown in a study with dogs [14,15]. The hypoenhanced region though, greatly underestimates total infarct size since the microvasculature might not be damaged in the whole necrotic region (**Figure 5**). The proportion of infarcted myocardium with microvascular obstruction may increase in the first two days after reperfused infarction but stabilizes between 2 and 10 days in a canine model of acute reperfused myocardial infarction [14].

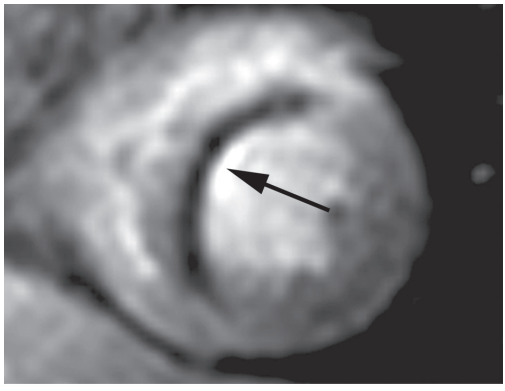

Figure 4: A patient with an acute occlusion of the left anterior descending coronary artery (LAD). Complete reperfusion was obtained with angioplasty within 4 hours after onset of symptoms. The hypoenhanced region in the septum indicates microvascular obstruction (patent LAD).

In conclusion: first-pass perfusion might be a less sensitive technique for the detection of myocardial viability in AMI, since non-viable myocardium might enhance normal.

(**3**) Delayed enhancement imaging
Myocardial infarct size and the transmural extent of infarction can be assessed with delayed contrast-enhanced MRI. An ECG-gated T1-weighted inversion-recovery fast gradient-echo sequence is applied. Images acquired between approximately 5 and 30 minutes after the administration of gadolinium-chelates show signal enhancement in necrotic regions, while the contrast agent is washed out of the healthy myocardium [16]. Although the exact mechanism is not yet clear, it is thought that gadolinium-chelates passively diffuse into the extracellular matrix that is increased in size due to interstitial edema and loss of myocyte membrane integrity [17,18].

The hyperenhanced region of the myocardium corresponds to the infarcted region found by post mortem triphenyltetrazolium chloride (TTC) staining in dogs for AMI as well as CIHD (chronic ischemic heart disease), although there seems to be a slight overestimation (10%) of infarct size due to partial volume effects [19]. Infarct size decreases in time with a factor of 3 to 4 between 3 days and 8 weeks in a study with dogs. Similar observations on infarct shrinkage have been reported in a human population [13,20].

Current MRI-techniques have sufficient spatial resolution (app. 1.5 x 2 x 6mm) to assess the transmural extent of infarction [21]. The transmural extent of infarction (TEI) in AMI predicts improvement in regional left ventricular function as shown in several studies [12,22-25]. The lower the extent of infarction the higher the probability of functional recovery. For example, in a patient with a dysfunctional segment and a TEI off less than 25 % the likelihood of functional improvement is between 65-75 %, while with a TEI of more than 75 % this will be around 35%. [22,23].

A delayed hypoenhanced (dark) subendocardial zone within the hyperenhanced region (imaged after 15 minutes) represents a region where microvasculature is compromised. This region corresponds to the hypoenhanced region as seen in the first-pass perfusion image, although size might be different (**Figure 5**,**6**). The hypoenhanced region will slowly enhance when contrast agent passively diffuses in [26]. Regions which show hypoenhancement after 10 to 30 minutes are severely injured and show no improvement on long term follow-up [23,25].

Chronic Ischemic Heart Disease
Patients with chronic ischemic heart disease (CIHD) might benefit from revascularization therapy if reversible dysfunctional (viable) myocardium is present [27].

Myocardial viability in CIHD can be assessed with the (**1**) evaluation of wall motion/thickening/thickness and (**2**) delayed enhancement imaging.

(**1**) Wall motion/thickening/thickness

Wall motion/thickening and wall thickness can be evaluated with MRI using an ECG-gated cine gradient-echo imaging technique (**Figure 7**). These parameters are not well suited for the differentiation between viable and necrotic myocardium. Normal wall motion/thickening indicates the presence of viable myocardium. A resting wall motion/thickening disorder does not differentiate between viable or non-viable myocardium, since stunned, hibernating, and necrotic myocardium exhibits contractile dysfunction. End-diastolic wall thickness is also proposed as a marker of viability in chronic ischemic heart disease. Echocardiography studies showed that regional end-

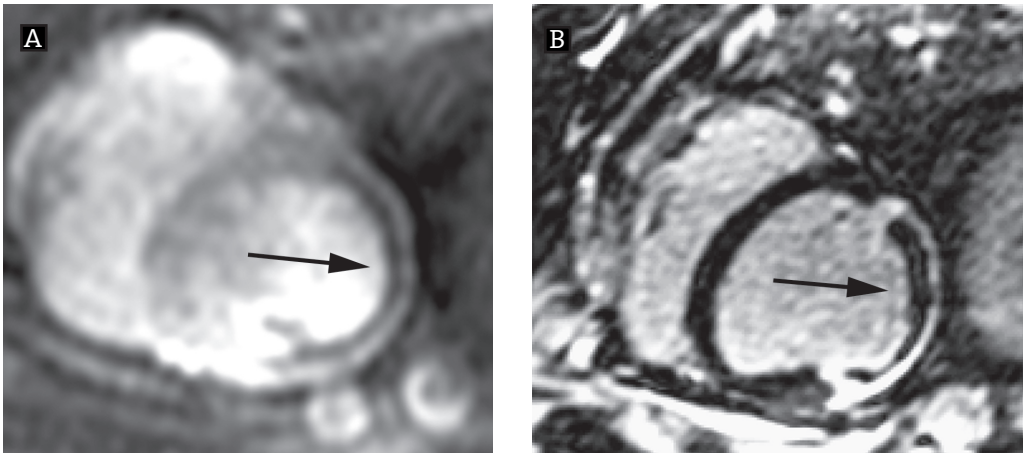

Figure 5: In a pig, a balloon was inflated for 2 hours in the left circumflex coronary artery followed by complete reperfusion. ce-MRI imaging was performed at five days. (**A**) First-pass perfusion imaging shows a region of hypoenhancement (*arrow*) in the lateral wall indicating microvascular obstruction (patent circumflex coronary artery). (**B**) The corresponding short axis view 15 minutes later shows a hypoenhanced area (microvascular obstruction) surrounded by a hyperenhanced region. Total infarct size: bright region including dark region.

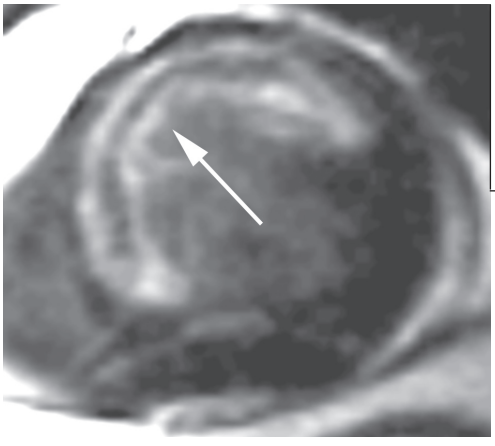

Figure 6: Patient presenting with acute myocardial infarction in the anterior wall. Angioplasty was performed within 6 hours and a ce-MRI was performed 3 days later. Delayed enhancement imaging reveals a region of transmural infarction (bright) in the anterior wall. The hypoenhanced area (dark) within the hyperenhanced region indicates an area of microvascular obstruction (arrow).

diastolic wall thickness of less than 6 mm was a good predictor of the lack of functional recovery [28]. However, with the introduction of high resolution contrast-enhanced MRI, segments with end-diastolic wall thickness of less than 6 mm are shown to be possibly viable and be able to recover function [29].

Low-dose dobutamine stress-MRI can be used to assess the functional reserve of dysfunctional myocardium. During administration of 5-10 microgram/kg/min dobutamine intravenously, stunned and hibernating myocardium will regain contractile function and show an increase in systolic wall thickening. Baer et al. showed a positive correlation between increased systolic wall thickening during stress and functional improvement after revascularization in patients with CIHD, indicating the presence of viable myocardium [30]. Wellnhofer et al. showed that dobutamine stress MRI performed better in predicting functional improvement than did contrast-enhanced MRI [31].

(**2**) Delayed enhancement imaging

Experimental studies of chronic myocardial infarction showed that MRI can accurately differentiate viable myocardium from scar tissue with high spatial resolution 19. The transmural extent of delayed enhancement in dysfunctional segments predicts functional outcome of these segments after revascularization therapy [32-34]. The lower the extent of enhancement (infarction), with subsequent higher extent of viable but dysfunctional myocardium, the higher the probability of functional recovery (**Figure 8, 9**). A dysfunctional segment without hyperenhancement has 80% chance of functional

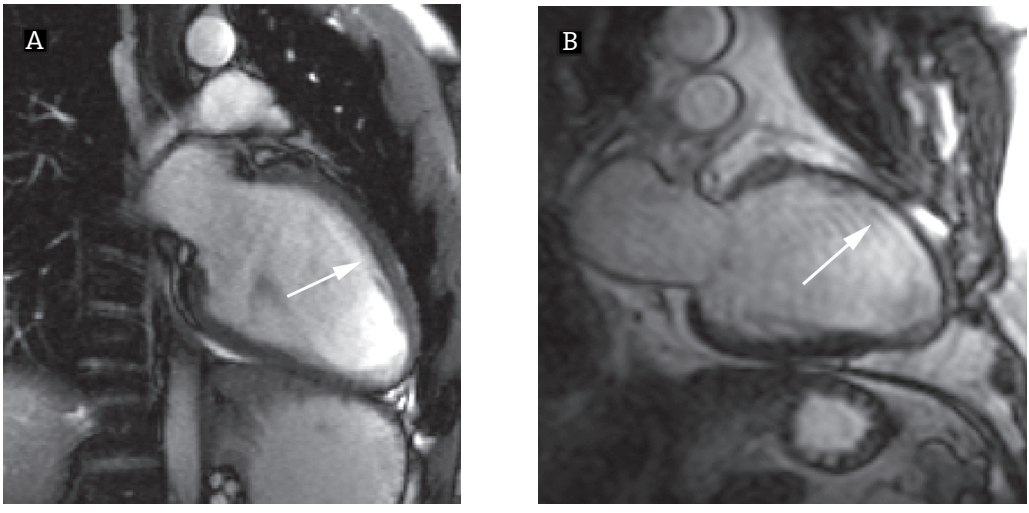

Figure 7: Assessment of wall thickness in a two-chamber view: (**A**) normal wall thickness in a healthy volunteer. (**B**) Decreased wall thickness in patient with history of myocardial infarction of the anterior wall. The question remains whether there is viable myocardium present in the anterior wall.

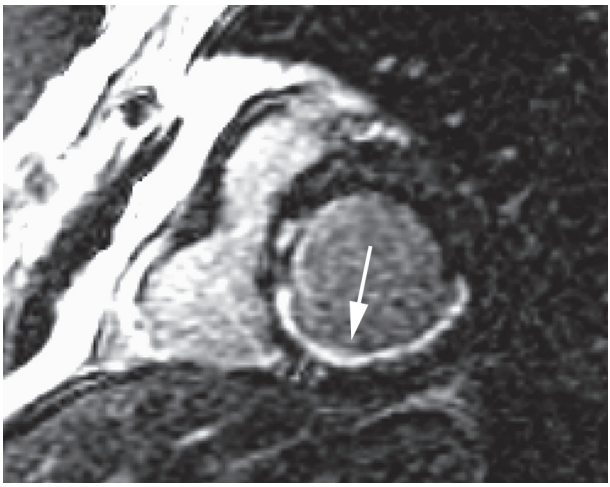

recovery. A segment with more than 50% transmural extent of hyperenhancement has little likelihood of improvement after revascularization therapy [34,35]. A recent study describes the effect of B-blocker therapy instead of revascularization therapy on chronic heart failure and an improvement of 10 % is seen in global left ventricular function if viable tissue is present as detected by MRI [36].

Figure 8: Patient presenting with exercise related chest pain and no clinical signs of acute myocardial infarction. Conventional coronary angiogram reveales a total occlusion of the RCA. ce-MRI imaging shows a delayed hyperenhanced subendocardial region in the basal part of the inferior wall, indicating the presence of epicardial viable myocardium.

Conclusion

Cardiovascular Magnetic Resonance (MRI) Imaging is a emerging diagnostic tool for the non-invasive assessment of ischemic heart disease. Contrast-enhanced MRI combines high temporal resolution with excellent spatial resolution for the assessment of myocardial viability. Myocardial viability is a clinical relevant issue in patients with dysfunctional myocardium due to ischemic heart disease. The extent of myocardial viability assessed with MRI is predictive for functional improvement after revascularization therapy.

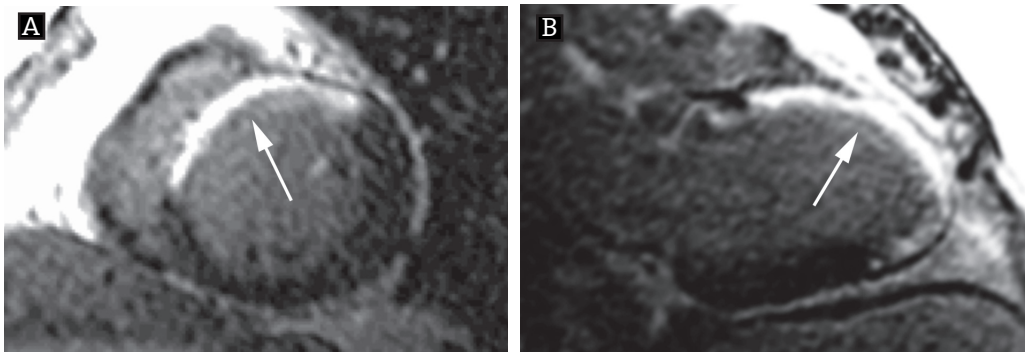

Figure 9: A patient with a history of ischemic heart disease develops symptoms of depressed left ventricular function. Ce-MRI imaging shows a transmural hyperenhanced region in the anterior wall indicating non-viable myocardium in (a) two-chamber view and (b) short axis view.

References

1. The clinical role of magnetic resonance in cardiovascular disease. Task Force of the European Society of Cardiology, in collaboration with the Association of European Paediatric Cardiologists. Eur Heart J. 1998;19:19-39.
2. Cerqueira MD, Weissman NJ, Dilsizian V, Jacobs AK, Kaul S, Laskey WK, Pennell DJ, Rumberger JA, Ryan T, Verani MS. Standardized myocardial segmentation and nomenclature for tomographic imaging of the heart: a statement for healthcare professionals from the Cardiac Imaging Committee of the Council on Clinical Cardiology of the American Heart Association. Circulation. 2002;105:539-42.
3. Weinmann HJ, Brasch RC, Press WR, Wesbey GE. Characteristics of gadolinium-DTPA complex: a potential NMR contrast agent. AJR Am J Roentgenol. 1984;142:619-24.
4. Nelson KL, Gifford LM, Lauber-Huber C, Gross CA, Lasser TA. Clinical safety of gadopentetate dimeglumine. Radiology. 1995;196:439-43.
5. Shellock FG, Shellock VJ. Metallic stents: evaluation of MR imaging safety. AJR Am J Roentgenol. 1999;173:543-7.
6. Gerber TC, Fasseas P, Lennon RJ, Valeti VU, Wood CP, Breen JF, Berger PB. Clinical safety of magnetic resonance imaging early after coronary artery stent placement. J Am Coll Cardiol. 2003;42:1295-8.
7. Ahmed S, Shellock FG. Magnetic resonance imaging safety: implications for cardiovascular patients. J Cardiovasc Magn Reson. 2001;3:171-82.
8. Sommer T, Naehle CP, Schild H. Magnetic resonance imaging in patients with cardiac pacemakers. J Am Coll Cardiol. 2005;46:561-2; author reply 562.
9. Braunwald E, Kloner RA. The stunned myocardium: prolonged, postischemic ventricular dysfunction. Circulation. 1982;66:1146-9.
10. Rahimtoola SH. The hibernating myocardium. Am Heart J. 1989;117:211-21.
11. Schroeder AP, Houlind K, Pedersen EM, Nielsen TT, Egeblad H. Serial magnetic resonance imaging of global and regional left ventricular remodeling during 1 year after acute myocardial infarction. Cardiology. 2001;96:106-14.
12. Gerber BL, Garot J, Bluemke DA, Wu KC, Lima JA. Accuracy of contrast-enhanced magnetic resonance imaging in predicting improvement of regional myocardial function in patients after acute myocardial infarction. Circulation. 2002;106:1083-9.
13. Baks T, van Geuns RJ, Biagini E, Wielopolski P, Mollet NR, Cademartiri F, van der Giessen WJ, Krestin GP, Serruys PW, Duncker DJ, de Feyter PJ. Effects of primary angioplasty for acute myocardial infarction on early and late infarct size and left ventricular wall characteristics. J Am Coll Cardiol. 2006;47:40-4.
14. Gerber BL, Rochitte CE, Melin JA, McVeigh ER, Bluemke DA, Wu KC, Becker LC, Lima JA. Microvascular obstruction and left ventricular remodeling early after acute myocardial infarction. Circulation. 2000;101:2734-41.

15. Ito H, Maruyama A, Iwakura K, Takiuchi S, Masuyama T, Hori M, Higashino Y, Fujii K, Minamino T. Clinical implications of the 'no reflow' phenomenon. A predictor of complications and left ventricular remodeling in reperfused anterior wall myocardial infarction. Circulation. 1996;93:223-8.
16. Amado LC, Gerber BL, Gupta SN, Rettmann DW, Szarf G, Schock R, Nasir K, Kraitchman DL, Lima JA. Accurate and objective infarct sizing by contrast-enhanced magnetic resonance imaging in a canine myocardial infarction model. J Am Coll Cardiol. 2004;44:2383-9.
17. Saeed M, Wendland MF, Watzinger N, Akbari H, Higgins CB. MR contrast media for myocardial viability, microvascular integrity and perfusion. Eur J Radiol. 2000;34:179-95.
18. Mahrholdt H, Wagner A, Judd RM, Sechtem U. Assessment of myocardial viability by cardiovascular magnetic resonance imaging. Eur Heart J. 2002;23:602-19.
19. Kim RJ, Fieno DS, Parrish TB, Harris K, Chen EL, Simonetti O, Bundy J, Finn JP, Klocke FJ, Judd RM. Relationship of MRI delayed contrast enhancement to irreversible injury, infarct age, and contractile function. Circulation. 1999;100:1992-2002.
20. Reimer KA, Jennings RB. The changing anatomic reference base of evolving myocardial infarction. Underestimation of myocardial collateral blood flow and overestimation of experimental anatomic infarct size due to tissue edema, hemorrhage and acute inflammation. Circulation. 1979;60:866-76.
21. Simonetti OP, Kim RJ, Fieno DS, Hillenbrand HB, Wu E, Bundy JM, Finn JP, Judd RM. An improved MR imaging technique for the visualization of myocardial infarction. Radiology. 2001;218:215-23.
22. Choi KM, Kim RJ, Gubernikoff G, Vargas JD, Parker M, Judd RM. Transmural extent of acute myocardial infarction predicts long-term improvement in contractile function. Circulation. 2001;104:1101-7.
23. Beek AM, Kuhl HP, Bondarenko O, Twisk JW, Hofman MB, van Dockum WG, Visser CA, van Rossum AC. Delayed contrast-enhanced magnetic resonance imaging for the prediction of regional functional improvement after acute myocardial infarction. J Am Coll Cardiol. 2003;42:895-901.
24. Hillenbrand HB, Kim RJ, Parker MA, Fieno DS, Judd RM. Early assessment of myocardial salvage by contrast-enhanced magnetic resonance imaging. Circulation. 2000;102:1678-83.
25. Baks T, van Geuns RJ, Biagini E, Wielopolski P, Mollet NR, Cademartiri F, Boersma E, van der Giessen WJ, Krestin GP, Duncker DJ, Serruys PW, de Feyter PJ. Recovery of left ventricular function after primary angioplasty for acute myocardial infarction. Eur Heart J. 2005;26:1070-7.
26. Judd RM, Lugo-Olivieri CH, Arai M, Kondo T, Croisille P, Lima JA, Mohan V, Becker LC, Zerhouni EA. Physiological basis of myocardial contrast enhancement in fast magnetic resonance images of 2-day-old reperfused canine infarcts. Circulation. 1995;92:1902-10.
27. Allman KC, Shaw LJ, Hachamovitch R, Udelson JE. Myocardial viability testing and impact of revascularization on prognosis in patients with coronary artery disease and left ventricular dysfunction: a meta-analysis. J Am Coll Cardiol. 2002;39:1151-8.
28. Schinkel AF, Bax JJ, Boersma E, Elhendy A, Vourvouri EC, Roelandt JR, Poldermans D. Assessment of residual myocardial viability in regions with chronic electrocardiographic Q-wave infarction. Am Heart J. 2002;144:865-9.

29. Kim RJ, Shah DJ. Fundamental concepts in myocardial viability assessment revisited: when knowing how much is "alive" is not enough. Heart. 2004;90:137-40.
30. Baer FM, Theissen P, Schneider CA, Voth E, Sechtem U, Schicha H, Erdmann E. Dobutamine magnetic resonance imaging predicts contractile recovery of chronically dysfunctional myocardium after successful revascularization. J Am Coll Cardiol. 1998;31:1040-8.
31. Wellnhofer E, Olariu A, Klein C, Grafe M, Wahl A, Fleck E, Nagel E. Magnetic resonance low-dose dobutamine test is superior to SCAR quantification for the prediction of functional recovery. Circulation. 2004;109:2172-4.
32. Kim RJ, Wu E, Rafael A, Chen EL, Parker MA, Simonetti O, Klocke FJ, Bonow RO, Judd RM. The use of contrast-enhanced magnetic resonance imaging to identify reversible myocardial dysfunction. N Engl J Med. 2000;343:1445-53.
33. Schvartzman PR, Srichai MB, Grimm RA, Obuchowski NA, Hammer DF, McCarthy PM, Kasper JM, White RD. Nonstress delayed-enhancement magnetic resonance imaging of the myocardium predicts improvement of function after revascularization for chronic ischemic heart disease with left ventricular dysfunction. Am Heart J. 2003;146:535-41.
34. Baks T, van Geuns RJ, Duncker DJ, Cademartiri F, Mollet NR, Krestin GP, Serruys PW, de Feyter PJ. Prediction of left ventricular function after drug-eluting stent implantation for chronic total coronary occlusions. J Am Coll Cardiol. 2006;47:721-5.
35. Kim RJ, Hillenbrand HB, Judd RM. Evaluation of myocardial viability by MRI. Herz. 2000;25:417-30.
36. Bello D, Shah DJ, Farah GM, Di Luzio S, Parker M, Johnson MR, Cotts WG, Klocke FJ, Bonow RO, Judd RM, Gheorghiade M, Kim RJ. Gadolinium cardiovascular magnetic resonance predicts reversible myocardial dysfunction and remodeling in patients with heart failure undergoing beta-blocker therapy. Circulation. 2003;108:1945-53.

Part 2

Experimental Application of Magnetic Resonance imaging

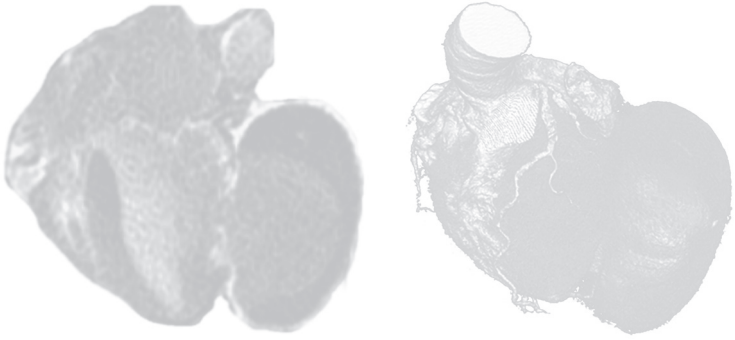

Infarct Size and Diastolic Function in Acute Reperfused Myocardial Infarction and the Impact on Left Ventricular Remodeling

Timo Baks, MD[1,2]; Robert-Jan van Geuns, MD, PhD[1,2]; Sharon Kirschbaum, MD[1,2]; Amber Moelker, MsC[1]; Willem J. van der Giessen, MD, PhD[1]; Dirk J. Duncker, MD, PhD[1]; Pim J. de Feyter, MD, PhD [1,2]

Institute:
Erasmus MC, Rotterdam, The Netherlands:
[1] Department of Cardiology, Thoraxcenter
[2] Department of Radiology

Submitted

3

1, 2 4, 5, 6, 7, 8, 9, 10, 11, 12, 13, 14, 15

Abstract

Aims

We studied the impact of infarct size on left ventricular diastolic function in swine and patients with reperfused acute myocardial infarction (AMI). Furthermore, we explored the predictive value of infarct size and diastolic function for left ventricular remodeling.

Methods and Results

Sixteen swine underwent 2 hours of balloon occlusion of the circumflex coronary artery followed by complete reperfusion. Eight healthy swine served as controls. At 5±1 days after AMI, all swine underwent contrast-enhanced Magnetic Resonance Imaging (MRI). Sixteen patients underwent MRI at 5±3 days and 5±1 months after mechanically reperfused first AMI. Diastolic function was calculated from volume-time curves. Infarct size was assessed with delayed-enhancement imaging. In swine with AMI, peak filling rate adjusted for end-diastolic volume (PFR/EDV) was significantly lower compared to healthy swine (3.3±1.0 versus 4.7±1.2/s;$p=0.006$). PFR/EDV was inversely related to infarct size ($R=0.88$;$p<0.0001$). Also in patients, PFR/EDV was inversely related to infarct size ($R=0.58$;$p=0.01$). Infarct size at 5 days was a stronger predictor than PFR/EDV for ejection fraction at 5 months ($R=0.79$;$p<0.001$, $R=0.41$;$p=0.05$ respectively).

Conclusion

Acute myocardial infarct size is a major determinant of left ventricular diastolic function. Infarct size is a stronger predictor of left ventricular remodeling and function than the extent of diastolic dysfunction.

Introduction

Myocardial infarct size and systolic and diastolic volumes and function of the left ventricle are all considered as predictors of left ventricular remodeling and cardiac mortality (1-5). Infarct size is a major determinant of left ventricular systolic (dys)function and remodeling in patients with a recent acute myocardial infarction (AMI) (3, 5), but the impact on left ventricular diastolic function is less well understood. Contrast-enhanced Magnetic Resonance Imaging (ce-MRI) allows refined assessment of left ventricular systolic and diastolic function and volumes and permits precise assessment of acute reperfused myocardial infarct size (6-9). Consequently, we studied the relation between infarct size and diastolic function using ce-MRI in a well defined porcine model of reperfused AMI. This relation was subsequently studied in patients who received successful drug-eluting stent implantation for first ST-segment elevation AMI. Finally, in these patients we explored the value of infarct size, ejection fraction and diastolic function at 5 days after reperfused AMI to predict left ventricular function and remodeling at 5 months.

Methods

Animal model

Sixteen Yorkshire-landrace swine (2-3 months old, 25-30 kg) were sedated (ketamine 20 mg/kg intramuscular and midazolam 1 mg/kg intramuscular), anaesthetized (thiopental, 12 mg/kg intravenously), intubated and mechanically ventilated (mixture of oxygen and nitrogen 1:2). Anaesthesia was maintained with fentanyl (12.5 microgram/kilogram/hour). All 16 swine then received a sheath in a carotid artery to allow coronary X-ray angiography. Under fluoroscopy guidance, a 2 hour balloon occlusion of the proximal left circumflex coronary artery was performed followed by reperfusion. Occlusion and reperfusion were verified using coronary angiography. Additionally, 8 healthy swine of the same age and weight were selected and served as controls. Of the 16 swine that underwent the 2 hour occlusion protocol, 2 swine were imaged with MRI at 3 days, 7 were imaged at 5 days and 7 were imaged at 7 days after reperfusion (mean 5±1). Also, all 8 control swine underwent a similar MRI protocol. The study complied with the regulations of the animal care committee of our hospital and the "Guide for the Care and Use of Laboratory Animals" (NIH publication 1996).

Patient Population

Sixteen patients with first AMI were included in the study (12 male, 54 ± 10 years old) (**Table 1**). Diagnosis of AMI was based on clinical symptoms, ST-segment elevation on

Table 1 Patient characteristics (n = 16)

Age (years)	54±10
Men	12 (75)
Smoking	6 (56)
Diabetes Mellitus	1 (5)
Hypertension	6 (38)
Hypercholesterolemia	3 (20)
Family history of coronary artery disease	12 (50)
Heart rate (bpm)	72 ±18
Creatine kinase peak (IU)	3296±2064
Anterior Infarction	12 (75)
Inferior	4(25)
Medication at follow-up	
ACE inhibitor	14 (88)
β - Blocker	15(100)
Clopidogrel	16 (100)
Statin	14 (88)
ASA	16 (100)

Values are presented as number (%) or mean ± standard deviation

electrocardiogram, angiographically demonstrated culprit lesion of a coronary artery and Thrombolysis In Myocardial Infarction (TIMI) flow grade ≤ 1. All culprit lesions were stented with a drug-eluting stent within 6 hours (mean 2.5 hours) of onset of symptoms. TIMI flow grade 3 was obtained in all vessels. Exclusion criteria consisted of any contraindication to MRI. All participants gave informed consent to the study protocol, which was approved by the medical ethics committee of the Erasmus MC University Hospital Rotterdam and complied with the Declaration of Helsinki. All 16 patients had both the first MRI scan at 5±3 days after admission and the second MRI scan at 5±1 months. Angiography at follow-up was not performed but no clinical evidence of recurrent myocardial ischemia was noted and all patients received a drug-eluting stent with very low numbers of restenosis reported.

MRI

A similar imaging protocol was applied for the swine and for the patients. A clinical 1.5-Tesla MRI scanner with a dedicated cardiac four element phased-array receiver coil

was used for imaging (Signa CV/i, GE Medical systems, Milwaukee, Wisconsin USA). Repeated breath-holds and gating to the electrocardiogram were applied to minimize the influence of cardiac and respiratory motion on data collection. No medication was administered to control heart rate. Cine-MRI was performed with a steady-state free-precession technique (FIESTA, GE) with the following imaging parameters: 24 temporal phases per slice; views per segment, 12; voxelsize of 1.8 x 1.5 x 8 mm for swine and app. 2.2 x 1.9 x 8 mm for patients; repetition time, 3.0 to 3.5ms; time to echo, 1.4ms; flip angle, 45°; bandwidth 83 kHz; number of averages, 0.75. These used parameters resulted in a temporal resolution per image of less than 42 ms. To cover the entire left ventricle, 6 to 12 consecutive slices of 8 mm were planned in short axis view perpendicular to the long axis of a double oblique four chamber view.

Myocardial distribution of delayed enhancement was studied 15 minutes following administration of Gadolinium-DTPA (0.2 mmol/kg, Magnevist®, Schering, Germany). A 2-dimensional T1-weighted inversion recovery segmented fast gradient-echo sequence with the following imaging parameters was used: voxelsize, 1.1 x 1.5 x 8 mm for swine and app. 1.4 x 1.8 x 8 mm for patients; repetition time, 7.3ms; time to echo, 1.6ms; flip angle, 20°; inversion pulse, 180°; number of averages, 1; bandwidth, 17.9 kHz; inversion time, 180-300 ms and data acquisition usually every second R-R interval. The trigger delay was adjusted to acquire data in mid to end-diastole and the inversion time was adjusted to null the signal of remote myocardium. Slice locations for delayed enhancement imaging were copied from slice locations of cine-imaging.

Data analysis

Cine-MRI images of all 24 swine and 32 patient data sets were loaded on a separate workstation with a commercially available analysis package (MASS, MEDIS, Leiden, the Netherlands). Endocardial contours were detected automatically and if necessary corrected manually in all short axis cine-images. Papillary muscles were considered as part of the left ventricular lumen. Volume-time curves were then calculated and the following parameters were assessed: ejection fraction, end-systolic volume, end-diastolic volume, peak filling rate corrected for end-diastolic volume (PFR/EDV) (10, 11) (**Fig 1**). Delayed enhancement MRI images of the 16 swine and the 16 baseline patient data sets were exported and transferred to a separate workstation with dedicated software (Cine Tool 3.4, GE Medical Systems, USA). The region with delayed hyper-enhancement was segmented manually (9). Infarct size was expressed as a percentage of the total left ventricular myocardial wall mass.

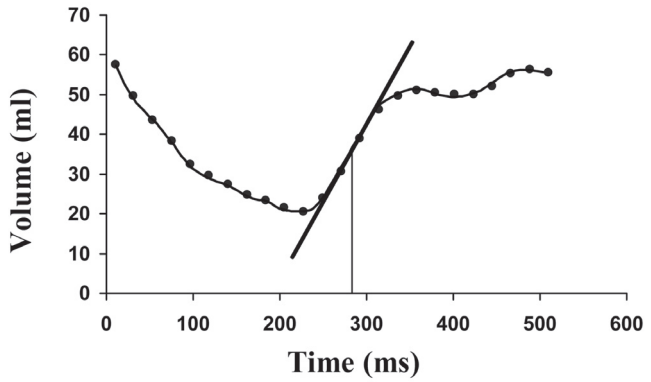

Figure 1A. An example of a volume time curve in a healthy swine. The line indicates the time where peak filling rate is measured.

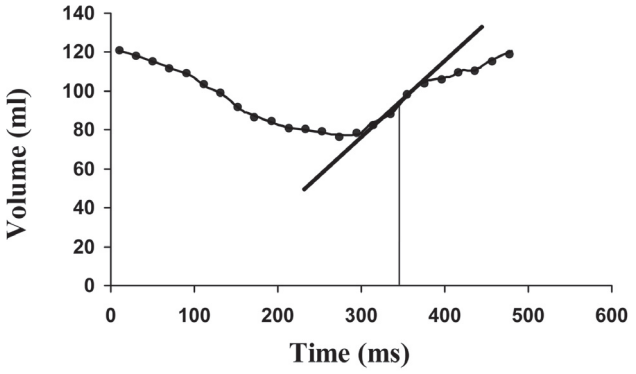

Figure 1B. An example of a volume time curve in a swine with AMI. The line indicates the time where peak filling rate is measured.

Statistical analysis

Data are presented as mean ± standard deviation. The dif- ference in measured parameters between healthy control swine and swine with AMI was assessed with unpaired Student`s t-tests. The relations be-tween infarct size, PFR/EDV, ejection fraction, end-systolic volume and end-diastolic volume were analysed with univariate linear regression analysis. All tests were performed two-sided and significance was accepted at p value of ≤ 0.05.

Results

Animal Model

All swine data sets were of good image quality and analysis could be performed with good confidence. Mean heart rate during the scan was 110±16 beats per minute in healthy swine and 97±18 in swine with AMI (p=0.08). Mean infarct size was 22±6% of left ventricular myocardial mass. In swine with AMI compared to healthy swine, mean end-systolic volume was significantly increased (51±14 ml versus 28±9 ml; p=0.0003) as well as end-diastolic volume (83±16 ml versus 57±11 ml; p=0.0005) while ejection fraction was significantly decreased (41±7 % versus 54±9%; p=0.0009). An inverse relation was observed between infarct size and ejection fraction (R=0.62; p=0.01). PFR/EDV was significantly lower in swine with AMI compared to healthy swine (3.3±1.0 versus 4.7±1.2 /s; p=0.006). A strong inverse relation was observed between infarct size and diastolic function as expressed as PFR/EDV (R=0.88, p<0.0001) (**Fig 2a**).

Patients

All patient data sets were of good image quality and analysis could be performed with good confidence. Mean heart rate during baseline scan was 72±18 beats per minute. Mean infarct size at 5 days was 25±13% of left ventricular myocardial mass. At 5 days, mean ejection fraction was 50±9%, mean end-systolic volume was 73±24 ml and mean end-diastolic volume was 151±38 ml. Mean PFR/EDV was 2.5±0.6 /s. Infarct size at 5 days was related to ejection fraction (R=0.69; p=0.004), end-systolic volume (R=0.74; p=0.001) and to end-diastolic volume (R=0.49; p=0.05) at 5 days. Diastolic function as expressed as PFR/EDV was inversely related to infarct size (R=0.58; p=0.01 (**Fig 2b**).

At 5 months, mean ejection fraction was 55±10%, mean end-systolic volume was 73±38 ml and mean end-diastolic volume was 158±50 ml. The value of infarct size, ejection fraction and PFR/EDV at 5 days to predict left ventricular function and volumes at 5 months was assessed with univariate linear regression analysis. Infarct size at 5 days appeared to be the best predictor for left ventricular function and volumes at 5 months (**Table 2**, **Fig 3**).

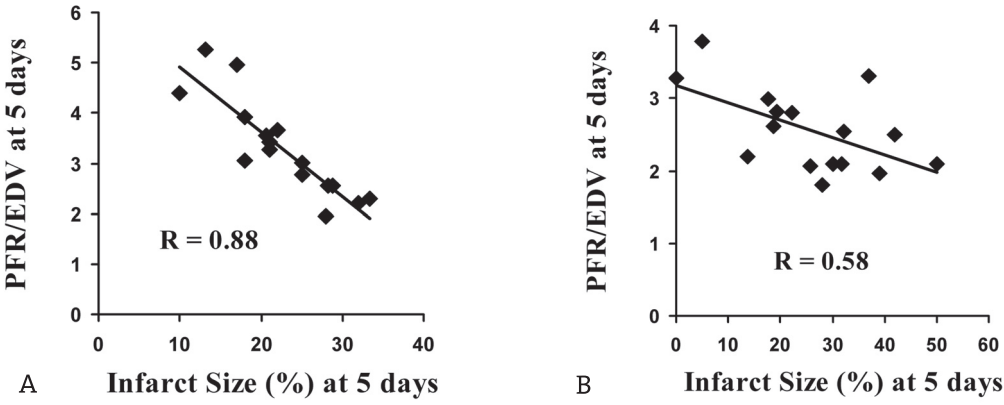

Figure 2A. The relation between infarct size and diastolic function in the porcine model. **B.** The relation between infarct size and diastolic function in patients at a mean of 5 days after reperfused first acute myocardial infarction.

Discussion

Our results show that acute myocardial infarct size is a major determinant of the extent of left ventricular diastolic dysfunction in the subacute phase of reperfused AMI. Second, acute infarct size appears to be a better predictor than either ejection fraction or the extent of diastolic dysfunction at 5 days for left ventricular function and remodeling at 5 months.

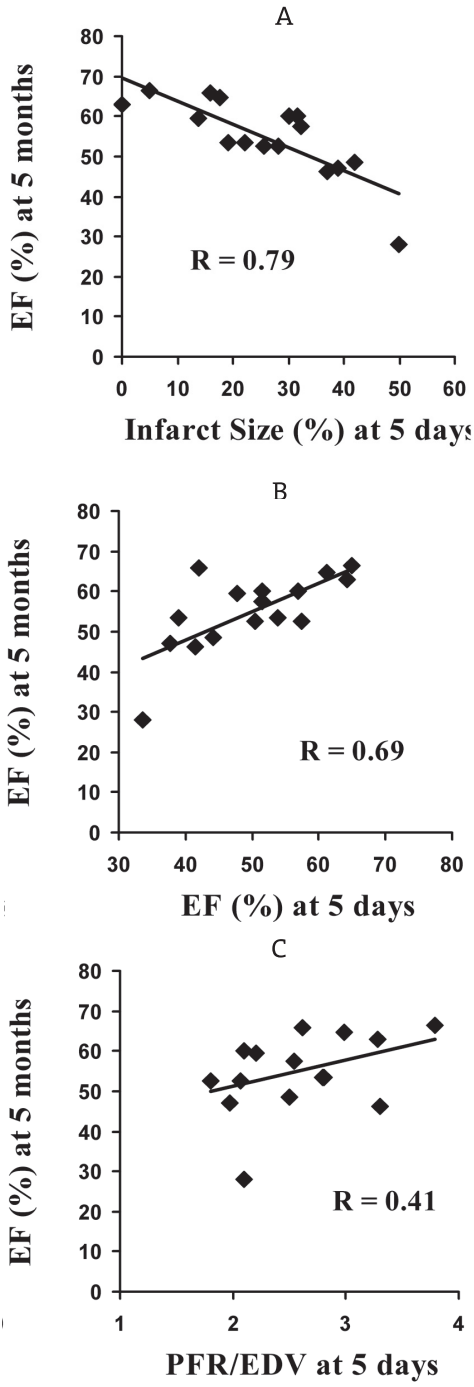

Technical developments in MRI now allow refined assessment of left ventricular systolic and diastolic function and volumes and permit precise assessment of acute reperfused myocardial infarct size (6-9). Using MRI, we observed that acute reperfused myocardial infarct size is a major determinant of left ventricular diastolic function. In the early seventies, Diamond et al. (12) observed that patients who had suffered AMI had an increased left ventricular wall stiffness resulting in a decreased left ventricular compliance.

This was recently confirmed by Azevedo et al. (13) who performed a detailed study of regional systolic and diastolic function in a canine model of reperfused AMI with tagged MRI. Infarcted myocardial tissue demonstrated decreased diastolic function compared to remote non-infarcted myocardium, expressed as reduced peak diastolic strain rate. Remote myocardium in the subacute phase of AMI may also exhibit reduced function as was observed in porcine studies and in patients (14, 15). Regional diastolic dysfunction of remote noninfarcted myocardium in swine is associated with modifications in Ca2+ handling proteins and myofilament function (15).

In the current study, infarct size was better related to the extent of diastolic dysfunction in the swine model than in patients. This finding might be explained

Figure 3A. The relation between infarct size at 5 days and ejection fraction at 5 months in patients. **B.** The relation between ejection fraction at 5 days and ejection fraction at 5 months in patients. **C.** The relation between peak filling rate adjusted for end-diastolic volume (PFR/EDV) at 5 days and ejection fraction at 5 months in patients.

by the presence of confounding variables in patients that influence the systolic and diastolic properties of the left ventricle. In our controlled experimental model, we were able to exclude the influence of these variables like persistent ischemia, differences in affected coronary artery perfusion territory, age, pharmacological therapy, pre-existent hypertension, diabetes mellitus, gender, body weight, heart rate, left sided valvular disease and the presence of stunned (post-ischemic reversible injured) myocardium, although the latter two are debatable (16-18). Mitral valve disease due to an ischemic papillary muscle can not be entirely excluded in the swine, but cine-MRI revealed no typical patterns of mitral valve regurgitation. Also, the presence of stunned myocardium can not be eliminated completely in the current study but swine have a negligible collateral circulation, making the occurrence of stunned myocardium less likely (19). Stunned myocardium may affect global diastolic function since stunned myocardium may demonstrate impaired diastolic function with preserved systolic function (13).

Infarct size at 5 days appeared to be a better predictor than either ejection fraction or the extent of diastolic dysfunction at 5 days for left ventricular function and remodeling at 5 months. Infarct size measured with MRI might be a better predictor because it is an anatomical parameter that is not influenced by other variables and because it represents only the necrotic myocardial tissue after AMI (6, 7, 9). However, one have to take into account the timing of infarct size measurement because infarct size decreases over time and is reduced by 30 to 35% at 5 months after AMI (20, 21). In contrast to infarct size, ejection fraction and diastolic function are not anatomical but functional parameters that are influenced by variables like the presence of stunned myocardium,

Table 2

		at 5 months					
		Ejection Fraction		End-systolic Volume		End-diastolic Volume	
		R	p	R	p	R	p
at 5 days	Infarct size	0.79	<0.001	0.71	0.001	0.56	0.02
	Ejection Fraction	0.69	0.002	0.48	0.05	0.22	0.41
	PFR/EDV	0.41	0.05	0.21	0.45	0.05	0.85

PFR/EDV = peak filling rate corrected for end-diastolic volume

infarct size, hemodynamics and the multiple aforementioned variables that influence the systolic and diastolic properties of the left ventricle. Unfortunately, the impact of these variables on ejection fraction and diastolic function cannot be measured with currently available techniques. For example, stunned myocardium might show systolic and diastolic functional recovery (5, 22, 23) resulting in an improved ejection fraction and diastolic function in patients over time (4, 24, 25). However, when and to what extent stunned myocardium may show functional recovery is currently not well understood.

Conclusion

Infarct size is a major determinant of the extent of left ventricular diastolic dysfunction in the subacute phase of reperfused AMI. Furthermore, acute infarct size appears to be a better predictor than either ejection fraction or the extent of diastolic dysfunction at 5 days for left ventricular function and remodeling at 5 months. Future studies on left ventricular systolic and diastolic (dys)function and left ventricular remodeling should include infarct size as a variable. An interesting question in this group of patients remains whether infarct size, left ventricular systolic (dys)function, end-systolic volume, the extent of diastolic dysfunction or a combination of these parameters is the major determinant of long-term survival after reperfused AMI.

References

1. White HD, Norris RM, Brown MA, Brandt PW, Whitlock RM, Wild CJ. Left ventricular end-systolic volume as the major determinant of survival after recovery from myocardial infarction. Circulation 1987;76(1):44-51.
2. Burns RJ, Gibbons RJ, Yi Q, Roberts RS, Miller TD, Schaer GL, Anderson JL, Yusuf S. The relationships of left ventricular ejection fraction, end-systolic volume index and infarct size to six-month mortality after hospital discharge following myocardial infarction treated by thrombolysis. J Am Coll Cardiol 2002;39(1):30-6.
3. Chareonthaitawee P, Christian TF, Hirose K, Gibbons RJ, Rumberger JA. Relation of initial infarct size to extent of left ventricular remodeling in the year after acute myocardial infarction. J Am Coll Cardiol 1995;25(3):567-73.
4. Nijland F, Kamp O, Karreman AJ, van Eenige MJ, Visser CA. Prognostic implications of restrictive left ventricular filling in acute myocardial infarction: a serial Doppler echocardiographic study. J Am Coll Cardiol 1997;30(7):1618-24.

5. Baks T, van Geuns RJ, Biagini E, Wielopolski P, Mollet NR, Cademartiri F, Boersma E, van der Giessen WJ, Krestin GP, Duncker DJ, Serruys PW, de Feyter PJ. Recovery of left ventricular function after primary angioplasty for acute myocardial infarction. Eur Heart J 2005;26(11):1070-7.
6. Kim RJ, Fieno DS, Parrish TB, Harris K, Chen EL, Simonetti O, Bundy J, Finn JP, Klocke FJ, Judd RM. Relationship of MRI delayed contrast enhancement to irreversible injury, infarct age, and contractile function. Circulation 1999;100(19):1992-2002.
7. Gerber BL, Rochitte CE, Melin JA, McVeigh ER, Bluemke DA, Wu KC, Becker LC, Lima JA. Microvascular obstruction and left ventricular remodeling early after acute myocardial infarction. Circulation 2000;101(23):2734-41.
8. Mahrholdt H, Wagner A, Holly TA, Elliott MD, Bonow RO, Kim RJ, Judd RM. Reproducibility of chronic infarct size measurement by contrast-enhanced magnetic resonance imaging. Circulation 2002;106(18):2322-7.
9. Baks T, Cademartiri F, Moelker AD, Weustink AC, van Geuns RJ, Mollet NR, Krestin GP, Duncker DJ, de Feyter PJ MSCT and MRI for the Assessment of Reperfused Acute Myocardial Infarction J Am Coll Cardiol. in press
10. Levy WC, Cerqueira MD, Abrass IB, Schwartz RS, Stratton JR. Endurance exercise training augments diastolic filling at rest and during exercise in healthy young and older men. Circulation 1993;88(1):116-26.
11. Bonow RO, Bacharach SL, Green MV, Kent KM, Rosing DR, Lipson LC, Leon MB, Epstein SE. Impaired left ventricular diastolic filling in patients with coronary artery disease: assessment with radionuclide angiography. Circulation 1981;64(2):315-23.
12. Diamond G, Forrester JS. Effect of coronary artery disease and acute myocardial infarction on left ventricular compliance in man. Circulation 1972;45(1):11-9.
13. Azevedo CF, Amado LC, Kraitchman DL, Gerber BL, Osman NF, Rochitte CE, Edvardsen T, Lima JA. Persistent diastolic dysfunction despite complete systolic functional recovery after reperfused acute myocardial infarction demonstrated by tagged magnetic resonance imaging. Eur Heart J 2004;25(16):1419-27.
14. Bogaert J, Bosmans H, Maes A, Suetens P, Marchal G, Rademakers FE. Remote myocardial dysfunction after acute anterior myocardial infarction: impact of left ventricular shape on regional function: a magnetic resonance myocardial tagging study. J Am Coll Cardiol 2000;35(6):1525-34.
15. van der Velden J, Merkus D, Klarenbeek BR, James AT, Boontje NM, Dekkers DH, Stienen GJ, Lamers JM, Duncker DJ. Alterations in myofilament function contribute to left ventricular dysfunction in pigs early after myocardial infarction. Circ Res 2004;95(11):e85-95.
16. Levy WC, Cerqueira MD, Weaver WD, Stratton JR. Early patency of the infarct-related artery after myocardial infarction preserves diastolic filling. Am J Cardiol 2001;87(8):955-8; A3.
17. Tseng WY, Liao TY, Wang JL. Normal systolic and diastolic functions of the left ventricle and left atrium by cine magnetic resonance imaging. J Cardiovasc Magn Reson 2002;4(4):443-57.
18. Akincioglu C, Berman DS, Nishina H, Kavanagh PB, Slomka PJ, Abidov A, Hayes S, Friedman JD, Germano G. Assessment of diastolic function using 16-frame 99mTc-sestamibi gated myocardial perfusion SPECT: normal values. J Nucl Med 2005;46(7):1102-8.

19. Patterson RE, Kirk ES. Analysis of coronary collateral structure, function, and ischemic border zones in pigs. Am J Physiol 1983;244(1):H23-31.
20. Baks T, van Geuns RJ, Biagini E, Wielopolski P, Mollet NR, Cademartiri F, van der Giessen WJ, Krestin GP, Serruys PW, Duncker DJ, de Feyter PJ. Effects of primary angioplasty for acute myocardial infarction on early and late infarct size and left ventricular wall characteristics. J Am Coll Cardiol 2006;47(1):40-4.
21. Wollert KC, Meyer GP, Lotz J, Ringes-Lichtenberg S, Lippolt P, Breidenbach C, Fichtner S, Korte T, Hornig B, Messinger D, Arseniev L, Hertenstein B, Ganser A, Drexler H. Intracoronary autologous bone-marrow cell transfer after myocardial infarction: the BOOST randomised controlled clinical trial. Lancet 2004;364(9429):141-8.
22. Choi KM, Kim RJ, Gubernikoff G, Vargas JD, Parker M, Judd RM. Transmural extent of acute myocardial infarction predicts long-term improvement in contractile function. Circulation 2001;104(10):1101-7.
23. Gerber BL, Garot J, Bluemke DA, Wu KC, Lima JA. Accuracy of contrast-enhanced magnetic resonance imaging in predicting improvement of regional myocardial function in patients after acute myocardial infarction. Circulation 2002;106(9):1083-9.
24. Cerisano G, Bolognese L, Carrabba N, Buonamici P, Santoro GM, Antoniucci D, Santini A, Moschi G, Fazzini PF. Doppler-derived mitral deceleration time: an early strong predictor of left ventricular remodeling after reperfused anterior acute myocardial infarction. Circulation 1999;99(2):230-6.
25. Temporelli PL, Giannuzzi P, Nicolosi GL, Latini R, Franzosi MG, Gentile F, Tavazzi L, Maggioni AP. Doppler-derived mitral deceleration time as a strong prognostic marker of left ventricular remodeling and survival after acute myocardial infarction: results of the GISSI-3 echo substudy. J Am Coll Cardiol 2004;43(9):1646-53.

Reduction in infarct size, but not functional improvement after bone marrow cell administration in a porcine model of reperfused myocardial infarction

Amber D. Moelker; Timo Baks; Wendy Kerver; Ewout J. van den Bos, Robert J. van Geuns; Heleen M.M. van Beusekom; Gabriel P. Krestin; Dirk J. Duncker; Willem J. van der Giessen

4

1, 2, 3, 5, 6, 7, 8, 9, 10, 11, 12, 13, 14, 15

Abstract

Aims

Stem cell therapy after myocardial infarction (MI) has been studied in models of permanent coronary occlusion. We studied the effect of intracoronary administration of unselected bone marrow (BM) as well as mononuclear cells (MNC) in a porcine model of reperfused MI.

Methods and results

In 34 swine, the left circumflex coronary artery was balloon-occluded for two hours followed by reperfusion. Ten swine without MI served as controls. All swine underwent magnetic resonance imaging (MRI) 1 week post-MI. The next day, 10 of the 30 surviving MI-swine received BM, 10 other MI-swine received MNC and the remaining MI-swine received medium intracoronary. Four weeks later all swine underwent a follow-up MRI.

One week after MI, end-diastolic volume (108±5 mL) and left ventricular (LV) weight (78±2 g) were greater, while ejection fraction (40±1 %) was lower then in controls (69±3 mL, 62±4 g and 53±2 %). Injection of BM or MNC had no effect on the MI-induced changes, nor on global or regional LV-function. But, there was a significant reduction in infarct size four weeks after MNC injection (-6%), compared to medium (-3%).

Conclusion

Intracoronary injection of BM or MNC in swine does not improve LV-function. However, MNC injection reduces infarct size four weeks later.

Introduction

Regeneration of infarcted myocardium by transplanting bone marrow (BM) derived stem cells into the infarct region has been proposed to prevent heart failure by angiogenesis and/or myogenesis.[1,2] Early experimental studies in animals with a myocardial infarction (MI) reported improvements in left ventricular (LV) function following cell therapy with bone marrow derived mononuclear cells (MNC),[3] or a cell sub-population selected from MNC.[1] These highly promising initial observations sparked a large number of non-randomized clinical trials, reporting beneficial effects of MNC therapy on global LV function and myocardial viability.[4,5,6,7,8] However, out of four recent randomized trials (BOOST-update, Leuven trial, REPAIR-AMI, ASTAMI),[9,10,11] three failed to show an improvement in global LV function,[9,10,11] although one reported a reduction in infarct size.[10]

In contrast to the discordant results obtained in clinical trials, to date the majority of experimental studies reported positive effects of MNC therapy on global LV function[3,12,13,14] although one study reported no effect.[15] However, the effects of MNC on infarct size, which has been observed clinically,[4,6,10] have not been investigated in these studies. Furthermore, all studies used a permanent coronary artery ligation, while all but one[14] (which injected the MNC cells in a coronary venous vessel) injected the MNC directly in the peri-infarct area. Hence, these experimental studies have a markedly different design compared to the clinical trials. Furthermore, most animal studies used more selected, enriched populations, such as the CD34+, c-kitpos or lin- bone marrow derived cells or bone marrow derived mesenchymal stem cells.

Consequently, we designed an experimental study that matches the clinical trial protocols more closely, using a porcine reperfused MI model. For this purpose, we first established cell survival and efficacy of the method of cell delivery in several pilot experiments. Subsequently, we studied the effect of bone marrow derived cell injection on LV geometry, function and infarct size. Myocardial infarction was induced by PTCA-balloon inflation followed by reperfusion. LV remodeling as well as global and regional LV function was assessed using cine-magnetic resonance imaging (cine-MRI). Contrast enhanced MR Imaging (Ce-MRI) was used to assess infarct size and infarct remodeling over time.

Although the clinical trials suggest that intracoronary BM derived cell delivery seems safe, recently Yoon et al.[16]demonstrated increased calcifications after unselected BM cell injection. Therefore we compared the effects of MNC to those of unselected BM.

Methods

Experiments were performed in 2-3 month old Yorkshire-Landrace pigs, in compliance with the "Guide for the Care and Use of Laboratory Animals" (NIH publication 1996) and after approval of the Animal Care Committee of the Erasmus MC.

Bone marrow

Approximately 40 mL of BM was aspirated from the iliac crest. MNC were isolated by Ficoll Paque-plus (Amersham Biosciences Europe GmbH, Freiburg, Germany) density gradient separation (25 min at 400g) and suspended in 10 mL Modified Eagle's Medium (MEM). Crude BM was prepared by filtering through a 100 micron filter. The BM and MNC were slowly (1mL/min) injected into the coronary artery.

Cell delivery study

To investigate the efficacy of cell delivery we tested injection with a selective, non flow-limiting injection catheter. Five animals were sedated (ketamine 20 mg/kg IM, and midazolam 1 mg/kg IM), anesthetised (thiopental, 12 mg/kg IV), intubated and mechanically ventilated with a mixture of oxygen and nitrogen (1:2 vol/vol). Anaesthesia was maintained with fentanyl (12.5 μg/kg/h) and isoflurane (0.6-0.8% started after onset of occlusion). Subsequently, animals received antibiotic prophylaxis (200 mg procainebenzylpenicillin and 250 mg dihydrostreptomycinesulfate IM) and underwent coronary catheterization through a carotid artery guided by fluoroscopy, followed by balloon occlusion of the proximal left circumflex coronary artery (LCX), for 2 hr followed by reperfusion. Heparin was administered every hour (5000 Units).
One week after MI, swine were sedated and heparinized as described above. Anesthesia was maintained with 1-1.5% isoflurane and all swine received an intracoronary injection of ~ 50·106 PKH-labelled MNC (PKH 26, Sigma-Aldrich, Schnelldorf, Germany) suspended in 10 mL saline into the LCX (infarct area) and into the left anterior descending coronary artery (LAD; non-infarct area). MNC were injected slowly (1 mL/min) into the coronary artery perfusing the MI area using a probing catheter (Multifunctional Probing, Boston Scientific Co, Boston, MA). The site of injection was identical to the position of the occlusion balloon during MI induction. Four days after cell injection animals were sacrificed for histological and immunocytochemical analyses.

Efficacy study

Thirty-four swine underwent MI as described above and 10 swine without MI served as controls for normal cardiac growth and function.

One week after induction of MI, all swine were anaesthetized as described above and underwent magnetic resonance imaging (MRI) to assess global and regional LV function. Then, 10 of the 30 surviving MI swine received an intracoronary (i.c.) injection of ~40 mL unselected autologous BM and 10 swine received an i.c. suspension of MNC, a total of ~ $5{\cdot}10^8$ cells in 10 mL MEM. The remaining 10 MI-swine received an i.c. injection of 10 mL of MEM. The site of injection was identical to the position of the occlusion balloon one week before.

Four weeks later, animals underwent follow-up MRI for assessment of LV function and infarct size, after which animals were sacrificed for histological analysis of the LCX perfused area and remote area of the left ventricle.

Magnetic Resonance Imaging

Data Acquisition

A clinical 1.5-Tesla MRI with a dedicated cardiac four element phased-array receiver coil was used for imaging (Signa CV/i, GE Medical systems, Milwaukee, WI, USA). Repeated breath-holds and gating to the ECG were applied to minimize the influence of cardiac and respiratory motion on data collection. Baseline and follow-up contrast enhanced (Ce) MRI protocol consisted of cine-MRI and Delayed Enhancement (DE) imaging. Cine-MRI was performed using steady-state free-precession technique (imaging parameters: 24 temporal phases per slice, FOV26-30, rect. FOV 75%, TR 3.4, TE 1.4, flip angle 45º, matrix 160x128, bandwidth 83 kHz, 0.75 NEX). To cover the entire left ventricle, six to eight consecutive slices of 8 mm were planned in the short axis view, perpendicular to the long axis four-chamber view of the left ventricle (gap=0). DE imaging was performed to assess total myocardial infarct mass 10-20 minutes after administration of gadolinium-DTPA (0.5 mmol/kg, Magnevist®, Schering) with a 2-dimensional T1-weighted inversion-recovery gradient-echo sequence (imaging parameters: slice thickness 8 mm, FOV26-30, rect FOV 75%, TR 7.3, TE 1.6, flip angle 20 degrees, TI 180-275 ms, matrix 256x192, 1 NEX, bandwidth 17.9 kHz). The inversion time was adjusted per animal to null the signal of remote myocardium. Locations were copied from the cine-images.

Image Analysis

The MR images were analyzed with dedicated cardiac software (Cine display application 3.0, General Electric medical systems, USA). End-diastolic volume (EDV), end-systolic volume (ESV) and left ventricular weight (LVW) were measured by manually drawing the endocardial and epicardial borders in the end- diastolic and end-systolic image of

each slice. Stroke volume (SV= EDV-ESV), ejection fraction (EF= [SV/EDV]x100%) and cardiac output (CO= SVxHR) were computed. End-diastolic wall thickness (EDT) and end systolic wall thickness (EST) was measured and expressed in millimeter in 36 sections per slice. Regional systolic wall thickening (SWT) was calculated as [EST-EDT]/EDTx100%. Baseline and endpoint scans were matched for location using anatomical landmarks like insertion of the right ventricle to the septum and the papillary muscles. The volume of DE was quantified by manually selecting the enhanced regions from the consecutive 2D slices encompassing the left ventricle. DE volume was multiplied by 1.05 g/ml to obtain myocardial infarct mass (1 millilitre corresponds to 1.05 gram as measured in our own laboratory). The anterior and posterior sections immediately adjacent to the akinetic infarct region were defined as border zone.

Histology and Immunohistochemistry

The hearts were excised and cut in 6-8 transverse slices similar to the MRI short axis slices (**Figure 1**). From the basal plane the first, third, fifth and seventh slice were fixed in 4% buffered formaldehyde and embedded in paraffin. The second, fourth, sixth and eight slice, were embedded in tissue tec OCT and frozen in liquid nitrogen. Sections (5 µm) were stained with hematoxylin eosin (HE) and resorcin-fuchsin (RF, collagen).

Sections were semi-quantitatively assessed as negative (0) or extent of positivity (1-5) for the amount of calcium deposition, collagen and vascularization.

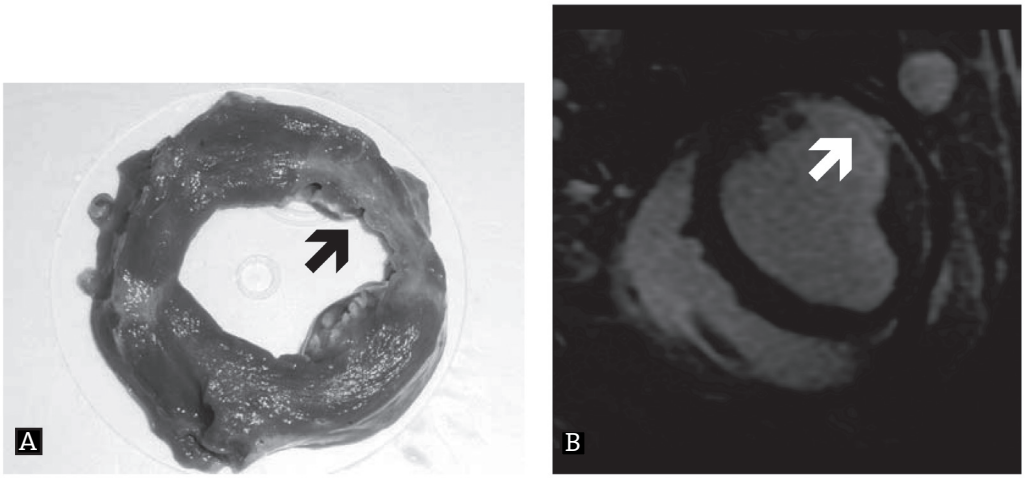

Figure 1. *Ex-vivo* short axis slice (**A**) compared with in vivo delayed enhancement (**B**). Arrow indicates infarct area. *

Statistical Analysis

Data were analyzed with SPSS 11.0. All data were analyzed using a one-way ANOVA and post-hoc analysis using unpaired t-testing with Bonferoni correction to test for significant intergroup differences at corresponding time points. Intragroup differences between baseline and endpoint were determined using paired t-testing with Bonferoni correction. Effect of BM and MNC therapy at the follow-up MRI was tested using analysis of co-variance (ANCOVA) with baseline values as covariate. Regression lines were compared using a linear regression analysis. Statistical significance was accepted when $P \leq 0.05$ (two-tailed). All data are presented as mean ± SEM.

Results

Cell delivery study

PKH labeled cells could be detected 4 days after injection into infarcted area (**Figure 2**). Only a few cells (< 1 cell/cm^2) could be detected in healthy LAD tissue. Systematic histological analysis did not reveal any myocardial damage in the normal (LAD-related) myocardium (**Figure 3**). Quantative analysis showed that an average of 260±52 PKH positive cells/cm^2 could be detected four days after injection with a probing catheter which corresponds to ~6.5% of the injected cells.

Efficacy study

A total of 44 swine entered the study. Four animals died prematurely, of which three died within 24 hours after induction of MI, while one animal died shortly after the baseline MRI (i.e. prior to any therapeutic intervention). Forty surviving animals completed the protocol.

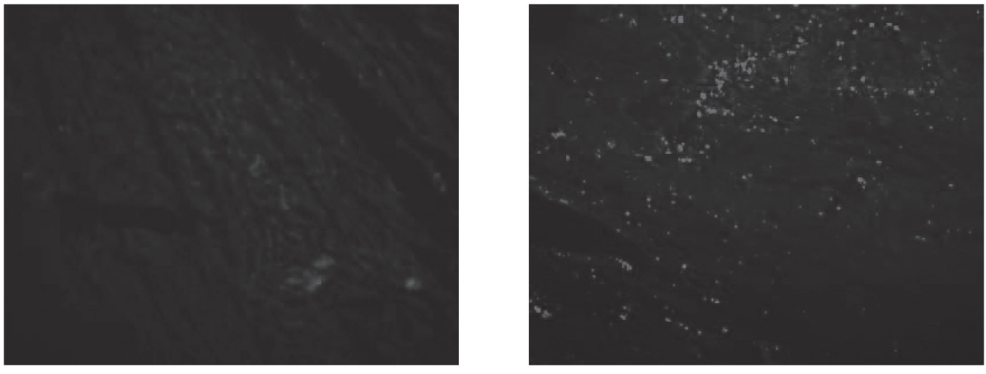

Figure 2. PKH-labeled cells do not home to healthy myocardium (**A**), but PKH positive cells (in red) home in infarcted myocardium after injection with a probing catheter (**B**). *

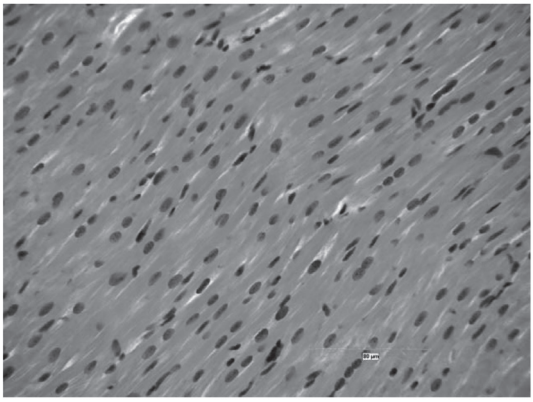

Figure 3. Healthy myocardium after injection of MNC. *

MRI

MI swine had a transmural myocardial infarction of the lateral left ventricular wall encompassing 14±1% of the left ventricle. There were no differences in body weight (BW), stroke volume (SV) or cardiac output (CO) between controls and MI-animals at baseline (**Table 1**). Due to normal growth four weeks later, BW increased in all four groups. SV also increased due to normal growth, which was significant in the MI-swine. There were no other significant differences in systemic hemodynamics (CO or heart rate) during the endpoint scan (**Table 1**).

Table 1: Systemic hemodynamics

		Control (n=10)	MI+medium (n=10)	MI+BM (n=10)	I+MNC (n=10)
BW (Kg)	Baseline	23 ± 2	26 ± 1	26 ± 1	24 ± 1
	Endpoint	40 ± 2*	43 ± 2*	43 ± 1*	39 ± 1*
HR (bpm)	Baseline	107 ± 4	87 ± 4†	103 ± 7	85 ± 7†
	Endpoint	83 ± 4*	84 ± 4	83 ± 5*	86 ± 6
SV (mL)	Baseline	37 ± 2	38 ± 3	36 ± 2	37 ± 3
	Endpoint	51 ± 3	60 ± 4*	56 ± 3*	50 ± 4*‡
CO (mL/min)	Baseline	3.9 ± 0.2	3.3 ± 0.3	3.8 ± 0.4	3.2 ± 0.4
	Endpoint	4.2 ± 0.3	5.0 ± 0.3*	4.6 ± 0.3	4.2 ± 0.3*

BW= body weight; HR= heart rate; SV= stroke volume; CO= cardiac output; Baseline = 1 wk post-MI; Endpoint = 5 wk post-MI. Data are mean ± SEM, *P<0.05 endpoint vs. baseline, †P<0.05 MI animals vs. corresponding Control, ‡P<0.05 change from baseline BM or MNC vs. medium-treated MI animals.

One week after MI, LVW, EDV and ESV were greater in MI swine, while EF was lower then in control swine (**Figure 4**). Changes in volumes and mass from baseline to four weeks after cell injection did not differ significantly between medium, BM and MNC treated MI-animals (**Figure 4**).

One week after MI systolic wall thickness was significantly decreased compared to control in the center MI as well as in the border zone (**Figure 5**). Systolic wall thickening in the LCX area was repressed in the MI animals compared to control, which was not restored by BM or MNC treatment.

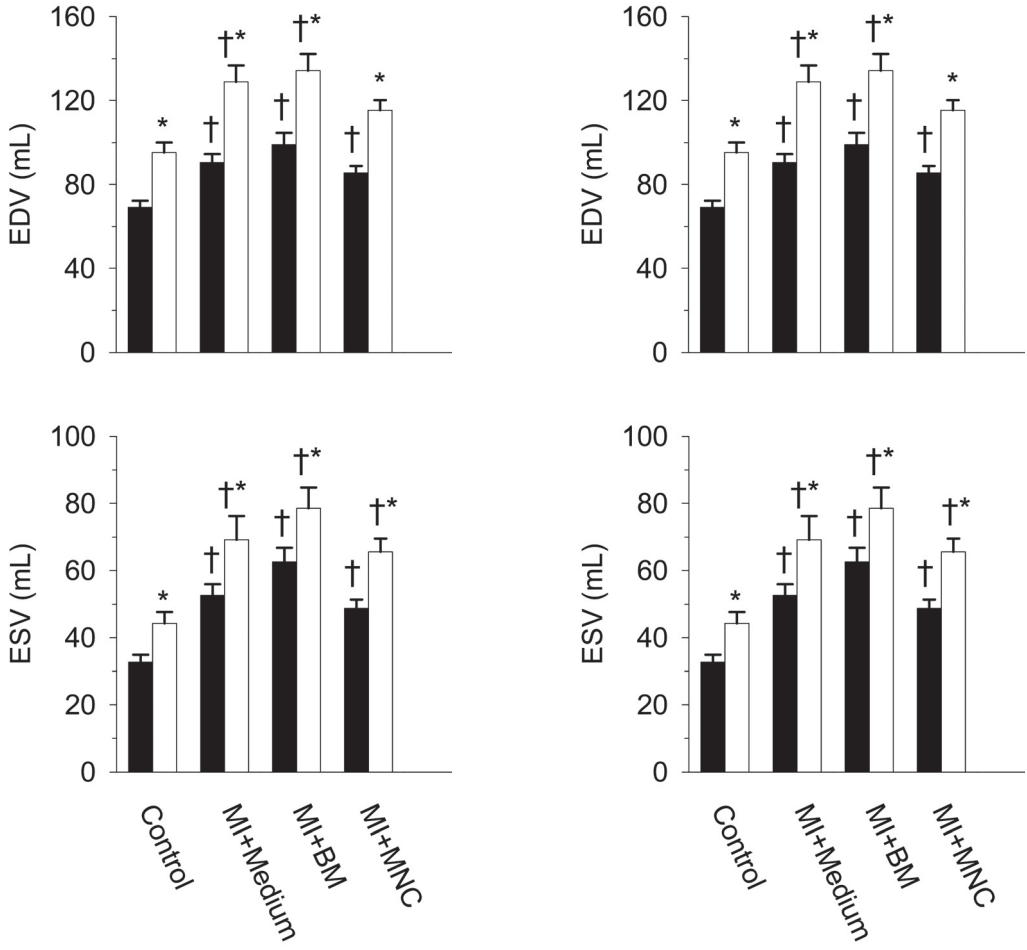

Figure 4. LV end-diastolic volume (EDV), LV weight (LVW), LV ejection fraction (EF) and end-systolic volume (ESV) at baseline (solid bars) and at endpoint (open bars) in Control swine, and MI swine receiving either medium, BM or MNC. *P<0.05 endpoint vs. baseline, †P<0.05 vs. corresponding control. There were no differences between BM, MNC and medium-treated MI animals either at baseline or endpoint, or in the response over the 4 wk follow-up period.

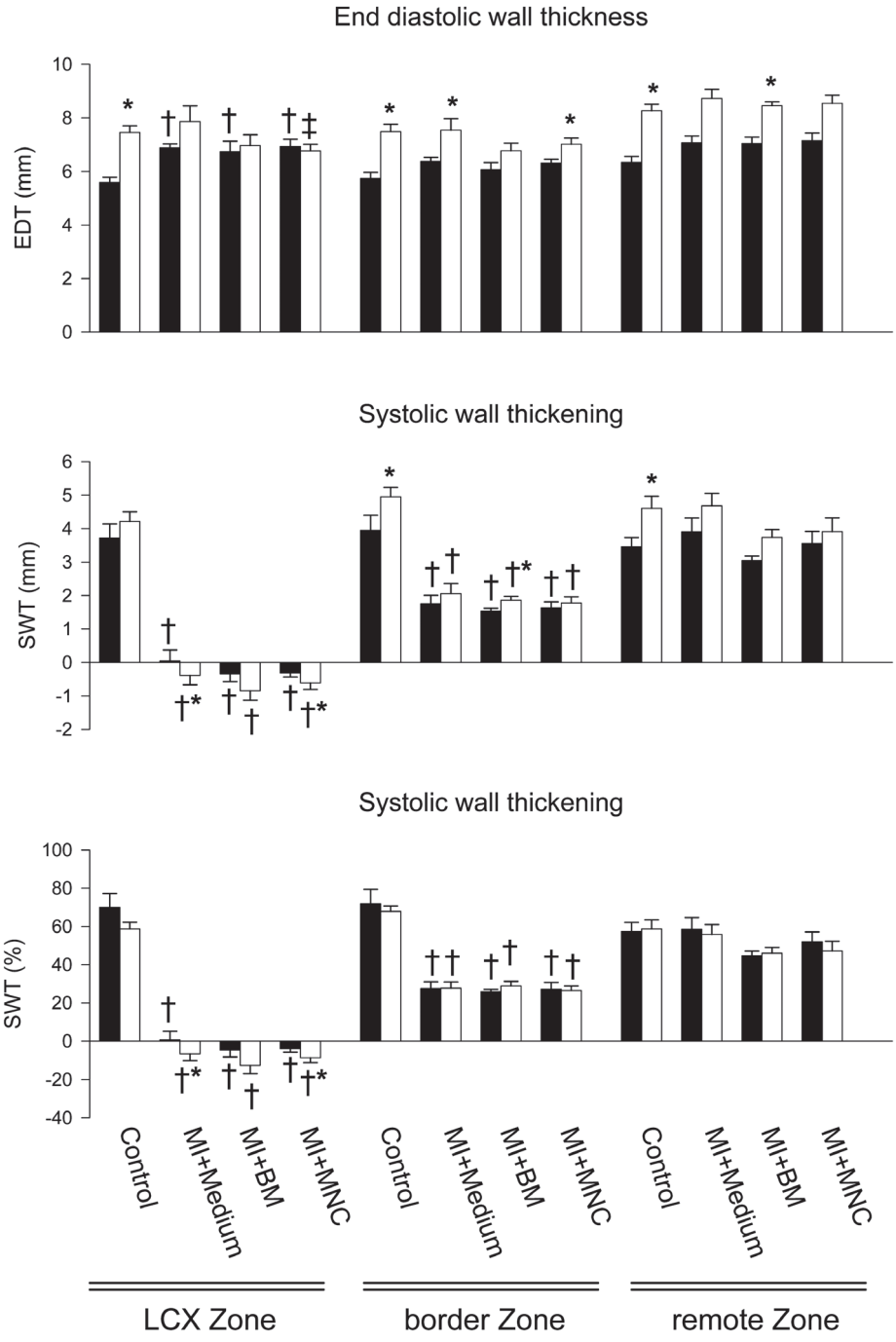

Figure 5. End diastolic wall thickness (EDT, upper panel), absolute end systolic wall thickening (SWT, middle panel) and percent Systolic wall thickening (SWT, lower panel) at baseline (solid bars) and at endpoint (open bars) in Control swine, and MI swine receiving either medium, BM or MNC. *P<0.05, **P=0.075 endpoint vs. baseline, †P<0.05 vs. correspond.

Infarct size measured with delayed enhancement revealed that five weeks after MI there was a significant decrease in infarct size in both BM (from 14.3±1.3 % to 10.0±1.5 %) as well as the MNC (from 14.3±2.0 % to 8.2±1.3 %) treated animals, compared to the medium treated swine (from 14.3±2.0 % to 11.0±1.3 %, **Table 2**). In the MNC treated animals, not only a change in infarct size in percentage of the LV was observed, but also a decrease in infarct mass was observed (from 10.8±1.7g to 8.7±1.5 g, P=0.054). There was also a significant difference in infarct size regression between medium and MNC treated MI-swine (**Figure 6**).

Histology

Histology showed that all the MI animals had a transmural infarct in the LCX region with total loss of viable myocardium, which matched the delayed enhancement scans performed at 1 and 5 weeks after MI (**Figure 1**). The medium and BM treated swine both showed a similar degree of fibroblasts and collagen (**Figure 7**), in the center of the infarct. There were no significant differences in calcium deposition, collagen or vascularization (**Table 3**).

Table 2: Infarct size measured by delayed enhancement

		MI + medium (n = 6)	MI + BM (n = 8)	MI + MNC (n = 10)
Infarctsize (g)	Baseline	11.1 ± 1.8	12.0 ± 1.2	10.8 ± 1.7
	Endpoint	12.3 ± 1.2	11.6 ± 2.0	8.2 ± 1.3**†
Infarctsize (%LV)	Baseline	14.3 ± 2.0	14.3 ± 1.3	14.3 ± 2.0
	Endpoint	11.0 ± 1.3	10.0 ± 1.5*	8.7 ± 1.5*†

Baseline = 1 wk post-MI; Endpoint = 5 wk post-MI; %LV = is as a percentage of the left ventricle. Data are mean ± SEM, *P<0.05, **P=0.054 endpoint vs. baseline, †P<0.05 change from baseline MNC vs. medium-treated MI animals.

Table 3: Semi-quantative histology score

	Calcium deposits	Collagen	Vascularization
MI + Medium	0.60 ± 0.29	3.95 ± 0.25	4.05 ± 0.30
MI + BM	1.37 ± 0.33*	4.11 ± 0.17	3.78 ± 0.23
MI + MNC	1.04 ± 0.31	4.36 ± 0.19	3.54 ± 0.25

Data are mean ± SEM. * P = 0.086, MI + BM vs MI + medium. There are no significant differences between groups

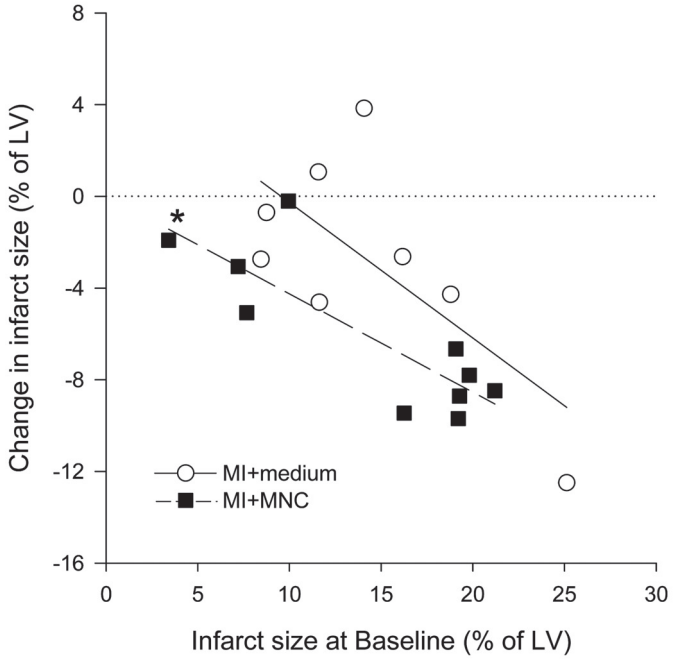

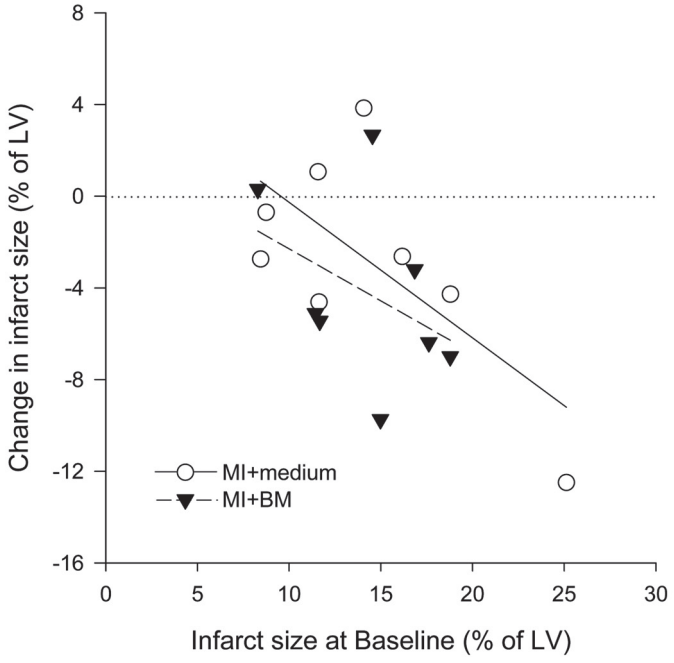

Figure 6. Change in infarct size from baseline in percentage of the LV. Regression lines; *P<0.05 vs. medium treated MI swine.

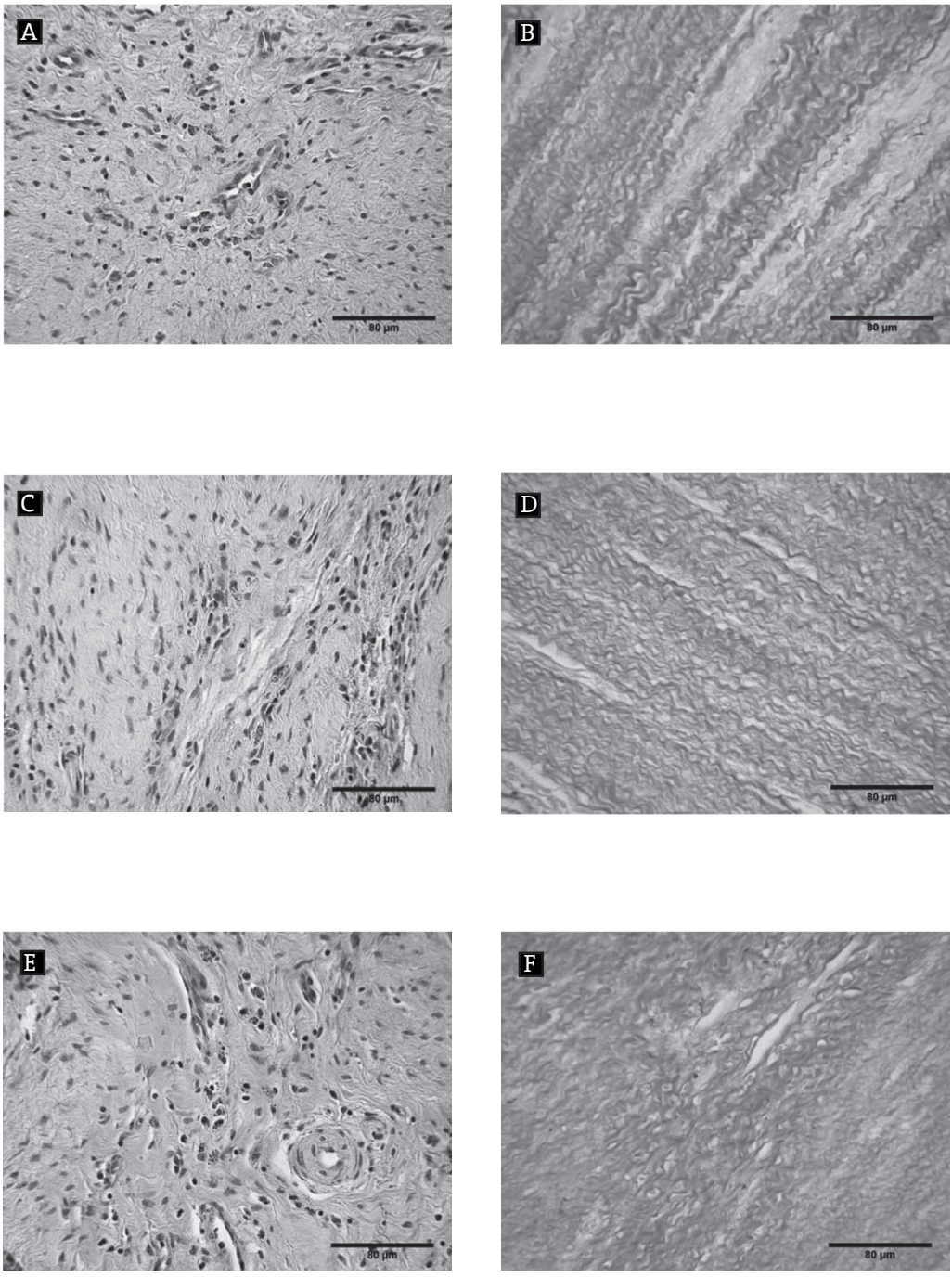

Figure 7. Infarct area of medium treated (A,B) compared with crude BM (C,D) and MNC (E,F) treated swine. HE staining (A,C,E) showed many fibroblasts. RF staining showed a lot of collagen (B,D,F). *

Discussion

The present study investigated the effect of intracoronary injection of MNC or BM on left ventricular function and histology at four weeks in a porcine model of acute myocardial infarction followed by reperfusion. Our study shows that in swine an intracoronary injection of both MNC and unselected BM one week after MI does not improve global or regional indices of LV function four weeks later. In addition, BM derived MNC or unselected BM treatment did not reverse the remodeling of the left ventricle induced by the MI. However, MNC reduced infarct size four weeks after injection, which was also observed in the clinical study by Janssens et al.[10]

Infarct size reduction

Comparison of histology (TTC staining) and MRI (delayed enhancement)[17] shows that both methods can measure infarct size accurately. Therefore, our observation, that infarct size is reduced after MNC administration is genuine. It remains unclear what the underlying mechanism for this infarct size reduction is. It has been shown that BM derived cells can differentiate into cardiomyocytes in vitro. But, it remains unclear whether BM derived stem cells are capable of differentiating into cardiomyocytes in vivo[18-20], especially in large mammals. It has been shown that stem cells do engraft in the myocardium and induce angiogenesis. It is therefore most likely that angiogenesis, especially in the border zone, leads to an improved perfusion. This will prevent further scar formation in the border zone because the better perfusion will rescue viable tissue in the border zone.

Although there was a reduction in infarct size after MNC treatment, there was no LV functional improvement. This is in contrast to previous studies, but it should be emphasized that the experimental protocol differed considerable (**Table 4**) Several explanations can be forwarded why in this model cardiac function failed to improve after intracoronary injection of MNC or BM in the MI zone.

Timing of cell administration

The optimal timing of stem cell delivery is not completely understood. We chose to inject cells one week after MI, which might not be optimal. However, the REPAIR-AMI trial showed that the optimal timing of cell injection seems to be at least five days after MI.[11] Also Bartunek et al.[21] suggest that 3 to 10 days post-MI is probably the optimal timing of cell therapy. Therefore, the lack of functional benefit of bone marrow derived cells in this study can not be explained by the timing of cell administration. It is likely that a proximal two hour during LCX occlusion, followed by reperfusion creates a transmural infarct which represents a too hostile environment for injected cells to contribute to LV function.

Table 4: Previous MNC studies

	Species	MI-model	Method of Injection	injection post MI	Time of Follow-up	# of cells	Effect MNC vs. control
Zhang[12]	Rat	LAD ligation	Intra myocardial	After MI	2 months	5x106	FS +18% vs. -1%
Ott[13]	Rat	LAD ligation	Intra myocardial	1 week	8 weeks	1x107	EF +1% vs. -15%
Bel[15]	Sheep	LCX ligation	Intra myocardial	3 weeks	2 months	422x106	EF -9% vs. -8%
Kamihata[3]	Swine	LAD ligation	Intra myocardial	60 minutes	3 weeks	1x108	EF +15% vs. +1%
Yokoyama[14]	Swine	LAD coil	Intra coronary vein	6 hours/2 weeks	4 weeks	3x109	EF +5% vs. -5%
Moelker	Swine	LCX occlusion reperfusion	Intra coronary LCX	1 week	4 weeks	5x108	EF +1% vs. +5%

Route of administration

In most clinical trials the intracoronary cell delivery involves repeated short periods of ischemia and reperfusion which is thought to lead to higher cell engraftment. A proximal balloon occlusion should prevent the cells to wash out by forward blood flow and it would increase the time to attachment of the injection cells onto the vascular wall.[22] Intracoronary injected cells are thought to disappear from circulation into liver, lung or kidney within a few hours. Our cell delivery study, with PKH labeled cells, showed that the above described injection technique does not result in better cell engraftment than selective i.c. injection. We did some additional experiments, in which 5 MI pigs were injected with an over the wire balloon catheter and sacrificed 4 days later. A similar number of PKH positive cells (246±40 cells/cm^2) could be detected as with the probing catheter.

The cell delivery study showed that injection of MNC in healthy myocardium (**Figure 3**) did not induce myocardial damage. In contrast, intracoronary injection of BM derived mesenchymal stromal stem cells have been shown to cause microinfarctions[23] in dogs.

Follow-up time

Several others[3,12,14] did report improvement in cardiac function after BM transplantation. It is possible that improvement does occur eventually, but not yet after four weeks. Studies with a longer follow-up period may be needed to assess the potential of BM derived cells in MI in large mammals. However, recent clinical trials11 such as the ASTAMI-trial, the BOOST-update[9] and the trial performed in Leuven10 do not suggest that a longer follow-up will lead to improvement. The BOOST-update showed that 18 months after MNC administration the intergroup comparison between MNC treated group and placebo was no longer significant. The ASTAMI-trial as well as the Leuven trial also did not see a beneficial effect on EF or EDV after MNC injection after 6 and 4 months. The preclinical study by Dai et al.[24] showed the same results as the BOOST-update, that the initial positive effect at four weeks is lost after six months. Therefore, it is hypothesized that in our model MNC injection only leads to an accelerated infarct healing. If that is the case, then the beneficial effect of MNC might be lost over time as well.

Infarct composition

There were no differences between the group receiving medium and both BM and MNC receiving MI-groups with respect to the histology. In all MI swine a transmural infarct was seen with transmural loss of viable myocytes. There were no signs of cardiomyocyte regeneration. A transmural infarct seems a hostile environment for the undifferentiated stem cells in the mononuclear fraction. It is not unlikely that MNC

will differentiate into fibroblasts in such an environment, and therewith contribute to infarct reduction by retraction, but do not contribute to contractility. In smaller, non-transmural infarcts BM derived cells might be able to differentiate into myocytes because there are myocytes still present in the infarct area.

Conclusions

In a porcine model of myocardial infarction followed by reperfusion, we could not demonstrate improvements in global or regional LV-function by injection of BM-derived MNC. Interestingly, we observed a reduction in infarct size four weeks after MNC-injection, which is similar to results obtained in patients[10].

References

1. Orlic D, Kajstura J, Chimenti S, Jakoniuk I, Anderson SM, Li B, Pickel J, McKay R, Nadal-Ginard B, Bodine DM, Leri A, Anversa P. Bone marrow cells regenerate infarcted myocardium. Nature. 2001;410:701-5.
2. Murry CE, Reinecke H, Pabon LM. Regeneration gaps: observations on stem cells and cardiac repair. J Am Coll Cardiol. 2006;47:1777-85.
3. Kamihata H, Matsubara H, Nishiue T, Fujiyama S, Tsutsumi Y, Ozono R, Masaki H, Mori Y, Iba O, Tateishi E, Kosaki A, Shintani S, Murohara T, Imaizumi T, Iwasaka T. Implantation of bone marrow mononuclear cells into ischemic myocardium enhances collateral perfusion and regional function via side supply of angioblasts, angiogenic ligands, and cytokines. Circulation. 2001;104:1046-52.
4. Strauer BE, Brehm M, Zeus T, Kostering M, Hernandez A, Sorg RV, Kogler G, Wernet P. Repair of infarcted myocardium by autologous intracoronary mononuclear bone marrow cell transplantation in humans. Circulation. 2002;106:1913-8.
5. Assmus B, Schachinger V, Teupe C, Britten M, Lehmann R, Dobert N, Grunwald F, Aicher A, Urbich C, Martin H, Hoelzer D, Dimmeler S, Zeiher AM. Transplantation of Progenitor Cells and Regeneration Enhancement in Acute Myocardial Infarction (TOPCARE-AMI). Circulation. 2002;106:3009-17.
6. Schachinger V, Assmus B, Britten MB, Honold J, Lehmann R, Teupe C, Abolmaali ND, Vogl TJ, Hofmann WK, Martin H, Dimmeler S, Zeiher AM. Transplantation of progenitor cells and regeneration enhancement in acute myocardial infarction: final one-year results of the TOPCARE-AMI Trial. J Am Coll Cardiol. 2004;44:1690-9.
7. Dobert N, Britten M, Assmus B, Berner U, Menzel C, Lehmann R, Hamscho N, Schachinger V, Dimmeler S, Zeiher AM, Grunwald F. Transplantation of progenitor cells after reperfused acute myocardial infarction: evaluation of perfusion and myocardial viability with FDG-PET and thallium SPECT. Eur J Nucl Med Mol Imaging. 2004;31:1146-51.

8. Mocini D, Staibano M, Mele L, Giannantoni P, Menichella G, Colivicchi F, Sordini P, Salera P, Tubaro M, Santini M. Autologous bone marrow mononuclear cell transplantation in patients undergoing coronary artery bypass grafting. Am Heart J. 2006;151:192-7.
9. Meyer GP, Wollert KC, Lotz J, Steffens J, Lippolt P, Fichtner S, Hecker H, Schaefer A, Arseniev L, Hertenstein B, Ganser A, Drexler H. Intracoronary bone marrow cell transfer after myocardial infarction: eighteen months' follow-up data from the randomized, controlled BOOST (BOne marrOw transfer to enhance ST-elevation infarct regeneration) trial. Circulation. 2006;113:1287-94.
10. Janssens S, Dubois C, Bogaert J, Theunissen K, Deroose C, Desmet W, Kalantzi M, Herbots L, Sinnaeve P, Dens J, Maertens J, Rademakers F, Dymarkowski S, Gheysens O, Van Cleemput J, Bormans G, Nuyts J, Belmans A, Mortelmans L, Boogaerts M, Van de Werf F. Autologous bone marrow-derived stem-cell transfer in patients with ST-segment elevation myocardial infarction: double-blind, randomised controlled trial. Lancet. 2006;367:113-21.
11. Cleland JG, Freemantle N, Coletta AP, Clark AL. Clinical trials update from the American Heart Association: REPAIR-AMI, ASTAMI, JELIS, MEGA, REVIVE-II, SURVIVE, and PROACTIVE. Eur J Heart Fail. 2006;8:105-10.
12. Zhang S, Guo J, Zhang P, Liu Y, Jia Z, Ma K, Li W, Li L, Zhou C. Long-term effects of bone marrow mononuclear cell transplantation on left ventricular function and remodeling in rats. Life Sci. 2004;74:2853-64.
13. Ott HC, Bonaros N, Marksteiner R, Wolf D, Margreiter E, Schachner T, Laufer G, Hering S. Combined transplantation of skeletal myoblasts and bone marrow stem cells for myocardial repair in rats. Eur J Cardiothorac Surg. 2004;25:627-34.
14. Yokoyama S, Fukuda N, Li Y, Hagikura K, Takayama T, Kunimoto S, Honye J, Saito S, Wada M, Satomi A, Kato M, Mugishima H, Kusumi Y, Mitsumata M, Murohara T. A strategy of retrograde injection of bone marrow mononuclear cells into the myocardium for the treatment of ischemic heart disease. J Mol Cell Cardiol. 2006;40:24-34.
15. Bel A, Messas E, Agbulut O, Richard P, Samuel JL, Bruneval P, Hagege AA, Menasche P. Transplantation of autologous fresh bone marrow into infarcted myocardium: a word of caution. Circulation. 2003;108 Suppl 1:II247-52.
16. Yoon YS, Park JS, Tkebuchava T, Luedeman C, Losordo DW. Unexpected severe calcification after transplantation of bone marrow cells in acute myocardial infarction. Circulation. 2004;109:3154-7.
17. Baks T, Cademartiri F, Moelker AD, Weustink AC, van Geuns RJ, Mollet NR, Krestin GP, Duncker DJ, de Feyter PJ. Multislice computed tomography and magnetic resonance imaging for the assessment of reperfused acute myocardial infarction. J Am Coll Cardiol. 2006;48:144-52.
18. Balsam LB, Wagers AJ, Christensen JL, Kofidis T, Weissman IL, Robbins RC. Haematopoietic stem cells adopt mature haematopoietic fates in ischaemic myocardium. Nature. 2004;428:668-73.
19. Kajstura J, Rota M, Whang B, Cascapera S, Hosoda T, Bearzi C, Nurzynska D, Kasahara H, Zias E, Bonafe M, Nadal-Ginard B, Torella D, Nascimbene A, Quaini F, Urbanek K, Leri A, Anversa P. Bone marrow cells differentiate in cardiac cell lineages after infarction independently of cell fusion. Circ Res. 2005;96:127-37.

20. Murry CE, Soonpaa MH, Reinecke H, Nakajima H, Nakajima HO, Rubart M, Pasumarthi KB, Virag JI, Bartelmez SH, Poppa V, Bradford G, Dowell JD, Williams DA, Field LJ. Haematopoietic stem cells do not transdifferentiate into cardiac myocytes in myocardial infarcts. Nature. 2004;428:664-8.
21. Bartunek J, Wijns W, Heyndrickx GR, Vanderheyden M. Timing of intracoronary bone-marrow-derived stem cell transplantation after ST-elevation myocardial infarction. Nat Clin Pract Cardiovasc Med. 2006;3 Suppl 1:S52-6.
22. Sherman W, Martens TP, Viles-Gonzalez JF, Siminiak T. Catheter-based delivery of cells to the heart. Nat Clin Pract Cardiovasc Med. 2006;3 Suppl 1:S57-64.
23. Vulliet PR, Greeley M, Halloran SM, MacDonald KA, Kittleson MD. Intra-coronary arterial injection of mesenchymal stromal cells and microinfarction in dogs. Lancet. 2004;363:783-4.
24. Dai W, Hale SL, Martin BJ, Kuang JQ, Dow JS, Wold LE, Kloner RA. Allogeneic mesenchymal stem cell transplantation in postinfarcted rat myocardium: short- and long-term effects. Circulation. 2005;112:214-23.

Intracoronary Delivery of Umbilical Cord Blood Derived Unrestricted Somatic Stem Cells is Not Suitable to Improve LV Function after Myocardial Infarction in Swine

Amber D. Moelker[1], Timo Baks[1,2], Dimitry Spitskovsky[3], Piotr A. Wielopolski[2], Heleen M.M. van Beusekom[1], Robert-Jan van Geuns[1,2], Stephan Wnendt[4], Dirk J. Duncker[1], Wim J. van der Giessen[1,5]

[1] Cardiology, Thoraxcenter, Erasmus MC Rotterdam, The Netherlands
[2] Radiology, Erasmus MC Rotterdam, The Netherlands
[3] Kourion Therapeutics AG, Langenfeld, Germany**
[4] Viacell, Cambridge, MA, USA**
[5] Interuniversity Cardiology Institute of the Netherlands

5

1, 2, 3, 4

6, 7, 8, 9, 10, 11, 12, 13, 14, 15

Abstract

Objective

Regeneration of infarcted myocardium by injecting stem cells has been proposed to prevent heart failure. We studied the i.c. administration of human umbilical cord blood stem cells (USSC) in a porcine model of myocardial infarction (MI) and reperfusion.

Methods

In 15 swine, MI was induced by balloon-occlusion of the circumflex coronary artery (LCX) for two hours followed by reperfusion. Five swine served as healthy controls. One week later, magnetic resonance imaging (MRI) was performed to assess left ventricular (LV) function and infarct size. Then, under immune suppression, 6 of the 12 surviving MI swine received intracoronary injection of ~10*8 human USSC in the LCX while the other MI-swine received medium. Four weeks later all swine underwent follow-up MRI, and were sacrificed for histology.

Results

One week after MI, end-diastolic volume (92±3 mL) and LV mass (75±2 g) were larger, while ejection fraction (42±2 %) was smaller than in healthy control (68±3 mL, 66±3 g and 55±3 %, $P<0.05$). Regional wall thickening (-7±4 %) in the LCX area became akinetic. No difference in global and regional LV function at five weeks was observed between MI animals receiving USSC or medium. Infarct size after USSC treatment was significantly larger (8±2 g vs 20±3 g, $P<0.05$). USSC survived only in the infarct border zone at 5 weeks.

Conclusion

In swine with a one week old MI, injection of USSC via the intracoronary route does not improve LV function four weeks later.

Introduction

Tissue regeneration after myocardial infarction (MI) via stem cell transplantation has shown potential as a novel therapy to prevent left ventricular (LV) remodeling and heart failure.[1-4] For example, direct injection of autologous skeletal muscle progenitor cells into the infarcted myocardium, resulted in improved LV function after MI in experimental studies[5] as well as in patients with an old MI and chronic heart failure.[6] Beneficial effects on LV function have also been reported for bone marrow derived stem cells[7]. Thus, in a large number of studies performed in small animal models of MI produced by permanent coronary artery ligation, injection of cells (either intravenously or directly into the infarcted area) within hours after ligation attenuated LV remodeling and dysfunction.[1,2] Clinical studies also showed similarly favorable, albeit smaller, effects of autologous bone marrow derived stem cells (injected into the coronary artery supplying the infarcted but reperfused myocardial region) on LV function after MI,[7-11] although more recent evidence suggests that the beneficial effects at 6 months were no longer different from controls at 18 months.[11]

Although transplantation of autologous cells has the obvious advantage of lack of rejection, therapy with autologous cells has also potential disadvantages. First, autologous cells are harvested from MI patients, who are likely to have risk factors that are associated with decreased precursor cell functionality.[12] In addition, the number of stem cells obtained during harvesting may be variable, resulting in non-standardized re-injections[12] or necessitating subsequent culture steps, particularly in the case of skeletal myoblasts.[5,6,13]

Human umbilical cord blood is a rich source of stem cells for hematopoietic reconstitution and other potential applications in regenerative medicine, especially with respect to the recently described Unrestricted Somatic Stem Cells (USSC) from human cord blood.[14] Recent evidence suggests that human umbilical cord blood derived cells may have a beneficial effect on LV remodeling and function after MI.[15-19] Importantly, all five studies produced MI by permanent coronary artery ligation, i.e. without reperfusion, which clearly differs from the clinical setting. Furthermore, cells were injected either intravenously[17,18] or directly into the infarcted territory,[15,16,19] whereas the intracoronary injection of bone marrow derived mononuclear cells are typically used in more recent clinical post-myocardial infarction studies.[11] Consequently, the present xenotransplantation study was designed to assess in a porcine model of reperfused acute MI the effects of intracoronary (i.c.) injection of human umbilical cord blood derived cultured USSC[19] on regional and global LV function, LV geometry as well as infarct size, using magnetic resonance imaging (MRI).[20] For this study USSC

cultured by Kourion Therapeutics were used, this cell line was ex vivo described by Kögler et al.[14] and exactly the same cell line was used for direct intramyocardial injection by Kim et al.[19]

Material and methods

Experiments were performed in 2-3 month old Yorkshire-landrace pigs, in compliance with the "Guide for the Care and Use of Laboratory Animals" (NIH publication 1996) and written approval of the Animal Care Committee of Erasmus MC.

Umbilical Cord Blood Derived Cells

USSC were established from human umbilical cord blood as described by Kögler et al.,[14] and were negative for CD14, CD33, CD34, CD45, and express CD13, CD29, CD44, CD49e and HLA-I.

Cell culture and preparation for transplantation was performed by Kourion Therapeutics AG (Langenfeld, Germany) according to proprietary methods.[14,19]

Experimental Protocols

Protocol I: Cell Injection and Survival

We first investigated the survival of human USSC in infarcted porcine myocardium in a pilot group of 4 swine. For this purpose, animals were sedated (ketamine 20 mg/kg intramuscular (i.m.), and midazolam 1 mg/kg i.m.), anesthetised (thiopental, 12 mg/kg intravenously (i.v.)), intubated and mechanically ventilated with a mixture of oxygen and nitrogen (1:2 vol/vol). Anesthesia was maintained with fentanyl (12.5 μg/kg/h, i.v.) and isoflurane (0.6-0.8% started after onset of occlusion). Subsequently, animals received antibiotic prophylaxis (200 mg procainebenzylpenicillin and 250 mg dihyd rostreptomycinesulfate i.m.) and underwent coronary catheterization through the carotid artery approach, followed by balloon occlusion of the proximal left circumflex coronary artery (LCX) for 2 hr followed by reperfusion. Heparin was administered every hour (5000 Units).

One week after MI, swine were anesthetized and heparinized as described above and received an i.c. injection of ~ fifty million DAPI-labelled USSC (Sigma-Aldrich, Schnelldorf, Germany) suspended in 10 mL Dulbecco's Modified Eagle's Medium (DMEM) in the infarct related artery. USSC were filtered (100 μm pore size) and injected slowly (1 mL/min) into the coronary artery perfusing the MI area using a delivery catheter (Multifunctional Probing, Boston Scientific Co, Boston, MA). The site of injection was identical to the position of the occlusion balloon during MI induction.

To prevent hyper-acute rejection, two out of the four swine received 600 mg mycophenolic acid mofetil (Novartis, The Netherlands) 6 hours prior to cell injection followed by 600 mg b.i.d. starting 24 hours after injection, and cyclosporine A (CsA, Novartis, The Netherlands) 4 mg/kg b.i.d. starting 24 hours after cell injection. The other two animals did not receive immune suppression. Four days after cell injection animals were sacrificed for histological and immunocytochemical analyses.

Protocol II: Effect of USSC on LV Remodeling, Global and Regional Function and Infarct Size

Experiments were performed in 21 swine. Six swine served as healthy controls for normal cardiac growth and function. Fifteen swine underwent MI as described above; 3 swine died within 24 h post-MI due to arrhythmias. One week after MI, swine were again anesthetized as described above and underwent magnetic resonance imaging (MRI) to assess LV geometry and global and regional function, and infarct size. One control animal did not recover from anesthesia. Subsequently, 6 MI swine received an intracoronary injection of ~ 100 million USSC suspended in 10 mL DMEM, while 6 MI swine received i.c. injection of 10 mL DMEM. All swine (including that receiving medium and the controls) received 300 mg prednisone 24 hours before cell or medium injection followed by 300 mg daily for 2 days. In addition, swine received CsA 4 mg/kg b.i.d. starting 24 h after cell or medium injection until sacrifice. Four weeks later all 17 swine underwent follow-up MRI, after which animals were sacrificed for histological and immunocytochemical analyses of the LCX perfused infarct area and remote areas of the LV.

Magnetic Resonance Imaging

Data Acquisition

A clinical 1.5-Tesla MRI with a dedicated cardiac four element phased-array receiver coil was used for imaging (Signa CV/i, GE Medical systems, Milwaukee, WI, USA). Repeated breath-holds and gating to the ECG were applied to minimize the influence of cardiac and respiratory motion on data collection. Baseline and follow-up contrast enhanced (ce) MRI protocol consisted of cine-MRI and Delayed Enhancement (DE) imaging. Cine-MRI was performed using steady-state free-precession technique (imaging parameters: 24 temporal phases per slice, FOV26-30, rect. FOV 75%, TR 3.4, TE 1.4, flip angle 45º, matrix 160x128, bandwidth 83 kHz, 0.75 NEX). To cover the entire left ventricle, six to eight consecutive slices of 8 mm were planned in the short axis view, perpendicular to the long axis four-chamber view of the left ventricle (gap=0). DE imaging was performed to assess total myocardial infarct mass 10-20 minutes after administration of gadolinium-DTPA (0.5 mmol/kg, Magnevist®, Schering) with

a 2-dimensional T1-weighted inversion-recovery gradient-echo sequence (imaging parameters: slice thickness 8 mm, FOV26-30, rect FOV 75%, TR 7.3, TE 1.6, flip angle 20 degrees, TI 180-275 ms, matrix 256x192, 1 NEX, bandwidth 17.9 kHz). The inversion time was adjusted per animal to null the signal of remote myocardium. Locations were copied from the cine-images.

Image Analysis

The MR images were analyzed with dedicated cardiac software (Cine display application 3.0, General Electric medical systems, USA). End-diastolic volume (EDV), end-systolic volume (ESV) and left ventricular weight (LVW) were measured by manually drawing the endocardial and epicardial borders in the end- diastolic and end-systolic image of each slice. Stroke volume (SV= EDV-ESV), ejection fraction (EF= [SV/EDV]x100%) and cardiac output (CO= SVxHR) were computed. End-diastolic wall thickness (EDT) and end systolic wall thickness (EST) was measured and expressed in millimeter in 36 sections per slice. Regional systolic wall thickening (SWT) was calculated as [EST-EDT]/EDTx100%. Baseline and endpoint scans were matched for location using anatomical landmarks like insertion of the right ventricle to the septum and the papillary muscles.[20] The volume of DE was quantified by manually selecting the enhanced regions from the consecutive 2D slices encompassing the left ventricle. DE volume was multiplied by 1.05 g/ml to obtain myocardial infarct mass (1 millilitre corresponds to 1.05 gram as measured in our own laboratory). The anterior and posterior sections immediately adjacent to the akinetic infarct region were defined as border zone.

Histology and Immunohistochemistry

The hearts were excised and cut in 6-8 transverse slices similar to the MRI short axis slices. From the basal plane the first ring, and all other odd rings, were fixed in 4% buffered formaldehyde and embedded in paraffin. The second ring, and all other even rings, were embedded in tissue tec OCT and frozen in liquid nitrogen. Sections (5 μm) were stained with hematoxylin eosin (HE), resorcin-fuchsin (RF, collagen), von Kossa (calcium). Immunocytochemistry was also performed for identification of leukocytes (CD45, Serotec, Kidlington, UK) and USSC (in situ hybridization for human chromosome one with PUC1.77 staining[21]).

Sections were semi-quantitatively assessed as negative (–) or extent of positivity (+, ++ or +++) for the amount of collagen, calcium deposition, CD45+ cells and vascularization.

Statistical Analysis

Data were analyzed with SPSS 11.0. All data were analyzed using two-way analysis of variance (ANOVA), followed by one-way ANOVA and post-hoc analysis using unpaired t-testing with Bonferoni correction to test for significant intergroup differences at

corresponding time points. Intragroup differences between baseline and endpoint were determined using paired t-testing with Bonferoni correction. Effect of USSC therapy was tested using analysis of co-variance (ANCOVA) with baseline values as covariate. Statistical significance was accepted when $P< 0.05$ (two-tailed). All data are presented as mean ± SEM.

Results

Cell Injection and Survival

DAPI labeled cells could be detected 4 days after injection into infarcted area both in the presence (**Figure 1A**) or absence (**Figure 1B**) of immune suppression. Mononucleated USSC were also detected with PUC 1.77 staining (**Figure 1C**) thereby excluding cell fusion. Histological analysis using HE, RF, and CD45 staining, showed similar numbers of fibroblasts, collagen deposition and inflammatory cell infiltration at 4 days after USSC injection in swine that did not, as compared to animals that did, receive immune suppression.

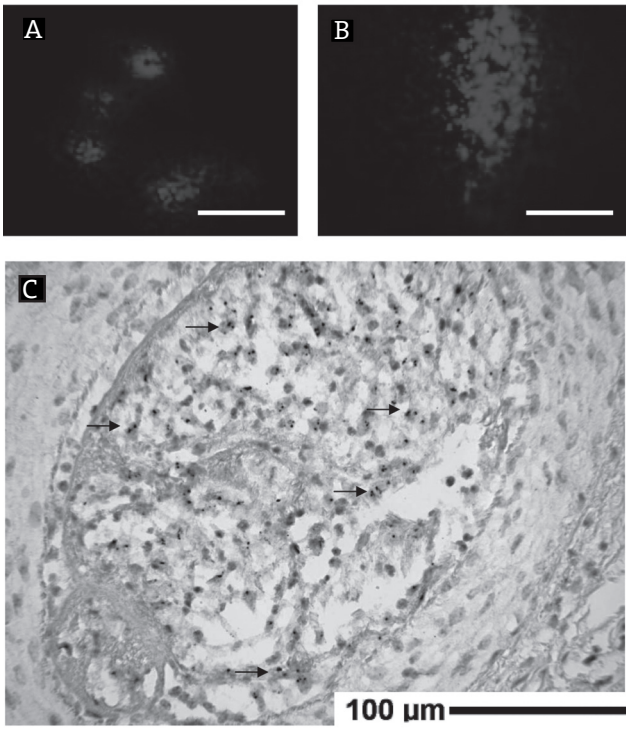

Figure 1. DAPI labeled USSC detected four days after injection into infarcted LCX region either with (photomicrograph **A**) or without (photomicrograph **B**) immune suppression. Photomicrograph 1**C** shows the presence of USSC as being positive for PUC1.77 (black dots indicated by black arrows) in an animal not receiving immune suppression. Each bar represents 100µm. *

Effect of USSC on LV Remodeling, Global and Regional Function and Infarct Size

Twenty-one animals entered the study. Four animals died prematurely, three of which died within 24 hours after induction of MI. One control animal did not recover from anesthesia after the baseline MRI. In all surviving MI animals, USSC or medium infusion was successful.

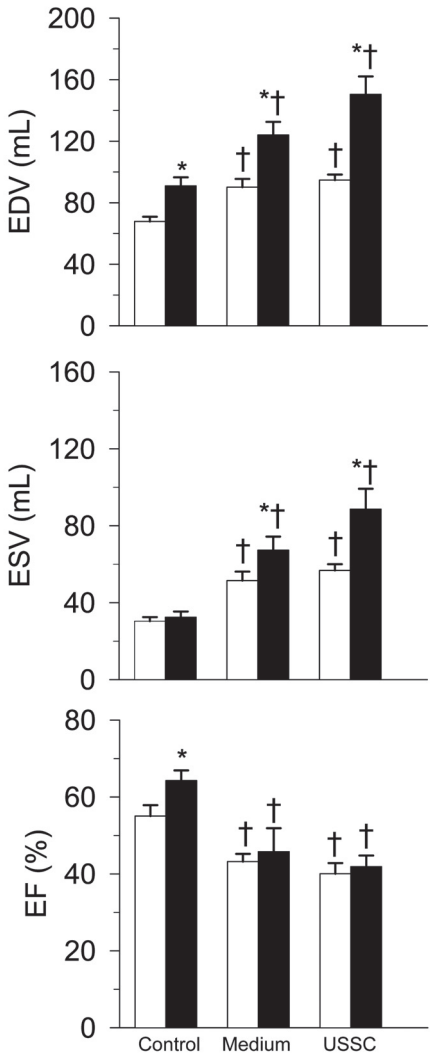

LV Remodeling and Global Function

One week after MI, significant LV remodeling as demonstrated by a higher end-diastolic volume (97±5 mL vs. 68±4 mL in control swine), end-systolic volume (54±3 mL vs. 32±3 mL) and LV weight (75±2 g vs. 66±3 g) in MI swine compared to control swine (all $P \leq 0.05$; **Table 1** and **Figure 2**) had already occurred. LV remodeling was accompanied by LV dysfunction resulting in a lower ejection fraction (42±2 % vs. 55±4 %, $P \leq 0.05$), but not in overt heart failure, as stroke volume (38±2 vs. 37±3 mL) was maintained (**Table 1**). LV-volumes increased between 1 and 5 weeks, but that was likely due to growth of the animals, since also the volumes in the control group increased (**Figure 2**). Importantly, the increases in LV weight and volumes over the 4 week follow-up period were not significantly different between medium- and USSC-treated MI swine. Furthermore, ejection fraction remained constant over the 4 week period in both medium- and USSC-treated animals (**Table 1** and **Figure 2**).

Figure 2. LV end-diastolic volume (EDV), LV end-systolic volume (ESV), and LV ejection fraction (EF) at baseline (open bars) and at endpoint (solid bars) in Control swine, and MI swine receiving either medium or USSC. *P<0.05 endpoint vs. baseline, †P<0.05 vs. corresponding control. There were no differences between USSC- and medium-treated MI animals either at baseline or endpoint, or in the response over the 4 wk follow-up period

Table 1: Hemodynamic and anatomical data

		Control Swine (n = 5)	MI Swine	
			Medium (n = 6)	USSC (n = 6)
BW (Kg)	Baseline	23 ± 1	24 ± 1	26 ± 0.4†
	Endpoint	35 ± 1*	38 ± 1*	39 ± 1*†
HR (bpm)	Baseline	108 ± 4	91 ± 5†	84 ± 5†
	Endpoint	83 ± 5*	93 ± 10	76 ± 5
SV (mL)	Baseline	37 ± 3	39 ± 2	38 ± 2
	Endpoint	58 ± 5	57 ± 6	59 ± 5
LVW (g)	Baseline	66 ± 3	76 ± 3†	74 ± 2†
	Endpoint	99 ± 6*	104 ± 5*	119 ± 5*§
Infarct size (g)	Baseline	-	9 ± 3	14 ± 3
	Endpoint	-	8 ± 2	20 ± 3*‡§
Infarct size (%)	Baseline	-	12 ± 3	19 ± 3
	Endpoint	-	7 ± 2**	17 ± 2‡§

BW = body weight; HR = heart rate; SV = stroke volume; LVW = left ventricular weight; Baseline = 1 wk post-MI; Endpoint = 5 wk post-MI. *P<0.05, **P=0.08 endpoint vs. baseline, †P<0.05 vs. corresponding Control, ‡ P<0.05 USSC vs. corresponding medium-treated MI animals, § P<0.05 change from baseline USSC- vs. medium-treated MI animals.

Regional LV Function

Analysis of regional LV function at 1 week post-MI showed akinesis of the infarcted lateral wall resulting in complete loss of systolic wall thickening in the central infarct zone (-7±2%) and partial loss of systolic wall thickening in the border zones (25±3%) as compared to systolic wall thickening of the lateral wall in control swine (62±7%; **Figure 3**). The abnormalities in regional function remained virtually unchanged during the next 4 weeks of the follow-up period. Furthermore, no differences were observed between medium- as well as USSC-treated animals in end-diastolic wall thickness or absolute or percent systolic wall thickening, either at baseline or 4 weeks after treatment (**Figure 3**).

Infarct Size

DE-MRI showed that at 1 week post-MI, the infarcted region encompassed 16±3% of LV weight (Table 1). During the 4 week follow-up period, the absolute weight of the

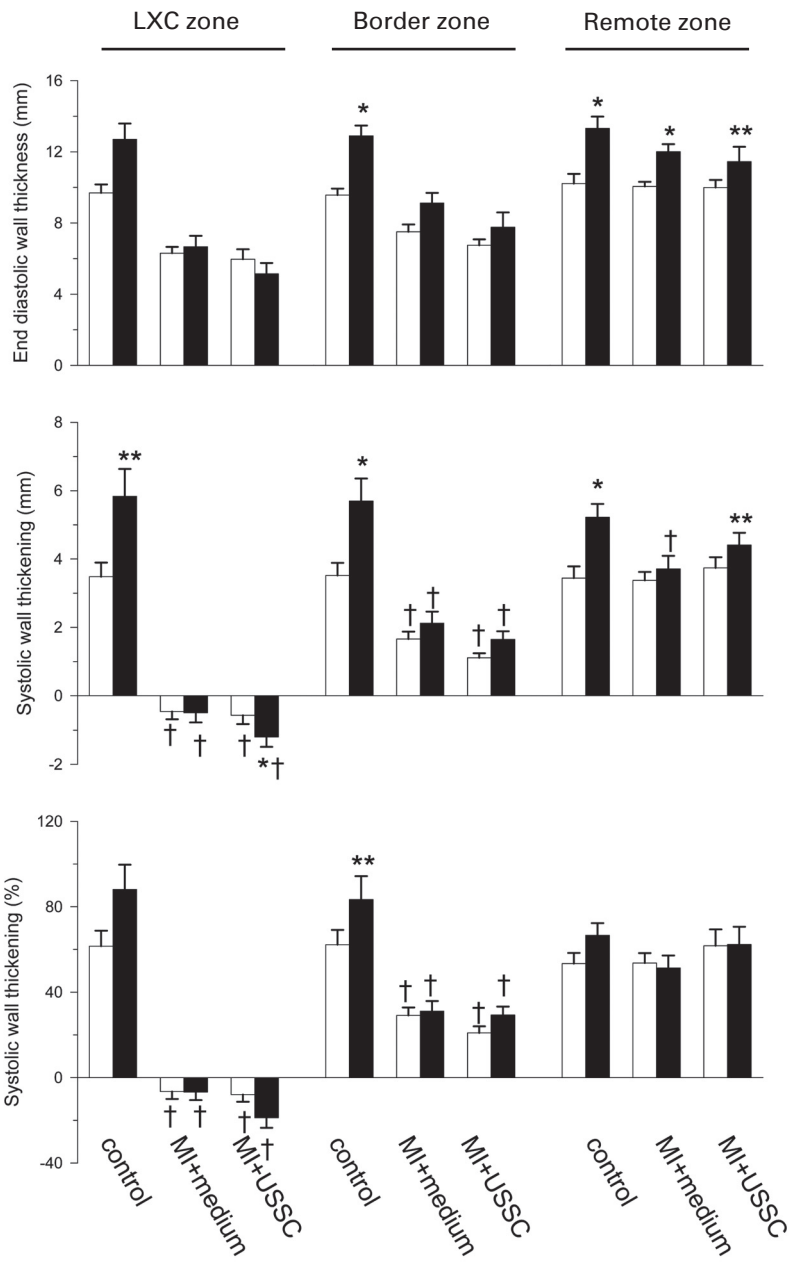

Figure 3. End-diastolic wall thickness (EDT, upper panel), absolute SWT (middle panel) and percent SWT (lower panel) at baseline (open bars) and at endpoint (solid bars) in Control swine, and MI swine receiving either medium or USSC. *P<0.05, **P<0.1 endpoint vs. baseline, †P<0.05 vs. corresponding control. There were no differences between USSC and medium treated MI animals.

infarcted region remained constant in the medium-treated swine, and considering the increase in total LV weight the relative infarct size thereby tended to decrease (from 12±3 % to 7±2 %; P=0.08). In contrast, in the USSC-treated swine absolute infarct size actually increased slightly and relative infarct size did not decrease. This change in infarct size over the four week period between the groups was statistically different (P<0.05).

Histology

Histology confirmed the presence of transmural infarcts in the LCX region with a nearly complete loss of viable tissue in all MI animals (**Figure 4A** and **4B**), matching the DE scans performed at 5 weeks after MI. The medium- and USSC-treated swine both showed abundant collagen (**Figure 4C** and **4D**) and fibrous tissue (**Figure 4E** and **4F**) in the center of the infarct. The amount of calcification (**4A**, **B**) and inflammatory cell infiltration (**4G**, **H**) appeared larger in USSC-treated compared to medium-treated swine. There were no discernible differences in histological appearance within the border zones between USSC- and medium-treated swine.

Using PUC1.77 staining we could not demonstrate the presence of USSC in the central infarct zone. However, a few USSC (2.0 ± 0.6 cells/cm2) could be detected in the border zone (**Figure 5**).

Discussion

The present study investigated the effects of intracoronary injection of USSC in a porcine model of reperfused MI. USSC were injected 1 week after reperfusion and swine were studied 4 weeks later. The main finding is that intracoronary injection of USSC does not attenuate MI-induced LV remodeling or ameliorate global and regional LV dysfunction. In addition, USSC resulted in a larger infarct size at 4 weeks follow-up, which was accompanied by increases in inflammatory cells and calcifications in the infarct zone compared to medium-treated swine. The implications of these findings will be discussed in detail.

Previous studies

To date a few studies have investigated the effects of cord blood derived cells on post-MI LV remodeling and dysfunction and infarct size (Table 2). In rats direct injection of CD34+, CD133+ or mononuclear cells from cord blood into viable myocardium, bordering the ischemic region, within 1 hour after permanent coronary artery ligation resulted in significantly better LV function at 4 weeks[16,17] or 4 months.[15] Intravenous injection of mononuclear cells from cord blood one day after permanent coronary

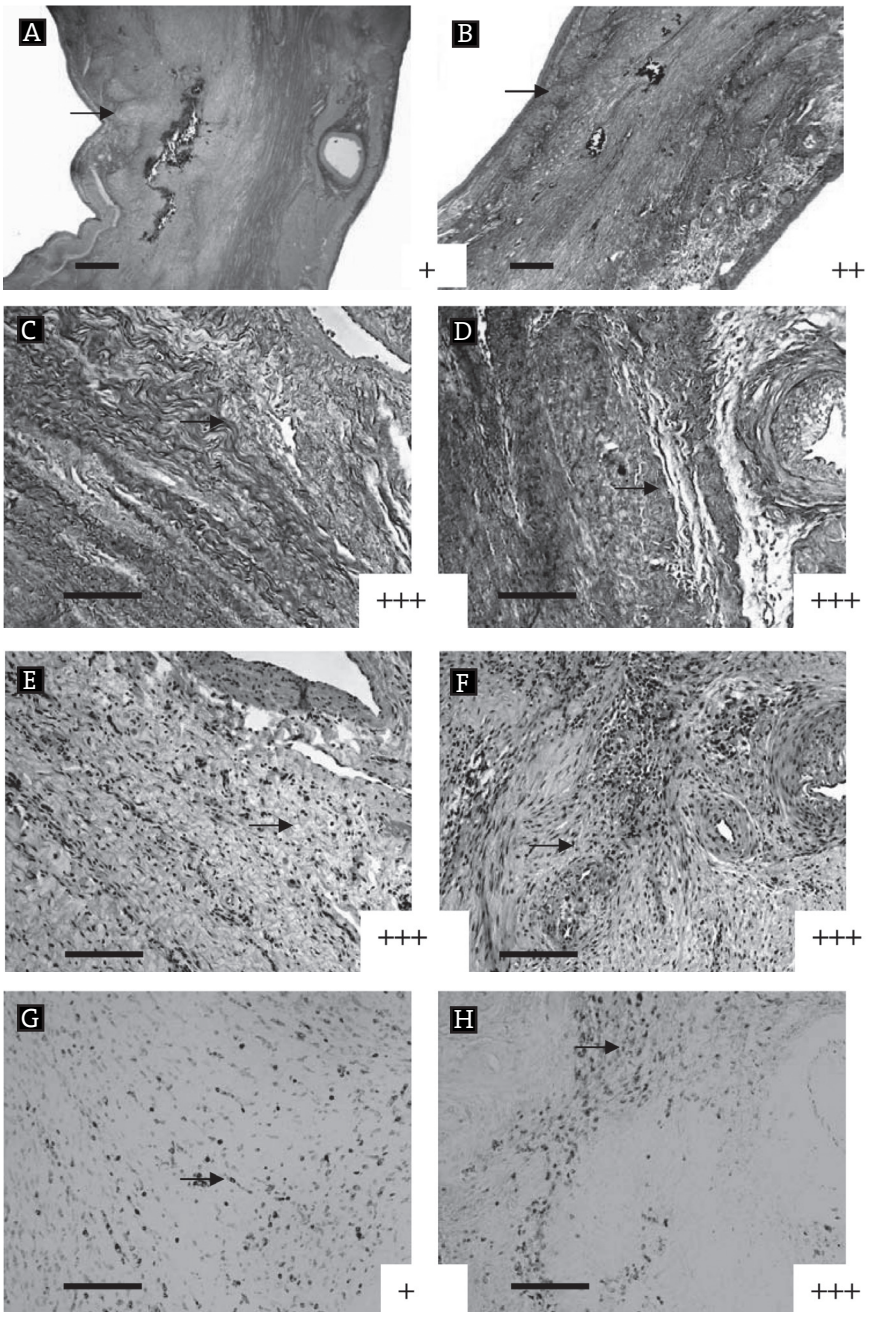

Figure 4. Infarct area of medium-treated (**A**,**C**,**E**,**G**) compared with USSC-treated (**B**,**D**,**F**,**H**) swine, showing transmural infarction (photomicrographs **A**,**B**; von Kossa staining; arrows point indicate endocardium), and abundant collagen (arrows in **C**,**D**; RF staining) and fibroblasts (arrows in **E**,**F**; HE staining), and inflammatory cells (arrows in G,H; panleucocyte marker CD45). The + symbols denotes the degree of calcification (**A**,**B**), collagen (**C**,**D**), vascularization (**E**,**F**) and CD45+ cells (**G**,**H**).
Bars denote 1mm (**A**,**B**) and 300 μm (**C**,**D**,**E**,**F**,**G**,**H**) *

artery ligation in mice was reported to reduce infarct size and enhance angiogenesis in the infarct border zone.[18] Recently, Kim et al.[19] reported in a porcine model of permanent ligation induced MI, that USSC directly injected into the border zone of the infarct area 4 weeks post-MI, resulted in significant reduction in end-diastolic volume and improvement of ejection fraction compared to medium-treated swine at 8 weeks post-MI. In addition, these authors observed a decrease in relative infarct size (as measured ex-vivo with planimetry). In contrast to the beneficial effects observed in studies that used direct intramyocardial injection in models of non-reperfused MI[19], the present study fails to reveal a beneficial effect of intracoronary injection of USSC on LV remodeling, function and infarct size in a model of reperfused MI, although the identical cell line was used. Several reasons could be forwarded to explain the negative results in the present study, including timing of USSC administration after MI, insufficient duration of follow-up in order to detect beneficial effects, insufficient cell survival, and/or route of administration.

Timing of cell administration

The optimal timing of progenitor cell administration after MI is still incompletely understood. Hence, it could be argued that USSC injection 7 days after MI was too early to be effective. However, this is unlikely as previous studies showed favorable effects of cord blood cell injection as early as 20-min,[16] 60-min,[15] or 1 day[18] after coronary ligation. We decided to inject USSC 7 days post- MI, as this approximates the time-point of injection that is often used in clinical trials.[7-9] Alternatively, one might forward that injection of USSC 7 days post-MI was too late to be effective. However, this is unlikely as Kim et al.[19] showed favorable effects of USSC injection as late as 4 weeks after ligation. Furthermore, the REPAIR-AMI trial11 suggests that optimal results are obtained when cells are injected at least 5 days after MI. Hence the timing

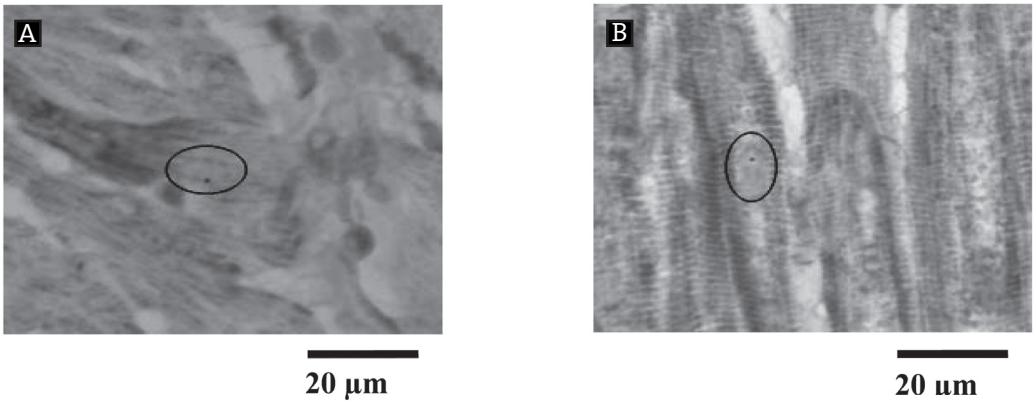

Figure 5. PUC 1.77 positive cell (encircled) in the border zone of the infarct area in two USSC-treated swine (A,B). *

of administration of USSC cannot explain the observed lack of benefit of USSC on LV remodeling, function or infarct size in the present study.

Follow-up time

Another reason for the lack of benefit observed in our study could be that the 4 week follow-up period was insufficient to allow detection of an effect of USSC transplantation. However, previous studies reported positive effects on LV remodeling, function, and infarct size as early as three18 or four[16,17,19] weeks after MI in rats,[16,17] mice[18] and swine,[19] indicating that 4 weeks should be sufficient.

Cell survival

An obvious concern when administrating human USSC to swine is low cell survival due to transplant rejection. USSC are purportedly hypo-immunogenic.[22] Furthermore, we detected DAPI-labeled USSC in the infarct zone 4 days after injection even in swine that did not receive immune-suppression, suggesting the absence of hyper-acute rejection. Nevertheless, we decided to use immune-suppression with prednisolone and CsA in our study, because injecting human cells in a pig is by definition a HLA-mismatched xenotransplantation. It is well known that even under immune suppression, cells will be lost by rejection in leukemia patients receiving cell transplants.

Using in-situ hybridization for human chromosome 1 (PUC1.77 staining),[21] we could not detect any USSC in the central infarct zone. However, surviving USSC were found in the border zone, at the site where the regenerative capacity of progenitor cells is considered most plausible.[4,11] Kim et al.[19] , who used the same cell line, observed survival of a number of USSC in the implanted area, 4 weeks after transplantation in swine, using a dose of CsA of 5 mg/Kg/day. In view of the higher dose of CsA that was administrated in the present study (8 mg/Kg/day), the low number of USSC found in the infarct area in the present study was unlikely the result of rejection due to insufficient dosing of CsA.

In the present study swine underwent a 2 hour coronary artery balloon occlusion followed by reperfusion to induce MI, which mimics the clinical procedure of percutaneous coronary intervention as closely as possible. Importantly, however, previous studies that reported beneficial effects of cord blood derived cells used an animal model in which MI was induced by permanent coronary ligation.[15-19] It is likely that reperfusion results in more abrupt and pronounced inflammation and hence creates a more hostile environment that is less appropriate for cell survival during the first few days after reperfusion[23]. In addition, the transmural, inflammatory infarct region will not stimulate the undifferentiated USSC to develop into a cardiomyocyte or

endothelial cell. It is more likely that USSC will develop into an inflammatory cell-type, which can contribute to the higher degree of inflammation and calcification which was observed in our study. This is why we injected USSC 7 days after reperfusion, as it also corresponds with the time of intracoronary injection of progenitor cells in clinical studies that reported beneficial effects.[8,9]

Route of administration causing micro infarctions

We purposely choose to inject USSC into the coronary artery supplying the infarct area, in view of this being the most common route of administration for stem cell therapy in the setting of AMI,[3] One advantage of intracoronary injection is that cells will follow blood flow distribution and reach areas that are well perfused, providing oxygen and nutrients to the transplanted cells which will enhance their survival.[4] Conversely, intracoronary injection of cells carries the risk of obstruction of the coronary vascular bed. Although this does not appear to be a major issue with purified bone marrow cells in most clinical trials, the risk for embolic complications seems to be more likely when infusing ex vivo expanded cells. Intracoronary injections of bone marrow derived mesenchymal stromal stem cells that were twice the size of freshly harvested bone marrow cells caused micro-infarctions in dogs.[24] In the present study, USSC increased inflammatory cells and calcification 4 weeks after injection into the infarct zone. To further explore the issue of micro-embolization in greater detail we injected ~ 50*106 USSC into the LAD of normal hearts in four swine. Four days after injection of USSC (which are ~20 μm in size) in normal healthy myocardium, extensive micro infarctions were observed in the injected area (**Figure 6**). USSC could be detected in the myocardium obstructing blood vessels. This induction of micro infarction may be the mechanism behind the increased infarct size in our USSC-group. These results show a potential complication of injection of USSC into the coronary circulation. In addition there is evidence that cells expanded in culture show increased expression of adhesion molecules compared to freshly isolated cells,[25] so that adhesion to the endothelium throughout the coronary vascular tree resulted in vascular obstruction. Hence, it cannot be excluded that a possible positive effect of USSC injection on LV function after MI was thus obscured by the induction of micro-infarctions caused by the intracoronary injection procedure. In conjunction with the positive results obtained with direct intramyocardial injection of the same USSC-cell line,[19] the present study indicates that intracoronary injection is not the preferred route of administration for cultured USSC. Future studies are needed to assess whether transendomyocardial injections (rather than intracoronary injections) could provide an alternative catheter-based approach to treatment with USSC in reperfused MI.

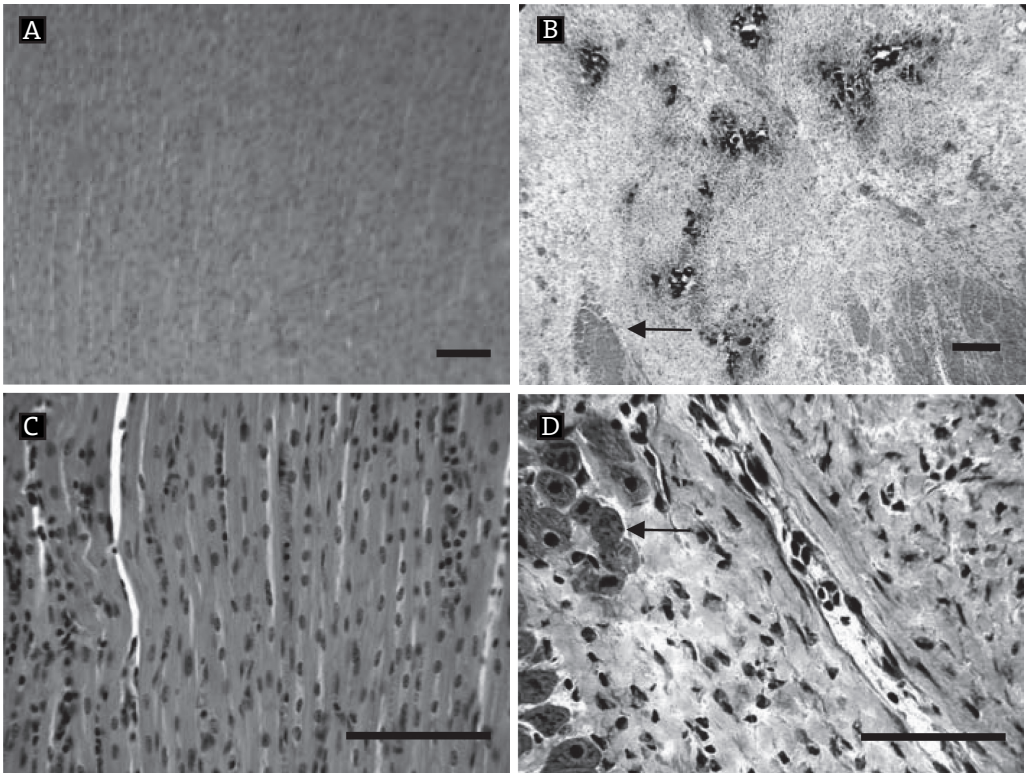

Figure 6. HE staining of normal LAD area showing healthy myocardium (A,C). HE staining of LAD area four days after injection of USSC (B,D) demonstrating extensive (micro)infarction. Arrows indicate surviving myocytes. Bars denote 100µm. *

References

1. Taylor DA, Atkins BZ, Hungspreugs P, Jones TR, Reedy MC, Hutcheson KA, Glower DD, Kraus WE. Regenerating functional myocardium: improved performance after skeletal myoblast transplantation. Nat Med 1998;4(8):929-33.
2. Murry EM, Field LJ, Menasche P. Cell-based cardiac repair: reflections at the 10-year point. Circulation 2005;112:3174-83.
3. Histrov M, Weber C. The therapeutic potential of progenitor cells in ischemic heart disease: Past present and future. Basic Res Cardiol 2005;100:1-7.
4. Dimmeler S, Zeiher AM, Schneider MD. Unchain my heart: the scientific foundations for cardiac repair. J Clin Invest 2005;115:572-83.
5. Van den Bos EJ, Thomson RB, Wagner A, Mahrholdt H, Morimoto Y, Thomson LEJ, Wang LH, Duncker DJ, Judd RM, Tayler DA. Functional assessment of myoblast transplantation for cardiac repair with magnetic resonance imaging. Eur J Heart Fail 2005;7(4):435-43.

6. Menasche P, Hagege AA, Vilquin JT, Desnos M, Bergel EA, Pouzet B, Bel A, Sarateanu S, Scorsin M, Schwartz K, Bruneval P, Benbunan M, Marolleau JP. Autologous skeletal myoblast transplantation for severe post infarction left ventricular dysfunction. Am Coll Cardiol 2003;41:1078-1083.
7. Bartunek J, Van der Heyden M, Vanderkerckhove B, Mansour S, De Bruyne B, de Bondt P, Van Haute I, Lootens N, Heyndrickx G, Wijns W. Intracoronary injection of CD133-positive enriched bone marrow progenitor cells promotes cardiac recovery after recent myocardial infarction: feasibility and safety. Circulation 2005;112(30, 9 Suppl):I178-83.
8. Wollert KC, Meyer GP, Lotz J, Ringes-Lichtenberg S, Lippolt P, Breidenbach C, Fichtner S, Korte T, Horning B, Messinger D, Arseniev L, Hertenstein B, Ganser A, Drexler H. Intracoronary autologous bone-marrow cell transfer after myocardial infarction: the BOOST randomized controlled clinical trial. Lancet 2004;364(9429): 141-8.
9. Strauer BE, Brehm M, Zeus T, Kostering M, Hernandez A, Sorg RV, Kogler G, Wernet P. Repair of infarcted myocardium by autologous intracoronary mononuclear bone marrow cell transplantation in humans. Circulation 2002;106:1913-1918.
10. Schachinger V, Assmus B, Britten MB, Honold J, Lehmann R, Teupe C, Abolmaali ND, Vogl TJ, Hofmann WK, Martin H, Dimmeler S, Zeiher AM. Transplantation of progenitor cells and regeneration enhancement in acute myocardial infarction: final one-year results of the TOPCARE-AMI Trial. J Am Coll Cardiol 2004;44:1690-1699.
11. Cleland JGF, Freemantle N, Coletta AP, Clark AL. Clinical trials update from the American Heart Association: REPAIR-AMI, ASTAMI, JELIS, MEGA, REVIVE-II, SURVIVE, and PROACTIVE. Eur J Heart Fail 2006;8:105-110.
12. Vasa M, Fichtlscherer S, Aicher A, Adler K, Urbich C, Martin H, Zeiher AM, Dimmeler S. Number and migratory activity of circulating endothelial progenitor cells inversely correlate with risk factors for coronary artery disease. Circ Res 2001;89(1):E1-7.
13. Smits PC, van Geuns RJ, Poldermans D, Bountioukos M, onderwater EE, Lee CH, Maat AP, Serruys PW. Catheter-based intramyocardial injection of autologous skeletal myoblasts as a primary treatment of ischemic heart failure: clinical experience with six-month follow-up. J Am Coll Cardiol 2003;42:2063-2069.
14. Kögler G, Senksen S, Airey js, Trapp T, Muschen M, Feldhahn N, Liedtke S, Sorg RV, Fischer J, Rosenbaum C, Greschat S, Knipper A, Bender J, Degistirici O, Gao J, Caplan AI, Colleti EJ, Almeida-Porada G, Muller HW, Zanjani E, Werner P. A new human somatic stem cell from placental cord blood woth intrinsic pluripotent differentiation potential. J Exp Med 2004;2:123-135.
15. Henning RJ, Abu-Ali H, Balis JU, Morgan MB, Willing AE, Sanberg PR. Human umbilical cord blood ononuclear cells for the treatment of acute myocardial infarction. Cell Transplant 2004;13(7-8):729-39.
16. Hirata Y, Sata M, Motomura N, Takanashi M, Suematsu Y, Ono M, Takamoto S. Human umbilical cord blood cells improve cardiac function after myocardial infarction. BBRC 2005;327: 609-614.
17. Leor J, Gyetta E, Feinberg MS, Galksi H, Bar I, Holbova R, Miller L, Zarin P, Castel D, Barbash IM, Nagler A. Human umbilical cord blood derived CD133+ cells enhance function and repair of the inf-

arcted myocardium. Stem Cells Express Epub ahead of print october 2005.

18. Ma N, Stamm C, Kaminski A, Li W, Kleine HD, Muller-Hilke B, Zhang L, Ladilov Y, Egger D, Steinhoff G. Human cord blood cells induce angiogenesis following myocardial infarction in NOD/scid-mice. Cardiovasc Res 2005;66(1):45-54.
19. Kim BO, Tian H, Prasongsukarn K, Wu J, Angoulvant D, Wnendt S, Muhs A, SpitkovskyD, Li RK. Cell transplantation improves ventricular function after a myocardial infarction: a preclinical study of human unrestricted somatic stem cells in a porcine model. Circulation 2005;112(9 Suppl):I96-104.
20. Baks T, van Geuns RJ, Biagini E, Wielopolski P, Mollet NR, Cademartiri F, Boersma E, van der Giessen WJ, Krestin GP, Ducnker DJ, Serruys PW, de Feyter PJ. Recovery of left ventricular function after primary angioplasty for acute myocardial infarction. Eur Heart J 2005;26(11):1070-7.
21. Verdoodt B, Charlette I, Maillet B, Kisch-Volders M. Numerical aberrations of chromosomes 1 and 17 in tumor cell lines of the exocrine pancreas as determined by fluorescence In Situ Hybridization. Cancer Genet Cytogenet 1997;94:125-30.
22. Rocha V, Gluckman E. Clinical use of umbilical cord blood hematopoietic stem cells. Biol Blood Marrow Transplant 2006;12:34-41.
23. Bartunek J, Wijns W, Heyndrickx GR, Vanderheyden M. Timing of intracoronary bone-marrow-derived stem cell transplantation after ST-elevation myocardial infarction. Nat Clin Pract Cardiovasc Med 2006;3(Suppl 1):S52-6.
24. Vulliet PR, Greeley M, Halloran SM, MacDonald KA, Kittleson MD. Intra-coronary arterial injection of mesenchymal stromal cells and microinfarction in dogs. Lancet 2004;363(9411): 783-4.
25. Liu B, Buckley SM, Lewis ID, Goldman AI, Wagner JE, van der Loo JCM. Homing defect of cultured human hematopoietic cells in the NOD/SCID mouse is mediated by Fas/CD95. Experimental Hematology 2003;31:824-832.

Magnetic resonance imaging of hemorrhage within reperfused myocardial infarcts: Possible interference with iron oxide–labeled cell tracking?

Ewout J. van den Bos; Timo Baks; Amber D. Moelker; Wendy Kerver; Willem J. van der Giessen; Dirk J. Duncker; Piotr A. Wielopolski

Eur Heart J. 2006 Jul;27(13):1620-6.

6

1, 2, 3, 4, 5, 7, 8, 9, 10, 11, 12, 13, 14, 15

Abstract

Aims

Magnetic resonance imaging (MRI) has been proposed as a tool to track iron oxide-labelled cells within myocardial infarction (MI). However, infarct reperfusion aggravates microvascular obstruction (MO) and causes haemorrhage. We hypothesized that haemorrhagic MI causes magnetic susceptibility-induced signal voids that may interfere with iron oxide-labelled cell detection.

Methods and Results

Pigs (n = 23) underwent 2 h occlusion of the left circumflex artery. Cine, T2*-weighted, perfusion, and delayed enhancement MRI scans were performed at 1 and 5 weeks, followed by ex vivo high-resolution scanning. At 1 week, MO was observed in 17 out of 21 animals. Signal voids were observed on T2*-weighted scans in five out of eight animals, comprising 24+/-22% of the infarct area. A linear correlation was found between area of MO and signal voids (R(2) = 0.87; P = 0.002). At 5 weeks, MO was observed in two out of 13 animals. Signal voids were identified in three out of sevenanimals. Ex vivo scanning showed signal voids on T2*-weighted scanning in all animals because of the presence of haemorrhage, as confirmed by histology. Signal voids interfered with the detection of iron oxide-labelled cells ex vivo (n = 21 injections).

Conclusion

Haemorrhage in reperfused MI produces MRI signal voids, which may hamper tracking of iron oxide-labelled cells.

Introduction

Transplantation of cells after myocardial infarction (MI) has emerged as a promising therapy to restore heart function.[1-4] To evaluate cell engraftment, non-invasive tracking of cells with magnetic resonance imaging (MRI) has been proposed as a valuable tool. Cells labeled with iron oxide, paramagnetic probes cause a T2* signal void[5] and can thus be detected up to single cell resolution in vitro.[6-8] In vivo, clusters of labeled cells could be detected after injection into infarcted myocardium of mouse,[9,10] rabbit[11] and pig hearts.[12-17]

However, in clinical practice acute MI is treated by reperfusion therapy,[18] aggravating microvascular obstruction (MO) and causing hemorrhage.[19,20] Hemoglobin degradation products, such as methemoglobin and hemosiderin, have strong magnetic susceptibility effects,[21] which may mimic the signal voids caused by iron oxide-labeled cells.

We hypothesized that hemoglobin degradation products in reperfused MI produce signal voids that interfere with reliable iron oxide-labeled cell tracking. Therefore, we evaluated the MRI characteristics of subacute (1 week old) and chronic (5 weeks old) infarcts in a porcine model of reperfused MI and compared the MRI findings with histology of the infarct tissue.

Methods

Myocardial infarction

Experiments were performed in 23 Yorkshire-Landrace pigs (2-3 months old, ~25 kg). The study complied with the regulations of the Animal Care Committee of the Erasmus MC and the National Institutes of Health Publication 86 to 23, revised 1996. Animals were sedated (ketamine, 20 mg/kg IM and midazolam, 1 mg/kg IM), anesthetized (thiopental, 12 mg/kg IV), intubated and mechanically ventilated (mixture of oxygen and nitrogen, 1:2). Analgesia was maintained initially with fentanyl (12 μg/kg/min IV). Subsequently, animals underwent left coronary catheterization, followed by balloon occlusion of the left circumflex coronary artery (LCx), proximal of the first margo obtusus branch. After 2 hours the balloon was deflated and the infarct reperfused, as confirmed by TIMI III flow on angiography. Anesthesia was maintained with isoflurane (0.6-0.8 %), starting after occlusion of the LCx.

Magnetic resonance imaging

A 1.5 T MRI scanner with a dedicated four-element phased array receiver coil was used (Signa CV/i; GE Medical Systems, Milwaukee, WI, USA). One week after MI, pigs were anesthetized and ventilated as described above and underwent clinically applied,[22] electrocardiogram (ECG)-gated cine, T2*-weighted, first-pass perfusion (FPP) and delayed enhancement (DE) MRI. The T2*-weighted sequence was applied in a subset of animals (n=8 and n=7 at 1 and 5 weeks, respectively), due to technical limitations of the scanner software at the start of the study. For detailed MRI protocols see supplemental information. Breath-holding was achieved by interrupting the ventilation.

After scanning, eight animals were euthanized using an overdose of pentobarbital. Hearts were excised, immersed in saline and scanned ex vivo using gradient echo (GE) and spin echo (SE) sequences with multiple echo times and flip angles to obtain T1-, proton density-, T2- and T2*-weighted images (T1W, PDW, T2W and T2*W, respectively). For detailed MRI protocols see supplemental information. The minimum time interval between in vivo scanning and sacrifice was at least 3 h and in most cases more than 12 hours (overnight), to make sure that all Gadolinium-DTPA had been washed out.

One animal died following the 1 week scan. Five weeks after infarction the remaining 14 animals underwent a follow-up MRI using a similar imaging protocol as at 1 week. In one animal at 1 week and again at 5 weeks no vascular access could be assured during scanning for injection of contrast, therefore in this animal no FPP and DE scans could be obtained. In one animal at 1 week, FPP scanning was not reliable for assement of MO due to movement artifacts, therefore it was not included in the analysis. Three infarct specimens were scanned a second time after standard paraffin embedding. Finally, of three animals no ex vivo scans could be obtained due to technical limitations during scanning.

In order to compare signal voids induced by the presence of iron oxide-labeled cells and hemoglobin degradation products, ex vivo scanning was repeated after local injections with either 0.1, 1 or 4 x106 iron oxide-labeled human umbilical vein endothelial cells. A total of 21 injections were performed in 4 subacute and 3 chronic infarct specimens. Cells were labeled as described previously,[8] resulting in ~9.2 pg iron per cell, and fixed in 4% formaldehyde.

A flow-chart (**Figure 1**) summarizes the protocol and the number of animals studied at each time point.

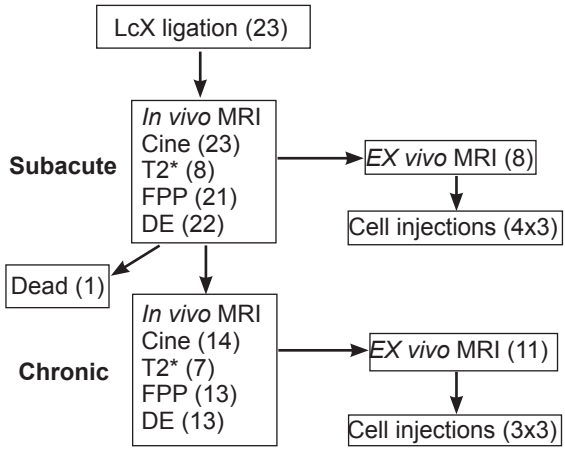

Figure 1. Flowchart of the study protocol. Numbers between brackets indicate the number of animals or specimens used at a certain time point.

Image analysis

MR images were analysed using Cine Display Application Version 3.0 (GE Medical systems, Milwaukee, WI, USA). Signal voids were identified on mid-papillary, single slice T2*W scans, and expressed as a percentage of the infarct area as defined by DE MRI. Signal void volumes were calculated by multiplying their area by slice thickness. MO was identified on mid-papillary, single slice FPP images as an area of persistent subendocardial hypoenhancement.[23] MI was identified on DE images as an area with delayed hyperenhancement and its size was expressed as a percentage of the left ventricular wall volume. Contrast-to-noise ratio (CNR) was measured in the T2*W in vivo and ex vivo scans at 1 and 5 weeks, according to the relation (CNR=[SImyo-SIvoid]/SDnoise), where SImyo represents signal intensity of remote or infarcted myocardium, SIvoid signal intensity of signal voids and SDnoise standard deviation of background noise measured in the air outside the pig. Total hemorrhagic areas were measured at mid-papillary levels in PD-T2*W ex vivo scans using Clemex Vision PE analysis software (Clemex Technologies, Longueuil, Canada) and expressed as a percentage of the total infarct area.

Histology

Hearts were transversally cut in ~1 cm thick slices and stained with 1% triphenyltetrazolium chloride (TTC; 37°C, 15 min; Sigma, St. Louis, MO) and subsequently with Prussian blue (PB), which stains hemosiderin deposits deep blue. After standard paraffin embedding, 5 µm serial sections were cut in the same plane as the MRI scans. Sections were stained with Hematoxylin Eosin (HE), von Kossa's (VK) or restained with PB. VK

was counterstained with von Gieson (VG). This approach allowed for identification of fat (HE), calcium (VK), collagen (VG) as well as hemosiderin (PB). Staining was analysed and compared with matching MR images at the same location and imaging plane.

Statistical analysis

Data are reported as mean ± SD. Data from subacute and chonic infarcts were compared using paired or unpaired t-testing as appropriate. The correlation between area of MO and signal voids was assessed using linear regression analysis, including all animals assessed by T2*W scanning. Proportions were compared using a z-test (SigmaStat software version 2.03; SPSS Inc., Chigago, IL). Sample size was determined with the following assumptions: Type I error of 0.05, power of 80%, an estimated proportion of animals with an in vivo MRI detectable hemorrhage-induced signal void of 35%, based upon the literature, with the assumption that a proportion of 5% would not be relevant. Therefore, 8 animals would yield 80% power to detect a significant proportion of animals with such a signal void. Based upon pilot studies, the proportion of ex vivo detected signal voids was estimated to be ~90%. A value of $P < 0.05$ (two-tailed) was considered statistically significant.

Results

In vivo MRI

In subacute infarcts, signal voids could be identified in five out of eight animals using the T2*W sequence (**Figure 2**). In the remaining 3 animals, signal voids were either not observed (n = 2) or could not be reliably discerned from the air-heart interface susceptibility artefact (n = 1). The size of the signal voids was 0.53 ± 0.51 cm^3. The area of signal voids comprised 24 ± 22% of the infarct area. MO was observed in 17 out of 21 animals, comprising 35 ± 23% of the infarct area (**Table 1**). A linear relationship was found between the area of signal voids on T2*W scans and the area of MO on the corresponding FPP scans at 1 week ($R^2 = 0.87$; $P = 0.002$; n = 8). Infarct size was 25 ± 6% of total left ventricular wall volume (n = 22). CNR between remote myocardium and areas of signal voids was 27 ± 16 and between infarcted, non-hemorrhagic myocardium and areas of signal voids 34 ± 11 (n = 5).

In chronic infarcts, an area of signal voids could be identified in 3 out of 7 animals, comprising 15 ± 19% of the infarct area. MO was identified in 2 out of 13 animals, comprising 13 ± 31% of the infarct area ($P = 0.0007$ and 0.02 versus 1 week, respectively; **Table 1**). Infarct size was 15 ± 5% ($P = 0.00003$ versus 1 week; n = 13). CNR between remote myocardium and areas of signal voids was 34 ± 21 and between infarcted, non-hemorrhagic myocardium and areas of signal voids was 23 ± 6 (n = 3).

Table 1. Results of MRI scanning.

	Subacute infarcts (number of animals)	Chronic infarcts (number of animals)	*P* value
In vivo MRI:			
LV wall volume (cm^3)	63±15 (23)	85±13 (14)	0.00006
Infarct volume (% of LV volume)	25±6 (22)	15±5 (13)	0.00003
Animals with FPP defect	17 (21)	2 (13)	0.0007
FPP defect area (% of infarct area)	35±23 (21)	13±31 (13)	0.02
Animals with T2* signal void	5 (8)	3 (7)	NS
Area of T2* signal void (% of infarct area)	24±22 (8)	15±19 (7)	NS
CNR signal void vs infarct area	34±11 (5)	23±6 (3)	NS
Ex vivo MRI			
Area of T2* signal void (% of infarct area)	42±5 (8)	19±7 (11)	0.00001
CNR signal voids vs infarct area	17±9 (8)	14±8 (11)	NS
CNR cells ($4x10^6$) vs infarct area	18±4 (4)	15±1 (3)	NS

LV=left ventricle; FPP=first-pass perfusion; CNR=contrast-to-noise ratio.

Ex vivo MRI and histology

In subacute infarcts, the ex vivo high-resolution scans showed rings of magnetic susceptibility-induced signal voids on T1W and PDW scans (**Figure 3**). The size of the signal voids increased with a longer TE (T1-T2*W). The rings surrounded large hyperintense areas on T1W scans, which appeared hypointense on T2W and PD-T2*W scans. At histology, these rings of signal voids corresponded with blue deposits on Prussian blue staining and surrounded large areas of erythrocytes.

In chronic infarcts, ex vivo scans showed magnetic susceptibility-induced signal voids on T1W, PDW, T2W and T1- or PD-T2*W scans throughout the infarct area (**Figure 4**). Hyperintense areas were observed on T1W scans, which appeared hypointense on T2W and T1- or PD-T2*W scans (data not shown). Furthermore, hyperintense areas were observed on T2W scans, which appeared hypointense on T1W scans (data not shown).

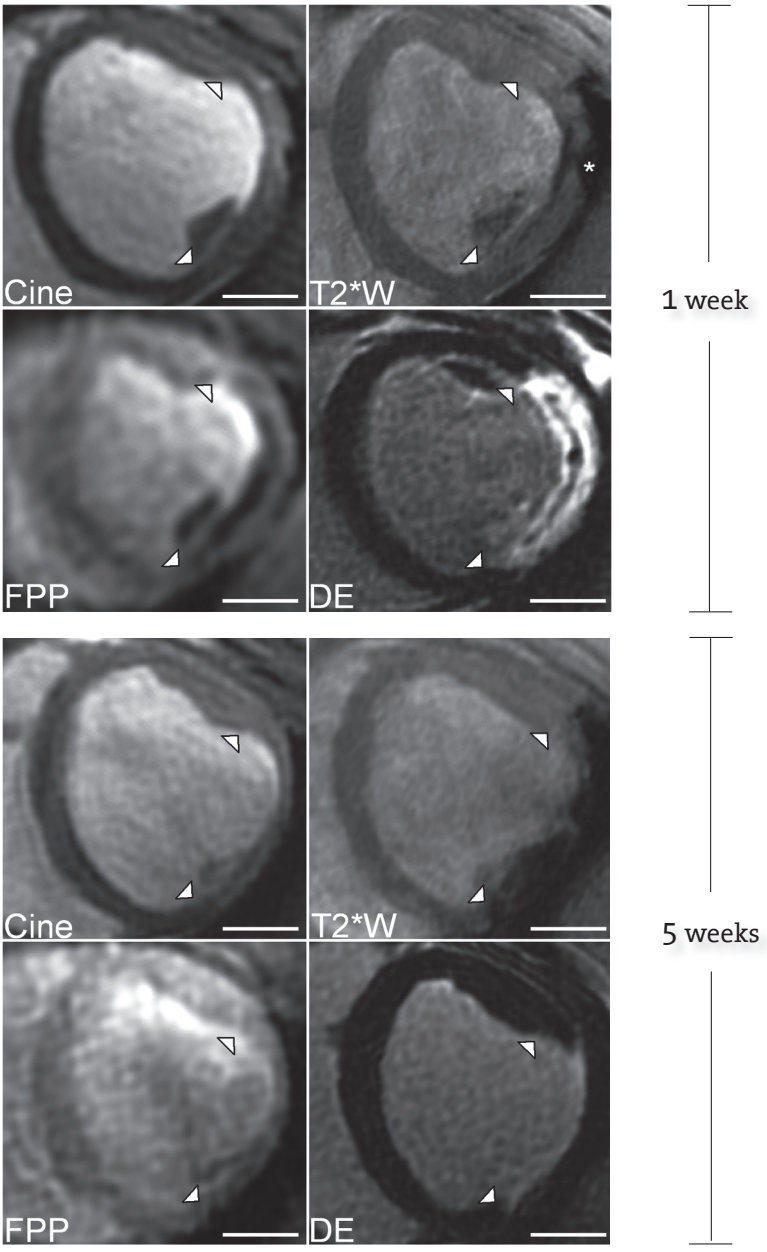

Figure 2. In vivo scans of one animal at 1 week (subacute) and 5 weeks (chronic) after infarction. Depicted are the end-diastolic frame of a cine, T2*W, FPP and DE scan at the same level. The infarct area is indicated by white arrows. In the T2*W image endo- and epicardial rims of signal voids are present at 1 week. The artifact caused by the heart-air interface is indicated by the asterisk. The rims of signal voids correspond with a zone of hypoperfusion in the FPP scan at 1 week, indicating MO. Furthermore, a zone of persistent hypoenhancement can be appreciated in the DE scan within the hyperenhanced infarct area. At 5 weeks, the area of signal voids in the T2*W image takes up a larger part of the infarct area. Neither MO nor an area of persistent hypoenhancement is observed in the FPP or DE scans. Bar indicates 2 cm.

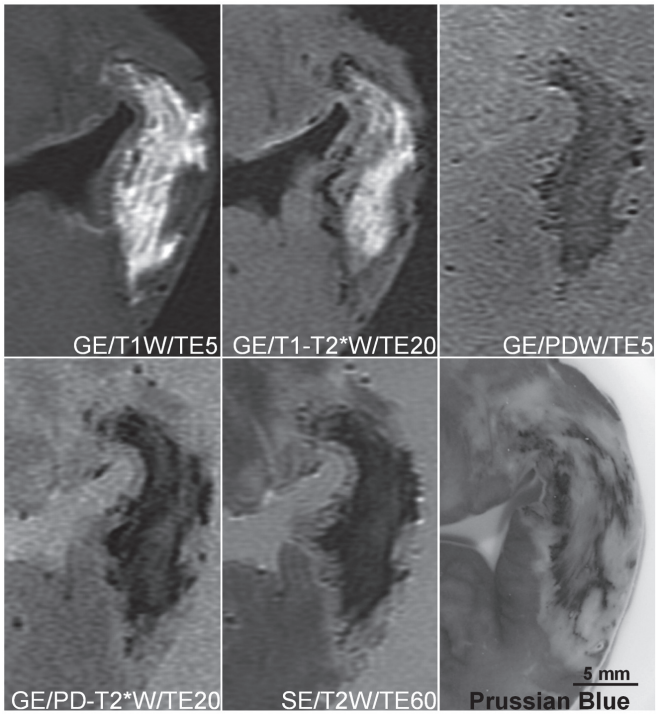

Figure 3. *Ex vivo* scans 1 week after infarction using different types of tissue contrast: T1W, PDW, T2W and T2*W with a TE of 5, 20 or 60 ms (TE5, TE20 or TE60, respectively). Either a gradient echo (GE) or spin echo (SE) sequence was used. A ring of black signal voids is identified best in the T1W scan with a TE of 20 ms (T1-T2*W). It corresponds with the blue hemosiderin deposits in the Prussian blue image. The ring surrounds a hyperenhanced area on T1W scans, which is hypoenhanced on SE/T2 and PD-T2*W scans, corresponding with methemoglobin within intact erythrocytes. *

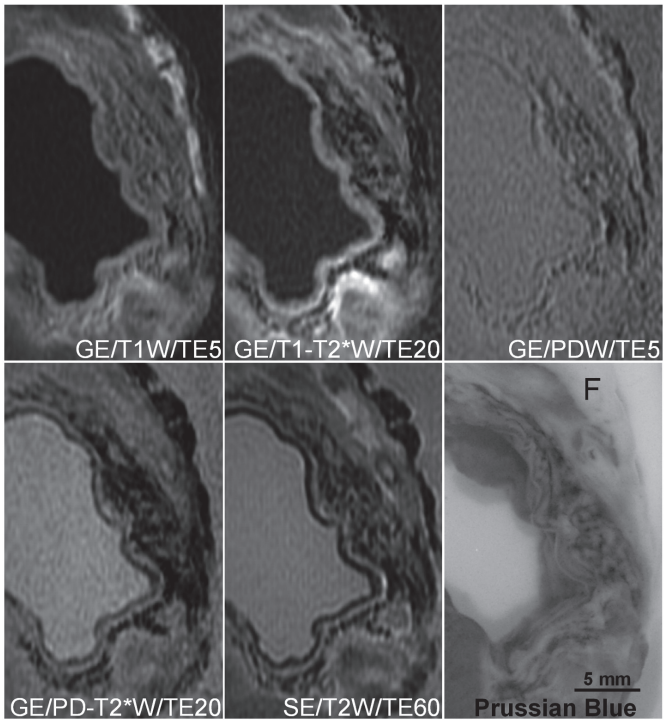

Figure 4. *Ex vivo* scans 5 weeks after infarction using various types of tissue contrast as described in Figure 3. Magnetic susceptibility-induced signal voids are observed throughout the infarct. Their size increases with T2*-weighting (TE 20 ms). Furthermore, signal voids correspond with blue hemosiderin deposits in the Prussian blue image. Epicardial fat, indicated by F, causes a hyperintense signal on the T1W scan and a hypointense signal on T2 and T2*W scans. *

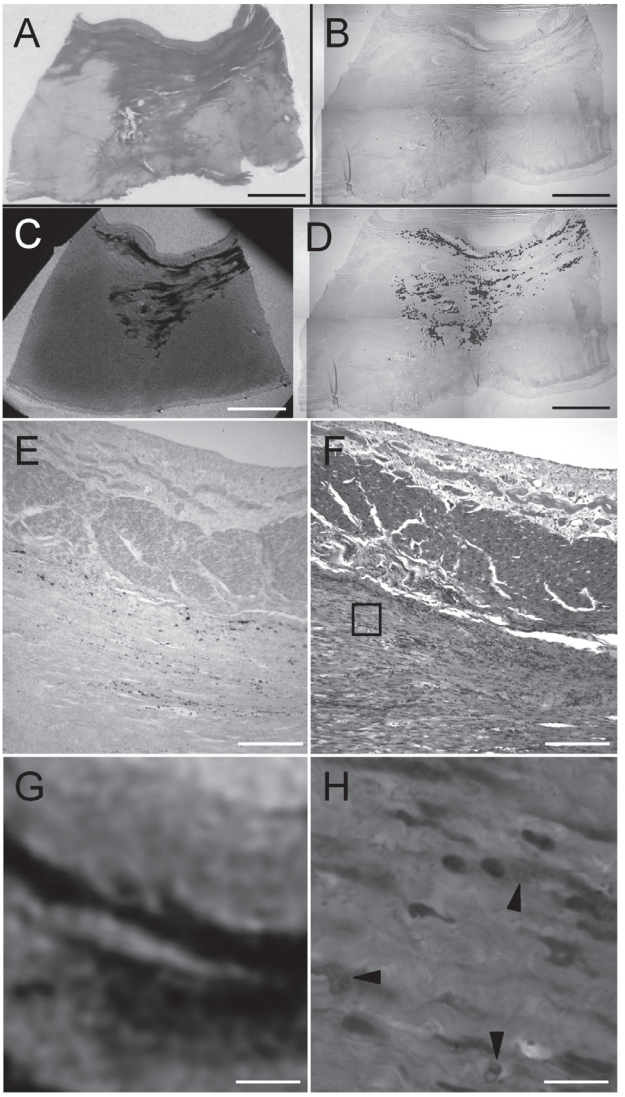

Figure 5. A tissue block from the infarct border of a 5-week old infarction was scanned at high-resolution ex vivo. *Panel A* shows the von Kossa's (calcium) and von Gieson (collagen) staining.

Red staining corresponds with collagenous (scar) tissue. Yellow staining corresponds with muscle fibers. Black calcium deposits were not observed in this section.

In *panel B* a serial section is shown after Prussian blue staining. *Panel C* shows the corresponding slice from the MRI T2*W data set. *Panel D* show the same section as in *panel B*, however blue regions are artificially enhanced. MRI signal voids correspond with blue hemosiderin particles and not with calcium, fat or collagenous tissue. *Panel E* shows the same section as in *panel B* at higher magnification. Blue hemosiderin deposits can be appreciated. *Panel F* shows a serial section after HE staining.

Panel G shows the corresponding region in the image of *panel A*. Area of signal voids correspond with blue hemosiderin deposits in *panel E*. *Panel H* shows the boxed region in *panel F* at higher magnification; hemosiderin deposits are visible as brownish particles (black arrows).

Bar indicates 1 cm in *panels A* to *D*. Bar indicates 400 μm in *panels E* to *G* and 40 μm in *panel H*. *

At histology, areas of signal voids matched the pattern of blue hemosiderin deposits after Prussian blue staining (**Figure 5**). No correlation was found with collagen, fat or calcium deposits.

Total hemorrhagic areas at mid-papillary level as a percentage of the total infarct area as determined by T2*W MRI were significantly larger in subacute than in chronic infarcts (P = 0.00001; n = 8 and 11, respectively; **Table 1**).

Post mortem injections with iron oxide-labeled cells could be located in remote, non-infarcted myocardium. CNR between depots of 4 x 106 labeled cells and infarcted, non-hemorrhagic myocardium was 18 ± 4 in subacute infarcts (n = 4) and 15 ± 1 in chronic infarcts (n = 3; **Table 1**). This was comparable with the CNR between hemorrhage-induced signal voids and infarcted, non-hemorrhagic myocardium in subacute infarcts (17 ± 9; n = 8) and chronic infarcts (14 ± 8; n = 11; Table 1). As a cause, in the infarct region, none of the injection sites could be reliably located and discerned from hemorrhage-induced signal voids (**Figure 6**).

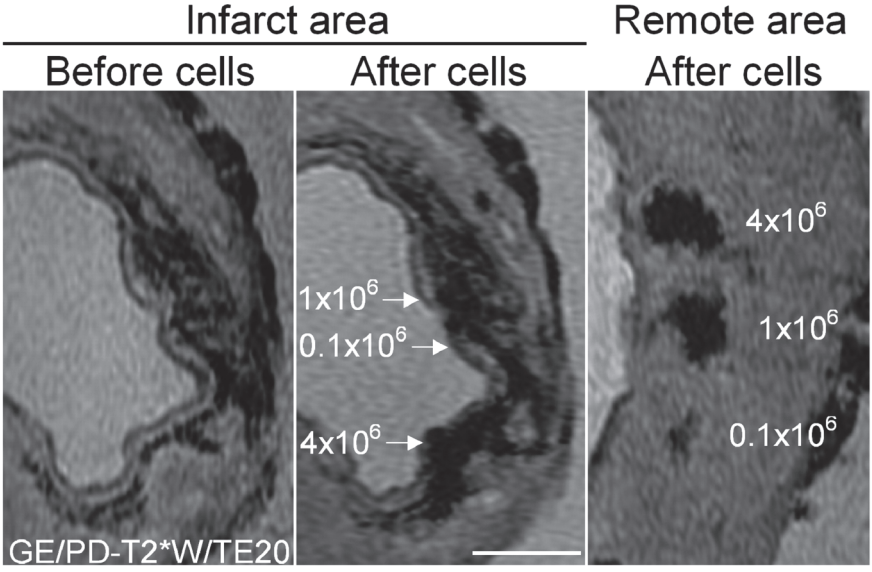

Figure 6. The left panel shows the GE/PD-T2*W/TE20 scan, depicted in Figure 4, before injection with iron oxide-labeled cells. The middle panel shows the same slice after injection with 0.1, 1 or 4 x106 iron oxide-labeled cells. The right panel shows a similar series of injections in remote, non-infarcted myocardium. Although the cell injections create larger areas of signal voids in the middle panel, their precise location cannot be determined due to the signal voids induced by the presence of hemoglobin degradation products. Bar indicates 0.5 cm.

Discussion

Myocardial infarct reperfusion and hemorrhage

Reperfusion of MI is known to induce progressive MO, also described as the "no-reflow" phenomenon.[19] As shown in both animal and clinical studies, MO is followed by the development of hemorrhage, probably due to loss of microvascular integrity.[20,24] The extent of the hemorrhagic area has been shown to correlate with the size of MO,[20] which was also observed in the present study.

Hemorrhage and MRI appearance

Few studies have been performed to evaluate the extent of the hemorrhagic area after reperfusion of MI using MRI.[24,25,26] One study demonstrated the presence of hemorrhage by spin echo imaging within 72h after reperfused MI in dogs.[25] Hypointense lesions corresponding with hemorrhage were found in 14 out of 16 animals. These lesions were not found in non-reperfused animals. Furthermore, in 2 clinical studies MRI was performed shortly after infarct reperfusion. The first study of 24 patients using gradient echo and contrast enhanced imaging showed hypointense areas within the infarct region in 38% of patients by both techniques.[24] In the second study, 39 patients were imaged using a T2*W GE sequence and hemorrhage could be identified as a hypointense zone within the infarct region in 33% of patients.[26] Because the 2 latter studies were done in patients, no histological comparison was possible. Furthermore, MRI was performed, on average, 6 days after MI, which is much shorter than the follow-up of 5 weeks used in the present study.

In contrast with intramyocardial hemorrhage, MRI appearance of intracranial hemorrhage has been given extensive attention.[21] Intracranial hemorrhage causes accumulation of deoxyhemoglobin within hours. Within days, deoxyhemoglobin is oxidized to methemoglobin, which causes T1 and T2 shortening due to its paramagnetic properties and magnetic susceptibility effect.[27,28] Therefore, the presence of methemoglobin within intact erythrocytes causes hyperintense signals on T1W scans and hypointense signals on T2W scans, a pattern observed in the present study in subacute infarcts. With further degradation, hemosiderin deposits are formed,[21] which remain chronically present.[29] Hemosiderin has a high magnetic susceptibility effect and thereby causes T2 shortening, resulting in signal voids on T1W, T2*W and T2W images surrounding the brain hemorrhage from 2 weeks onwards, the so called "ring" pattern. In the present study, the same ring pattern was observed in subacute infarcts in the ex vivo scans. This difference in time course might be due to the higher in plane resolution of ex vivo scanning, allowing early detection of such a pattern.

Iron oxide-labeled cell detection by MRI

Detection of iron oxide-labeled cells within MI has been described for mouse[9,10] and rabbit[11] models. Recently, several studies showed the feasibility of using iron oxide-labeled cells for clinically relevant, catheter-based delivery and cell tracking within MI in pigs. Infarcts were created by permanent coil occlusion[16,17] or a 60-90 min balloon occlusion followed by reperfusion of the infarct artery.[12,13,15] Cells were injected immediately after infarction[12,14] or into 1 day,[17] 1 week[15] or 4 week[13] old infarcts.

None of these studies mentioned the presence of MO or hemorrhage within the infarct center. In contrast, in the present study, MO was present in 17 out of 21 animals in subacute infarcts and signal voids were identified in all animals on the ex vivo scans corresponding with hemorrhage on histology. The high frequency of MO and hemorrhage could possibly be explained by the longer occlusion times used in our study (i.e. 2 hours versus 60 or 90 min),[12,13,15] approximating the time to reperfusion in the clinical setting more closely. The frequency of MO in the present study is indeed comparable to the frequency in patients reperfused early after MI.[22] Despite the longer occlusion times, it has been shown that hemorrhage already occurs in the pig heart after coronary occlusions more than 45 minutes.[30]

In a previous study, examining iron oxide-labeled cell detection in a mouse cryoinfarction model,[10] the presence of "spontaneous" signal voids within the infarct region was discussed. These signal voids were attributed to necrosis and fibrosis within the infarct scar. However, a recent study showed that cryoinfarction results in large areas of hemorrhage,[31] which have most likely caused those signal voids. Furthermore, the problem of those spontaneous signal voids was purportedly solved by using a combination of PD- and T2*-weighted scanning: the areas with signal voids that were exclusively due to the tissue lesions would lead to similar signal void sizes in both imaging modalities. In contrast, the size of the signal voids generated by the presence of labeled cells, was proposed to increase on T2*-weighted scans, thereby making unequivocal detection possible. However, Figures 3 and 4 clearly illustrate that the usefulness of this method could not be demonstrated in the present study, as the size of the hemorrhage-induced signal voids increased with a longer TE.

In studies of spinal cord regeneration by transplanted iron oxide-labeled cells,[32,33] interference of hemorrhage with cell detection has been described as an important confounding factor. In one study, the discrimination between cells and hemorrhage was made by assessing the "blooming" effect induced by iron oxide-labeled cells, where the distortion of the magnetic field occurs over a greater area than the presence of the contrast agent.[32] In another study, the use of imaging sequences less susceptible to hemorrhage-induced signal voids was proposed as a solution.[33]

For cell detection in vivo a certain number of labeled cells is necessary to obtain sufficient contrast with background tissue. For MI the smallest number of cells needed for detection was reported to be 105 cells/150 µl,[14] generating signal void volumes of 0.36 cm^3. This study however was performed in a model of permanent occlusion in pigs. In 3 studies of porcine, reperfused infarct models the number of cells per injection exceeded 28 x 106.[12,13,15] In the present study, the hemorrhage-associated signal voids in the in vivo scans had a mean total size of 0.53 ± 0.51 cm^3 in subacute infarcts, and therefore would possibly obscure detection of cell groups of ~105 cells. Furthermore, CNR of signal voids identified on the T2*W in vivo scans were similar to the values previously reported for groups of iron oxide-labeled cells using similar scanning sequences.[14] Finally, the ex vivo injections of iron oxide-labeled cells in the present study generated signal voids with a CNR similar to the hemorrhage-induced signal voids, thereby interfering with detection of the injected cells.

The presence of hemorraghe and visualisation with longer TE's is important in relation to the injection route as visualization of labeled cells was reported with local injections[12-17] while intracoronary injections have been used in most human studies.[3] Using iron labeling to track these cells, which will presumably spread over a larger area, requires sequences with long TE and the artifacts described in the present study are to be expected.

Study limitations

Since it is a very subjective process to match the image locations of in vivo scans with the locations of ex vivo scans based upon anatomical landmarks only, and since the slice thickness of in vivo scans was 6 or 8 mm as compared with 0.8 mm of ex vivo scans, we chose to describe in vivo and ex vivo findings separately. Therefore, our data do not allow for a direct comparison between in vivo and ex vivo scans.

In the present study a model of reperfused MI was used, causing large areas of hemorrhage. Therefore, it is not clear whether there is a difference in hemorrhage-induced artifacts in reperfused versus non-reperfused infarcts in porcine models in vivo, although in similar canine models no hemorrhage was observed when perfusion was not reinstated.[25]

Only intramyocardial injections were performed in the present study using fixed, iron oxide-labeled cells, which were imaged after tissue preparation. Future studies are required to investigate whether hemorrhage-induced signal voids cause similar interference with cell detection after intracoronary injection in vivo.

Conclusion

The present study demonstrates that hemorrhage in reperfused MI produces MRI signal voids, which may interfere with reliable tracking of iron oxide-labeled cells.

References

1. Orlic D, Kajstura J, Chimenti S, Jakoniuk I, Anderson SM, Li B, Pickel J, McKay R, Nadal-Ginard B, Bodine DM, Leri A, Anversa P. Bone marrow cells regenerate infarcted myocardium. Nature 2001;410:701-705.
2. van den Bos EJ, Thompson RB, Wagner A, Mahrholdt H, Morimoto Y, Thomson LE, Wang LH, Duncker DJ, Judd RM, Taylor DA. Functional assessment of myoblast transplantation for cardiac repair with magnetic resonance imaging. Eur J Heart Fail 2005;7:435-443.
3. Schachinger V, Assmus B, Britten MB, Honold J, Lehmann R, Teupe C, Abolmaali ND, Vogl TJ, Hofmann WK, Martin H, Dimmeler S, Zeiher AM. Transplantation of progenitor cells and regeneration enhancement in acute myocardial infarction: final one-year results of the TOPCARE-AMI Trial. J Am Coll Cardiol 2004;44:1690-1699.
4. Smits PC, van Geuns RJ, Poldermans D, Bountioukos M, Onderwater EE, Lee CH, Maat AP, Serruys PW. Catheter-based intramyocardial injection of autologous skeletal myoblasts as a primary treatment of ischemic heart failure: clinical experience with six-month follow-up. J Am Coll Cardiol 2003;42:2063-2069.
5. Yeh TC, Zhang W, Ildstad ST, Ho C. Intracellular labeling of T-cells with superparamagnetic contrast agents. Magn Reson Med 1993;30:617-625.
6. Foster-Gareau P, Heyn C, Alejski A, Rutt BK. Imaging single mammalian cells with a 1.5 T clinical MRI scanner. Magn Reson Med 2003;49:968-971.
7. Shapiro EM, Skrtic S, Sharer K, Hill JM, Dunbar CE, Koretsky AP. MRI detection of single particles for cellular imaging. Proc Natl Acad Sci U S A 2004;101:10901-10906.
8. Zhang Z, van den Bos EJ, Wielopolski PA, de Jong-Popijus M, M. Bernsen, Duncker DJ, Krestin GP. In vitro imaging of single living human umbilical vein endothelial cells with a clinical 3.0T MRI scanner. MAGMA 2005;18:175-185.
9. Himes N, Min JY, Lee R, Brown C, Shea J, Huang X, Xiao YF, Morgan JP, Burstein D, Oettgen P. In vivo MRI of embryonic stem cells in a mouse model of myocardial infarction. Magn Reson Med 2004;52:1214-1219.
10. Kustermann E, Roell W, Breitbach M, Wecker S, Wiedermann D, Buehrle C, Welz A, Hescheler J, Fleischmann BK, Hoehn M. Stem cell implantation in ischemic mouse heart: a high-resolution magnetic resonance imaging investigation. NMR Biomed 2005;18:362-370.
11. van den Bos EJ, Wagner A, Mahrholdt H, Thompson RB, Morimoto Y, Sutton BS, Judd RM, Taylor DA. Improved efficacy of stem cell labeling for magnetic resonance imaging studies by the use of cationic liposomes. Cell Transplant 2003;12:743-256.

12. Kraitchman DL, Heldman AW, Atalar E, Amado LC, Martin BJ, Pittenger MF, Hare JM, Bulte JW.In vivo magnetic resonance imaging of mesenchymal stem cells in myocardial infarction. Circulation 2003;107:2290-2293.
13. Garot J, Unterseeh T, Teiger E, Champagne S, Chazaud B, Gherardi R, Hittinger L, Gueret P, Rahmouni A. Magnetic resonance imaging of targeted catheter-based implantation of myogenic precursor cells into infarcted left ventricular myocardium. J Am Coll Cardiol 2003;41:1841-1846.
14. Hill JM, Dick AJ, Raman VK, Thompson RB, Yu ZX, Hinds KA, Pessanha BS, Guttman MA, Varney TR, Martin BJ, Dunbar CE, McVeigh ER, Lederman RJ.Serial cardiac magnetic resonance imaging of injected mesenchymal stem cells. Circulation 2003;108:1009-1014.
15. Baklanov DV, Demuinck ED, Thompson CA, Pearlman JD. Novel double contrast MRI technique for intramyocardial detection of percutaneously transplanted autologous cells. Magn Reson Med 2004;52:1438-1442.
16. Karmarkar PV, Kraitchman DL, Izbudak I, Hofmann LV, Amado LC, Fritzges D, Young R, Pittenger M, Bulte JW, Atalar E. MR-trackable intramyocardial injection catheter. Magn Reson Med 2004;51:1163-1172.
17. Dick AJ, Guttman MA, Raman VK, Peters DC, Pessanha BS, Hill JM, Smith S, Scott G, McVeigh ER, Lederman RJ. Magnetic resonance fluoroscopy allows targeted delivery of mesenchymal stem cells to infarct borders in Swine. Circulation 2003;108:2899-2904.
18. Giugliano RP, Braunwald E; The TIMI Study Group. Selecting the best reperfusion strategy in ST-elevation myocardial infarction: it's all a matter of time. Circulation 2003;108:2828-2830.
19. Rochitte CE, Lima JA, Bluemke DA, Reeder SB, McVeigh ER, Furuta T, Becker LC, Melin JA. Magnitude and time course of microvascular obstruction and tissue injury after acute myocardial infarction. Circulation 1998;98:1006-1014.
20. Reffelmann T, Kloner RA. Microvascular reperfusion injury: rapid expansion of anatomic no reflow during reperfusion in the rabbit. Am J Physiol Heart Circ Physiol 2002;283:H1099-H1107.
21. Bradley WG Jr. MR appearance of hemorrhage in the brain. Radiology 1993;189:15-26.
22. Baks T, van Geuns RJ, Biagini E, Wielopolski P, Mollet NR, Cademartiri F, Boersma E, van der Giessen WJ, Krestin GP, Duncker DJ, Serruys PW, de Feyter PJ. Recovery of left ventricular function after primary angioplasty for acute myocardial infarction. Eur Heart J 2005;26:1070-1077.
23. Lund GK, Stork A, Saeed M, Bansmann MP, Gerken JH, Muller V, Mester J, Higgins CB, Adam G, Meinertz T. Acute myocardial infarction: evaluation with first-pass enhancement and delayed enhancement MR imaging compared with 201Tl SPECT imaging. Radiology 2004;232:49-57.
24. Asanuma T, Tanabe K, Ochiai K, Yoshitomi H, Nakamura K, Murakami Y, Sano K, Shimada T, Murakami R, Morioka S, Beppu S. Relationship between progressive microvascular damage and intramyocardial hemorrhage in patients with reperfused anterior myocardial infarction: myocardial contrast echocardiographic study. Circulation 1997;96:448-453.
25. Lotan CS, Bouchard A, Cranney GB, Bishop SP, Pohost GM. Assessment of postreperfusion myocardial hemorrhage using proton NMR imaging at 1.5 T. Circulation 1992;86:1018-1025.

26. Ochiai K, Shimada T, Murakami Y, Ishibashi Y, Sano K, Kitamura J, Inoue S, Murakami R, Kawamitsu H, Sugimura K. Hemorrhagic myocardial infarction after coronary reperfusion detected in vivo by magnetic resonance imaging in humans: prevalence and clinical implications. J Cardiovasc Magn Reson 1999;1:247-256.
27. Vymazal J, Brooks RA, Patronas N, Hajek M, Bulte JW, Di Chiro G. Magnetic resonance imaging of brain iron in health and disease. J Neurol Sci 1995;134:19-26.
28. Anzalone N, Scotti R, Riva R. Neuroradiologic differential diagnosis of cerebral intraparenchymal hemorrhage. Neurol Sci 2004;25:S3-S5.
29. Hardy PA, Kucharczyk W, Henkelman RM. Cause of signal loss in MR images of old hemorrhagic lesions. Radiology 1990;174:549-555.
30. Garcia-Dorado D, Theroux P, Alonso J, Elizaga J, Botas J, Fernandez-Aviles F, Soriano J, Munoz R, Solares J. Intracoronary infusion of superoxide dismutase and reperfusion injury in the pig heart. Basic Res Cardiol 1990;85:619-629.
31. van den Bos EJ, Mees BM, de Waard MC, de Crom R, Duncker DJ. A Novel Model of Cryoinjury-Induced Myocardial Infarction in the Mouse: A Comparison with Coronary Artery Ligation. Am J Physiol Heart Circ Physiol 2005;289:H1291-H1300.
32. Dunning MD, Lakatos A, Loizou L, Kettunen M, ffrench-Constant C, Brindle KM, Franklin RJ. Superparamagnetic iron oxide-labeled Schwann cells and olfactory ensheathing cells can be traced in vivo by magnetic resonance imaging and retain functional properties after transplantation into the CNS. J Neurosci 2004;24:9799-9810.
33. Dunn EA, Weaver LC, Dekaban GA, Foster PJ. Cellular imaging of inflammation after experimental spinal cord injury. Mol Imaging 2005;4:53-62.

Part 3

Clinical Application of Magnetic Resonance Imaging

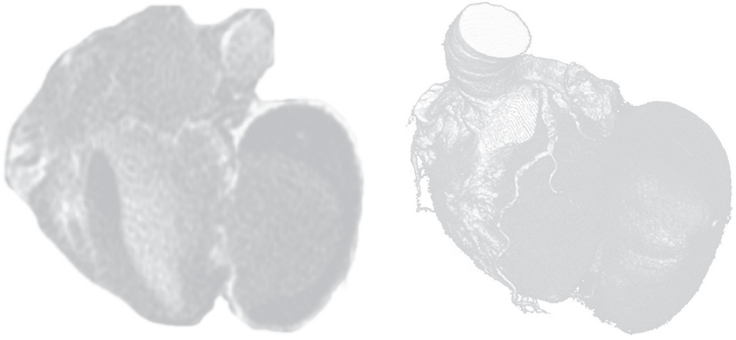

Recovery of Left Ventricular Function after Primary Angioplasty for Acute Myocardial Infarction

Timo Baks; Robert-Jan van Geuns; Elena Biagini; Piotr Wielopolski; Nico R. Mollet; Filippo Cademartiri; Willem J. van der Giessen; Gabriel P. Krestin; Dirk J. Duncker; Patrick W. Serruys; Pim J. de Feyter

Eur Heart J. 2005;26:1070-7

7

1, 2, 3, 4, 5, 6, 8, 9, 10, 11, 12, 13, 14, 15

Abstract

Aim

To study recovery of segmental wall thickening (SWT), ejection fraction (EF) and end-systolic volume (ESV) after acute myocardial infarction (AMI) in patients who underwent primary stenting with drug-eluting stents. Additionally, to evaluate the predictive value of magnetic resonance imaging (MRI)-based myocardial perfusion and delayed enhancement (DE) imaging.

Methods and Results

Twenty-two patients underwent cine-MRI, first-pass perfusion and DE imaging 5 days after successful placement of a drug-eluting stent in the infarct-related coronary artery. Regional myocardial perfusion and the transmural extent of DE were evaluated. A per patient perfusion score was calculated and consisted of a summation of all segmental scores. Myocardial infarct size was quantified by measuring the volume of DE. At 5 months after AMI, cine-MRI was performed and SWT, EF and ESV were quantified. EF increased from 48 ± 11% to 55 ± 9% ($p<0.01$). SWT at 5 months was inversely related to baseline segmental DE scores ($p<0.001$) and segmental perfusion scores ($p<0.001$). EF and ESV at 5 months were related to acute infarct size ($R^2 = 0.65$; $p < 0.001$ and $R^2 = 0.78$; $p < 0.001$ respectively) and the calculated perfusion score ($R^2 = 0.23$; $p = 0.02$ and $R^2 = 0.14$;$p = 0.09$ respectively) at baseline.

Conclusions

Marked recovery of left ventricular function was observed in patients receiving a drug-eluting stent for AMI. DE imaging appears to be a better prognosticator than perfusion imaging.

Abbreviations

ce-MRI	-	contrast-enhanced Magnetic Resonance Imaging
AMI	-	acute myocardial infarction
EF	-	ejection fraction
ESV	-	end systolic volume
EDV	-	end diastolic volume
SWT	-	segmental wall thickening
DE	-	delayed enhancement
CPK	-	Phosphocreatine Kinase

Introduction

At present, the preferred reperfusion treatment for patients with acute myocardial infarction (AMI) is early primary angioplasty with the placement of a drug-eluting stent in the infarct related coronary artery [1-3]. Early restoration of coronary blood flow by primary angioplasty salvages myocardium at risk and reduces infarct size, but may also lead to distal embolization and microvascular plugging, resulting in microvascular obstruction [4,5]. These regions with microvascular obstruction within the infarcted myocardium can be detected by first-pass perfusion imaging performed with Magnetic Resonance Imaging (MRI)[6]. Total myocardial infarct size (region with myocyte necrosis) and the transmural extent of infarction can be demonstrated with delayed enhancement (DE) imaging performed 10-20 minutes following perfusion imaging [7]. Although previous studies demonstrated the value of perfusion and DE imaging for predicting regional and global myocardial function at long term follow-up after AMI [8-13], the results of these studies have been equivocal. Differences in outcome may have been caused by differences in reperfusion therapy, time to reperfusion, and timing of baseline scan. In the present study, a well-defined group of patients who suffered AMI underwent myocardial perfusion and DE imaging 5 days after primary stenting with a drug-eluting stent. Specifically, we studied segmental wall thickening (SWT), ejection fraction (EF), end-systolic (ESV) and end-diastolic volume (EDV) at 5 months after AMI. Additionally, we investigated the predictive values of perfusion and DE imaging.

Methods

Patient Population

Patients with an AMI who received a drug-eluting stent in the infarct related coronary artery within 6 h of onset of symptoms were possible candidates for the present study. Inclusion of patients was hampered by the fact that patients referred from other hospitals were transferred back within a few hours after primary angioplasty. Eventually, we studied 30 patients (25 male, 53 ± 10 years old) admitted to the coronary care unit with AMI. Three possible candidates refused to participate: one patient was visiting from another country, two patients were claustrophobic. Diagnosis of AMI was based on clinical symptoms, ST-segment elevation on electrocardiogram and angiographically demonstrated occlusion of a coronary artery. All culprit lesions were stented with a drug-eluting stent within 6 hours (mean 2.5 hours) of onset of symptoms. Thrombolysis In Myocardial Infarction (TIMI) flow grade 3 was obtained in all vessels. Exclusion criteria consisted of any contraindication to MRI. All participants

gave informed consent to the study protocol, which was approved by the medical ethics committee of the Erasmus MC University Hospital, Rotterdam. Of the original study population, 22 patients had both the first MRI scan 5 ± 3 days after admission and the second MRI scan 20 ± 7 weeks later. Eight patients did not undergo a second scan; 1 patient died of a stroke (non-cardiac death), 2 patients had a defibrillator implanted and 5 patients refused to come back.

MRI protocol

A clinical 1.5-Tesla MRI scanner with a dedicated cardiac four element phased-array receiver coil was used for imaging (Signa CV/i, GE Medical systems, Milwaukee, Wisconsin). Repeated breath-holds and gating to the electrocardiogram were applied to minimize the influence of cardiac and respiratory motion on data collection. The first ce-MRI protocol consisted of cine-MRI, first-pass perfusion imaging and DE imaging. The second MRI protocol consisted of cine-MRI alone.

SWT and left ventricular volumes were assessed with cine-MRI using a steady-state free-precession technique (FIESTA) with the following imaging parameters: 6-10 seconds per breath-hold per slice (depending on heart rate), 24 phases per slice location, Field of View: 36 x 36 cm; TR 3.4; TE 1.4; flip angle 45 degrees; matrix 160 x 128, bandwidth 83 kHz, 0.75 NEX.) To cover the entire left ventricle, 9 to 12 consecutive slices of 8 mm were planned in short axis view (gap of 2 mm) perpendicular to the horizontal long axis (4-chamber view) of the left ventricle.

First-pass perfusion imaging was performed during 30-40 consecutive heart beats after administration of Gadolinium-DTPA (0.1 mmol/kg, Magnevist®, Schering). The pulse sequence consisted of a preparation sequence followed by an interleaved gradient-echo echo-planar sequence[14]. The temporal resolution per slice was 120 ms and allowed imaging of 5-8 slices within each R - R interval depending on heart rate. The following imaging parameters were used: FOV: 36 x 36, rectFOV 0.75, TR 6.8, TE 1.2, ET 4, bandwidth 125 kHz, flip angle 20 degrees, matrix 128/96. Perfusion images were planned to cover the basal, mid and apical part of the left ventricle in the same direction as the cine images.

Myocardial distribution of DE was studied 10-20 minutes following perfusion imaging with a 2-dimensional T1-weighted inversion recovery gradient-echo sequence with the following imaging parameters; FOV: 40 x 32 cm, slice thickness 8 mm gap 2 mm, TR 7.3, TE 1.6, flip angle 20 degrees, TI 180 - 275 ms, matrix 256 x192, 1 NEX, bandwidth 17.9 kHz. The inversion time was adjusted per patient to null the signal of remote myocardium. Slice locations of the DE-images were copied from the cine images.

Data analysis and Definitions

First-pass perfusion, DE, and cine-MR images were matched for position using anatomical landmarks like papillary muscles and the insertion of the right ventricle. For regional analysis, the left ventricle was divided in 16 myocardial segments. Two investigators (T.B. and RJ.v.G.), blinded to the clinical data, analysed all perfusion and DE segments and a decision was made on the basis of consensus.

Dedicated post-processing software was used to quantify left ventricular wall thicknesses and left ventricular volume (centreline method; Mass, Medis, Leiden, the Netherlands). SWT was calculated by subtracting the end-diastolic wall thickness from the end-systolic wall thickness and was expressed in millimetres. ESV and EDV were quantified by drawing endocardial and epicardial contours on the short axis series of the cine-MR images and EF was calculated as: (EDV – ESV)/ EDV * 100%. Papillary muscles were considered as part of the left ventricular lumen and hence included in the left ventricular volume.

Myocardial perfusion was evaluated per segment and scored as: 1, normal perfusion (homogeneous enhancement of myocardium); 2, mild perfusion defect (subendocardial layer of hypoenhancement); and 3, severe perfusion defect (> 30% transmural extent of hypoenhancement) (**Figure 1**).

A myocardial perfusion score was calculated per patient and consisted of a summation of all segmental perfusion scores. All patients had the same amount of segments (sixteen) in the calculated perfusion score. DE-myocardium was clearly differentiated from remote myocardium (nulled signal) with the use of an inversion recovery pulse

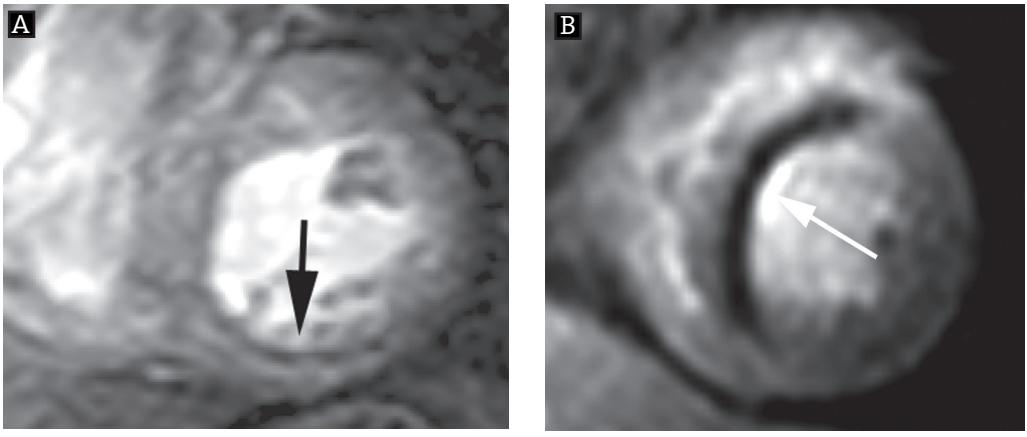

Figure 1. First-pass perfusion images in patients 5 days after AMI indicating (**A**) subendocardial perfusion defect (score 2) in the inferior wall and (**B**) a severe perfusion defect in the interventricular septum extending the subendocardium (score 3).

sequence. The volume of DE was quantified by manually selecting the enhanced regions from the consecutive 2D slices encompassing the left ventricle. DE volume was multiplied by 1.05 gr/ml to obtain myocardial infarct mass (1 millilitre corresponds to 1.05 gram). Also, the transmural extent of DE was scored per segment as: 1 = 0 % (no DE), 2 = 1–25 % (transmural extent of DE), 3 = 26–50 %, 4 = 51–75 % ; 5 = 76–100 %. A myocardial segment was judged as non-assessable if the region of DE could not be differentiated clearly from the healthy myocardium (breathing artifacts, erroneous ECG triggering).

Statistical analysis

Continuous data are expressed as mean ± standard deviation, and dichotomous data are expressed as numbers and percentages. Paired Student`s t-tests were applied to evaluate differences in EF, ESV, and EDV between baseline (i.e. 5 days post-AMI) and follow-up (i.e. 5 months post-AMI). The relation between the baseline DE scores and follow-up SWT was analyzed by one-way-analysis of variance (ANOVA). However, these analyses should be interpreted with care since possible correlations between segments within patients might exist with consequent possible underestimates for the standard errors and hence for the corresponding P-values. Univariate linear regression analyses were applied to evaluate the relationship between the separate prediction variables (CPK, the per patient calculated perfusion score, acute infarct mass) and EF, ESV and EDV at follow-up. Similar analyses were performed to study the relation between the separate prediction variables and the change in EF, ESV, and EDV between baseline and follow-up. Multiple linear regression analyses were then applied to evaluate to what extent the separate prediction variables had additive predictive value for EF, ESV and EDV at follow-up. The first model evaluated the additive predictive value of the calculated perfusion score in addition to CPK. The second model evaluated the additive predictive value of acute infarct mass in addition to CPK. The third model evaluated the additive predictive value of the calculated perfusion score and the acute infarct mass in addition to CPK. All prediction variables were put in the model at once (no elimination procedure). The linearity assumption was assessed by examining the scatter plots (**Figure 3** and **5**) and these demonstrated that no other than linear relationships were to be expected. Furthermore, a normal distribution of the residuals was found (p-p plots of regression standardized residuals) and the mean value of the residuals was zero. We report regression coefficients (β) with 95%-confidence intervals, P-values and model R^2-values (percentage of variance in the outcome variable explained by the prediction variable). All tests were 2-sided, and statistical significance was accepted at $p \leq 0.05$. SPSS for Windows, release 11.0.1, SPSS Inc, was used for all analyses.

Table 1 Patient characteristics (n = 22)

Age (years)	52±12
Men	16 (73)
Smoking	15 (68)
Diabetic Mellitus	1 (5)
Hypertension	6 (27)
Hypercholesterolemia	5 (23)
Family history of coronary artery disease	12 (55)
Post acute myocardial infarction	
Left ventricular ejection fraction (%)	48 ±11
Creatine kinase peak (IU)	3112±2001
Anterior Infarction	15 (68)
Inferior/Lateral infarction	6 (27)
Abciximab	14 (64)
ACE inhibitor	18 (82)
β - Blocker	22 (100)
Clopidogrel	22 (100)
Statin	20 (91)
ASA	22 (100)

Values are presented as number (%) or mean ± standard deviation

Results

Patient population

Fifteen patients had an anterior AMI, while 7 patients had an AMI of the inferior or lateral wall. Mean peak CPK level in all patients was 3112 ± 2001 U/l (range 187 to 7359 U/l). More patient characteristics are listed in Table 1. EF increased from 48±11% at baseline to 55±9% ($p < 0.01$) at follow-up. ESV remained unchanged (84±4 ml to 81±4 ml; $p = 0.6$), but EDV increased from 160±44 ml to 172±55 ml at follow-up ($p = 0.03$).

Regional analysis

Myocardial perfusion could be evaluated in all 352 segments. In 30 (9%) segments a mild subendocardial perfusion defect was detected and 30 (9%) segments exhibited a severe perfusion defect extending beyond the subendocardium (**Figure 1**, **Table 2**).

All perfusion defects were located within the perfusion territory of the infarct related coronary artery. An inverse relation was found for the perfusion status of the microvasculature at 5 days after AMI and SWT at 5 months after AMI ($p<0.001$; **Figure 2**). The transmural extent of DE could be evaluated in 320 segments. Thirty-two segments (9%) were not assessable due to image quality. In 105 (32%) segments, a pattern of DE was detected located within the perfusion territory of the infarct related coronary artery (Table 2). An inverse relation was found for the transmural extent of DE at 5 days after AMI and SWT at 5 months after AMI ($p<0.001$; **Figure 3**).

	segmental Delayed Enhancement score					
segmental Perfusion score	***1***	***2***	***3***	***4***	***5***	**Total # segments**
1	212	18	11	11	8	260
2	3	3	14	5	5	30
3	0	0	4	6	20	30
Total # segments	215	21	29	22	33	**320**

Table 2. An overview of all segmental perfusion and DE scores.

Global left ventricular analysis

A positive correlation between time to reperfusion and the perfusion score ($R = 0.48$; $p < 0.05$) was observed. Univariate regression analysis revealed that the per patient calculated perfusion score was statistically significant related to EF at follow-up, such that patients with lowest perfusion score had highest EF ($R2 = 0.23$; **Figure 4**, **Table 3**). Baseline calculated perfusion scores were not related to ESV and EDV at follow-up. Also,

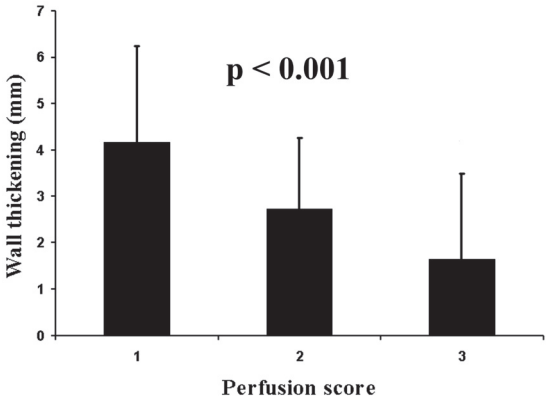

Figure 2. Myocardial segments with mild or severe perfusion defects demonstrated impaired SWT at 5 months post AMI (ANOVA; $p < 0.001$). 1 = normal perfusion; 2 = subendocardial perfusion defect ; 3 = severe perfusion defect (also Figure 1).

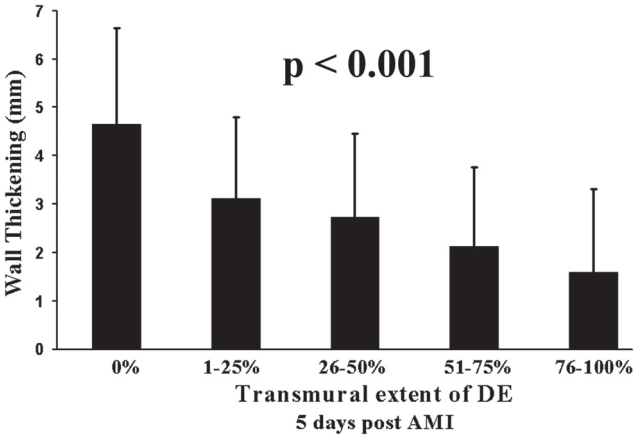

Figure 3. Segmental wall thickening at 5 months post AMI is inversely related to the transmural extent of DE at 5 days post-AMI. (ANOVA; $p < 0.001$)

no relation was found for the calculated perfusion score and the change in EF, ESV, and EDV between baseline and follow-up. Univariate regression analysis revealed that quantified acute infarct mass was statistically significant related to EF ($R^2 = 0.65$), ESV ($R^2 = 0.78$), and EDV ($R^2 = 0.68$) at 5 months post AMI (**Figure 5**, **Table 3**). Acute infarct mass was also associated with the change in ESV ($R^2 = 0.37$) and EDV ($R^2 = 0.44$), but not with the change in EF ($R^2 = 0.19$). Quantified acute myocardial infarct mass was correlated with peak CK concentrations ($R = 0.76$, $p < 0.001$). Univariate regression analyses revealed that CPK peak concentrations were statistically significant related to EF ($R^2 = 0.33$), ESV ($R^2 = 0.28$), and EDV ($R^2 = 0.22$) at follow-up. The results of the multiple regression ana-lyses are listed in **Table 3**. The calculated perfusion score had no additive predictive value in addition to CPK with regard to EF, ESV, and EDV at follow-up. Acute infarct mass had additive predictive value in addition to CPK with regard to EF, ESV, and EDV at follow-up. Finally, with all prediction variables in the model, acute infarct mass was the only significant predictor of EF, ESV, and EDV at 5 months after infarction.

Discussion

The present study demonstrates the recovery of left ventricular function in patients who suffered AMI and were treated with a drug-eluting stent in the infarct related coronary artery within 6 h of onset of symptoms. Additionally, the predictive value of perfusion and DE imaging performed at 5 days after AMI was evaluated. The main findings were that (i) a marked increase in overall mean EF was observed compared to previously published data [9,11], (ii) EF, ESV, and EDV at 5 months after AMI can be estimated by performing ce-MRI 5 days after AMI. DE imaging appears to be a better prognosticator than perfusion imaging, and (iii) although epicardial coronary blood flow was restored in all patients within 6 h of onset of symptoms, microvascular obstruction was identified with perfusion imaging at 5 days post AMI in 19 patients (87%).

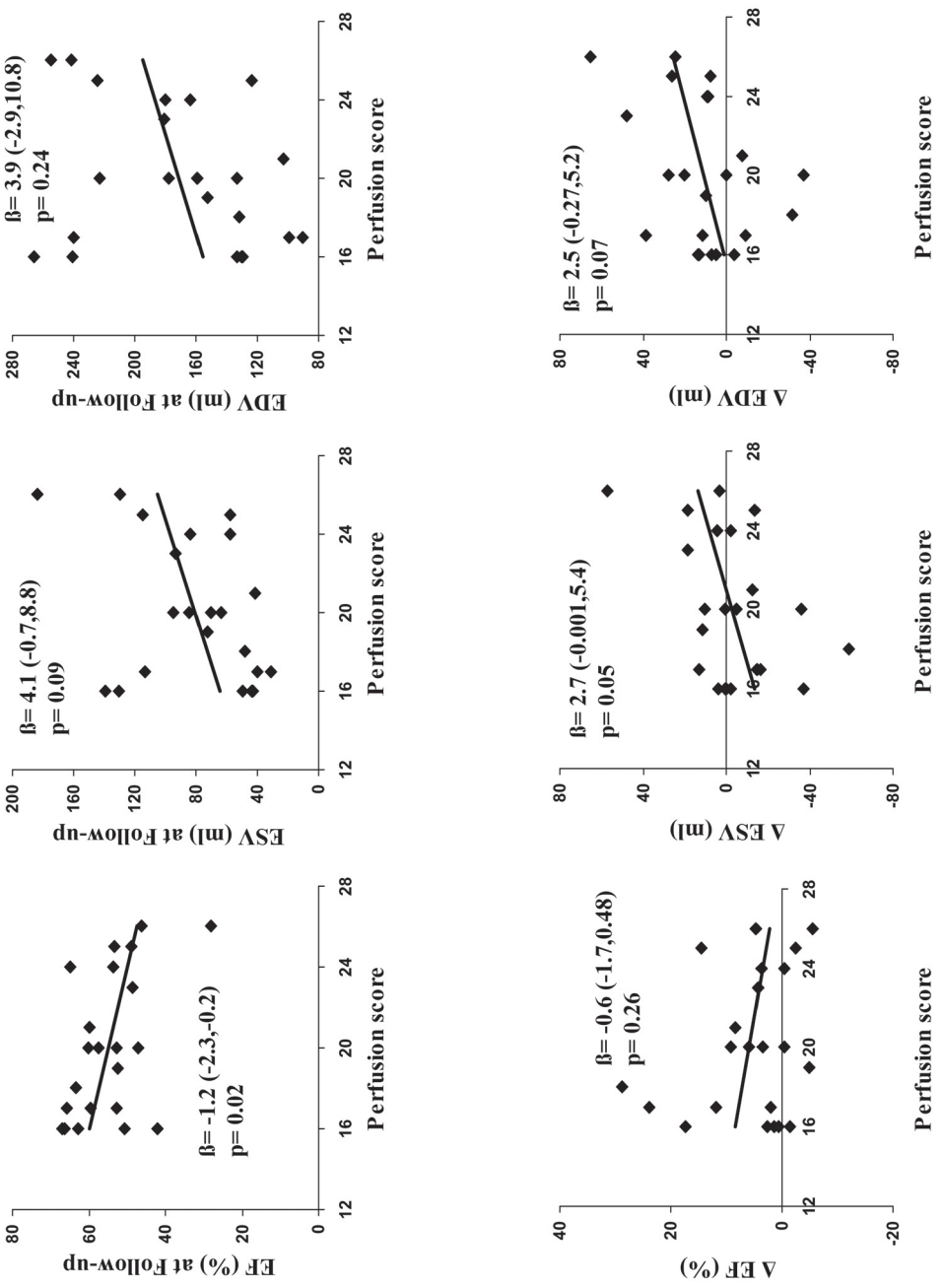

Figure 4. The calculated perfusion score per patient correlated better with EF at 5 months after AMI than the change in EF between 5 days and 5 months post-AMI. The calculated perfusion score was not related to ESV and EDV at 5 months follow-up and the change in ESV and EDV between 5 days and 5 months post AMI. (Δ = change between 5 days and 5 months)

Previous studies have investigated the recovery of regional and global left ventricular function in patients who suffered AMI by performing ce-MRI. However, results of these studies have been equivocal. Gerber et al.[10] performed perfusion and DE imaging 4 days after AMI and found that perfusion imaging was less accurate than DE imaging in predicting regional contractile recovery at 7 months. In contrast, Taylor et al.[13] performed perfusion imaging in patients within 24 h after AMI and reported that a delayed wash-in of contrast in the infarcted myocardium was a better predictor than DE imaging of recovery of SWT and EF 3 months after AMI. In the present study, EF, ESV, and EDV at 5 months after AMI appeared to be better predicted by DE imaging than by perfusion imaging. Furthermore, an inverse relation between DE and regional contractile function after 5 months of follow-up was observed, with minimal SWT in segments with >75% transmural extent of DE. The majority of the studies using only DE imaging reported an inverse relation between the transmural extent of DE and improvement in regional contractile function, with generally minimal improvement in dysfunctional segments with a >75% transmural extent of DE. For example, Ingkanisorn et al.[11] assessed SWT in patients after AMI and reported an inverse relationship between de transmural extent of DE and SWT at follow-up study. Choi et al. [8], reported that only 5% of segments with a >75% transmural extent of DE demonstrated an improved contractile function at follow-up, whereas Beek et al. [9] reported improvement in 29% of these segments, although severe dysfunction remained present in the majority of these segments. In contrast with all other studies, Petersen et al. [12] reported that only segments with a >75% transmural extent of DE improved.

The different outcomes in the various studies are difficult to explain, but could be caused by a number of confounding factors. First, patients with different reperfusion strategies for AMI like primary angioplasty, thrombolysis, and spontaneous resolution of infarct symptoms, were included. Primary PCI with the placement of a drug-eluting stent in the infarct related artery is presently the preferred reperfusion treatment for AMI. TIMI 3 flow in the infarct related artery can be accomplished in most cases and very low numbers of restenosis have been reported. Residual stenosis or restenosis of an infarct-related artery is often found in patients treated with thrombolysis and this influences the remodelling process. Secondly, time to reperfusion varied from < 6 h [13] to 1 month[11] after onset of symptoms. Time to reperfusion determines the amount of stunned (salvaged) and necrotic myocardium [15] and the integrity of the microvasculature [4,5]. Thirdly, baseline scans were performed between < 24 h [13] up to 21 days after AMI [12]. Myocardial infarct evolution is a complex process of early infarct expansion (up to 48 h post-AMI) [16] followed by myocardial infarct shrinkage in time [11]. Perfusion and DE imaging parameters will subsequently alter with proceeding time after AMI. Infarct size might be underestimated with DE imaging if performed too

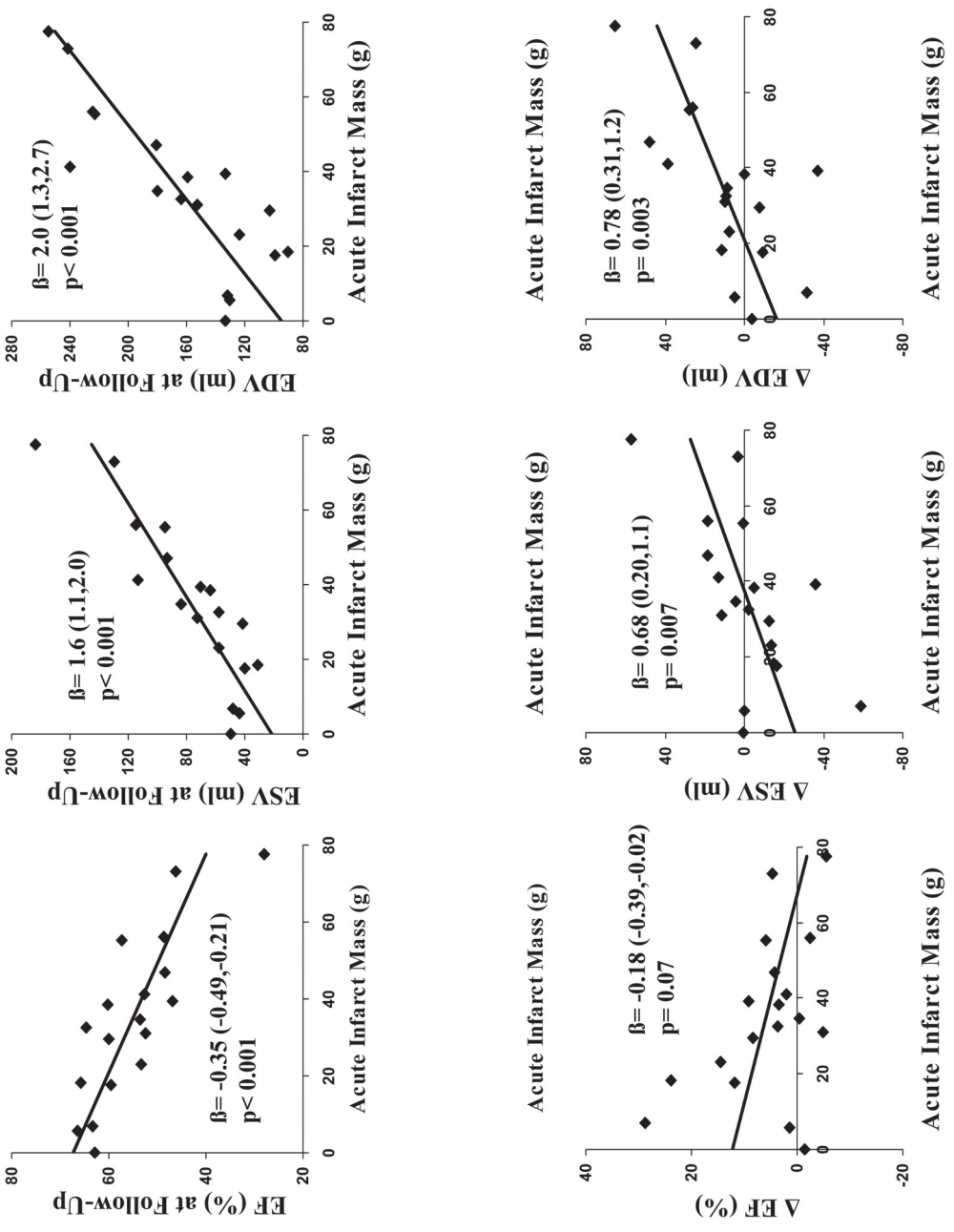

Figure 5. Acute myocardial infarct mass correlated better with EF, ESV, and EDV at 5 months after AMI than the change in EF, ESV, and EDV between 5 days and 5 months post AMI. (Δ = change between 5 days and 5 months).

early after AMI. We performed baseline scans in a clinically applicable time interval between completing stabilization on the coronary care unit and discharge home from the cardiology ward. Fourthly, the chosen endpoints per study varied from the change in regional contractile function and EF to contractile function and EF at follow-up. In the present study, a marked increase in overall mean EF was observed from 48 ± 11% at baseline to 55 ± 9% at follow-up. However, a moderate correlation was found between DE and perfusion imaging and the change in EF, ESV, and EDV between 5 days and 5 months post-AMI. Improvement of myocardial contractile function is dependent on recovery of stunned myocardium and compensatory hypertrophy of salvaged myocardium during left ventricular remodelling. It is still unknown in what time span recovery of contractile function of dysfunctional stunned myocardium can be expected and the degree of compensatory hypertrophy is influenced by numerous factors, such as: neurohumoral stimulation, medication etc. Although a marked increase in EF was observed in the present study, it is possible that with baseline scans performed earlier after AMI we might have observed an even greater improvement in EF. Predicting the change in EF, ESV, and EDV during this complex process of left ventricular remodelling might lead to false interpretations of recovery since baseline values may fluctuate during the first period after AMI. For this reason, we correlated perfusion and DE imaging with EF, ESV, and EDV at 5 months after AMI. EF, ESV and EDV were chosen as endpoints as several studies showed that these endpoints are major determinants of clinical outcome after AMI [17].

Although the number of patients in the present study is relatively small, DE imaging appears to be a better prognosticator than perfusion imaging. DE imaging might be a better predictor EF, ESV, and EDV at 5 months after AMI as total infarct size remains underestimated with perfusion imaging. Myocardial perfusion defects, as identified with perfusion imaging, correspond to the region of microvascular obstruction within the infarcted region, but do not include necrotic myocardium with an intact microvasculature and hence normal perfusion [16] (**Table 2**). In contrast, with DE imaging entire myocardial infarct size including the region with microvascular obstruction, is assessed. In a canine model of AMI, total infarct size (DE imaging) and the extent of microvascular obstruction (perfusion imaging) corresponded to post-mortem histology findings [16]. DE imaging allows the visualization of infarcted myocardium since a contrast agent like Gadolinium-DTPA enhances the signal in regions with myocyte necrosis. X-ray microanalysis showed an accumulation of Gadolinium-DTPA exclusively in the infarcted myocardium 10-20 minutes after intravenous administration [18]. The results of this study show that an imaging technique, which allows the differentiation between viable and non-viable myocytes might be preferred above an imaging technique that visualizes solely the integrity of the microvasculature. Contrast echocardiography,

		EF at follow-up				ESV at follow-up				EDV at follow-up			
Univariate analyses		**ß**	**ß (CI)**	**P-value**	**R^2**	**ß**	**ß (CI)**	**P-value**	**R^2**	**ß**	**ß (CI)**	**P-value**	**R^2**
	CPK	**$-2.7*10^{-3}$**	**-0.004,-0.001**	**0.005**	**0.33**	**0.01**	**0.003,0.018**	**0.01**	**0.28**	**0.01**	**0.002,0.02**	**0.03**	**0.22**
	Perfusion score	**-1.2**	**-2.3,-0.2**	**0.02**	**0.23**	**4.1**	**-0.7,8.8**	**0.09**	**0.14**	**3.9**	**-2.9,11**	**0.24**	**0.02**
	Infarct Mass	**-0.35**	**-0.49,-0.21**	**<0.001**	**0.65**	**1.6**	**1.1,2.0**	**<0.001**	**0.78**	**2.0**	**1.3,2.7**	**<0.001**	**0.68**
Multivariate Analyses													
Model 1	**CPK**	**$-2.2*10^{-3}$**	**-0.005,0.001**	**0.09**	**0.34**	**0.01**	**-0.001,0.02**	**0.06**	**0.28**	**0.02**	**0,0.033**	**0.05**	**0.23**
	Perfusion score	**-0.35**	**-1.8,1.1**	**0.63**		**-0.46**	**-7.1,6.1**	**0.9**		**-2.7**	**-12,6.5**	**0.50**	
Model 2	**CPK**	**$-0.9*10^{-3}$**	**-0.0003,0.001**	**0.39**	**0.67**	**$-0.5*10^{-3}$**	**-0.007,0.008**	**0.88**	**0.78**	**$-0.8*10^{-3}$**	**-0.01,0.01**	**0.90**	**0.68**
	Infarct Mass	**-0.28**	**-0.50,-0.07**	**0.01**		**1.5**	**0.82,2.3**	**< 0.001**		**2.1**	**0.89,3.2**	**0.002**	
Model 3	**CPK**	**$-0.8*10^{-3}$**	**-0.003,0.002**	**0.50**	**0.67**	**$1.3*10^{-3}$**	**-0.007,0.01**	**0.75**	**0.78**	**$1.3*10^{-3}$**	**-0.01,0.01**	**0.84**	**0.70**
	Perfusion score	**-0.11**	**-1.5,1.3**	**0.87**		**-0.93**	**-5.6,3.7**	**0.68**		**2.6**	**-10,4.8**	**0.46**	
	Infarct mass	**-0.28**	**-0.52,-0.035**	**0.04**		**1.6**	**0.84,2.4**	**0.001**		**2.2**	**0.94,3.5**	**0.002**	

Table 3. Univariate and Multivariate linear regression analyses, ß = regression coefficient, CI = 95%-confidence interval.

besides having the great advantage of being a bedside imaging tool, only allows the assessment of microvasculature integrity and does not provide accurate information regarding infarct size. Another currently available non-invasive imaging modality is nuclear medicine, which allows the differentiation between regions with viable and non-viable myocytes but is hampered by the currently offered low spatial resolution. ce-MRI allows the assessment of total infarct size and provides detailed information on regional and global left ventricular function. Unfortunately, its availability is still limited.

Methodological Considerations

The size of the present study population is relatively small and conclusions for subgroups such as patients with diabetics, women vs. men, etc., cannot be drawn. Furthermore, a possible selection bias could have been present in this study since eight patients were unable or refused to undergo a second MRI. Importantly, none of these patients dropped out due to cardiac death or sever heart failure making a selection bias unlikely. In the present study we did not perform angiographic follow-up to exclude in-stent restenosis, but all patients received a drug-eluting stent in the infarct related coronary artery with very low numbers of restenosis reported [3]. There was no clinical evidence of recurrent myocardial ischemia. Quantification of the volume of microvascular obstruction is hampered by the low spatial resolution offered by the currently available acquisition technique and the temporal resolution that does not allow coverage of the whole ventricle in one R-R interval.

Clinical Implications

In the era of primary stenting with drug-eluting stents as reperfusion treatment for patients with AMI, marked recovery of left ventricular function is observed. Global left ventricular function at 5 months post AMI can be estimated by performing ce-MRI at 5 days post-AMI. DE imaging appears to be a better prognosticator than perfusion imaging.

References

1. Andersen HR, Nielsen TT, Rasmussen K, Thuesen L, Kelbaek H, Thayssen P, Abildgaard U, Pedersen F, Madsen JK, Grande P, Villadsen AB, Krusell LR, Haghfelt T, Lomholt P, Husted SE, Vigholt E, Kjaergard HK, Mortensen LS. A comparison of coronary angioplasty with fibrinolytic therapy in acute myocardial infarction. N Engl J Med. 2003;349:733-42.
2. Keeley EC, Boura JA, Grines CL. Primary angioplasty versus intravenous thrombolytic therapy for acute myocardial infarction: a quantitative review of 23 randomised trials. Lancet. 2003;361:13-20.

3. Lemos PA, Saia F, Hofma SH, Daemen J, Ong AT, Arampatzis CA, Hoye A, McFadden E, Sianos G, Smits PC, van der Giessen WJ, de Feyter P, van Domburg RT, Serruys PW. Short- and long-term clinical benefit of sirolimus-eluting stents compared to conventional bare stents for patients with acute myocardial infarction. J Am Coll Cardiol. 2004;43:704-8.
4. Henriques JP, Zijlstra F, Ottervanger JP, de Boer MJ, van 't Hof AW, Hoorntje JC, Suryapranata H. Incidence and clinical significance of distal embolization during primary angioplasty for acute myocardial infarction. Eur Heart J. 2002;23:1112-7.
5. Verma S, Fedak PW, Weisel RD, Butany J, Rao V, Maitland A, Li RK, Dhillon B, Yau TM. Fundamentals of reperfusion injury for the clinical cardiologist. Circulation. 2002;105:2332-6.
6. Wu KC, Kim RJ, Bluemke DA, Rochitte CE, Zerhouni EA, Becker LC, Lima JA. Quantification and time course of microvascular obstruction by contrast-enhanced echocardiography and magnetic resonance imaging following acute myocardial infarction and reperfusion. J Am Coll Cardiol. 1998;32:1756-64.
7. Judd RM, Lugo-Olivieri CH, Arai M, Kondo T, Croisille P, Lima JA, Mohan V, Becker LC, Zerhouni EA. Physiological basis of myocardial contrast enhancement in fast magnetic resonance images of 2-day-old reperfused canine infarcts. Circulation. 1995;92:1902-10.
8. Choi KM, Kim RJ, Gubernikoff G, Vargas JD, Parker M, Judd RM. Transmural extent of acute myocardial infarction predicts long-term improvement in contractile function. Circulation. 2001;104:1101-7.
9. Beek AM, Kuhl HP, Bondarenko O, Twisk JW, Hofman MB, van Dockum WG, Visser CA, van Rossum AC. Delayed contrast-enhanced magnetic resonance imaging for the prediction of regional functional improvement after acute myocardial infarction. J Am Coll Cardiol. 2003;42:895-901.
10. Gerber BL, Garot J, Bluemke DA, Wu KC, Lima JA. Accuracy of contrast-enhanced magnetic resonance imaging in predicting improvement of regional myocardial function in patients after acute myocardial infarction. Circulation. 2002;106:1083-9.
11. Ingkanisorn WP, Rhoads KL, Aletras AH, Kellman P, Arai AE. Gadolinium delayed enhancement cardiovascular magnetic resonance correlates with clinical measures of myocardial infarction. J Am Coll Cardiol. 2004;43:2253-9.
12. Petersen SE, Voigtlander T, Kreitner KF, Horstick G, Ziegler S, Wittlinger T, Abegunewardene N, Schmitt M, Schreiber WG, Kalden P, Mohrs OK, Lippold R, Thelen M, Meyer J. Late improvement of regional wall motion after the subacute phase of myocardial infarction treated by acute PTCA in a 6-month follow-up. J Cardiovasc Magn Reson. 2003;5:487-95.
13. Taylor AJ, Al-Saadi N, Abdel-Aty H, Schulz-Menger J, Messroghli DR, Friedrich MG. Detection of acutely impaired microvascular reperfusion after infarct angioplasty with magnetic resonance imaging. Circulation. 2004;109:2080-5.
14. Slavin GS, Wolff SD, Gupta SN, Foo TK. First-pass myocardial perfusion MR imaging with interleaved notched saturation: feasibility study. Radiology. 2001;219:258-63.
15. Christian TF, Schwartz RS, Gibbons RJ. Determinants of infarct size in reperfusion therapy for acute myocardial infarction. Circulation. 1992;86:81-90.

16. Gerber BL, Rochitte CE, Melin JA, McVeigh ER, Bluemke DA, Wu KC, Becker LC, Lima JA. Microvascular obstruction and left ventricular remodeling early after acute myocardial infarction. Circulation. 2000;101:2734-41.
17. White HD, Norris RM, Brown MA, Brandt PW, Whitlock RM, Wild CJ. Left ventricular end-systolic volume as the major determinant of survival after recovery from myocardial infarction. Circulation. 1987;76:44-51.
18. Rehwald WG, Fieno DS, Chen EL, Kim RJ, Judd RM. Myocardial magnetic resonance imaging contrast agent concentrations after reversible and irreversible ischemic injury. Circulation. 2002;105:224-9.

Effects of Primary Angioplasty for Acute Myocardial Infarction on Early and Late Infarct Size and Left Ventricular Wall Characteristics

Timo Baks; Robert-Jan van Geuns; Elena Biagini; Piotr Wielopolski; Nico R. Mollet; Filippo Cademartiri; Willem J. van der Giessen; Gabriel P. Krestin; Patrick W. Serruys; Dirk J. Duncker; Pim J. de Feyter

J Am Coll Cardiol 2006;47:40-4

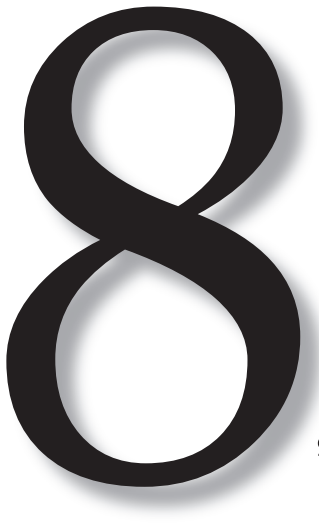

1, 2, 3, 4, 5, 6, 7, 9, 10, 11, 12, 13, 14, 15

Abstract

Objectives

We aimed to study the effects of early successful primary angioplasty for ST-segment elevation acute myocardial infarction (AMI) on early and late infarct size and left ventricular (LV) wall characteristics.

Background

Early reperfusion treatment for AMI preserves LV function, but the effects on early and late infarct size, end-diastolic wall thickness (EDWT) and segmental wall thickening (SWT) are not well known.

Methods

In 22 patients with successful primary angioplasty for first AMI, cine-magnetic resonance imaging (MRI), first-pass perfusion and delayed-enhancement imaging was performed at five days and five months. The extent of microvascular obstruction was evaluated on perfusion images. Infarct shrinkage was defined as the difference between the volume of delayed-enhancement at five days and five months. The EDWT and SWT were quantified on cine-MRI.

Results

Infarct shrinkage occurred to the same extent in small and large infarctions ($R = 0.92$; $p<0.001$), with a mean decrease of 31% (35 ± 21 g to 24 ± 17 g). Dysfunctional segments without microvascular obstruction had an increased EDWT at five days compared with remote myocardium (9.2 ± 1.7 mm versus 8.4 ± 1.7 mm; $p < 0.001$). At five months, EDWT in these segments became comparable to the thickness of remote myocardium (7.8 ±1.6 mm versus 7.6 ± 1.4 mm; $p = 0.60$) and SWT improved (21 ± 15% to 40 ± 24%; $p < 0.001$) but remained impaired (40 ± 24% versus 71 ± 29%; $p < 0.001$). Segments with microvascular obstruction demonstrated wall thinning at 5 months (6.4 ± 1.3 versus 7.6 ± 1.4 mm; $p = 0.006$) and no significant recovery in SWT (12 ± 14% to 17 ± 20%; $p = 0.15$).

Conclusions

Infarct size decreased with 31%. Segments without microvascular obstruction had early increased wall thickness and late partial functional recovery. Segments with microvascular obstruction showed late wall thinning and no functional recovery at 5 months.

Introduction

Early restoration of epicardial coronary blood flow reduces infarct size in patients with acute myocardial infarction (AMI) and has a beneficial effect on post-infarction myocardial infarct healing and left ventricular (LV) remodeling (1-3). Early reperfusion, however, might also lead to endothelial dysfunction and extravasation of fluids to the interstitium (4). Understanding the natural course of infarct healing and the effect of early reperfusion on ischemic myocardium might contribute to understanding and developing new therapies for ischemic heart disease. Recently, it was shown that contrast-enhanced Magnetic Resonance Imaging (ce-MRI) allows the assessment of myocardial perfusion, infarct size and left ventricular wall thickness/function with good reproducibility and excellent correlation with histology in animal models of acute and chronic MI (5-11). Therefore, we performed ce-MRI in patients who suffered AMI and were treated within 6 hours with successful drug-eluting stent implantation to study the effects on early and late infarct size and left ventricular wall characteristics.

Methods

Patient Population

We studied 30 patients (25 male, 53±10 years old) admitted to the coronary care unit with first AMI. Patient characteristics are listed in **Table 1**. Diagnosis was based on clinical symptoms, ST-segment elevation on electrocardiogram and angiographically demonstrated occlusion of a coronary artery. All vessels were stented with a drug-eluting stent within 6 h (mean 2.5 h) of onset of symptoms resulting in Thrombolysis In Myocardial Infarction (12) flow grade 3. Exclusion criteria consisted of any contraindication to MRI. All participants gave written informed consent to the study protocol, which was approved by the medical ethics committee of the Erasmus MC, Rotterdam. The study population consisted of 22 patients who had the first MRI scan 5 ± 3 days after admission and the second MRI scan 20 ± 7 weeks later. Eight patients did not undergo a second scan: one patient died (non-cardiac death), 2 patients had a defibrillator implanted and 5 patients refused to come back. Angiographic follow-up was performed in 8 patients (36%) and no in-stent restenosis was seen. In the other patients, there was no clinical evidence of recurrent myocardial ischemia and all patients received a drug-eluting stent in the infarct related coronary artery with very low numbers of restenosis reported (13).

Table 1 Patient characteristics (n = 22)

Age (yrs)	52 ± 12
Men	16 (73)
Smoking	15 (68)
Diabetes Mellitus	1 (5)
Hypertension	6 (27)
Hypercholesterolemia	5 (23)
Family history of coronary artery disease	12 (55)
Creatine kinase peak (IU)	3112 ± 2001
Anterior Infarction	15 (68)
Inferior/lateral infarction	7 (32)
Abciximab peri-procedural	14 (64)
ACE inhibitor baseline / follow-up	1 (5) / 18 (82)
Beta-Blocker baseline / follow-up	3 (14) / 22 (100)
Clopidogrel	22 (100)
Statin follow-up	20 (91)
ASA follow-up	22 (100)
Ejection Fraction 5 days (%)	48±11
Ejection Fraction 5 months (%)	55±9

Values are presented as number (%) or mean ± standard deviation

MRI protocol

A clinical 1.5-Tesla MRI with a dedicated cardiac four element phased-array receiver coil was used for imaging (Signa CV/i, GE Medical systems, Milwaukee, Wisconsin). Baseline and follow-up ce-MRI protocol consisted of cine-MRI, first-pass perfusion, and Delayed Enhancement imaging. Cine-MRI was performed with a steady-state free-precession technique (FIESTA, GE Medical Systems) with the following imaging parameters: 24 temporal phases per slice, field of view 32 to 36 x 32 to 36 cm; rectangular field of view 0.75; repetition time 3.2 to 3.7; time to echo 1.4; flip angle 45°; matrix 160x128, bandwidth 83 kHz, number of averages 0.75. To cover the entire left ventricle, nine to 12 consecutive slices of 8 mm were planned in short axis view (gap of 2 mm) on the horizontal long axis (4-chamber view) of the left ventricle. First-pass perfusion imaging was performed during 30-40 consecutive heartbeats immediately after administration of gadolinium-DTPA (0.1 mmol/kg, Magnevist®, Schering: 4 ml/second in an antecubital vein followed by 15 ml of saline at 4 ml/second). A special

presaturation scheme with a notched excitation followed by a segmented gradient-echo/echo-planar readout was used (14) with the following imaging parameters: field of view 32 to 36 x 32 to 36 cm, rectangular field of view 0.75, repetition time 6.8, inversion time 150-175ms, saturation pulse 90°, time to echo 1.2, echo train length 4, number of averages 0.75, bandwidth 125 kHz, flip angle 20°, matrix 128/96, slice thickness 8 mm. The temporal resolution per slice of 120 ms allowed imaging of 5-8 slices per R-R interval (maximum heart rate of 90 bpm). Perfusion images were planned to cover the basal, mid and apical part of the left ventricle in the same orientation as the cine images. Delayed enhancement imaging was performed with a 2-dimensional T1-weighted inversion-recovery fast gradient-echo sequence 10-20 minutes following perfusion imaging with the following parameters: field of view 32 to 36 x 32 to 36 cm, rectangular field of view 0.75; slice thickness 8 mm, gap 2 mm, repetition time 7.3, time to echo 1.6, flip angle 20°, inversion pulse of 180°, matrix 256x192, number of averages 1, bandwidth 17.9 kHz, inversion time 180-275 ms (adjusted per patient to null the signal of remote myocardium). Slice locations of the delayed enhancement images were copied from the cine images.

Definitions and Data analysis

Cine, perfusion and delayed enhancement images were all matched for position using anatomical landmarks like papillary muscles and the insertion of the right ventricle. To quantify end diastolic wall thickness (EDWT), end systolic wall thickness (ESWT), left ventricular volumes and left ventricular mass, epicardial and endocardial contours were detected automatically and corrected manually on short axis cine-MRI images in 16 myocardial segments per patient using the centerline method (Mass, Medis, Leiden, the Netherlands). Segmental wall thickening (SWT) was calculated by (ESWT-EDWT)/ EDWT *100. Myocardial segments were considered dysfunctional if SWT was 45% or less (15). Myocardial perfusion was evaluated qualitatively on first-pass perfusion images and scored as: 1 = no microvascular obstruction (homogeneous enhancement of myocardium), 2 = presence of microvascular obstruction (hypoenhanced region). No perfusion study had to be excluded from the analysis due to lack of image quality. Infarcted myocardium was clearly differentiated from remote myocardium with a delayed enhancement inversion-recovery pulse sequence. Infarct size was quantified by manually tracing the delayed enhanced regions from the consecutive 2D slices encompassing the left ventricle. Delayed enhancement volume was multiplied by 1.05 g/ml to obtain myocardial infarct mass. Total infarct mass was judged as non-assessable in four baseline scans since the region of delayed enhancement could not be differentiated clearly from the healthy myocardium in all myocardial segments (breathing artifacts, erroneous electrocardiographic triggering). These data were left out from the regression analysis.

Statistical analysis

All data are expressed as mean ± standard deviation. Segmental data were stratified on baseline perfusion images in 3 groups: first, dysfunctional segments without microvascular obstruction; second, dysfunctional segments with microvascular obstruction; and third, remote myocardium. One-way analysis of variance was used for the comparison of EDWT measurements (at 5 days and at 5 months) between the 3 groups, followed by unpaired t tests. Two-way analysis of variance with repeated measures over time was used to compare changes in SWT between 5 days and 5 months and to evaluate the difference in these changes between the 3 groups. Bonferroni correction was applied to adjust for multiple comparisons. Univariate linear regression analysis was used to evaluate the relationship between infarct mass at 5 days and 5 months. Significance was accepted at p value of ≤ 0.05.

Results

Myocardial Infarct size

Infarct size decreased significantly with 31% from 35 ± 21 g at 5 days to 24 ± 17 g at 5 months ($p<0.001$), which was 26 ± 14% to 20 ± 11% of left ventricular mass. Infarct size decreased relatively with the same extent in small and large infarctions ($R = 0.92$; $p < 0.001$) (**Figure 1**). Anterior infarctions decreased from a mean of 36 g to 25 g (30% reduction) which was as much as inferolateral infarctions which decreased from 33 g to 22 g (33% reduction). Remote left ventricular mass decreased slightly but not statistically significant from 100 ± 26 g to 94 ± 23 g ($p=0.18$).

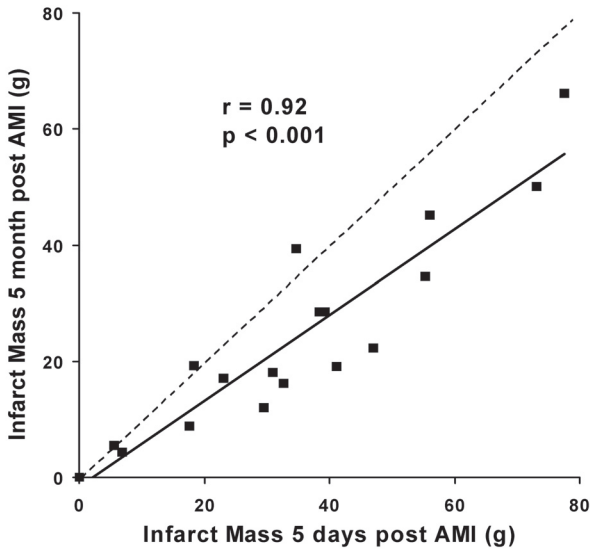

Figure 1. Relation between myocardial infarct mass at five days and five months after Acute Myocardial Infarction (AMI) (solid line). Equation: y = 0.71x – 1.5. Dashed line represents the line of unity (i.e., infarct mass at baseline is infarct mass at follow-up).

Left ventricular wall characteristics

Dysfunctional segments without microvascular obstruction had an increased EDWT at 5 days compared to remote myocardium (9.2 ± 1.7 mm vs.

8.4 ± 1.7 mm; p < 0.001) and segments with microvascular obstruction despite a stented and patent coronary artery (8.4 ± 1.7 mm; p = 0.07) (**Figure 2A**). At 5 months, segments without microvascular obstruction had a reduced EDWT comparable to the thickness of remote segments (7.8 ± 1.6 mm vs. 7.6 ± 1.4 mm; p = 0.60) (**Figure 2B**) and demonstrated improvement in SWT (21 ± 15% to 40 ± 24%; p<0.001), although function remained impaired compared to remote myocardium (40 ± 24% versus 71 ± 29%; p<0.001) (**Figure 3**). Segments with microvascular obstruction demonstrated wall thinning at 5 months compared to remote segments (6.4 ± 1.3 mm vs. 7.6 ± 1.4 mm; p=0.006) and no significant recovery of SWT (12 ± 14% to 17 ± 20%; p = 0.15).

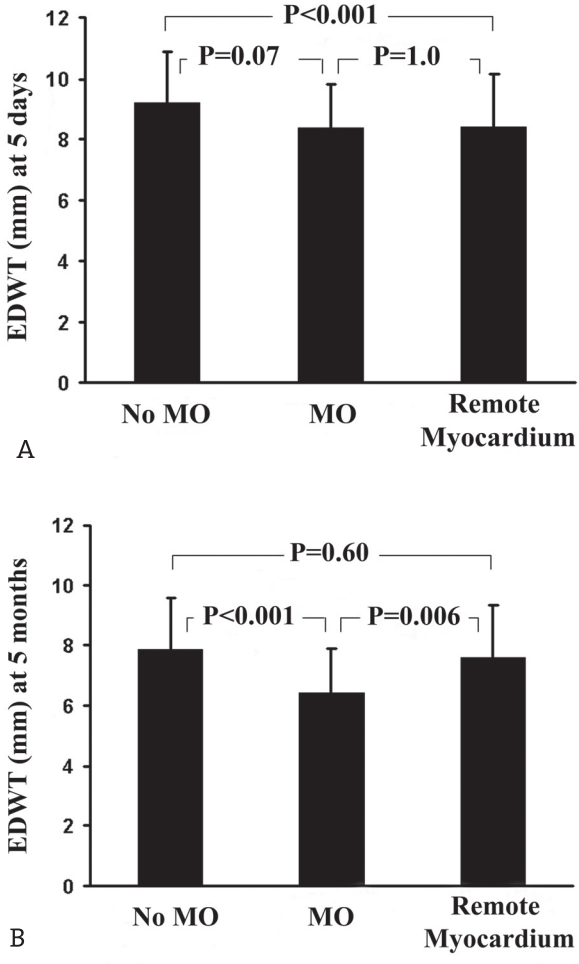

Figure 2. A: Dysfunctional segments without microvascular obstruction (MO) had an increased end-diastolic wall thickness (EDWT) at five days compared with remote myocardium and myocardium with microvascular obstruction.

B: At five months, segments with microvascular obstruction (MO) demonstrated wall thinning compared to remote myocardium and myocardium without microvascular obstruction. End-diastolic wall thickness of myocardium without microvascular obstruction became comparable to remote myocardium.

Discussion

In our study of 22 patients who underwent successful drug-eluting stent implantation within 6 hours of onset of symptoms, we first demonstrated that infarct size decreased relatively to the same extent in small and large infarctions with a mean decrease of 31%. Second, we observed that dysfunctional segments without microvascular obstruction exhibited an increased EDWT compared to remote myocardium. These segments showed a significant improvement in wall

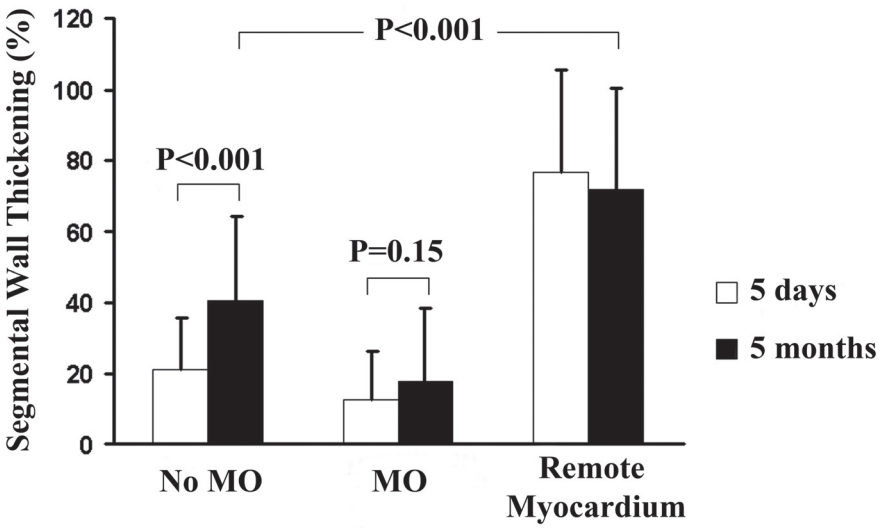

Figure 3. Dysfunctional myocardial segments without microvascular obstruction (MO) demonstrated improved segmental wall thickening at follow-up but function remained impaired compared to remote myocardium. *Open bars* = five days; *Solid bars* = five months

thickening. Third, segments with microvascular obstruction, despite a stented coronary artery, demonstrated wall thinning at 5 months and showed no significant improvement in wall thickening at follow-up.

The pathophysiology of infarct healing and left ventricular remodeling has been studied in a canine model of AMI (16). Infarct healing appeared to be an ongoing process with early infarct expansion (4 days) followed by infarct resorption, scar formation, and wall thinning (6 weeks). Necrotic myocytes, interstitial oedema, hemorrhage, and inflammatory cells were resorbed and replaced by collagenous scar tissue. Infarct healing might be further enhanced by repopulation of the border zones of the infarcted area by circulating stem-cells (17). Remote myocardial mass increased in an animal study of AMI (3), whereas in our study, a small but non-significant reduction in remote myocardial mass was observed. This observation in our study might be explained by early and chronic treatment with angiotensin-converting enzyme inhibition in 18 patients (82%) and beta-blockers in 22 patients (100%).

Studying infarct size reduction in patients has recently become possible with the introduction of high resolution ce-MRI. Ce-MRI allows the differentiation of necrotic and viable myocardium with DE imaging, besides the assessment of myocardial wall thickening with cine-MRI and myocardial perfusion and microvascular obstruction

with first-pass perfusion imaging (3,5,8,11,18,19). Therefore, ce-MRI is a suitable non-invasive imaging tool to evaluate the natural course of infarct healing and to evaluate stem-cell therapy for AMI. Promising but contradictory results have been reported (20-22). The non-randomized Transplantation of Progenitor Cells and Regeneration Enhancement in Acute Myocardial Infarction (TOPCARE-AMI) trial studied acute infarct patients who were treated with coronary stenting with a mean time of reperfusion of 23 h, followed by coronary infusion of adult progenitor cells at four days. They demonstrated an increase in ejection fraction of 5% at 4 months and of 9% at 12 months. Infarct size decreased approximately 20% at 4 months and 34% at 12 months. In the randomized Bone Marrow Transfer to Enhance ST-elevation Infarct Regenaration (BOOST) trial, patients were eligible for inclusion if admitted within 5 days of onset of symptoms. Ejection fraction increased by 7% in patients treated with bone-marrow cells and 1% in patients treated conventionally. Infarct size decreased in both patient groups with approximately 30% to 35% in six months. Ingkanisorn et al. (23) studied patients with acute or subacute (up to one month) revascularization therapy and observed an increase in ejection fraction of 5% and a decrease in infarct size of approximately 34% in 5 months. In the present study, patients were revascularized within 6 hours and received optimal pharmacological treatment for AMI. An improvement in ejection fraction of 7% was demonstrated, and infarct size decreased with 31% in five months. From these studies it might be concluded that there seems to be no difference in decrease of infarct size (approx. 30-35%) between patients treated with mechanical perfusion alone or with the combination of either infusion of bone marrow or adult progenitor cells and mechanical reperfusion. The increase in ejection fraction ranged between approximately 5% and 7 % and only in the control group of the BOOST trial did the ejection fraction remain nearly unchanged. It remains to be seen whether infarct size or ejection fraction or the combination needs to be taken as the primary endpoint in the investigations of reperfusion strategies in AMI.

Restoration of epicardial coronary flow by primary angioplasty is highly successful in patients with AMI, and the occurrence of target vessel restenosis has been reduced dramatically since the introduction of drug-eluting stents (13); however, the effect of restoration of epicardial coronary blood flow on ischemic myocardium is not well understood. In a porcine model of AMI, restoration of myocardial perfusion was followed by an increase in EDWT presumed to be due to hyperemia and extravasation of fluids (24,25). Histology of reperfused segments with increased EDWT revealed massive extra-cellular oedema but an intact microvasculature (24). In line with these experimental studies we observed that segments without microvascular obstruction demonstrated an increased EDWT. However, restoration of epicardial coronary blood flow is not always followed by restored microvascular perfusion. Microvascular

obstruction might occur owing to obstructing microthrombi originating from the primary occluding thrombus, microvascular plugging by the influx of inflammatory cells and/or locally emerging thrombi caused by endothelial damage by oxygen radicals (4,26). In our study, myocardial segments with microvascular obstruction did not demonstrate an increased EDWT. This was most likely caused by reduced blood-flow in myocardium with microvascular obstruction and subsequently less extravasation of fluids to the interstitium. Interestingly, these segments demonstrated wall-thinning at follow-up, and myocardial contractility remained severely depressed.

References

1. Keeley EC, Boura JA, Grines CL. Primary angioplasty versus intravenous thrombolytic therapy for acute myocardial infarction: a quantitative review of 23 randomised trials. Lancet 2003;361:13-20.
2. Christian TF, Schwartz RS, Gibbons RJ. Determinants of infarct size in reperfusion therapy for acute myocardial infarction. Circulation 1992;86:81-90.
3. Fieno DS, Hillenbrand HB, Rehwald WG, et al. Infarct resorption, compensatory hypertrophy, and differing patterns of ventricular remodeling following myocardial infarctions of varying size. J Am Coll Cardiol 2004;43:2124-31.
4. Verma S, Fedak PW, Weisel RD, et al. Fundamentals of reperfusion injury for the clinical cardiologist. Circulation 2002;105:2332-6.
5. Gerber BL, Rochitte CE, Melin JA, et al. Microvascular obstruction and left ventricular remodeling early after acute myocardial infarction. Circulation 2000;101:2734-41.
6. Mahrholdt H, Wagner A, Holly TA, et al. Reproducibility of chronic infarct size measurement by contrast-enhanced magnetic resonance imaging. Circulation 2002;106:2322-7.
7. Yang Z, Berr SS, Gilson WD, Toufektsian MC, French BA. Simultaneous evaluation of infarct size and cardiac function in intact mice by contrast-enhanced cardiac magnetic resonance imaging reveals contractile dysfunction in noninfarcted regions early after myocardial infarction. Circulation 2004;109:1161-7.
8. Judd RM, Lugo-Olivieri CH, Arai M, et al. Physiological basis of myocardial contrast enhancement in fast magnetic resonance images of 2-day-old reperfused canine infarcts. Circulation 1995;92:1902-10.
9. Wu KC, Kim RJ, Bluemke DA, et al. Quantification and time course of microvascular obstruction by contrast-enhanced echocardiography and magnetic resonance imaging following acute myocardial infarction and reperfusion. J Am Coll Cardiol 1998;32:1756-64.
10. Amado LC, Kraitchman DL, Gerber BL, et al. Reduction of "no-reflow" phenomenon by intra-aortic balloon counterpulsation in a randomized magnetic resonance imaging experimental study. J Am Coll Cardiol 2004;43:1291-8.
11. Kim RJ, Fieno DS, Parrish TB, et al. Relationship of MRI delayed contrast enhancement to irreversible injury, infarct age, and contractile function. Circulation 1999;100:1992-2002.

12. Chesebro JH, Knatterud G, Roberts R, et al. Thrombolysis in Myocardial Infarction (TIMI) Trial, Phase I: A comparison between intravenous tissue plasminogen activator and intravenous streptokinase. Clinical findings through hospital discharge. Circulation 1987;76:142-54.
13. Lemos PA, Saia F, Hofma SH, et al. Short- and long-term clinical benefit of sirolimus-eluting stents compared to conventional bare stents for patients with acute myocardial infarction. J Am Coll Cardiol 2004;43:704-8.
14. Slavin GS, Wolff SD, Gupta SN, Foo TK. First-pass myocardial perfusion MR imaging with interleaved notched saturation: feasibility study. Radiology 2001;219:258-63.
15. Holman ER, Buller VG, de Roos A, et al. Detection and quantification of dysfunctional myocardium by magnetic resonance imaging. A new three-dimensional method for quantitative wall-thickening analysis. Circulation 1997;95:924-31.
16. Richard V, Murry CE, Reimer KA. Healing of myocardial infarcts in dogs. Effects of late reperfusion. Circulation 1995;92:1891-901.
17. Orlic D, Hill JM, Arai AE. Stem cells for myocardial regeneration. Circ Res 2002;91:1092-102.
18. Rehwald WG, Fieno DS, Chen EL, Kim RJ, Judd RM. Myocardial magnetic resonance imaging contrast agent concentrations after reversible and irreversible ischemic injury. Circulation 2002;105:224-9.
19. Baks T, van Geuns RJ, Biagini E, et al. Recovery of left ventricular function after primary angioplasty for acute myocardial infarction. Eur Heart J 2005;26:1070-7.
20. Britten MB, Abolmaali ND, Assmus B, et al. Infarct remodeling after intracoronary progenitor cell treatment in patients with acute myocardial infarction (TOPCARE-AMI): mechanistic insights from serial contrast-enhanced magnetic resonance imaging. Circulation 2003;108:2212-8.
21. Schachinger V, Assmus B, Britten MB, et al. Transplantation of progenitor cells and regeneration enhancement in acute myocardial infarction: final one-year results of the TOPCARE-AMI Trial. J Am Coll Cardiol 2004;44:1690-9.
22. Wollert KC, Meyer GP, Lotz J, et al. Intracoronary autologous bone-marrow cell transfer after myocardial infarction: the BOOST randomised controlled clinical trial. Lancet 2004;364:141-8.
23. Ingkanisorn WP, Rhoads KL, Aletras AH, Kellman P, Arai AE. Gadolinium delayed enhancement cardiovascular magnetic resonance correlates with clinical measures of myocardial infarction. J Am Coll Cardiol 2004;43:2253-9.
24. Turschner O, D'Hooge J, Dommke C, et al. The sequential changes in myocardial thickness and thickening which occur during acute transmural infarction, infarct reperfusion and the resultant expression of reperfusion injury. Eur Heart J 2004;25:794-803.
25. Pislaru C, Bruce CJ, Seward JB, Greenleaf JF. Distinctive changes in end-diastolic wall thickness and postsystolic thickening in viable and infarcted myocardium. J Am Soc Echocardiogr 2004;17:855-62.
26. Kloner RA, Ganote CE, Jennings RB. The "no-reflow" phenomenon after temporary coronary occlusion in the dog. J Clin Invest 1974;54:1496-508.

Prediction of Left Ventricular Function after Drug-eluting Stent Implantation for Chronic Total Coronary Occlusions

Timo Baks; Robert-Jan van Geuns; Dirk J. Duncker; Filippo Cademartiri; Nico R. Mollet; Gabriel P. Krestin; Patrick W. Serruys; Pim J. de Feyter

J Am Coll Cardiol 2006;47:721-5

9

1, 2, 3, 4, 5, 6, 7, 8, 10, 11, 12, 13, 14, 15

Abstract

Objectives

We studied the effect of drug-eluting stent implantation for chronic total coronary occlusion (CTO) on left ventricular volumes and function and assessed the predictive value of magneticresonance imaging (MRI) performed before revascularization.

Background

The effect of recanalization of CTO on long-term left ventricular function and the value of myocardial viability assessment with MRI is incompletely understood.

Methods

Twenty-seven patients underwent contrast-enhanced MRI before and five months af ter successful drug-eluting stent implantation for CTO. A CTO was defined as a complete occlusion of a major epicardial coronary artery existing for at least six weeks (mean, 7 ± 5 months). Myocardial wall thickening and left ventricular volumes were quantified on cine-images, and the transmural extent of infarction (TEl) was scored on delayed enhancement images.

Results

A significant decrease in mean end-systolic volume index (34 ± 13 ml/m^2 to 31 ± 13 ml/m^2; p = 0.02) and mean end-diastolic volume index (84 ± 15 ml/m^2 to 79 ± 15 ml/m^2; p < 0.002) was observed, whereas the mean ejection fraction did not change significantly (61 ± 9% to 62 ± 11%; P = 0.54). The extent of the left ventricle that was dysfunctional but viabie before revascularization was related to improvement in end-systolic volume index (R = 0.46; P = 0.01) and ejection fraction (R = 0.49; P = 0.01) but not to the end-diastolic volume index (R = 0.10; P = 0.53). Segmental wall thickening improved significantly in segments with <25% TEl (21 ± 15% to 35 ± 25%; P < 0.001), tended to improve in segments with 25% to 75% TEl (18 ± 22% to 27 ± 22%; P = 0.10), whereas segments with >75% TEl did not improve (4 ± 14% to -9 ± 14%; P = 0.54)

Conclusions

Drug-eluting stent implantation for a CTO has a beneficial effect on left ventricular volumes and function that can be predicted by performing MRI before revascularization.

Introduction

Chronic total coronary occlusions (CTO) are observed in 35% to 50% of patients with significant coronary disease undergoing diagnostic angiography (1,2). Percutaneous coronary intervention (PCI) for CTO is increasingly used as treatment strategy and accounts for 10% to 15% of all angioplasties. New catheter-based techniques have led to higher success rates of PCI (3), and drug-eluting stents significantly reduce the incidence of restenosis and reocclusion (4). However, the effect of PCI on myocardial contractility and left ventricular volumes of the individual patient with CTO is incompletely understood. Previous studies used left ventricular angiography to study left ventricular function and volumes after balloon angioplasty or bare-metal stents for CTO, but results have been equivocal (5-7). These equivocal results may partly be caused by the rather crude measurements offered by left ventricular angiography in conjunction with the high restenosis and reocclusion rate after balloon angioplasty or bare-metal stent implantation. The use of contrast-enhanced magnetic resonance imaging (ce-MRI) permits refined assessment of myocardial contractility, left ventricular volumes, and the transmural extent of infarction (TEl) (8). We used ce-MRI to study the effect of drug-eluting stent implantation for CTO on left ventricular volumes and function and to evaluate the diagnostic value of ce- MRI to predict improvement in regional and global left ventricular function.

Materials and methods

Patients

Patients scheduled for percutaneous revascularization of a CTO of a native coronary artery and without contraindications for MRI were prospectively selected for enrollment in this study. Of 50 selected patients, 3 patients refused to participate, 47 patients underwent MRI at 16 ± 16 days before PCI, and 27 patients underwent follow-up MRI at 5 ± 1 months after PCI. Twenty patients did not undergo follow-up MRI; in 13 patients, PCI was not successful, 1 patient gained too much weight to fit into the scanner, 1 patient had a defibrillator implanted, and 5 patients refused re-investigation. All procedures were performed by operators highly experienced in the treatment of CTO, with the interventional strategy left to the discretion of the operator.

Abbreviations and Acronyms

ce-MRI	=	contrast-enhanced magnetic resonance imaging
CTO	=	chronic total coronary occlusion
PCI	=	percutaneous coronary intervention
SWT	=	segmental wall thickening
TEI	=	transmural extent of infarction

All participants gave written informed consent to the study protocol, which was approved by the medical ethics committee of the Erasmus MC, Rotterdam. More patient characteristics are listed in **Table 1.**

Table 1: Baseline Patient Characteristics (n = 27)

Baseline patient characteristics	n = 27
Age (years)	64 ± 10
Men	22 (81)
Smoking	9 (33)
Diabetic Mellitus	5 (19)
Hypertension	6 (22)
Hypercholesterolemia	5 (19)
Family history	12 (44)
History of Myocardial Infarction	14 (52)
Delayed Enhancement before PCI	17 (63%)
Duration of procedure (min.)	143 ± 62
Duration of occlusion (months)	7 ± 5
Collateral filling (grade)	2 to 3
Time to follow-up (months)	5 ± 1
Baseline Ejection fraction (%)	61 ± 9
ACE inhibitor	8 (30)
Beta- Blocker	22 (81)
Clopidogrel (after PCI)	27 (100)
Statin	26 (96)
ASA	27 (100)

Values are presented as number (%) or mean ± standard deviation PCI, Percutaneous Coronary Intervention

MRI protocol

A 1.5-Tesla MRI scanner with a dedicated four element phased-array receiver coil was used for imaging (Signa CV/i, GE Medical systems, USA). Cine-MRI was performed at baseline and follow-up with a steady-state free-precession technique. Sequence details have been published previously (9). To cover the entire left ventricle, 9 to 12 consecutive slices of 8 mm in the short-axis view were planned on the four chamber view (gap

of 2 mm). Delayed enhancement imaging was performed at the baseline scan 10 to 20 minutes after administration of Gadolinium-DTPA (0.1 mmol/kg intravenously, Magnevist®, Schering, Germany). A two-dimensional T1-weighted inversion recovery gradient-echo sequence was used as described previously (9). The inversion time was adjusted per patient to null the signal of remote myocardium. Slice locations were copied from the locations of the cine-images.

Definitions and Data analysis

All conventional angiograms before revascularization were evaluated by two experienced observers (Drs. Baks and van Geuns). Collateral function was scored on a four-points scale (10). A CTO was defined as a complete occlusion of a major coronary artery existing for at least six weeks as obtained from either the date from the previous angiogram or the clinical history of prolonged anginal chest pain or myocardial infarction. Left ventricular volumes and mass were quantified using a dedicated software package (Mass, Medis, the Netherlands). Papillary muscles were considered as part of the left ventricular volume. Regional analysis per patient was assessed using a 16 segments model excluding the apex (11). Segmental wall thickening (SWT) was calculated by (end-systolic minus end-diastolic wall thickness)/ end-diastolic wall thickness X 100%. Myocardial segments were considered dysfunctional if SWT was 45% or less (12). To study the effect of revascularization on SWT, segments in the perfusion territory of a CTO (defined on conventional angiogram) were analyzed for wall thickening at baseline and at five months.

Two investigators (Drs. Baks and van Geuns), blinded for the clinical data, analyzed delayed enhancement images for the TEI, and decision was made on the basis of consensus. TEI was calculated by dividing the hyperenhanced area by the total area in 16 segments per patient as: 1 = 0 % (TEI), 2 = 1 to 25 %, 3 = 26 to 50 %, 4 = 51 to 75%, 5 = 76 to 100 %. A myocardial segment with a 0 to 25 % TEI was considered viable (13). The percentage of dysfunctional but viable myocardium per patient was calculated by dividing the sum of all dysfunctional but viable segments by the total amount of segments.

Statistical analysis

Data are presented as mean ± standard deviation. Two-way analysis of variance with repeated measures over time followed by Bonferroni correction (4 groups) was used to compare changes in SWT in viable segments (<25% TEI), possible viable segments (26 to 75% TEI), non-viable segments (>75% TEI) and remote segments between baseline and follow-up and to evaluate differences in SWT at baseline and at follow-up. The change in left ventricular volume indexes was tested with paired Student t tests. The

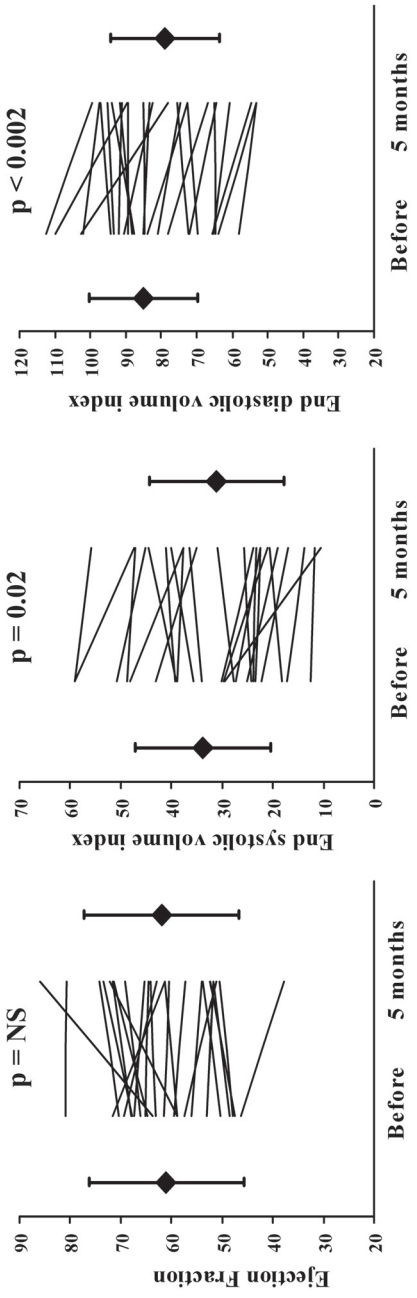

Figure 1. The change in left ventricular volume indexes between baseline and five months follow-up measured with MRI. Mean ejection fraction remained unchanged but end-systolic and end-diastolic volume index decreased significantly.

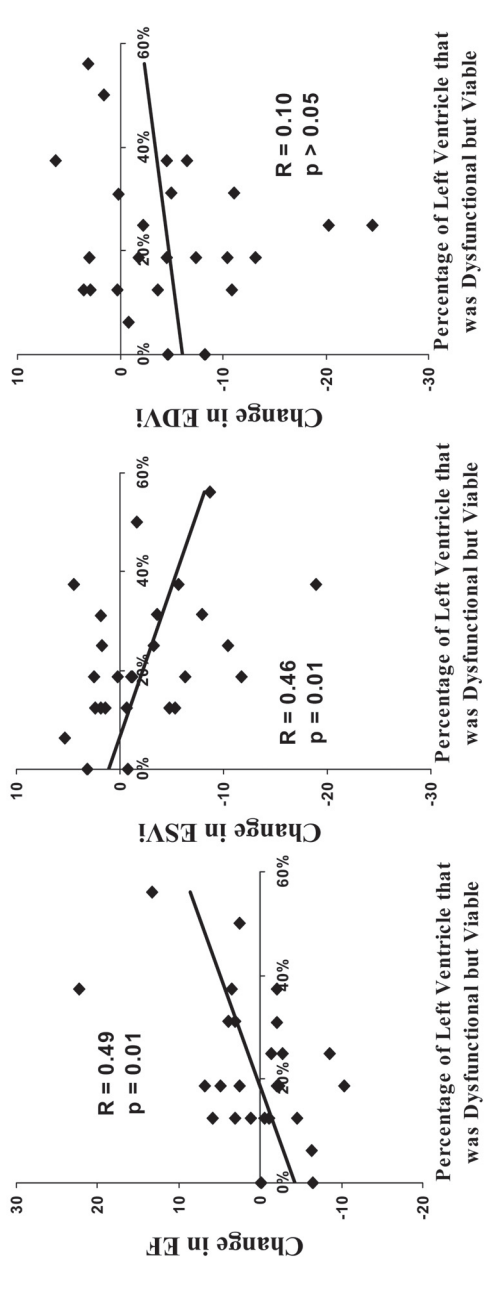

Figure 2. Improvement in end-systolic volume index (ESVi) and ejection fraction (EF) was related to the extent of dysfunctional but viable myocardium before revascularization.No relation was found for end-diastolic vo-lume index (EDVi).

relationship between the viability score per patient and the change in left ventricular volumes was analyzed with univariate linear regression analysis. All tests were performed two-sided, and significance was accepted at p value of ≤ 0.05.

Results

Patient population

CTO was found in the left anterior descending coronary artery in 14 patients, in the right coronary artery in 10 patients, and in the circumflex coronary artery in 3 patients. Mean duration of occlusion was 7 ± 5 months. The overall mean procedural time was 143 ± 62 min. A total of 432 segments were available for analysis, and no segments had to be excluded because of image quality.

Left Ventricular Function and Volumes

Mean end-systolic volume index decreased significantly from 34 ± 13 ml/m^2 to 31 ± 13 ml/m^2 (p = 0.02; 66 ± 29 ml to 60 ± 28 ml, p = 0.02) and mean end-diastolic volume index decreased significantly from 84 ± 15 ml/m^2 to 79 ± 15 ml/m2 (p < 0.002; 162 ± 38 ml to 153 ± 36 ml, p = 0.002) Overall mean ejection fraction remained unchanged from 61 ± 9% to 62 ± 11% (p = 0.54) (**Figure 1**). The extent of the left ventricle that was dysfunctional but viable before revascularization was related to improvement in end-systolic volume index (R = 0.46; p = 0.01) and ejection fraction (R = 0.49; p = 0.01) but not to the end-diastolic volume index (R = 0.10; p = 0.53) (**Figure 2**).

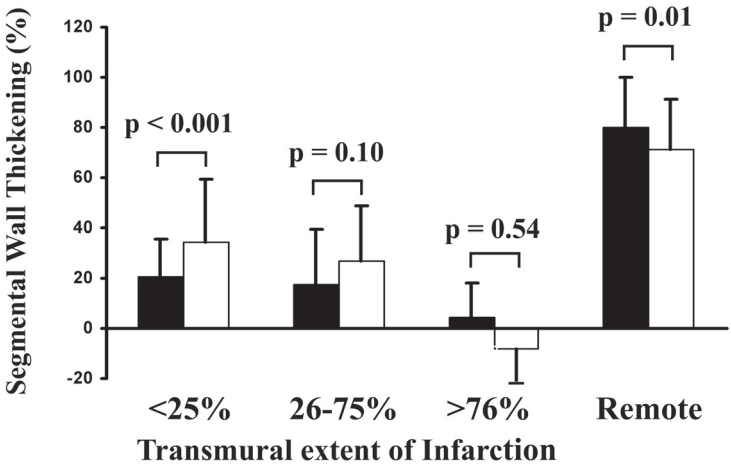

Figure 3. Improvement in segmental wall thickening (SWT) was related to the transmural extent of infarction assessed with MRI before revascularization. Solid bars = before revascularization; open bars: five months after revascularization

In dysfunctional but viable segments (<25% TEI), mean SWT improved significantly from 21 ± 15% to 35 ± 25% ($p < 0.001$) while mean SWT tended to improve from 18 ± 22% to 27 ± 22% ($p = 0.10$) in segments with 25% to 75% TEI and did not improve (4 ± 14% to -9 ± 14%; $p = 0.54$) in segments with >75% TEI (**Figure 3**).

Improvement of more than 10% in absolute SWT was observed in 76% of dysfunctional segments (16 of 21) with TEI 0%, in 67% (4 of 6) with TEI 1% to 25%, 35% (6 of 17) with TEI 26% to 50%, 35% (5 of 14) with TEI 51% to 75% and in 0% (0 of 4) with TEI >75%. The sensitivity, specificity, positive and negative predictive values of MRI for predicting segmental improvement were 65% (20 of 31), 77% (24 of 31), 74% (20 of 27), 69% (24 of 35) respectively, using <25% TEI as the threshold for viability. Left ventricular mass index did not change significantly from 64 ± 13 g/m^2 to 63 ± 11 g/m^2 ($p = 0.25$; 127 ± 27 g to 122 ± 22 g, $p=0.26$).

Discussion

We showed the beneficial effect of successful drug-eluting stent implantation for CTO on end-systolic and end-diastolic volumes and SWT. Furthermore, we showed that the extent of dysfunctional but viable myocardium before revascularization was related to improvement in end-systolic volume, ejection fraction, and SWT.

Previous sudies investigated the effect of successful PCI for CTO on left ventricular function (5,14-18). Overall, the average of left ventricular improvement is not overwhelming and is likely to escape detection by crude measurements of global left ventricular ejection fraction and appears to be limited to fairly recent occlusions. In the current study, we used up-to-date methodology to study a well-defined group of patients with a duration of occlusion of more than six weeks and well developed collaterals making PCI feasible. All patients received a drug-eluting stent with reported low restenosis/reocclusion rates and all patients underwent MRI before and after PCI, permitting refined assessment of left ventricular volumes and myocardial viability. The magnitude of change observed in global left ventricular indexes was relatively small but in line with previously reported data on patients studied after myocardial infarction (19,20).

In the present study, ce-MRI predicted 74% of dysfunctional but viable segments correctly for showing improvement in function after revascularization. The remaining 26% of segments did not improve, although >75% of the wall consisted of viable myocardium as defined by ce-MRI. Experimental studies demonstrated that ce-MRI

can accurately differentiate viable myocardium from scarred myocardium in dogs 8 weeks after reperfused infarction (8). However, viable myocardium in patients with chronic ischemic heart disease might undergo changes determined by the severity of the coronary artery stenosis, the duration and frequency of limited flow to the myocardium and the quality of myocardial perfusion at rest. Myocardial biopsies in patients with chronic myocardial ischemia demonstrated signs of atrophy and degeneration in chronic ischemic but predominantly viable myocardium (21). These microscopic changes of ischemic myocardium are not depicted with currently available imaging techniques, but might explain the variation observed in the reversibility of dysfunctional but viable myocardium as defined by ce-MRI. Additional techniques such as dobutamine stress MRI performed before revascularization might identify reversible dysfunctional myocardium better than ce-MRI since it allows a direct assessment of the contractile reserve of dysfunctional myocardium (22). However, a lack of functional improvement does not preclude a beneficial effect of restoring blood flow to dysfunctional but predominantly viable myocardium. In the present study, restoring blood flow to dysfunctional but viable myocardium led to a moderate improvement in function and a reduction in adverse remodeling in a majority of patients with a CTO, but other beneficial effects like prevention of arrhythmias and prevention of recurrent myocardial ischemia were not assessed.

Limitations

Angiography at follow-up was not performed but no clinical evidence of recurrent myocardial ischemia was noted and all patients received a drug-eluting stent with very low numbers of restenosis reported (4). The definition for CTO was arbitrarily set at six weeks in the present study while previous studies defined CTO as seven days till until three months of occlusion time. Delayed enhancement patterns at follow-up were not studied but might provide further insight in the pathophysiological mechanisms underlying recovery of function of viable myocardium.

Conclusion

Implantation of a drug-eluting stent in patients with a chronic total coronary occlusion has a beneficial effect on myocardial contractility and left ventricular volumes. Improvement in regional and global left ventricular function after revascularization is related to the extent of dysfunctional but viable myocardium assessed with MRI before revascularization.

References

1. Christofferson RD, Lehmann KG, Martin GV, Every N, Caldwell JH, Kapadia SR. Effect of chronic total coronary occlusion on treatment strategy. Am J Cardiol 2005;95:1088-91.
2. Kahn JK. Angiographic suitability for catheter revascularization of total coronary occlusions in patients from a community hospital setting. Am Heart J 1993;126:561-4.
3. Suero JA, Marso SP, Jones PG, et al. Procedural outcomes and long-term survival among patients undergoing percutaneous coronary intervention of a chronic total occlusion in native coronary arteries: a 20-year experience. J Am Coll Cardiol 2001;38:409-14.
4. Hoye A, Tanabe K, Lemos PA, et al. Significant reduction in restenosis after the use of sirolimus-eluting stents in the treatment of chronic total occlusions. J Am Coll Cardiol 2004;43:1954-8.
5. Sirnes PA, Myreng Y, Molstad P, Bonarjee V, Golf S. Improvement in left ventricular ejection fraction and wall motion after successful recanalization of chronic coronary occlusions. Eur Heart J 1998;19:273-81.
6. Danchin N, Angioi M, Cador R, et al. Effect of late percutaneous angioplastic recanalization of total coronary artery occlusion on left ventricular remodeling, ejection fraction, and regional wall motion. Am J Cardiol 1996;78:729-35.
7. Van Belle E, Blouard P, McFadden EP, Lablanche JM, Bauters C, Bertrand ME. Effects of stenting of recent or chronic coronary occlusions on late vessel patency and left ventricular function. Am J Cardiol 1997;80:1150-4.
8. Kim RJ, Fieno DS, Parrish TB, et al. Relationship of MRI delayed contrast enhancement to irreversible injury, infarct age, and contractile function. Circulation 1999;100:1992-2002.
9. Baks T, van Geuns RJ, Biagini E, et al. Recovery of left ventricular function after primary angioplasty for acute myocardial infarction. Eur Heart J 2005;26:1070-7.
10. Rentrop KP, Cohen M, Blanke H, Phillips RA. Changes in collateral channel filling immediately after controlled coronary artery occlusion by an angioplasty balloon in human subjects. J Am Coll Cardiol 1985;5:587-92.
11. Cerqueira MD, Weissman NJ, Dilsizian V, et al. Standardized myocardial segmentation and nomenclature for tomographic imaging of the heart: a statement for healthcare professionals from the Cardiac Imaging Committee of the Council on Clinical Cardiology of the American Heart Association. Circulation 2002;105:539-42.
12. Holman ER, Buller VG, de Roos A, et al. Detection and quantification of dysfunctional myocardium by magnetic resonance imaging. A new three-dimensional method for quantitative wall-thickening analysis. Circulation 1997;95:924-31.
13. Kim RJ, Wu E, Rafael A, et al. The use of contrast-enhanced magnetic resonance imaging to identify reversible myocardial dysfunction. N Engl J Med 2000;343:1445-53.
14. Dzavik V, Carere RG, Mancini GB, et al. Predictors of improvement in left ventricular function after percutaneous revascularization of occluded coronary arteries: a report from the Total Occlusion Study of Canada (TOSCA). Am Heart J 2001;142:301-8.

15. Singh A, Murray RG, Chandler S, Shiu MF. Myocardial salvage following elective angioplasty for total coronary occlusion. Cardiology 1987;74:474-8.
16. Pfisterer ME, Buser P, Osswald S, Weiss P, Bremerich J, Burkart F. Time dependence of left ventricular recovery after delayed recanalization of an occluded infarct-related coronary artery: findings of a pilot study. J Am Coll Cardiol 1998;32:97-102.
17. Melchior JP, Doriot PA, Chatelain P, et al. Improvement of left ventricular contraction and relaxation synchronism after recanalization of chronic total coronary occlusion by angioplasty. J Am Coll Cardiol 1987;9:763-8.
18. Bellenger NG, Yousef Z, Rajappan K, Marber MS, Pennell DJ. Infarct zone viability influences ventricular remodelling after late recanalisation of an occluded infarct related artery. Heart 2005;91:478-83.
19. Pfeffer MA, Lamas GA, Vaughan DE, Parisi AF, Braunwald E. Effect of captopril on progressive ventricular dilatation after anterior myocardial infarction. N Engl J Med 1988;319:80-6.
20. Mitchell GF, Lamas GA, Vaughan DE, Pfeffer MA. Left ventricular remodeling in the year after first anterior myocardial infarction: a quantitative analysis of contractile segment lengths and ventricular shape. J Am Coll Cardiol 1992;19:1136-44.
21. Canty JM, Jr., Fallavollita JA. Hibernating myocardium. J Nucl Cardiol 2005;12:104-19.
22. Wellnhofer E, Olariu A, Klein C, et al. Magnetic resonance low-dose dobutamine test is superior to SCAR quantification for the prediction of functional recovery. Circulation 2004;109:2172-4.

Automatic Quantitative Left Ventricular Analysis of Cine Magnetic Resonance Images using Three-Dimensional Information for Contour Detection

Robert Jan M. van Geuns, Timo Baks, Ed H. B. M. Gronenschild, Jean-Paul M. M. Aben, Piotr A. Wielopolski, Filippo Cademartiri, and Pim J. de Feyter

Department of Cardiology and Radiology Erasmus MC, University Hospital Rotterdam, the Netherlands

Radiology. 2006 Jul;240(1):215-21

10

Abstract

We validated an automatic contour detection algorithm for the left ventricle (LV) which uses three dimensional information available in magnetic resonance imaging scans in an institutional review board approved study with obtained consent from 25 patients and volunteers. The outline of the LV was indicated manually in the horizontal and vertical long-axis images. The calculated intersections points with the short-axis (SA) images are the basis of the automatic contour detection.

Automatically derived volumes correlated highly with manually derived (SA based) volumes (r^2 = 0.98). Ejection fraction (EF) and mass showed a correlation of r^2 = 0.95 and r^2 = 0.93, respectively. The automatic contour detection reduced the inter-observer variability to 0.1 ml for endocardial end-diastolic volume (EDV) and end-systolic volume (ESV), to 1.1 ml for epicardial EDV and ESV, to 0.01% for EF and 1.1 g for mass. Thus the algorithm realized an excellent task in obtaining reliable and highly reproducible LV parameters.

Introduction

Accurate and reproducible assessment of left ventricular volumes and ejection fraction is essential for the prognosis of patients with heart diseases and for evaluating therapeutic responses. (1), (2) MR imaging has proven to be an accurate and reproducible imaging modality for the quantitative analysis of left ventricular function.(3),(4) Left ventricular volume and mass as well as regional functional parameters such as wall motion and wall thickening are usually obtained in the true short-axis plane of the left ventricle.(5)(6) (7) (8) These short-axis views minimize partial volume effects and are perpendicular to the direction of wall motion and wall thickening.

Automatic segmentation of the left ventricle in MR images is not trivial. One of the main obstacles is caused by the transitions in gray levels across the endocardial and epicardial boundaries, which are not sharp and differ in sign (bright to dark and vice versa). Moreover, large variations in image quality in MR imaging and large variations in shape of the left ventricle poses even more challenges for such an image processing task. Several approaches for border recognition have been developed, ranging from manual to semi-automatic and fully automatic techniques. (9) (10) (11) (12) (13) (14) (15)(16) (17) (18) (19). The applied techniques range from purely data driven (edge detection, region growing) to model driven (model fitting).

Because of the limited or partial successful performance of the reported methods we have developed an automatic boundary detection algorithm. The proposed algorithm does not make any anatomical assumptions and requires only a set of manual epicardial contours in the two- and four-chamber images at end-systole and end-diastole as single user input. It takes advantage of the three-dimensional information obtained from the MRI system in order to start the segmentation process for both the endocardial and epicardial contours in all short-axis slices. An obvious benefit of such an approach is its intrinsic high reproducibility.

The purpose of our study was to evaluate the automatic boundary detection algorithm of the left ventricle in MR short-axis images with the essential restriction of no manual corrections.

Materials and Methods

Patient selection

The study population consisted of 13 patients and 12 healthy volunteers. The patients (9 male, 4 female, mean age 47 years) were studied for left ventricular function in a

protocol on experimental cell therapy for ischemic heart failure. The volunteers (11 male, mean age 30 years, all employees of the Erasmus MC or Pie Medical Imaging) reported no history of cardiac disease or present health problems. On six patients and nine volunteers cine MR imaging was performed twice with a time interval of one hour up to one year. This resulted in a total of 40 scans included in this study. All patients and volunteers gave informed consent to this study that was approved by the institutional review board.

Data acquisition

All patients and healthy volunteers were examined on a 1.5 Tesla whole-body MRI system (Sonata, Siemens, Erlangen, Germany). Cine MRI was performed using an electrocardiogram triggered breath-hold steady state free precession acquisition technique in a supine position with a 4-channel quadrature body phased array coil placed over the thorax. Imaging parameters were: TR = 3.2 ms, TE = 1.6 ms, flip angle was 65 degrees, temporal resolution was 47 ms, slice thickness was 8 mm, with a slice gap of 2 mm, field of view was 300 x 340 mm, and matrix size was 224 x 256. Using standard techniques to identify the major cardiac axes, two-chamber, four-chamber, and short-axis cine sequences were acquired during breath hold in end expiratory phase. Typically, eleven cine breath-hold short-axis slices were acquired to encompass the entire left ventricle from apex to base. The number of images per cardiac cycle was dependent on the heart rate and varied between 18 and 24. The total imaging time for a complete scans was about 20 minutes.

Image analysis

All the scans were transferred to a Microsoft Windows™ based personal computer for further analysis with the current algorithm which is implemented in the CAAS-MRV 1.0 program (Pie Medical Imaging BV, the Netherlands). Two experienced investigators (9 and 2 years cardiac MRI experience) independently traced both the endocardial and epicardial contours manually in the short-axis views in the end-diastolic (ED) and end-systolic (ES) heart phases, which served as reference results. One observer (RvG) traced all 40 scans and subsequently a subset of 10 scans (first 7 patients, first 3 volunteers) in order to derive the intra-observer variability. An independent second observer (TB) traced contours in the same subset of 10 scans to derive the inter-observer variability. Papillary muscles and trabeculations were treated as being part of the blood pool volume.

For the automatic left ventricle segmentation a total of four epicardial contours are required, one in each of the two-chamber ED and ES views and one in each of the four-chamber ED and ES views. These contours can be drawn relatively quickly, by

indicating the valve plane by two points followed by the apex position. An open spline curve is then fitted through these points. Adding, adjusting or removing points will tailor the curve to the desired shape. Typically, eight points are sufficient to indicate the epicardial wall. Again one observer (RvG) traced al 40 scans, the second investigator (TB) traced the same 10 scans as for the full manual analysis. By using the absolute system coordinates obtained from the MRI system (through the DICOM headers) the short-axis (SA) images can be cross-referenced with the orthogonal two- and four-chamber long-axis (LA) views, as depicted in **Figure 1**. This results in four intersection points of the LA epicardial borders with each SA slice. A closed spline curve is automatically fitted to these points, yielding a first guess of the SA epicardial border. Starting from this first guess a segmentation algorithm derives the endocardial borders in this slice for all (18–24) cardiac phases. This algorithm heavily draws on the concept of fuzzy objects in which image elements (pixels/voxels) exhibit a similarity or "hanging togetherness" both in geometry and in grey-scale values.[Udupa, 1996 #804] The algorithm will properly differentiate the papillary muscles located inside the left ventricle from the blood volume. A smooth convex hull produces the final endocardial contour, now including the papillary muscles as part of the LV volume. Guided by this endocardial contour, the epicardial contour is subsequently obtained on the basis of a radial minimum cost algorithm. This step is repeated for all short axis slices covering the left ventricle as defined in the long axis views. The average segmentation time is about two minutes on a 2.4GHz Pentium IV. Within this time the full set of multiphase and multislice SA scans (typically 300 images) is segmented. We have to stress here that for the current study no manual corrections are performed afterwards.

Each endocardial and epicardial volume is computed using Simpson's rule: it is the summation over all slices of the areas within the endocardial and epicardial contours multiplied by the slice thickness (including the inter-slice gap). Myocardial mass is calculated by taking the difference of the ED endocardial volume and the ED epicardial volume multiplied by 1.05 g/cm^3, the standard mass for each cubic centimeter. Finally, the ejection fraction (EF) is derived by calculating the stroke volume from ED and ES endocardial volumes divided by the ED endocardial volume.

Statistical analysis

To assess the reliability of the automatic segmentation algorithm, the derived ED and ES ventricular volumes (EDV and ESV, respectively) for the endocardium as well as epicardium, the EF and the myocardial mass were compared with the manually derived values of observer RvG. The agreement between the manual and automatic segmentation is expressed as the mean and standard deviation of the paired differences in each data set. A two-tailed, paired Student t-test was performed to determine the

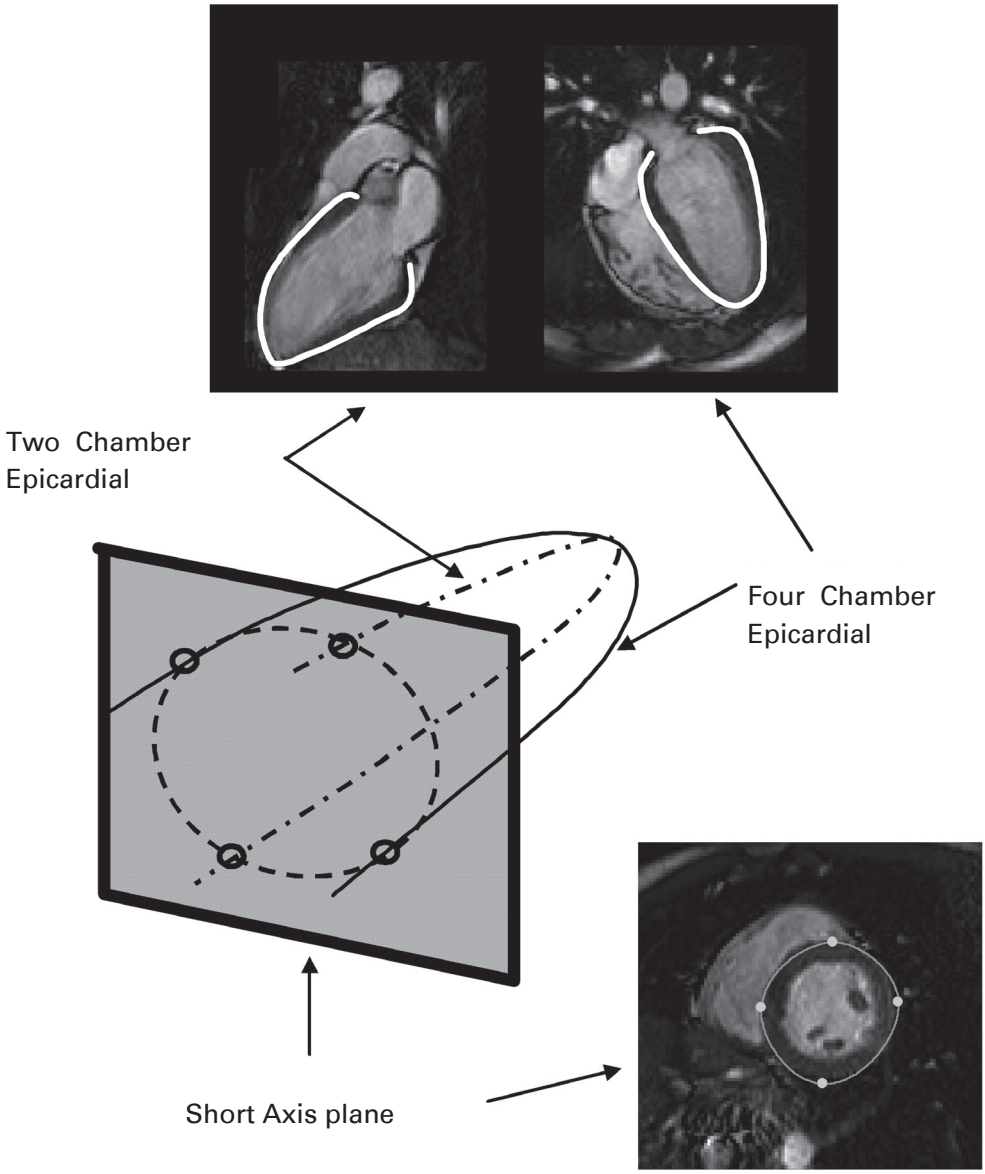

Figure 1. Based on the epicardial boundaries in the 2-chamber and 4-chamber images, four intersection points with each SA image can be determined. A spline is fitted to these four points that subsequently starts the automatic left ventricle segmentation algorithm.

statistical significance of the observed differences. A p-value of less then 0.05 was considered to be statistically significant. The percentage difference relative to the average value of the paired manual volumes was also calculated. A linear regression analysis was applied to quantify the correlation between the automatic and manual volumes.

To be able to put the observed differences in perspective we also determined the inter- and intra-observer variabilities of the measurements based on a repeated manual tracing of the ventricular borders. Two comparison sets were obtained, each based on 10 scans: RvG.1 (first time) versus RvG.2 (second time) (Intra) and the averaged difference of RvG.1 versus TB and RvG.2 versus TB (Inter).

As described above, the automatic segmentation is started from manually drawn two-chamber and four-chamber epicardial contours. To assess the reproducibility of the automatic segmentation algorithm these contours were drawn twice by RvG and independently once by TB, all in the same 10 scans. An essential prerequisite for determining the reproducibility is that no manual corrections are made afterwards. Based on the available three sets of contours an estimate of the true reproducibility of the algorithm was derived.

In view of the small number of paired values (n = 10), a Wilcoxon signed-ranks test was applied to determine the statistical significant differences between intra- and inter-observer variabilities and between observer variabilities of manual and automatic segmentation.

Results

For the volunteers the manual average end-diastolic volume was 125 +/- 27 ml, end-systolic volumes was 49 +/- 11 ml. Ejection fraction and mass were 60 +/- 6 % and 124 +/- 23 g, respectively. These results are concordant with the literature.

For the patients the manual average end-diastolic volume was 201 +/- 94 ml, end-systolic volume was 132 +/- 77 ml. Ejection fraction and mass were 36 +/- 16 % and 196 +/- 62 g respectively.

Intra- and inter-observer variabilities of manual volumes, EF and mass

In the manual measurements there was a significant difference between the first and second measurement of the first observer for the two endocardial volumes, ES epicardial volume and mass. (**Table I**). A significant difference also existed between

both observers for all measurements, except for EF. There was an agreement between the two observers on a level of about 17 ml (8 %) for the endocardial volumes and about 15 ml (4 %) for the epicardial volumes. For EF the level of agreement was about 2 percentage points (5%). For the myocardial mass the intra-observer variability was about 7 g (4%) whereas the inter-observer variability was much larger (approximately 33 g (20%)) because there was a systematic positive difference for endocardial volumes combined with a negative difference for epicardial volumes between the two observers. For all measurements the inter-observer-variability was significantly larger than the intra-observer variability.

Reliability of automatic volumes, EF and mass

There was an excellent agreement (R^2adj:0.93 to 0.98) between the automatic and manual measurement of the left ventricular volumes, EF and myocardial mass (**Table II**). We observed a slight underestimation in the endocardial volumes of about 5% and a slight overestimation in the epicardial volume(mean: 2%), resulting in a moderately overestimated myocardial mass (approximately 6%). The EF was also slightly overestimated as compared to the manually derived value (5%). The results are comparable to the inter-observer variabilities listed in Table I and slightly worse than the intra-observer variabilities. The results are further detailed in Bland-Altman plots (**Figure 2**) showing the differences for each of the two paired measurements versus their averages.

Reproducibility of automatic volumes, EF and mass

For the automatic contour detection no significant differences could be observed between the first and second measurement of the first observer or between the first and second observer(**Table III**).

The reproducibility of the automatic analysis is high for the endocardial volumes; compared to the manual intra- and inter-observer variabilities it can be noticed that the average difference as well as the standard deviation was dramatically decreased to a level of ≤ 0.35 ml (0.20%) and ≤ 1.32 ml (0.61%), respectively. For the epicardial volumes, EF and myocardial mass the reproducibility was significantly higher as compared to the inter-observer variabilities, whereas it was similar to the intra-observer variabilities.

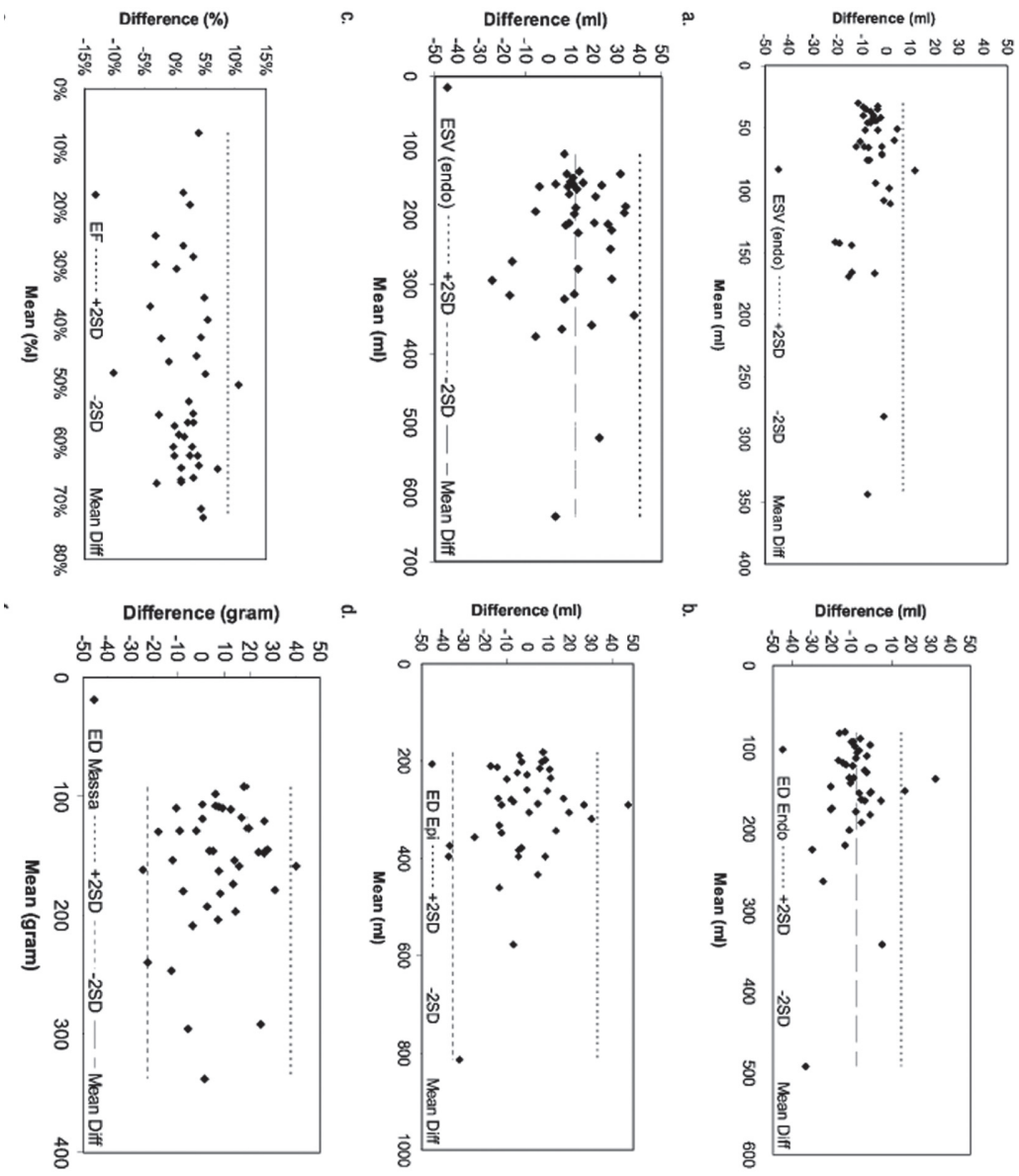

Figure 2. Comparison of manually derived LV volumes with automatically derived volumes. The results are presented in Bland-Altman plots for the endocardial ESV (**A**), and EDV (**B**), the epicardial ESV (**C**) and EDV (**D**), EF (**E**) and mass (**F**). The dashed lines show the respective means of the volume differences and the dotted lines the ± 2 standard deviations.

Table I. Intra- and inter-observer variabilities (ml and %) based on the manually drawn contours (n=10)

	Intra[1]	Intra [%]	Av. Inter[2]	Av. Inter [%]
Endocardial EDV[3]	-6.18 ± 3.63 ml*	-2.57 ± 1.51	16.07 ± 13.90 ml*	6.46 ± 5.58#
Endocardial ESV[4]	-3.20 ± 3.96 ml*	-2.07 ± 2.56	17.72 ± 14.85 ml*	10.61 ± 8.89#
Epicardial EDV	0.46 ± 4.03 ml	0.11 ± 0.97	-15.21 ± 12.41 ml*	-3.74 ± 3.05#
Epicardial ESV	4.37 ± 7.46 ml*	1.35 ± 2.30	-15.36 ± 12.70 ml*	-4.77 ± 3.95#
EF5	-0.08 ± 2.49 %	-0.20 ± 6.15	-2.37 ± 2.53 %	-5.57 ± 5.95#
Mass	6.98 ± 6.83 g*	3.82 ± 3.74	-32.85 ± 20.54 g*	-19.76 ± 12.35#

* Statistically significant ($p < 0.05$)
\# Statistically significant ($p < 0.05$) compared to intra-observer variability
[1] Difference RvG.2 – RvG.1
[2] Averaged difference TB – RvG.1 and TB – RvG.2
[3] EDV = end-systolic volume
[4] ESV = end-systolic volume
[5] EF = ejection fraction

Table II. Results of comparing automatic with manual LV measurements (n=40).

	Auto–Manual	Auto-Manual [%]	Linear regression	R^2adj[1] SE[2]
Endocardial EDV[3]	-8.15 ± 11.46 ml*	-5.05 ± 7.10	0.95x + 0.33	0.9810.86 ml
Endocardial ESV[4]	-5.95 ± 6.34 ml*	-6.71 ± 7.15	0.98x - 4.19	0.996.28 ml
Epicardial EDV	-1.30 ± 17.11 ml	-0.42 ± 5.48	0.94x + 16.87	0.9815.78 ml
Epicardial ESV	12.12 ± 13.96 ml*	5.25 ± 6.05	0.98x + 17.25	0.9813.93 ml
EF5	1.61 ± 3.53%	5.06 ± 13.12	1.00x + 1.55	0.953.63 %
Mass	7.19 ±15.00 g*	5.91 ± 10.52	0.93x + 18.93	0.9314.76 g

* Statistically significant ($p < 0.05$)
[1] R^2adj = squared adjusted multiple correlation
[2] SE = the standard error of the residuals
[3] EDV = end-systolic volume
[4] ESV = end-systolic volume
[5] EF = ejection fraction

Table III. Intra- and inter-observer variabilities (ml and %) based on the automatic contours (n=10).

	Intra1	Intra [%]	Av. Inter2	Av. Inter [%]
Endocardial EDV[3]	-0.35 ± 1.32 ml	-0.16 ± 0.61#	-0.08 ± 0.32 ml	-0.04 ± 0.15#
Endocardial ESV[4]	-0.28 ± 0.54 ml	-0.20 ± 0.37#	-0.07 ± 0.45 ml	-0.05 ± 0.30#
Epicardial EDV	-4.53 ± 6.82 ml	-1.11 ± 1.68	-1.11 ± 6.33 ml	-0.27 ± 1.55#
Epicardial ESV	-1.35 ± 6.77 ml	-0.37 ± 1.84	-1.05 ± 9.63 ml	-0.29 ± 2.63#
EF5	-0.21 ± 0.36 %	-0.52 ± 0.88#	-0.02 ± 0.26 %	-0.05 ± 0.69#
Mass	-4.38 ± 6.97 g	-2.19 ± 3.49	-1.08 ± 6.65 g	-0.52 ± 3.1#

Statistically significant ($p < 0.05$) as compared to manual intra- or inter-observer variability
[1] Difference RvG.2 – RvG.1
[2] Averaged difference TB – RvG.1 and TB – RvG.2
[3] EDV = end-systolic volume
[4] ESV = end-systolic volume
[5] EF = ejection fraction

Table IV. Comparison with literature

	Endocardial			
	EDV [ml]	ESV [ml]	EF [%]	Mass [g]
Van der Geest et al.1997 [10]	-5.5 ± 9.7	-3.6 ± 6.5	1.7 ±4.1	7.2 ± 15.0
Nachtomy et al 1998 [12]	15.3 ± 13.7	-1.4 ± 7.1	0.85 ± 7.0	27.1 ± 40.6
Furber et al 1998 [11]	--	--	--	8.5 ± 6.1
Lalande et al 1999 [13]	--	--	4.7± 2.7	--
Graves et al. 2000[15]	-8.8 ± 5.3	-2.2 ± 3.6	-0.9 ± 3.1	--
Young et al. 2000 [14]	2.2 ± 4.6	2.3 ± 3.8	1.1 ± 2.5	1.8 ± 4.9
Barkhausen et al 2001 [16]	-4.8±9.2	-3.8 ± 6.75	0.5 ± 3.2	--
Francois et al 2004 [18]	--	--	--	5.0 ± 7.2
Van der Geest et al.2004 [vd G	-2.9 ± 13.2	-5.1 ± 18.9	0.0 ± 6.8	-1.2 ± 14.1
Current study	-8.15 ± 11.46	-5.95 ± 6.34	1.6 ± 3.5	7.19 ± 15.00

Discussion

An automatic left ventricle segmentation algorithm has been developed that requires only a set of epicardial contours in the two-chamber and four-chamber ED and ES slices as single user input. In this study no manual contour editing was performed, allowing a reliable comparison with manual measurements and a true assessment of the reproducibility of the segmentation technique.

The automatically derived endocardial and epicardial volumes highly correlate with the volumes obtained from manual analysis, although a statistical significant systematic difference for some measurements is present. Obtaining a high correlation between two measurements is more important than obtaining a small absolute difference especially when no golden standard is available. In addition, the systematic differences are of the same order as the intra- and inter-observer variabilities for the manual measurements. Also in this respect, the automatic segmentation performed equally well as an experienced observer. Moreover, the reliability of the endocardial volumes is similar to those reported in literature (**Table IV**). It should be noted that values for the epicardial volumes are not present in literature known to us. Usually, however, myocardial mass is reported which is implicitly dependent on both the epicardial and endocardial contours. The results for myocardial mass using our technique without manual corrections are comparable to techniques involving manual corrections. The summary of the results in Table IV shows an interesting finding: in all cases but one the endocardial volumes are underestimated compared to the manually derived volumes. The explanation of this deviation is not completely understood. Most probably other considerations than purely based on pixel grey-scale values play a role in the manual delineation of the ventricular borders by a clinician. With this in mind there may be some room for future improvements here.

A basic requirement for any automatic algorithm is that it is highly reproducible. To assess the reproducibility we varied the input of the algorithm by repeating the manual tracing of the long-axis contours by the same investigator (RvG) and by an independent second investigator (TB). This resulted in a strong reduction of the intra- and inter-observer variabilities from about 18 ml (10.6%) to about 0.35 ml (0.2%) for the endocardial volumes and from about 15 ml (4.8%) to about 4.5 ml (1.1%) for the epicardial volumes. Restricting the comparison to the inter-observer variabilities the reduction is even more spectacular: from about 17 ml (10-%) to less than 0.1 ml (0.05%)for the endocardial volumes and from about 15 ml (4.8%) to about 1.1 ml (0.3%) for the epicardial volumes. For the associated myocardial mass the reduction is from about 33 g (20%) to about 1 g (0.5%) and for EF from about 2 percentage points

(6%) to 0.01 percentage points (0.04%). Such a high reproducibility can be expected for the approach we took to perform an automatic segmentation. To our knowledge this is the first time that the reproducibility of a LV automatic segmentation algorithm has been assessed.

Whereas almost all techniques are based on only SA image stacks, only Graves et al. (15) describe a technique, which makes use of the two-chamber and four-chamber slices. A severe limitation of their method is that only endocardial contours are derived while the epicardial contours are manually drawn. The power of our algorithm is that the epicardial contour is also automatically detected.

Additional advantages of the method of segmentation presented herein are the following. Although the described validation has been performed only for the end-diastolic and end-systolic cardiac phases, the segmentation algorithm is able to detect the endocardial and epicardial border in all acquired cardiac phases, without any further user interaction. Furthermore, information not present in the SA images can be incorporated in the analysis. For instance, localization of the mitral valve annulus as separator between ventricular and atrial volume is difficult in SA images and can be better defined in two-chamber and four-chamber images. These images also show the motion of the annulus during cardiac motion and the delineation of the apex more clearly. Due to an improved localization of the mitral valve and the apex, it is possible to make corrections to the ventricular volume derived from the contours.

For optimal cross-referencing of the long-axis and short-axis acquisitions reproducibility of breath-hold position is important. Inconsistency in breath-holding will hamper cross referencing but will also lead to impaired image quality of short axis images making reliable assessment of left ventricular volumes more difficult. Our volunteers and patients were only shortly (< 1 minute) instructed of breath-hold techniques during which end-expiratory and a relaxed position was explained.

One limitation of this study is the lack of experience with MR scanners from other manufacturers. On the Siemens scanner, using a large phased array chest coil, surface coil inhomogeneity was limited and the fuzzy connectedness algorithm functioned excellent. For studies obtained on other type of scanners with sometimes smaller surface coils, inhomogeneity artifacts may impair the performance of the algorithm, however, only partially because of the designed underlying affinity function. This potential problem can be solved or reduced using existing dedicated algorithms provided by the manufactures.

In conclusion, we have developed an accurate and highly reproducible algorithm to perform automatic measurement of the left venticular endocardial and epicardial volumes and the associated parameters like myocardial mass and ejection fraction.

References

1. Levy D, Garrison RJ, Savage DD, Kannel WB, Castelli WP. Prognostic implications of echocardiographically determined left ventricular mass in the Framingham Heart Study. N Engl J Med 1990; 322:1561-1566.
2. Koren MJ, Devereux RB, Casale PN, Savage DD, Laragh JH. Relation of left ventricular mass and geometry to morbidity and mortality in uncomplicated essential hypertension. Ann Intern Med 1991; 114:345-352.
3. Pattynama PM, Lamb HJ, van der Velde EA, van der Wall EE, de Roos A. Left ventricular measurements with cine and spin-echo MR imaging: a study of reproducibility with variance component analysis. Radiology 1993; 187:261-268.
4. Bellenger NG, Davies LC, Francis JM, Coats AJ, Pennell DJ. Reduction in sample size for studies of remodeling in heart failure by the use of cardiovascular magnetic resonance. J Cardiovasc Magn Reson 2000; 2:271-278.
5. Fisher MR, von Schulthess GK, Higgins CB. Multiphasic cardiac magnetic resonance imaging: normal regional left ventricular wall thickening. AJR Am J Roentgenol 1985; 145:27-30.
6. von Schulthess GK, Higashino SM, Higgins SS, Didier D, Fisher MR, Higgins CB. Coarctation of the aorta: MR imaging. Radiology 1986; 158:469-474.
7. Higgins CB. Prediction of myocardial viability by MRI. Circulation 1999; 99:727-729.
8. Holman ER, Vliegen HW, van der Geest RJ, et al. Quantitative analysis of regional left ventricular function after myocardial infarction in the pig assessed with cine magnetic resonance imaging. Magn Reson Med 1995; 34:161-169.
9. Baldy C, Douek P, Croisille P, Magnin IE, Revel D, Amiel M. Automated myocardial edge detection from breath-hold cine-MR images: evaluation of left ventricular volumes and mass. Magn Reson Imaging 1994; 12:589-598.
10. van der Geest RJ, Buller VG, Jansen E, et al. Comparison between manual and semiautomated analysis of left ventricular volume parameters from short-axis MR images. J Comput Assist Tomogr 1997; 21:756-765.
11. Furber A, Balzer P, Cavaro-Menard C, et al. Experimental validation of an automated edge-detection method for a simultaneous determination of the endocardial and epicardial borders in short-axis cardiac MR images: application in normal volunteers. J Magn Reson Imaging 1998; 8:1006-1014.
12. Nachtomy E, Cooperstein R, Vaturi M, Bosak E, Vered Z, Akselrod S. Automatic assessment of cardiac function from short-axis MRI: procedure and clinical evaluation. Magn Reson Imaging 1998; 16:365-376.

13. Lalande A, Legrand L, Walker PM, et al. Automatic detection of left ventricular contours from cardiac cine magnetic resonance imaging using fuzzy logic. Invest Radiol 1999; 34:211-217.
14. Young AA, Cowan BR, Thrupp SF, Hedley WJ, Dell'Italia LJ. Left ventricular mass and volume: fast calculation with guide-point modeling on MR images. Radiology 2000; 216:597-602.
15. Graves MJ, Berry E, Eng AA, et al. A multicenter validation of an active contour-based left ventricular analysis technique. J Magn Reson Imaging 2000; 12:232-239.
16. Barkhausen J, Ruehm SG, Goyen M, Buck T, Laub G, Debatin JF. MR evaluation of ventricular function: true fast imaging with steady-state precession versus fast low-angle shot cine MR imaging: feasibility study. Radiology 2001; 219:264-269.
17. Latson LA, Powell KA, Sturm B, Schvartzman PR, White RD. Clinical validation of an automated boundary tracking algorithm on cardiac MR images. Int J Cardiovasc Imaging 2001; 17:279-286.
18. Francois CJ, Fieno DS, Shors SM, Finn JP. Left ventricular mass: manual and automatic segmentation of true FISP and FLASH cine MR images in dogs and pigs. Radiology 2004; 230:389-395.
19. van der Geest RJ, Lelieveldt BP, Angelie E, et al. Evaluation of a new method for automated detection of left ventricular boundaries in time series of magnetic resonance images using an Active Appearance Motion Model. J Cardiovasc Magn Reson 2004; 6:609-617.

Comparison between contrast echocardiography and magnetic resonance imaging to predict improvement of myocardial function after primary coronary intervention

Biagini E, van Geuns RJ, Baks T, Boersma E, Rizzello V, Galema TW, de Feyter PJ, ten Cate FJ.

Am J Cardiol. 2006 Feb 1;97(3):361-6

11

Abstract

The relative merits of myocardial contrast echocardiography (MCE) and magnetic resonance imaging (MRI) to predict myocardial function improvement after percutaneous coronary intervention have not been evaluated until now. We studied 35 consecutive patients with acute myocardial infarction who underwent percutaneous coronary intervention using MCE and MRI and first-pass imaging for evaluation of myocardial perfusion. Delayed-enhanced MRI was included as another method to differentiate viable from infarcted tissue. MCE was performed by power modulation and intravenous Sonovue. A 16-segment model of the left ventricle was used to analyze all myocardial contrast echocardiograms and magnetic resonance images. At 60 days of follow-up, MCE showed improvement of function in 115 of 192 (60%) dysfunctional segments. The sensitivity, specificity, and accuracy for the prediction of functional improvement were comparable among MCE (87%, 90%, and 88%), first- pass MRI (87%, 60%, and 79%), and delayed-enhancement MRI (75%, 100%, and 82%, respectively, all p = NS). In conclusion, MCE and MRI allowed for prediction of myocardial function improvement after percutaneous coronary intervention. MCE had a comparable accuracy and, as a bedside technique, may be an alternative tool in the acute phase of acute myocardial infarction.

Introduction

Restoration of coronary blood flow in acute myocardial infarction (AMI) after percutaneous coronary intervention (PCI) is related to improved clinical outcome.[1] However, successful recanalization of the occluded vessel does not always result in recovery of myocardial function, because the microvascular integrity and myocytes may be irreversibly damaged after AMI.[2] The lack of contractile function after PCI may be caused by reversible (myocardial stunning) or irreversible (necrosis) myocardial damage. The distinction between these two pathophysiologic entities may help to define patient-tailored therapy, justifying the use of mechanical support, as well relative caution regarding inotropic therapy for patients with myocardial stunning.[3] Myocardial contrast echocardiography (MCE) and contrast-enhanced magnetic resonance imaging (MRI) are noninvasive techniques able to assess myocardial function and perfusion. Additionally, delayed contrast-enhanced MRI is able to assess irreversible cellular damage. Several studies have confirmed the ability of MCE to predict the improvement of myocardial function after reperfusion in AMI.[4–12] Recently, it has become clear that contrast-enhanced MRI can be performed in humans early after AMI and allows for prediction of functional improvement.[13–19] Contrast-enhanced MRI can be performed to evaluate myocardial perfusion during the first pass of the contrast agent or, alternatively, to detect necrosis using delayed contrast-enhanced MRI 20 minutes after contrast injection. The relative merits of these noninvasive techniques are not yet clear. The aim of this study was to compare MCE and contrast-enhanced MRI to assess myocardial perfusion/viability and to predict improvement of myocardial function after PCI for AMI.

Methods

Patients and study protocol

This prospective study comprised 42 consecutive patients with ST-elevation AMI who underwent PCI within 6 hours of symptom onset. The diagnosis of AMI was made on the basis of symptoms consistent with myocardial ischemia for 30 minutes and 2 mm ST-segment elevation in 2 contiguous electrocardiographic leads. The infarct-related artery was identified by the site of coronary occlusion during coronary angiography and electrocardiographic criteria. Stent implantation was performed in all patients. The local hospital ethics committee approved the study protocol, and all patients gave informed consent. MCE was performed within 48 hours after coronary intervention and not more then 48 hours before MRI, although in most cases, the 2 techniques were performed on the same day. In 5 patients, MRI could not

be performed because of claustrophobia in 2 patients and the necessity of an aortic balloon device in 3 patients who presented with unstable clinical conditions. Two patients were excluded because of nonoptimal delayed-enhancement image quality. Therefore, the final population consisted of 35 patients. All 35 patients had adequate myocardial contrast echocardiographic studies. Improvement of resting regional and global contractile function was assessed with follow-up MCE at 60 days in all patients, using left ventricular opacification for better detection of the endocardial border, exactly as in the baseline examinations. The mean interval between the baseline and follow-up studies was 68 ± 7 days.

Contrast echocardiographic studies

Echocardiography was performed with a Philips Sonos 5500 system (Andover, Massachusetts) using second harmonic imaging (1.8 MHz/3.6 MHz), 24 to 48 hours after revascularization to assess regional and global left ventricular function. After recording the baseline images, myocardial perfusion images were obtained during contrast injection in real-time (power modulation) using a low mechanical index (0.1). A slow bolus of 0.75 ml of sulfur hexafluoride (Sonovue, Bracco, Italy) was intravenously injected, followed by a slow saline flush (5 ml) for 5 seconds. If left ventricular opacification and myocardial perfusion were not optimal, additional doses of 0.5 ml of contrast agent were injected. Real-time power modulation imaging began before contrast injection, and "flash" imaging with a high mechanical index (1.6) was used at peak contrast intensity to destroy the microbubbles in the myocardium to exclude artifacts and to visualize myocardial contrast replenishment (15 cycles). After the real-time perfusion study, left ventricular opacification images for endocardial border assessment were recorded using a 0.4 mechanical index to improve quantitative assessment of regional and global myocardial function.[20] Left ventricular volumes and ejection fraction were measured using the modified biplane Simpson rule.[21] An improvement in left ventricular ejection fraction of ≥ 5% at follow-up was considered clinically significant.[22] Images were digitally stored on the Philips Sonos S500 System (Eindhoven, The Netherlands).

Analysis of echocardiographic studies

Regional wall motion and myocardial perfusion were scored by 2 observers who had no knowledge of the clinical, MRI, or angiographic data, using standard parasternal long- and short-axis views and apical 2-, 3-, and 4-chamber views. The left ventricle was divided according to a standard 16-segment model.[21] Only segments related to the acute infarct territory were considered for analysis. The myocardial segments were assigned to the coronary arteries as previously described.[23] Segments were scored as 1 = normal; 2 = hypokinetic; 3 = akinetic; and 4 = dyskinetic. Myocardial

contrast perfusion was scored semiquantitatively using a 3-point scale: grade 0, no opacification; grade 1, reduced/ patchy opacification; and grade 2, normal/ homogenous opacification. Segments with a hypokinetic or akinetic wall motion pattern were considered dysfunctional. Recovery of contractile function was defined as an improvement of segmental wall motion score by 1 grade at follow-up. As previously reported,[7] in each patient, a myocardial contrast echocardiographic score index was derived by averaging the perfusion scores from each dysfunctional segment divided by the number of dysfunctional segments. A patient was considered to have adequate reperfusion if the score index was 1.7

Contrast-enhanced MRI studies

All patients were studied in a supine position, with a 4-channel quadrature body phased-array coil placed over the thorax, in a 1.5-T whole body MRI system (General Electric, Milwaukee, Wisconsin; Signa CV/i, with an amplitude of 40 mTm^{-1} and a slew rate of 150 Tm^{-1} $second^{-1}$). For semiquantitative analysis, 2-, 3-, 4-chamber and approximately 10 to 12 cine short-axis series (slice thickness 8 mm, gap 2 mm) covering the heart from base to apex were acquired using a breath-hold, cardiac-triggered, steady-state, free-precession sequence with a repetition time and echo time of 3.5 and 1.3 ms, respectively, and a flip angle of 45°. The additional imaging parameters were as follows: field of view 360 x 270 mm, matrix 160 x 128 pixels, and number of shots 12, resulting in a temporal resolution of 42 ms. After the cine images were acquired, the patients received an intravenous bolus of 0.1 mmol/kg gadolinium-diethylenetriamine pentaacetic acid (Magnevist, Schering, Berlin, Germany) at a rate of 5 ml/s using an infusion pump. A first-pass perfusion scan was acquired simultaneously with the bolus injection for 40 to 50 heartbeats. First-pass perfusion images (early hypoenhancement) were acquired using an electrocardiographic-gated saturation recovery interleaved gradient echo- planar imaging pulse sequence, covering the heart with 5 to 8 evenly spaced lices every heart beat. The imaging parameters were as follows: repetition time 6.8 ms, echo time 1.2 ms, echo train length 4, image matrix 96 x 128 interpolated to 256 x 256 pixels, saturation pulse 90°, flip angle 20°, bandwidth 125 kHz, spatial resolution 2.8 x 3.75 x 8 mm. A rectangular field of view of 75% was used. The acquisition window of 1 image/slice location was approximately (0.75 x 96 x 6.8)/4 x 120 ms. Using the slice selective "notched" prepulse and interleaved acquisitions strategy, an effective time to inversion of approximately 160 ms was achieved.[24] At 10 to 20 minutes after injection, delayed-enhancement images (hyperenhancement) were acquired using an inversion-recovery prepared gated fast-gradient echo-pulse sequence, similar to that recently described.[25] Imaging was performed with the following parameters: repetition time 7.3 ms, echo time 1.6 ms, image matrix 256 x 192, rectangular field

of view 75%, flip angle 20°, inversion pulse 180°, inversion time 200 to 250 ms, and spatial resolution 1.6 x 1.6 x 8 mm. The delayed- image prescriptions had the same slice thickness and spacing as the cine short-axis images.

MRI analysis

Regional MRI myocardial perfusion and delayed hyperenhancement imaging were scored using the 2-chamber, 4-chamber, and short-axis series using the same 16-segment model as MCE. Only segments related to the acute infarct territory were considered for the analysis. Using the last 5 images of the first-pass imaging series, regional myocardial early hypoenhancement was graded using a 3-point grade scale: grade 0, severe hypoenhancement; grade 1, subendocardial hypoenhancement; grade 2, no hypoenhancement. Delayed hyperenhancement imaging on inversion-recovery MRI was scored using a 5-point grading scale assessing the transmural extent of hyperenhancement: grade I, no hyperenhancement; grade II, 1% to 25% of the wall thickness; grade III, 26% to 50%; grade IV, 51% to 75%; and grade V, 76% to 100% of the wall thickness. MRI scans were scored by 2 observers unaware of the clinical, myocardial contrast echocardiographic, and angiographic data. Similar to MCE, in each patient, an MRI score index regarding hypo- and hyperenhancement was derived by averaging the perfusion scores from each dysfunctional segment and dividing by the number of dysfunctional segments. A patient was considered to have adequate reperfusion if the hypoenhancement score index was 1 and the hyperenhancement score index was 3 (50% of the wall thickness), and inadequate otherwise.

Statistical analysis

All continuous data are expressed as the means ± SDs. Differences between proportions were compared using the chi-square test. The patient values of sensitivity, specificity, and accuracy of each technique to predict improvement of myocardial function were calculated on the basis of an improvement at follow-up of left ventricular ejection fraction of ≥ 5% in patients with or without adequate reperfusion. These values were compared using McNemar's analysis. Two-way repeated measurements analysis of variance was applied to evaluate differences in left ventricular end-diastolic volume (EDV), end- systolic volume, and ejection fraction between the baseline and follow-up (repeated measurements) data and to evaluate differences in these values between patients with and without adequate reperfusion. All tests were 2-sided. Statistical significance for all tests was stated at the classic tests multiple times. A p value 0.05 was considered statistically significant.

Results

Patient characteristics and perfusion/enhancement pattern at baseline

The baseline characteristics of the 35 patients (30 men; mean age 52 ± 12 years) are listed in Table 1. The mean time from symptom onset to the first balloon inflation was 4.1 ± 1.8 hours. In 3 of the 35 patients (8%), the infarct-related coronary artery was suboccluded with a Thrombolysis In Myocardial Infarction grade 3 flow when angiography was performed. No residual angiographic stenosis was found in the target coronary vessel. In 241 segments related to the acute infarct territory, 72 (30%) were defined as hypokinetic and 120 (63%) as akinetic according to MCE. At 60 days of follow-up, 115 of 192 (60%) dysfunctional segments evaluated by MCE showed an improvement in function.

Table 1: Patient characteristics (n35)

Age (yrs)	52 ± 12
Men	30(86%)
Smoking	22(63%)
Diabetesmellitus	3(1%)
Hypertension	12(34%)
Hypercholesterolemia	9(26%)
Family history of coronaryartery disease	12(34%)
Left ventricular ejection fraction	42 ± 8
Creatinekinase peak(IU)	3418 ± 2462
Creatinekinase MB peak(IU)	299 ± 237
Anterior infarction	20(57%)
No. of diseased vessels	1.6 ± 0.8

Improvement in myocardial function at follow-up

At 6 days of follow-up, 58 (95%), 53 (66%), and 4 (8%) segments with normal, partial, and no perfusion detected by MCE exhibited improvement in function. Considering cine MRI with first-pass perfusion imaging (hypoenhancement), 66 (81%) segments with no defects, 46 (71%) with a subendocardial defect, and 3 (6%) with severe hypo-enhancement showed improvement in regional myocardial function. Delayed-enhanced MRI demonstrated that 38 of 39 segments (97%) without hyperenhancement improved compared with 31 (96%), 36 (92%), 7 (22%), and 3 (6%) segments with grades II, III, IV, and V, respectively, showing improvement at follow-up.

Relation of adequate reperfusion assessed by MCE and contrast-enhanced MRI to improvement of global myocardial function

The sensitivity, specificity, predictive value, and accuracy for MCE and contrast-enhanced MRI in predicting myocardial function improvement were analyzed on a per patient basis (**Figure 1**). One patient did not show any myocardial dysfunction and was not considered in the analysis. Of 22 patients with adequate reperfusion by MCE, 21 (95%) showed improvement in the left ventricular ejection fraction at follow-up. Conversely, 3 of 12 patients (25%) without adequate reperfusion showed improvement in ejection fraction. On the MRI hypoenhancement evaluation, 21 of 25 patients (84%) with adequate reperfusion showed improvement in ejection fraction at follow-up compared with 3 of 9 patients (33%) without adequate reperfusion who did so. Finally, all 18 patients with a hyperenhancement MRI score index of ≤ 3 showed an increase in ejection fraction compared with only 6 of 16 (37%) with improvement at follow-up. The sensitivity, specificity and accuracy for the prediction of functional improvement were comparable among MCE, first-pass MRI, and delayed-enhancement MRI (all p NS). **Figure 2** illustrates the relation between MCE and MRI using first-pass and delayed-enhancement imaging (hypo- and hyperenhancement patterns) in patients who underwent PCI of the left anterior descending and circumflex coronary arteries. To study the time course of left ventricular remodeling after PCI, the EDV was compared with the results of MCE and first-pass perfusion and

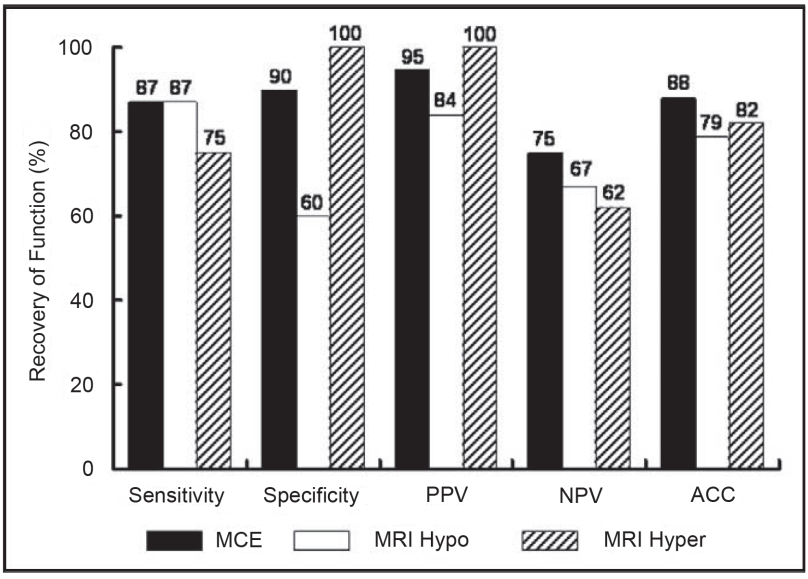

Figure 1. Sensitivity, specificity, and positive and negative predictive values (PPV and NPV, respectively), and accuracy (ACC) of MCE (black bars), first-pass perfusion MRI (white bars), and delayed-enhancement MRI (slashed bars) to predict improvement of myocardial function after PCI.

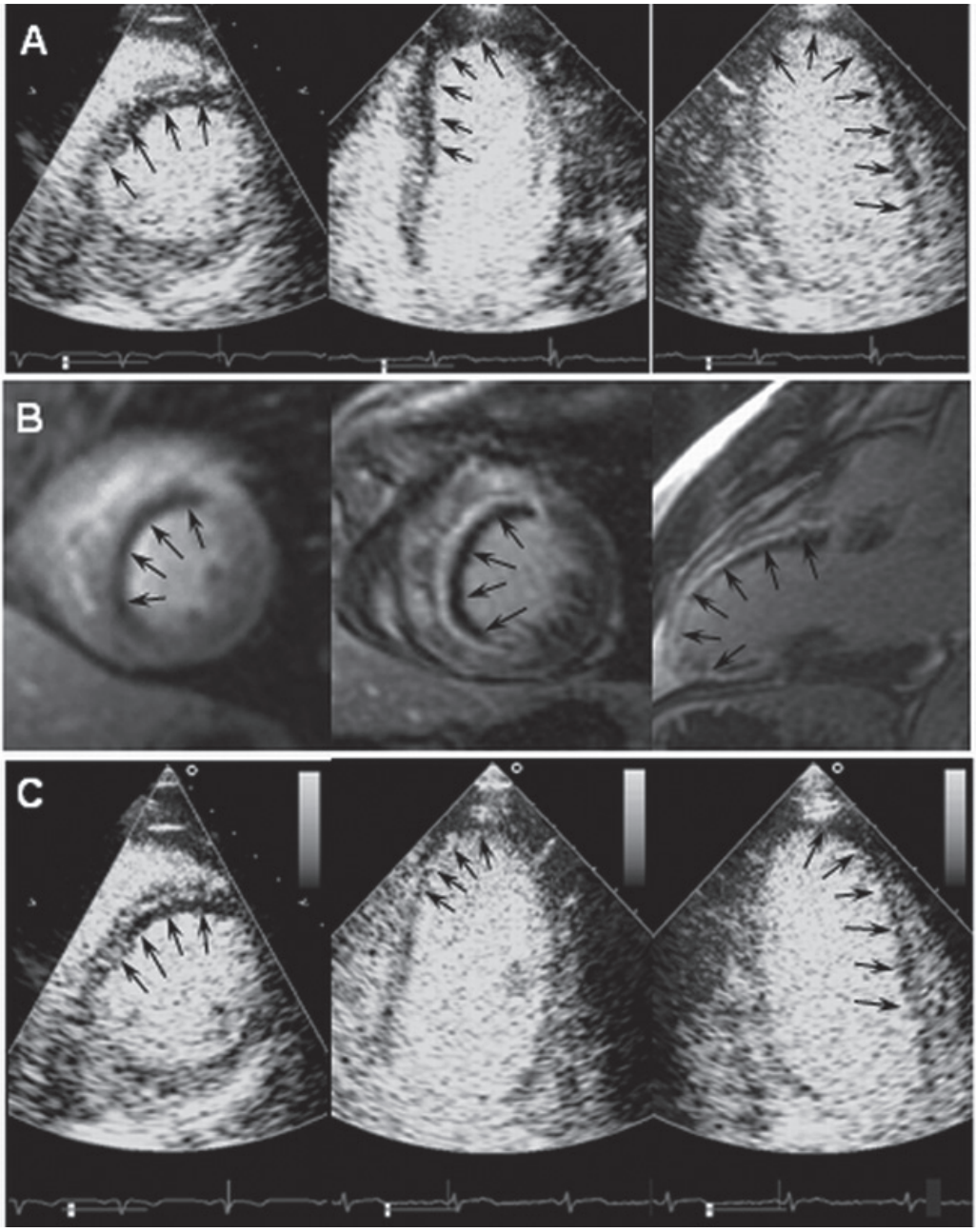

Figure 2. MCE and MRI of patient who underwent PCI of the left anterior descending coronary artery. (A) Myocardial contrast echocardiogram showing defect of perfusion involving anterior and posterior septum to apex in short- axis, 4-, and 3-chamber views. (B) MRI scan showing defect of perfusion detected by first-pass imaging (hypoenhancement) and transmural delayed hyperenhancement involving anterior and posterior myocardial septum (short- axis images on left and middle part, respectively). Delayed hyperenhancement involved all anterior septum to apex (3-chamber view on right). (C) MCE at 2 months of follow-up showing persistence of perfusion defect involving anterior and posterior septum to apex in short-axis, 4- and 3-chamber views. *

Table 2. Changes over time of left ventricular volumes and ejection fraction (EF) in patients with adequate reperfusion versus patients with inadequate reperfusion detected by myocardial contrast echocardiography (MCE), magnetic resonance imaging (MRI) first-pass perfusion, and MRI delayed-enhancement

	EDV			ESV			EF		
	Baseline	Follow-up	Δ	Baseline	Follow-up	Δ	Baseline	Follow-up	Δ
MCE									
Adequate reperfusion	121 ± 31	118 ± 29	−3 ± 7	66 ± 21	52 ± 17	−13 ± 9	46 ± 7	56 ± 8	10 ± 4
Inadequate reperfusion	125 ± 38	149 ± 45	24 ± 20	79 ± 25	92 ± 31	13 ± 14	37 ± 4	39 ± 6	2 ± 3
p Value			<0.001			<0.001			<0.001
MRI first-pass imaging									
Adequate reperfusion	123 ± 31	125 ± 35	1.7 ± 15	70 ± 23	60 ± 29	−9 ± 16	44 ± 8	53 ± 11	9 ± 5
Inadequate reperfusion	120 ± 39	140 ± 43	20 ± 21	74 ± 24	82 ± 27	8 ± 14	38 ± 3	41 ± 2	3 ± 3
p Value			0.008			0.007			0.003
MRI delayed-enhancement									
Adequate reperfusion	121 ± 34	117 ± 31	−4 ± 6	64 ± 23	49 ± 16	−15 ± 9	48 ± 6	58 ± 4	11 ± 4
Inadequate reperfusion	124 ± 33	142 ± 41	18 ± 20	78 ± 22	86 ± 29	7 ± 16	37 ± 5	40 ± 7	3 ± 3
p Value			<0.001			<0.001			<0.001

EF = ejection fraction; ESV = end-systolic volume.

delayed enhancement MRI. Patients with adequate reperfusion had a small decrease in EDV during follow-up, and patients with inadequate reperfusion had adverse LV remodeling with a gradual increment of EDV over time **(Table 2**).

Discussion

In patients who underwent PCI for AMI, MCE and contrast- enhanced MRI allowed early assessment of microvascular integrity and prediction of improvement of myocardial function. The main finding of the present study was that these modalities provided a comparable sensitivity, specificity, and accuracy for the assessment of recovery of contractile function after PCI.

Comparison of MCE with contrast-enhanced MRI to predict improvement in myocardial function

Previous studies have shown the efficacy of MCE to assess microvascular flow restoration after revascularization in AMI and the ability of MCE to distinguish stunned from nonreperfused myocardium.[9] Ito and colleagues[26] used MCE to define the "no-reflow" phenomenon after revascularization in AMI and showed how this phenomenon was related to subsequent increased postinfarction complications.[27] Previously, MRI studies showed that a hypoenhancement pattern detected by first-pass perfusion MRI, representing the noreflow area after AMI, is associated with permanent dysfunction at follow-up.[13,28] The present data have confirmed and extended the findings of the previous studies in line with pathologic findings that have indicated that hypoenhanced myocardium represents myocardial tissue with microvascular damage and obstruction (no-reflow phenome- non).[29,30] In contrast, delayed hyperenhancement in AMI appears to be related to myocardial necrosis, considering that gadolinium is a contrast agent able to pass through microvascular vessel walls and the membrane of damaged cells. Conversely, the contrast agents used for MCE remain inside the microvascular circulation, allowing the exclusive detection of microvascular integrity and, therefore, myocardial perfusion. An additional benefit of contrast-enhanced MRI is the higher spatial resolution that allows assessment of the transmural extent of necrosis in the infarct region. In the present study, MRI achieved 100% specificity and was superior to MCE in correctly identifying patients who did not improve in function after revascularization. Moreover, data on improvement of regional myocardial function noted as predictive accuracy for MCE was high for segments with normal or absent perfusion, but was limited for segments with a "patchy" perfusion pattern (around 70%). In contrast, the finer scale applied with MRI using the delayed-enhancement technique allowed a better distinction between segments with high

or low probability for functional recovery, with a sharp demarcation at the 50% transmural hyperenhancement level. MCE and MRI can be used to assess the recovery of contractile function after PCI. The choice of either MCE or MRI mainly depends on the patient characteristics and local availability and expertise. MCE is a rapid realtime bedside technique that can be easily performed in intensive care units during the acute phase of myocardial infarction, as well as in unstable patients. Moreover, this technique is less time-consuming compared with contrast-enhanced MRI and is a relatively inexpensive tool. Additionally, not all patients can be safely referred for MRI because of the presence of intra-aortic balloon devices, pacemakers, or claustrophobia. However, MCE is not yet widely applied in clinical routine, mainly because of a lack of standardized image acquisition and contrast administration protocols and image interpretation. In contrast, these issues are largely resolved for MRI using the delay-enhancement technique. Moreover, MRI may be the preferred modality in patients with a poor acoustic window.

Study limitations

Several limitations of this study need to be addressed. No formal sample size calculation was done. The number of patients was based on practical considerations. Although a 16-segment model of the left ventricle was used for MCE and MRI, some misalignment between the different images may have occurred. Due to the limited time slots available for MRI, these examinations were not always performed on the same day. To minimize the influence of time, MRI and MCE were correlated to wall motion scores using the same technique on the same day. Patients with intra-aortic balloon devices or who were clinically unstable for 48 hours were not included in the study. Although a quantitative analysis of MCE could have been advisable, this technique is not still widely used in daily clinical practice.

Clinical implications and conclusion

This study compared the value of MCE with contrast-enhanced MRI to predict myocardial functional improvement in patients after PCI for AMI. The 2 techniques allow prediction of myocardial function improvement after PCI. MCE has comparable accuracy to that of MRI and, as a bedside technique, may be an alternative tool in the acute phase of myocardial infarction.

References

1. Keeley EC, Boura JA, Grines CL. Primary angioplasty versus intravenous thrombolytic therapy for acute myocardial infarction: a quantitative review of 23 randomised trials. Lancet 2003;361:13–20.
2. Simes RJ, Topol EJ, Holmes DR Jr, White HD, Rutsch WR, Vahanian A, Simoons ML, Morris D, Betriu A, Califf RM, et al, for the GUSTO-I Investigators. Link between the angiographic substudy and mortality outcomes in a large randomized trial of myocardial reperfusion: im- portance of early and complete infarct artery reperfusion. Circulation 1995;91:1923–1928.
3. Marwick TH. The viable myocardium: epidemiology, detection, and clinical implications. Lancet 1998;351:815– 819.
4. Rocchi G, Kasprzak JD, Galema TW, de Jong N, Ten Cate FJ. Usefulness of power Doppler contrast echocardiography to identify reperfusion after acute myocardial infarction. Am J Cardiol 2001;87:278 –282.
5. Galiuto L, DeMaria AN, May-Newman K, Del Balzo U, Ohmori K, Bhargava V, Flaim SF, Iliceto S. Evaluation of dynamic changes in microvascular flow during ischemia-reperfusion by myocardial con- trast echocardiography. J Am Coll Cardiol 1998;32:1096 –1101.
6. Ragosta M, Camarano G, Kaul S, Powers ER, Sarembock IJ, Gimple LW. Microvascular integrity indicates myocellular viability in patients with recent myocardial infarction: new insights using myocardial con- trast echocardiography. Circulation 1994;89:2562–2569.
7. Bolognese L, Carrabba N, Parodi G, Santoro GM, Buonamici P, Cerisano G, Antoniucci D. Impact of microvascular dysfunction on left ventricular remodeling and long-term clinical outcome after primary coronary angioplasty for acute myocardial infarction. Circulation 2004;109:1121–1126.
8. Balcells E, Power ER, Lepper W, Belcik T, Wei K, Ragosta M, Samady H, Lindner JR. Detection of myocardial viability by contrast echocardiography in acute infarction predicts recovery of resting func- tion and contractile reserve. J Am Coll Cardiol 2003;41:827– 833.
9. Main ML, Magalski A, Morris BA, Coen MM, Skolnick DG, Good TH. Combined assessment of microvascular integrity and contractile reserve improves differentiation of stunning and necrosis after acute anterior wall myocardial infarction. J Am Coll Cardiol 2002;40:1079 – 1084.
10. Lepper W, Hoffmann R, Kamp O, Franke A, de Cock CC, Kuhl HP, Sieswerda GT, Dahl J, Janssens U, Voci P, Visser CA, Hanrath P. Assessment of myocardial reperfusion by intravenous myocardial contrast echocardiography and coronary flow reserve after primary percutaneous transluminal coronary angiography in patients with acute myocardial infarction. Circulation 2000;101:2368 –2374.
11. Kamp O, Lepper W, Vanoverschelde JL, Franke A, de Cock CC, Kuhl HP, Sieswerda GT, Dahl J, Janssens U, Voci P, Visser CA, Hanrath P. Serial evaluation of perfusion defects in patients with a first acute myocardial infarction referred for primary PTCA using intravenous myocardial contrast echocardiography. Eur Heart J 2001;22:1485-1495.

12. Marques KM, Visser CA. Myocardial contrast echocardiography in the assessment of pharmacologic intervention of the reperfusion injury. Eur Heart J 2003;24:19 –20.
13. Wu KC, Zerhouni EA, Judd RM, Lugo-Olivieri CH, Barouch LA, Schulman SP, Blumenthal RS, Lima JA, et al. Prognostic significance of microvascular obstruction by magnetic resonance imaging in patients with acute myocardial infarction. Circulation 1998;97:765–772.
14. Kramer CM, Rogers WJ Jr, Mankad S, Theobald TM, Pakstis DL, Hu YL. Contractile reserve and contrast uptake pattern by magnetic resonance imaging and functional recovery after reperfused myocardial infarction. J Am Coll Cardiol 2000;36:1835–1840.
15. Choi KM, Kim RJ, Gubernikoff G, Vargas JD, Parker M, Judd RM. Transmural extent of acute myocardial infarction predicts long-term improvement in contractile function. Circulation 2001;104:1101–1107.
16. Gerber BL, Garot J, Bluemke DA, Wu KC, Lima JA. Accuracy of contrast-enhanced magnetic resonance imaging in predicting improve- ment of regional myocardial function in patients after acute myocardial infarction. Circulation 2002;106:1083–1089.
17. Beek AM, Kuhl HP, Bondarenko O, Twisk JW, Hofman MB, van Dockum WG, Visser CA, van Rossum AC. Delayed contrast-enhanced magnetic resonance imaging for the prediction of regional functional improvement after acute myocardial infarction. J Am Coll Cardiol 2003;42:895–901.
18. Rademakers F, Van de Werf F, Mortelmans L, Marchal G, Bogaert J. Evolution of regional performance after an acute anterior myocardial infarction in humans using magnetic resonance tagging. J Physiol 2003;546:777–787.
19. Taylor AJ, Al-Saadi N, Abdel-Aty H, Schulz-Menger J, Messroghli DR, Friedrich MG. Detection of acutely impaired microvascular reperfusion after infarct angioplasty with magnetic resonance imaging. Circulation 2004;109:2080 –2085.
20. Thomson HL, Basmadjian AJ, Rainbird AJ, Razavi M, Avierinos JF, Pellikka PA, Bailey KR, Breen JF, Enriquez-Sarano M. Contrast echocardiography improves the accuracy and reproducibility of left ventricular remodeling measurements: a prospective, randomly assigned, blinded study. J Am Coll Cardiol 2001;38:867– 875.
21. Schiller NB, Shah PM, Crawford M, DeMaria A, Devereux R, Feigenbaum H, Gutgesell H, Reichek N, Sahn D, Schnittger I, et al, for the American Society of Echocardiography Committee on Standards, Subcommittee on Quantitation of Two-Dimensional Echocardiograms. Recommendations for quantitation of the left ventricle by two- dimensional echocardiography. J Am Soc Echocardiogr 1989;2:358 –367.
22. Bax JJ, Poldermans D, Elhendy A, Cornel JH, Boersma E, Rambaldi R, Roelandt JR, Fioretti PM. Improvement of left ventricular ejection fraction, heart failure symptoms and prognosis after revascularization in patients with chronic coronary artery disease and viable myocardium detected by dobutamine stress echocardiography. J Am Coll Cardiol 1999;34:163–169.
23. Marwick TH, D'Hondt AM, Baudhuin T, Willemart B, Wijns W, Detry JM, Melin J. Optimal use of dobutamine stress for the detection and evaluation of coronary artery disease: combination with echocardiography, scintigraphy or both? J Am Coll Cardiol 1993;22:159 –167.

24. Slavin GS, Wolff SD, Gupta SN, Foo TK. First-pass myocardial perfusion MR imaging with interleaved notched saturation: feasibility study. Radiology 2001;219:258 –263.
25. Simonetti OP, Kim RJ, Fieno DS, Hillenbrand HB, Wu E, Bundy JM, Finn JP, Judd RM. An improved MR imaging technique for the visualization of myocardial infarction. Radiology 2001;218:215–223.
26. Ito H, Tomooka T, Sakai N, Higashino Y, Fujii K, Masuyama T, Kitabatake A, Minamino T. Lack of myocardial perfusion immediately after successful thrombolysis. A predictor of poor recovery of left ventricular function in anterior myocardial infarction. Circulation 1992;85:1699 –1705.
27. Ito H, Maruyama A, Iwakura K, Takiuchi S, Masuyama T, Hori M, Higashino Y, Fujii K, Minamino T. Clinical implications of the 'no reflow' phenomenon: a predictor of complications and left ventricular remodeling in reperfused anterior wall myocardial infarction. Circulation 1996;93:223–228.
28. Rogers WJ Jr, Kramer CM, Geskin G, Hu YL, Theobald TM, Vido DA, Petruolo S, Reichek N. Early contrast-enhanced MRI predicts late functional recovery after reperfused myocardial infarction. Circulation 1999;99:744 –750.
29. Lima JA, Judd RM, Bazille A, Schulman SP, Atalar E, Zerhouni EA. Regional heterogeneity of human myocardial infarcts demonstrated by contrast-enhanced MRI: potential mechanisms. Circulation 1995;92: 1117–1125.
30. Rochitte CE, Lima JA, Bluemke DA, Reeder SB, McVeigh ER, Furuta T, Becker LC, Melin JA. Magnitude and time course of microvascular obstruction and tissue injury after acute myocardial infarction. Circulation 1998;98:1006 –1014

Chronic Pseudoaneurysm of the Left Ventricle

Timo Baks; Filippo Cademartiri; H. Spierenburg; Pim J. de Feyter

Int J Cardiovasc Imaging 2005 Nov 30;1-3

12

Abstract

We present a case of a 55-year-old men who suffered a silent myocardial infarction four years earlier and presented with exertional dyspnoea. Cardiac Magnetic Resonance Imaging (CMR) and Multislice Computed Tomography (MSCT) was performed and revealed a giant pseudoaneursym of the lateral wall of the left ventricle with the presence of a thrombus in the lateral wall of the pseudoaneursym. We present this case since excellent non-invasive evaluation of the pseudoaneursym was feasible using state-of-the-art imaging modalities. Information on left ventricular geometry and function as well as myocardial viability and coronary anatomy is available when both MSCT and CMR are performed. This combined approach of these two imaging modalities provide clinically relevant information and may guide therapeutic decision making.

Introduction

Formation of a pseudoaneurysm of the left ventricle is a rare complication of acute myocardial infarction and occurs most frequently in the inferior wall. The wall of the pseudoaneurysm contains pericardium and/or scar tissue and not myocardium as is observed in a true aneurysm of the left ventricle (1). The diagnosis might be difficult to make since a pseudoaneurysm is easily confused with a true aneurysm of the left ventricle (2). A pseudoaneurysm often needs urgent surgical treatment while a true aneurysm might be treated medically (3). Advanced non-invasive imaging modalities like cardiac Magnetic Resonance Imaging (CMR) and Multislice Computed Tomography (MSCT) provide clinically relevant information on coronary anatomy, left ventricular function and myocardial viability (4-6). We present a patient with a pseudoaneurysm of the left ventricle 4 years after acute myocardial infarction and performed CMR and MSCT to evaluate left ventricular geometry and function as well as myocardial viability and coronary anatomy.

CT protocol

The examination was performed using a 16-row MSCT scanner (Sensation 16, Siemens, Germany; collimation 16 x 0.75 mm, rotation time 420 ms, table feed 3.0 mm/rotation, tube voltage 120 kV, tube current 400-450 mAs). After intravenous administration of 120 ml of non-ionic contrast material (Visipaque® 320, Amersham Health, UK), an automatic bolus tracking technique triggered the start of the MSCT-scan. Images were reconstructed using retrospective ECG-gating during the mid- to end-diastolic phase to provide nearly motion-free image quality.

CMR protocol

A clinical 1.5-Tesla CMR scanner with a dedicated cardiac four element phased-array receiver coil was used for imaging (Signa CV/*i*, GE Medical systems, Milwaukee, Wisconsin USA). Repeated breath-holds and gating to the electrocardiogram were applied to minimize the influence of cardiac and respiratory motion on data collection. Cine-CMR was performed with a steady-state free-precession technique (FIESTA, GE) using the following imaging parameters: 24 temporal phases per slice; field of view 32 to 36 x 32 to 36 cm; rectangular field of view 75-100%; repetition time 3.4; time to echo 1.4; flip angle 45°; matrix 192x160; bandwidth 83 kHz; number of averages 0.75. To cover the entire left ventricle 9 to 12 consecutive slices of 8 mm were planned in short-axis view (gap of 2 mm) on the 4-chamber view of the left ventricle.

Myocardial distribution of delayed enhancement was studied 10-20 minutes following administration of Gadolinium-DTPA (0.2 mmol/kg, Magnevist®, Schering, Germany). A 2-dimensional T1-weighted inversion recovery gradient-echo sequence with the following imaging parameters was used: field of view 32 to 36 x 32 to 36 cm; rectangular field of view 75-100%; slice thickness 8 mm; gap 2 mm; repetition time 7.3; time to echo 1.6; flip angle 20°; inversion pulse 180°; matrix 256x192; 1 number of averages; bandwidth 17.9 kHz; inversion time 180-300 ms. The inversion time was adjusted to null the signal of remote myocardium. Slice locations were copied from the locations of the cine-images. (**Fig. 1**)

Case Report

A 55-year-old men suffered a silent myocardial infarction four years earlier diagnosed by the occurrence of new Q-waves on an electrocardiogram. Recently, he presented with complaints of exertional dyspnoea. A transthoracic echocardiogram was suspicious for a pseudoaneurysm. More detailed anatomy was obtained with cardiovascular magnetic resonance (CMR) imaging and multislice computed tomography (MSCT). CMR revealed a pseudoaneurysm in the lateral wall of the left ventricle with a volume of 351 ml and a diameter of the neck of 1.4 cm. Left ventricular systolic function was depressed (ejection fraction 42%). A large non contrast-enhanced filling defect was seen at the lateral wall

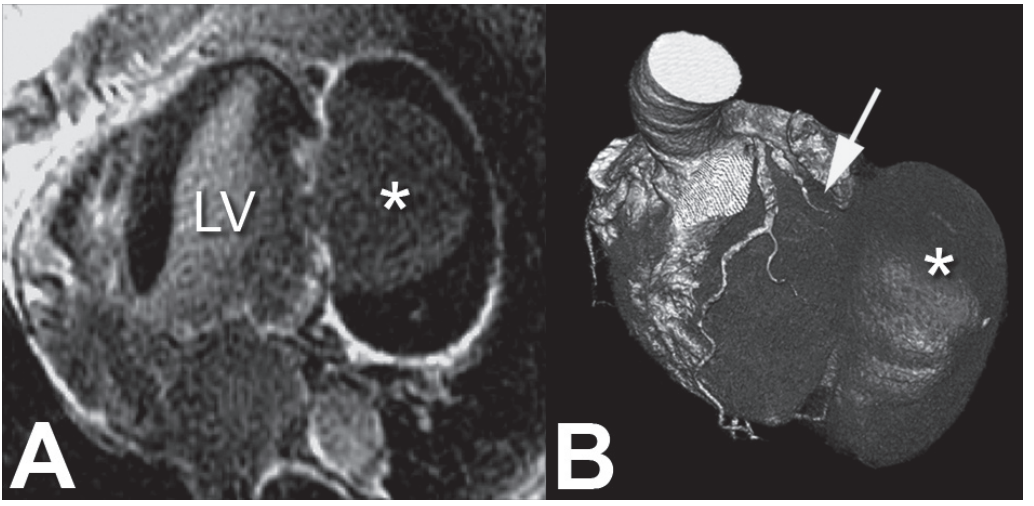

Figure 1 A: Cardiovascular Magnetic Resonance (1.5 Tesla) performed 15 minutes after administration of 0.2 mmol/kg Gadolinium-DTPA demonstrates a pseudoaneurysm in the lateral wall of the left ventricle. * = pseudoaneurysm; LV = left ventricle. **B:** Multislice Computed Tomography (16-slice) demonstrated the 3-dimensional reconstruction of the pseudoaneurysm. The left circumflex coronary artery is totally occluded (arrow). *

of the pseudoaneurysm indicating a mural thrombus. The thrombus was surrounded by a bright enhanced rim of pericardium, indicating scar/fibrous tissue. Three-dimensional reconstruc-tion of the MSCT images provided the location and the size of the pseu-doaneurysm and an occluded circumflex coro-nary artery. Surgical intervention was based on the combined information of both imaging modalities and consisted of resection of the pseudoaneurysm with insertion of a pericardial patch and additional coronary artery bypass grafting of the occluded circumflex coronary artery. The postoperative course was uneventful and six months after surgery the patient could tolerate exercise well. Left ventricular ejection fraction was assessed with CMR after resection of the pseudoaneurysm and was increased from 42% to 46%.

Discussion

CMR and MSCT provide clinically relevant information in patients with a postinfarction pseudoaneurysm of the left ventricle. CMR provides information on left ventricular function and the location and extent of the pseudoaneurysm. Moreover, 10-30 minutes after administration of gadolinium-derivates, the extent of myocardial viability can be assessed (7). MSCT provides a 3 dimensional data set that can be reconstructed to give an overview of the often complicated geometry of the left ventricle and pseudoaneurysm (8). MSCT also provides information on coronary artery stenosis, although an increased heart rate (>70 beats per minute) might hinder evaluation. The combined information on left ventricular geometry and function, myocardial viability and coronary anatomy may guide therapeutic decision making. In the currently presented case, the surgeon was able to resect the pseudoaneurysm with good result.

Other non-invasive imaging modalities have been proposed for the diagnosis of a pseudoaneurysm of the left ventricle. Left ventricular angiography can be helpful, although it is limited by a 2 dimensional view of the pseudoaneurysm making assumptions on 3 dimensional geometry necessary. Radionuclide ventriculography is also used to assess left ventricular geometry, but diagnostic accuracy is limited due to the limited spatial resolution. Echocardiography is commonly used in clinical practice and provides relevant information. However, echocardiography requires a sufficient acoustic window and it might be difficult to differentiate thrombus from myocardium and pericardium. The presence of a thrombus might subsequently lead to an underestimation of the dimensions of the pseudoaneurysm. Contrast echocardiography is a promising technique that may improve image quality. In conclusion, CMR and MSCT are the preferred non-invasive imaging modalities to evaluate patients with a pseudoaneurysm of the left ventricle.

References

1. Vlodaver Z, Coe JI, Edwards JE. True and false left ventricular aneurysms. Propensity for the altter to rupture. Circulation 1975;51(3):567-72.
2. Frances C, Romero A, Grady D. Left ventricular pseudoaneurysm. J Am Coll Cardiol 1998;32(3):557-61.
3. Brown SL, Gropler RJ, Harris KM. Distinguishing left ventricular aneurysm from pseudoaneurysm. A review of the literature. Chest 1997;111(5):1403-9.
4. Mollet NR, Cademartiri F, Krestin GP, McFadden EP, Arampatzis CA, Serruys PW, et al. Improved diagnostic accuracy with 16-row multi-slice computed tomography coronary angiography. J Am Coll Cardiol 2005;45(1):128-32.
5. Baks T, van Geuns RJ, Biagini E, Wielopolski P, Mollet NR, Cademartiri F, et al. Recovery of left ventricular function after primary angioplasty for acute myocardial infarction. Eur Heart J 2005;26(11):1070-7.
6. Ohnesorge BM, Hofmann LK, Flohr TG, Schoepf UJ. CT for imaging coronary artery disease: defining the paradigm for its application. Int J Cardiovasc Imaging 2005;21(1):85-104.
7. Kim RJ, Fieno DS, Parrish TB, Harris K, Chen EL, Simonetti O, et al. Relationship of MRI delayed contrast enhancement to irreversible injury, infarct age, and contractile function. Circulation 1999;100(19):1992-2002.
8. Boxt LM. CT anatomy of the heart. Int J Cardiovasc Imaging 2005;21(1):13-27.

Hypertrophic obstructive cardiomyopathy: septal ablation with overlapping sirolimus-eluting and covered stents after failed alcoholization and concomitant coronary artery disease

Georgios Sianos; Michail I. Papafaklis; Eleni C. Vourvouri; Jurgen T. Ligthart; Timo Baks; Folkert J. Ten Cate; Patrick W. Serruys

Accepted for publication in Circulation

13

1, 2, 3, 4, 5, 6, 7, 8, 9 ,10, 11, 12, 14, 15

Case Report

A 61-year-old man with exertional dyspnea was diagnosed with hypertrophic obstructive cardiomyopathy. The echocardiogram demonstrated an interventricular septum with a thickness of 18 mm, marked systolic anterior motion and mitral regurgitation grade 3. The left ventricular outflow tract (LVOT) gradient was 100 mmHg. The patient was treated with percutaneous transluminal septal myocardial alcohol ablation (PTSMA) resulting in a residual LVOT gradient of 20 mmHg. Mild coronary artery disease of the proximal left anterior descending coronary artery (LAD) and the first diagonal branch (D1) [40% diameter stenosis by quantitative coronary angiography (QCA)] was left untreated.

The patient remained asymptomatic for 6 months and then he developed again exertional dyspnea. The echocardiogram revealed relapse of the LVOT gradient (80mmHg). Repeat PTSMA was decided. The invasive LVOT gradient was 77 mmHg. Coronary angiography demonstrated progression of the disease of both lesions in the LAD and D1 (70% by QCA). Due to the concomitant coronary artery disease, the treatment plan was changed. The LAD and the D1 were treated with sirolimus-eluting stent (SES) implantation. Instead of injecting ethanol, a polytetrafluoroethylene-covered stent was implanted within the borders of the SES stent over the ostium of the septal artery. The procedure resulted in occlusion of the septal branch and immediate reduction of the LVOT gradient to 12 mmHg. The Creatine Kinase rose to 789 IU/L. At 12 months follow-up, the patient remains asymptomatic. Repeat angiography revealed no restenosis and intravascular ultrasound complete absence of neointima formation. Furthermore, no signs of septal collateralization through the right coronary artery were noted. There was no rest gradient. Multislice-CT imaging demonstrated good stent patency while magnetic resonance imaging with gadolinium demonstrated the region of the infarcted inter-ventricular septum. Septal reperfusion through collaterals leading to treatment failure after occlusion with covered stents, has been previously reported.[1,2] In our case this has been prevented probably due to myocardial fibrosis and destruction of the microcirculation after the initial alcoholization.

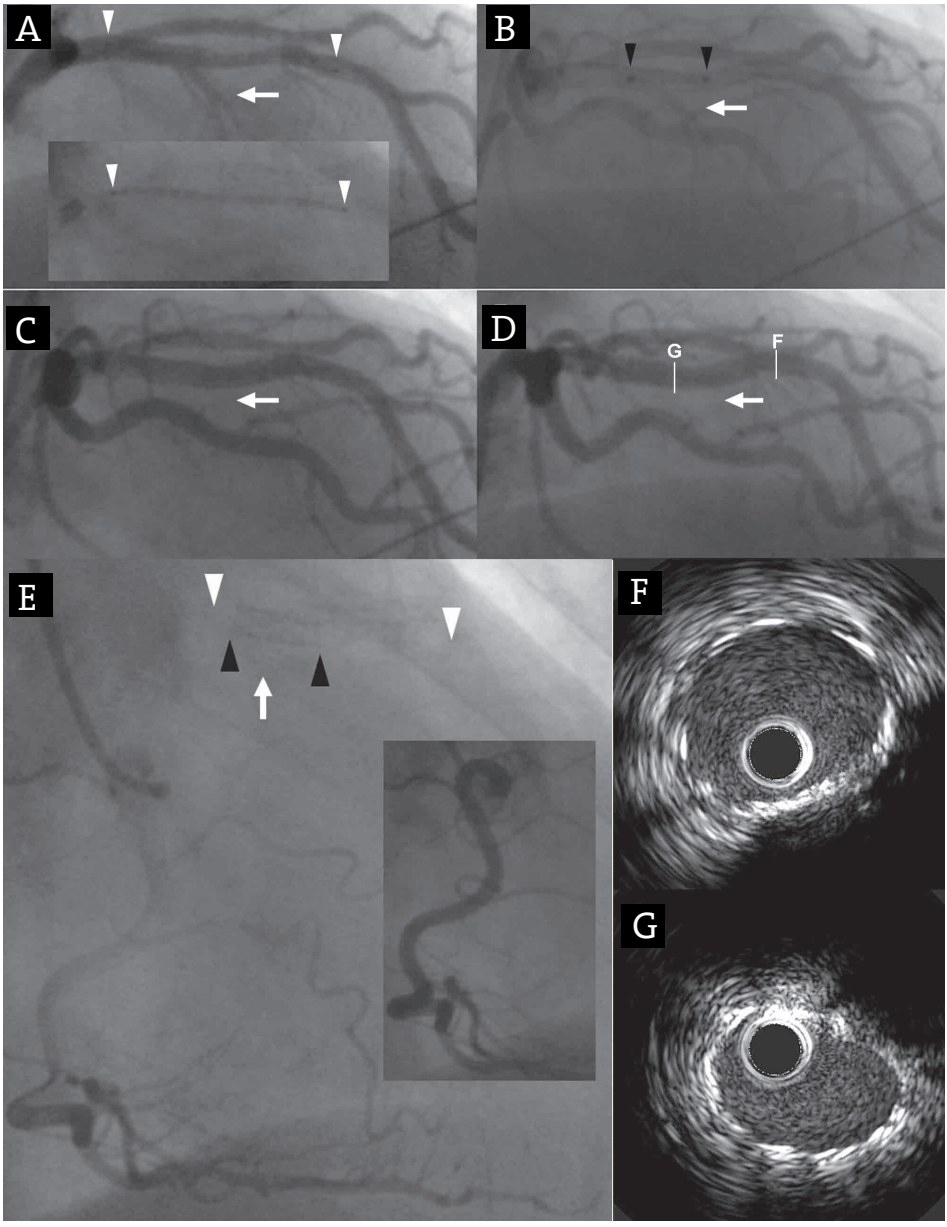

Figure 1. **Top**: Angiographic images demonstrating (A) the placement of a 3.5x28mm sirolimus-eluting stent (SES) (white arrowheads) in the left anterior descending coronary artery (LAD) over the septal branch (SB) (white arrow), (B) the placement of a 3.5x12mm polytetrafluoethylene-covered stent (black arrowheads) within the SES over the ostium of the septal branch, (C) the post-procedural result with complete absence of opacification of the SB (white arrow) and (D) the 12-month follow-up result with no signs of restenosis and persistent SB occlusion. **Bottom**: Follow-up angiography of the right coronary artery (insert) depicting the SES (white arrow) during the delayed phase of contrast dye injection (E). The patency of the stented LAD without neointima formation was also affirmed by intravascular ultrasound both in the SES only region (F: single strut layer) and in the region of overlapping stents (G: triple strut layer).

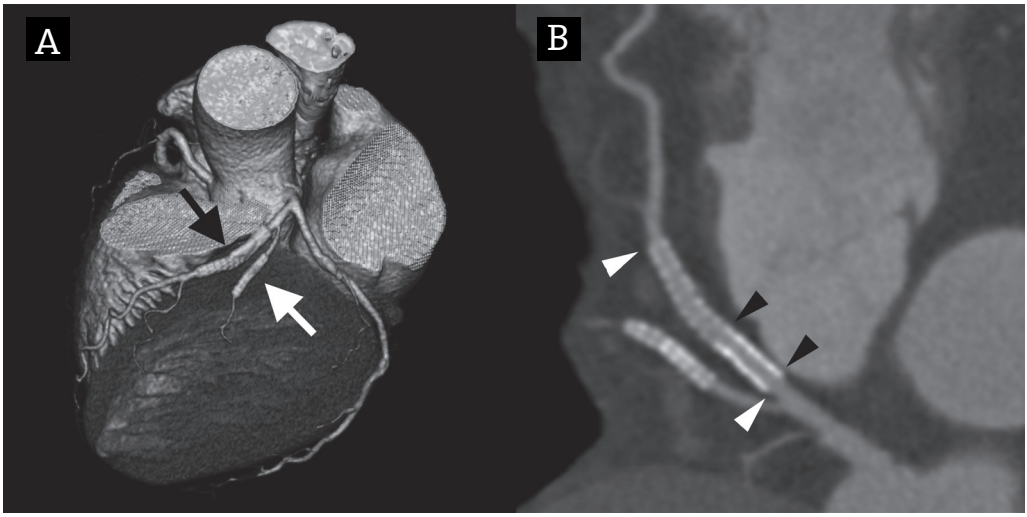

Figure 2. 64-slice CT angiogram. **A**: Volume-rendered image demonstrating the stented left anterior descending coronary artery (LAD; black arrow) and first diagonal branch (D1; white arrow). **B**: Multiplanar reconstructed image showing the sirolimus-eluting stent (white arrowheads) and the polytetrafluoethylene-covered stent (black arrowheads) in the LAD and the sirolimus-eluting stent in the D1 (white arrow). The lumen within the stents is clearly visible without signs of neointima formation. *

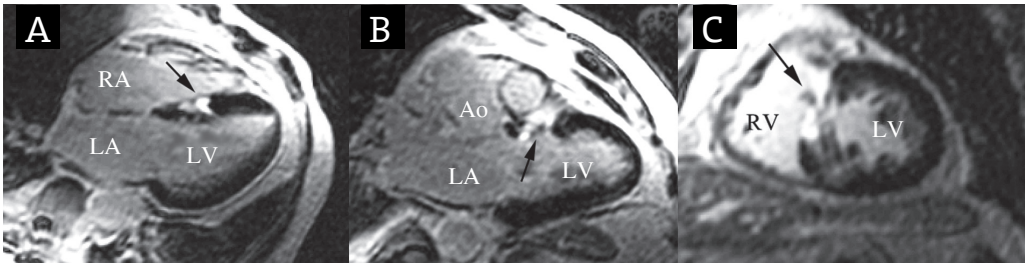

Figure 3. Magnetic Resonance Imaging (1.5 Tesla) depicting the infarcted area (black arrows pointing at bright region) of the septum in 4-chamber (**A**), left ventricular outflow tract (**B**) and short axis view (**C**) using an inversion recovery T1-weighted gradient echo sequence 15 minutes after administration of 0.2 mmol/kg gadolinium-DTPA. RA: right atrium; LA: left atrium; LV: left ventricle; RV: right ventricle; Ao: aortic root

References

1. Fifer MA, Yoerger DM, Picard MH, Vlahakes GJ, Palacios IF. Covered stent septal ablation for hypertrophic obstructive cardiomyopathy: initial success but ultimate failure resulting from collateral formation. Circulation. 2003;107:3248-9.
2. Anzuini A, Uretsky BF. Covered stent septal ablation for hypertrophic obstruction cardiomyopathy. Circulation. 2004;109:e6.

Part 4

Innovation in Viability Imaging

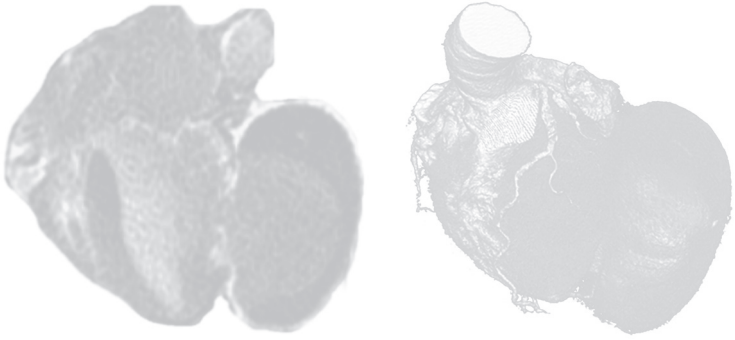

MSCT and MRI for the Assessment of Reperfused Acute Myocardial Infarction

Timo Baks; Filippo Cademartiri; Amber Moelker; Robert-jan van Geuns; Gabriel P. Krestin; Dirk J. Duncker; Pim J. de Feyter

J Am Coll Cardiol. 2006 Jul 4;48(1):144-52

14

Abstract

Objective

We evaluated the accuracy of in-vivo delayed enhancement Multislice Computed Tomography (DE-MSCT) and delayed enhancement Magnetic Resonance Imaging (DE-MRI) for the assessment of myocardial infarct size using postmortem triphenyltetrazolium chloride (TTC) pathology as standard of reference.

Background

The diagnostic value of DE-MSCT for the assessment of acute reperfused myocardial infarction is currently unclear.

Methods

In 10 domestic swine (25 to 30kg), the circumflex coronary artery was balloon-occluded for 2 h followed by reperfusion. After 5 days (3 to 7 days), DE-MRI (1.5-T) was performed 15 min after administration of 0.2 mmol/kg gadolinium-DTPA using an inversion recovery gradient echo technique. On the same day, DE-MSCT (64-slice) was performed 15 min after administration of 1 gI/kg of iodinated contrast material. One day after imaging, hearts were excised, sectioned in 8 mm short axis slices, and stained TTC. Infarct size was defined as the hyperenhanced area on DE-MSCT and DE-MRI images and the TTC negative area on TTC pathology slices. Infarct size was expressed as percentage of total slice area.

Results

Infarct size determined by DE-MSCT and DE-MRI showed a good correlation with infarct size assessed with TTC pathology ($R^2 = 0.96$; $p < 0.001$ and $R^2 = 0.93$; $p < 0.001$, respectively). The correlation between DE-MSCT and DE-MRI was also good ($R^2 = 0.96$; $p < 0.001$). The relative difference in CT attenuation value of infarcted myocardium compared to remote myocardium was 191 ± 18%. The relative MR signal intensity between infarcted myocardium and remote myocardium was 554 ± 156%.

Conclusion

We demonstrated that DE-MSCT can assess acute reperfused myocardial infarction in good agreement with in-vivo DE-MRI and TTC pathology.

Introduction

Acute myocardial infarct size is a predictor of long-term left ventricular function and geometry and clinical outcome in patients who have suffered acute myocardial infarction (1,2). Delayed enhancement Magnetic Resonance Imaging (DE-MRI) is a well established non-invasive imaging modality that allows assessment of myocardial infarct size (3-5). In recent years, Multislice Computed Tomography (MSCT) technology has made great strides, and non-invasive assessment of coronary artery stenosis is now feasible with high diagnostic accuracy using a 64-slice scanner (6,7). Delayed enhancement MSCT (DE-MSCT) has been proposed as an alternative non-invasive imaging modality for the detection of myocardial infarction. However, different imaging protocols have been proposed at different time points after myocardial infarction and the diagnostic accuracy is currently unclear (8-11). We performed DE-MSCT and DE-MRI in a porcine model of reperfused acute myocardial infarction at a mean of five days after infarction. We evaluated the accuracy of in-vivo DE-MSCT and DE-MRI for the assessment of acute reperfused myocardial infarct size and used post-mortem viability staining with triphenyltetrazolium chloride (TTC) as standard of reference.

Material and Methods

Animal model

Fourteen Yorkshire-landrace swine (2 to 3 months old, 25 to 30 kg) were sedated (ketamine 20 mg/kg intramuscular and midazolam 1 mg/kg intramuscular), anesthetized (thiopental, 12 mg/kg intravenously), intubated, and mechanically ventilated (mixture of oxygen and nitrogen 1:2). Anaesthesia was maintained with fentanyl (12.5 microgram/kilogram/hour). All swine then received a sheath in a carotid artery to allow coronary X-ray angiography. Under fluoroscopy guidance, balloon occlusion of the left circumflex coronary artery was performed. In 2 swine, the balloon was deflated after 15 min of occlusion to produce severely ischemic but reversible injured (stunned) myocardium. In 12 swine, the balloon was deflated after 2 hours of occlusion to allow reperfusion of the infarcted area. Reperfusion was proven by coronary angiography. Of the animals who underwent 2 hours of occlusion, 1 pig died after 1 day and 1 pig died after 3 days after balloon occlusion. The study complied with the regulations of the animal care committee of our hospital and the "Guide for the Care and Use of Laboratory Animals" (NIH publication 1996).

All swine were anaesthetized as described above before imaging. First, DE-MRI was performed and 93 ± 23 min later DE-MSCT imaging. The two swine that underwent 15 min of balloon occlusion underwent imaging at 3 days and 4 days, respectively, after induction of ischemia. Of the 10 remaining swine that underwent the 2 hour occlusion protocol, 2 swine were imaged at 3 days, 6 at 5 days and 2 at 7 days after reperfusion. One day after the DE-MSCT and DE-MRI imaging session, all animals were sacrificed and the hearts excised. The ex-vivo hearts were stiffened using alginate impression material (Cavex Holland BV, Haarlem, the Netherlands). The myocardium of the left ventricle was then sectioned in 8 mm consecutive slices in short axis view perpendicular to the long axis of the left ventricle using a commercially available meatslicer. To obtain a viability staining, the slices were embedded in a solution of 1% TTC and 0.2 mol/L Sorensen's buffer (pH 7.4) at 37°C for 15 min, followed by fixation in 4% formalin. Slices that showed a TTC negative area were photographed digitally after 24 hours of exposure to formalin. Exposure to formalin allows delineation between necrotic but hemorrhagic myocardium (which has a red appearance due to the presence of blood) and viable tissue (which stains red due to the conversion of TTC to the bright red formazan stain). By exposing the TTC stained tissue to formalin, the hemorrhagic necrotic areas acquire a dark brown color, while the red formazan precipitate remains bright red (Fig 1). Unfortunately, a limitation of this approach was the asymmetric shrinkage (causing the slices to bend) in 9 out of a total of 67 slices (in 10 animals), hampering the accurate assessment of infarct size in these slices, that were excluded from analysis for this reason.

DE-MSCT

A 64-slice clinical CT scanner was used for imaging (Sensation 64®, Siemens, Forchheim, Germany) with the following characteristics: number of detector rows, 32 x 2 (oversampling in the z-axis obtained with flying focal spot (12)); individual detector width, 0.6 mm; gantry rotation time, 330 ms; effective temporal resolution, 165 ms. The delayed enhancement protocol was performed 15 min after administration of 1 gI/kg of iodinated contrast agent through an ear vein at a injection speed of 1.5 ml/s (Iomeprol 400mgI/ml, Iomeron®, Bracco, Italy). The following scan parameters were used: tube voltage, 120 kV; tube current, 900 mAs; table feed per rotation, 3.84 mm; scan direction, cranio-caudal and retrospective ECG gating. Voxelsize at acquisition was 0.3 x 0.3 x 0.4 mm. The estimated radiation dose if applied in humans was calculated with dedicated software as 15/21 milliSievert for male/female (WinDose, Institute of Medical Physics, Erlangen, Germany). Mean heart rate decreased to 51±9 beats per minute after administration of Zatebradine (10 mg/kg intravenously). An instrumented breath hold was applied to minimize the influence of respiratory motion on data collection. DE-MSCT datasets were reconstructed at −300ms, −350ms,

and –400 ms before the next R wave (end-diastolic phase of the cardiac cycle). From the dataset with optimal image quality, axial slices with a slice thickness of 1 mm and an increment of 0.5 mm were reconstructed using a field of view of 150 x 150 mm, a 5122 reconstruction matrix and a medium smooth convolution filter (B30f). MSCT short axis slices with a slice thickness of 1 mm were then reconstructed perpendicular to the long axis of a double oblique true four chamber view using a dedicated software platform with multiplanar capabilities (Leonardo, Siemens, Forchheim, Germany).

DE-MRI

A clinical 1.5-T MRI scanner with a dedicated cardiac four-element phased-array receiver coil was used for imaging (Signa CV/i, GE Medical systems, Milwaukee, Wisconsin, USA). Repeated instrumented breath-holds and gating to the electrocardiogram were applied to minimize the influence of cardiac and respiratory motion on data collection. No medication was administered to control heart rate. Cine-MRI was performed with a steady-state free-precession technique (FIESTA, GE) with the following imaging parameters: 24 temporal phases per slice, voxel size of 1.8 x 1.5 x 8 mm; repetition time, 3.4 ms; time to echo, 1.4 ms; flip angle, 45°; bandwidth 83 kHz; number of averages, 0.75. To cover the entire left ventricle, 6 to 8 consecutive slices of 8 mm were planned in short axis view perpendicular to the long axis of a double oblique true four-chamber view.

Myocardial distribution of delayed enhancement was studied 15 min after administration of Gadolinium-DTPA (0.2 mmol/kg, Magnevist®, Schering, Germany). A 2-dimensional T1-weighted inversion recovery segmented fast gradient-echo sequence with the following imaging parameters was used: voxel size of 1.1 x 1.5 x 8 mm; repetition time, 7.3 ms; time to echo, 1.6 ms; flip angle, 20°; inversion pulse, 180°; number of averages, 1; bandwidth, 17.9 kHz; inversion time, 180 to 300 ms; data acquisition every second R-R interval. The trigger delay was adjusted per pig to acquire data in mid- to end-diastole and the inversion time was adjusted per pig to null the signal of remote myocardium. Slice locations for delayed enhancement imaging were copied from slice locations of short-axis cine-imaging.

Data analysis

DE-MSCT, DE-MRI and TTC pathology images were coregistered using anatomical landmarks like the insertion of the right ventricle to the septum and the presence of papillary muscles. Infarct size per slice was calculated by dividing the infarcted area by the total slice area of left ventricular myocardium. The digitalized TTC pathology slices were loaded in a separate workstation with a commercially available analysis package (SigmaScan® Pro 5.0). The TTC negative area (including the dark-brown

subendocardial area) was considered to be the infarcted area and was segmented manually. Reconstructed DE-MSCT images and DE-MRI images were exported and transferred to a separate workstation with dedicated software (Cine Tool 3.4; GE Medical Systems). Image quality was evaluated on a per-slice basis and classified as good (defined as the absence of any image-degrading artifacts related to motion or miss-triggering), adequate (presence of image-degrading artifacts but evaluation possible), or poor (presence of image-degrading artifacts but evaluation possible with moderate confidence). The region with delayed hyper-enhancement was segmented manually by two different observers (T.B. and A.M.) blinded to the results of the other imaging modality and TTC pathology. Regional wall thickening was assessed on cine-MRI images at the core of the infarction and in remote non-infarcted myocardium of the septum using dedicated software based on the centerline method (CAAS MRV 2.1, Pie Medical Imaging, Maastricht, the Netherlands). CT attenuation values (expressed in Hounsfield Units, HU) were measured using the scanner software by drawing three 10 mm^2 regions of interest in delayed enhanced myocardium, remote myocardium and the left ventricular cavity in a short axis slice located at the center of the infarction of each pig (11). Noise was considered to be the standard deviation of the CT value in a region of interest of 25 mm^2 placed in the descending thoracic aorta. MRI signal intensity values were measured using the scanner software by drawing 30 mm^2 regions of interest in delayed enhanced and remote myocardium and were expressed as arbitrary units (AU) (13). Signal intensity of the left ventricular blood pool was measured by drawing a >100mm^2 region of interest in the left ventricular cavity. Noise was considered to be the standard deviation of the signal measured in a region of interest >300mm^2 placed in the imaged air outside of the pig.

Statistical Analysis

All data are presented as mean ± standard deviation. The relation between infarct size assessed with DE-MSCT, DE-MRI and TTC pathology was evaluated with univariate linear regression analysis. Agreement between DE-MSCT, DE-MRI and TTC pathology for the assessment of infarct size and intra –and interobserver variability was determined with Bland Altman analysis. Differences in regional wall thickening were tested with an unpaired t test. Differences in CT attenuation values and MR signal intensity values between infarcted myocardium, remote myocardium and left ventricular blood pool were tested with one-way analysis of variance followed by post hoc Bonferroni correction to adjust for multiple comparisons.

Results

The two swine that underwent 15 min of balloon occlusion of the circumflex coronary artery showed hypokinesia of the lateral wall on echocardiography performed 20 min after reperfusion, indicating the presence of stunned myocardium. DE-MSCT and DE-MRI imaging demonstrated no regions with delayed enhancement. TTC staining confirmed that there was no infarcted myocardium.

In 10 swine that underwent 2 hour balloon occlusion of the circumflex coronary artery, acute reperfused myocardial infarction was accu-rately detected by both DE-MSCT and DE-MRI (**Figs. 1, 2**). DE-MSCT image quality was classified as good in 83% (48 of 58), moderate in 10% (6 of 58), and poor in 7% (4 of 58) of slices. DE-MRI image quality was classified as good in 75% (43 of 58), moderate in 17% (10 of 58), and poor in 8% (5 of 58) of slices. No delayed enhancement was seen in myocardium outside the perfusion territory of the circumflex coronary artery. Mean infarct size was 21 ± 15% on DE-MSCT images, 22 ± 16% on DE-MR images and 20 ± 15% on TTC pathology images. Infarct size assessed with DE-MSCT correlated well with infarct size measured on TTC pathology slices ($R^2 = 0.96$; $p < 0.001$). Also, infarct size assessed with DE-MRI correlated well with infarct size measured on TTC pathology slices ($R^2 = 0.93$; $p < 0.001$). Accordingly, infarct size assessed with DE-MSCT correlated well with infarct size assessed with DE-MRI ($R^2 = 0.96$; $p < 0.001$) (**Fig 3a**). Bland-Altman analyses demonstrated a good agreement for the assessment of infarct size between DE-MSCT, DE-MRI and TTC pathology (**Fig. 3b**). The intraobserver variability for the assessment of infarct size was 1.0 ± 3.9% for DE-MSCT and 0.5 ± 4.6% for DE-MRI. The interobserver variability for the assessment of infarct size was 2.1 ± 5.6% for DE-MSCT and 3.0 ± 5.9% for DE-MRI. Regional wall thickening was significantly decreased in infarcted myocardium of the lateral wall compared to remote non-infarcted myocardium of the septum (0 ± 14% versus 50 ± 14%; $p<0.001$) (**Fig. 4**).

Mean CT attenuation value of delayed enhanced myocardium was significantly different from CT attenuation value of remote myocardium (126 ± 20 versus 66 ± 6 HU; $p < 0.001$; 3 pair-wise comparisons) (**Fig. 5**). The relative difference in CT attenuation value between delayed enhanced and remote myocardium was 191 ± 18%. Noise measured in the descending aorta was 17±3 HU. Mean MR signal intensity value of delayed enhanced myocardium was significantly higher than MR signal intensity of remote myocardium (154 ± 37 AU versus 28 ± 6 AU; $p < 0.001$; 3 pairwise comparisons) (**Fig. 5**). Relative MR signal intensity value of delayed enhanced myocardium compared to remote myocardium was 554 ± 156%. Noise measured in the air outside the pig was 6 ± 1 AU.

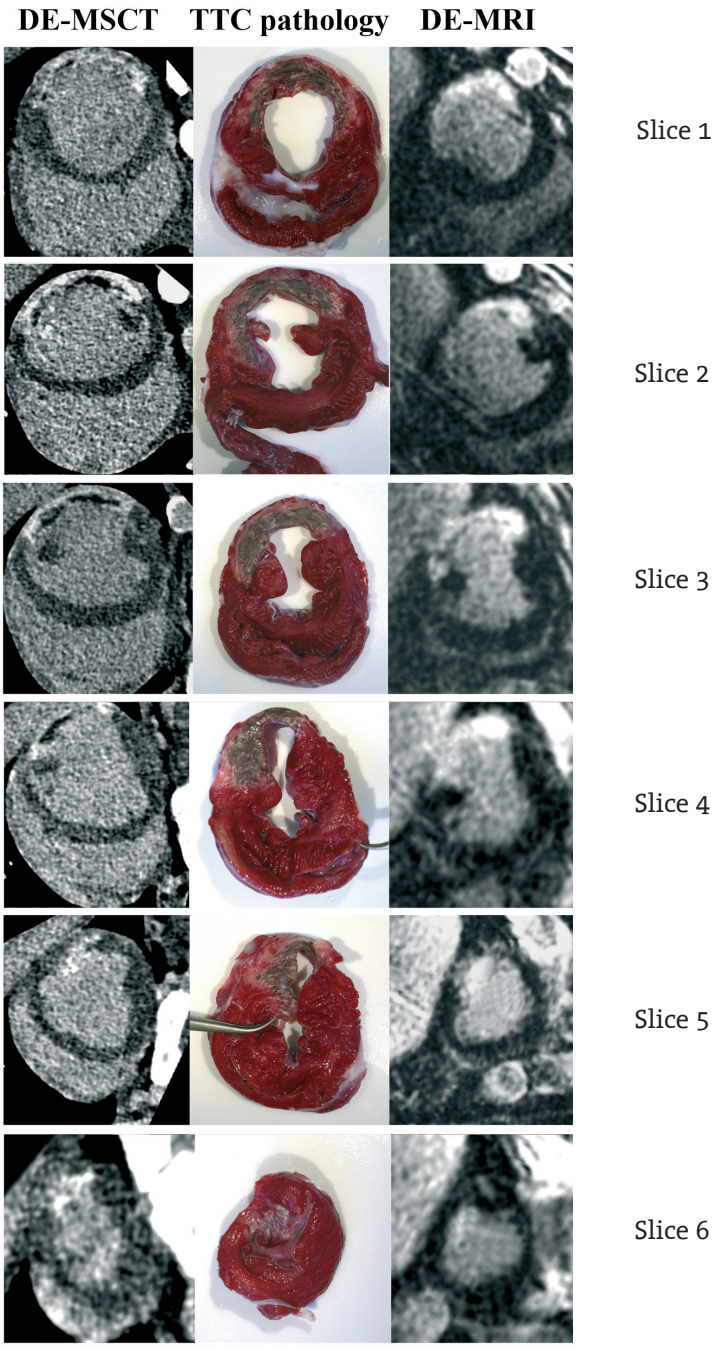

Figure 1. Acute reperfused myocardial infarction can be assessed accurately with delayed enhancement multislice computed tomography (DE-MSCT) and delayed enhancement magnetic resonance imaging (DE-MRI) compared to postmortem TTC pathology. The left ventricle is shown from base (*Slice 1*) to apex (*Slice 6*). The DE-MSCT images represent 1 mm slices compared to the photographed TTC pathology slices and the DE-MRI slices of 8 mm.

Discussion

Our results demonstrate that DE-MSCT can assess acute reperfused myocardial infarction in good agreement with in-vivo DE-MRI and post-mortem TTC pathology.

Delayed Enhancement Imaging

Delayed enhancement imaging is feasible with MSCT and MRI since both iodinated contrast agents and gadolinium chelates passively diffuse into the increased extracellular matrix of infarcted myocardium (14). Higgins et al. (15) demonstrated elevated concentrations of iodinated con-trast material in infarcted tissue compared to uninfarcted tissue if assessed more than 5 min after administration of these contrast materials. Rehwald et al. (16) showed significantly higher con-centrations of gadolinium chelates in infarcted myocardium compared to remote myocardium after a delay of 10 min. Because accumulation of contrast agents in necrotic myocardium is a passive process, the timing between administration of contrast agents and imaging might be crucial to accurately assess infarct size. Amado et al. (17) performed DE-MRI between 6 and 30 min after administration of gadolinium-chelates and observed no difference in measured infarct size. The optimal time delay for performing DE-MSCT after administration of iodinated contrast agents remains to be determined since no data are available for DE-MSCT in infarctions more than 2 days old. The pharmacokinetic

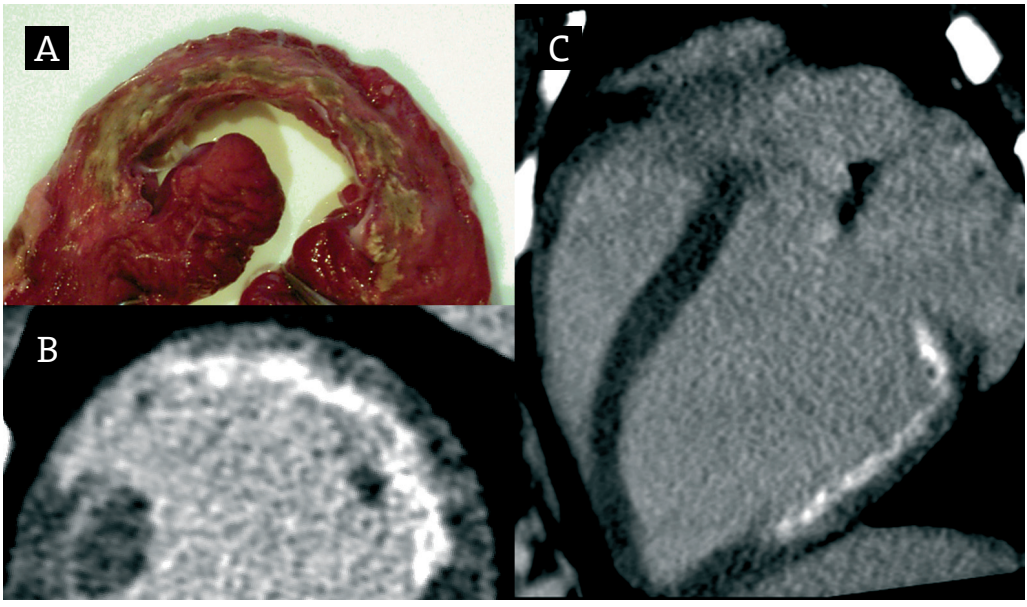

Figure 2. In this pig with subendocardial infarction, the transmural differentiation of viable and non-viable myocardium is demonstrated with DE-MSCT in short axis view (**B**) and long axis view (**C**) with TTC pathology as standard of reference (**A**)

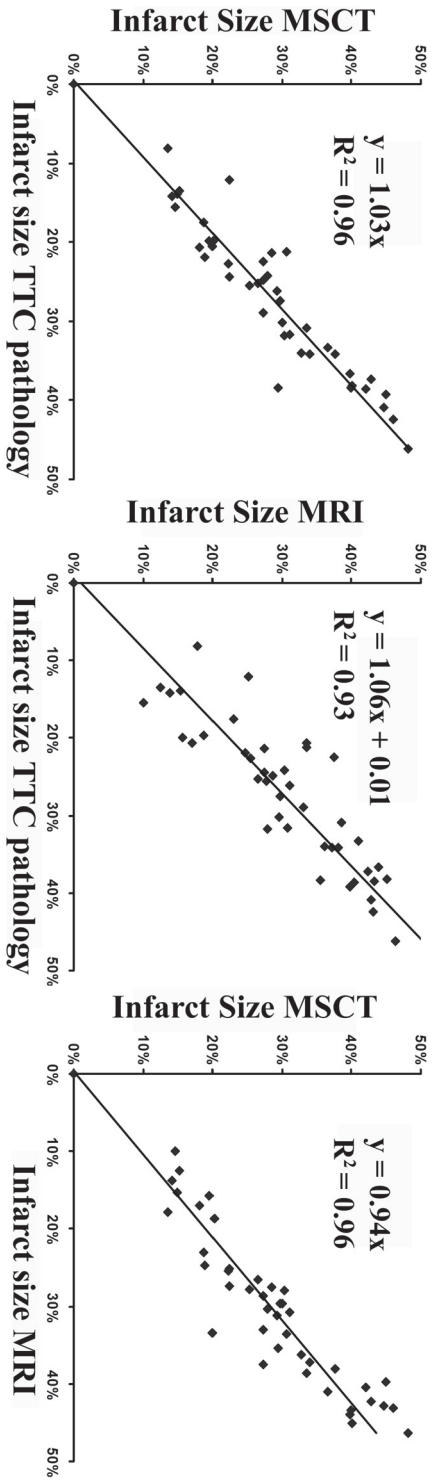

be-havior of gadolinium chelates and iodinated contrast agents is relatively similar but differences in molecule size may influence the rate of diffusion in infarcted myocardium (18).

DE-MSCT

Delayed enhancement CT for the assessment of myocardial infarction was performed as early as the late 1970s, and these initial results were encouraging (19). However, practical use of this technique was hampered by insufficient image quality mainly caused by cardiac motion. Computerized Tomography technology has developed rapidly during the last decade, and with the introduction of spiral and later multislice spiral CT a marked increase in temporal and spatial resolution was obtained. Three recent experimental studies demonstrated the excellent diagnostic accuracy of 4-, 16-, and 32-slice CT for the assessment of non-reperfused and reperfused myocardial infarction if performed within 5 h after induction of infarction (10,11,20). However, infarct morphology may change after myocardial infarction with early infarct expansion (<2 days) and late infarct shrinkage (>10 days) (5,21), and the ability of DE-MSCT to assess more than 5 h old infarctions is currently unknown. To assess infarct size between 2 and 7 days after infarction is clinically relevant since infarct size predicts long term left ventricular remodeling and clinical outcome (1,22-24). In the current study, we demonstrated that DE 64-slice CT can assess infarct size between 3 and 7 days after infarction and can differentiate between necrotic myocardium and severely ischemic

Figure 3a. The relation between infarct size assessed with DE-MSCT, DE-MRI and postmortem TTC pathology.

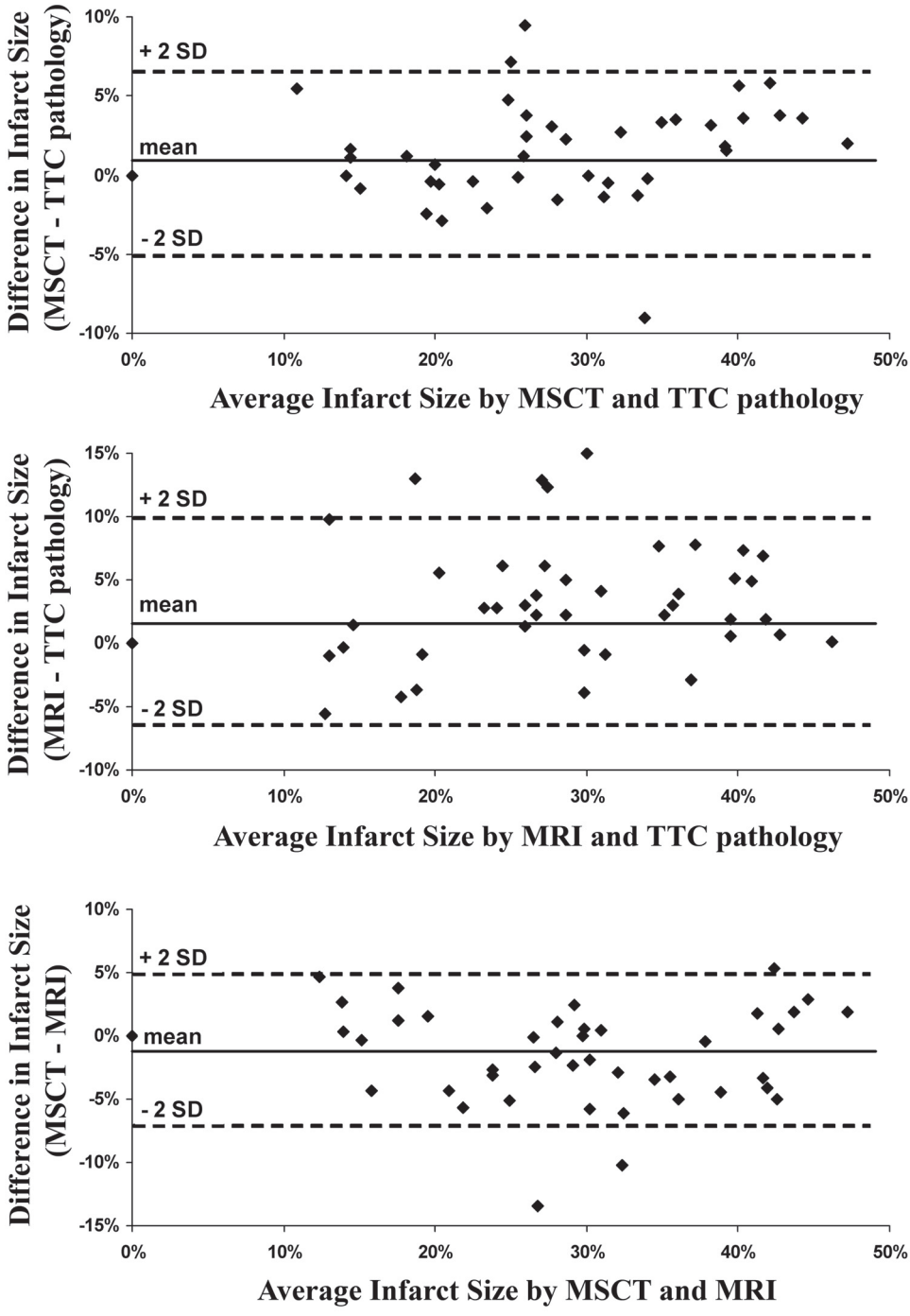

Figure 3b. Bland Altman analyses show the excellent agreement between infarct size assessed with DE-MSCT, DE-MRI and post mortem TTC pathology. Abbreviations as in Fig. 1.

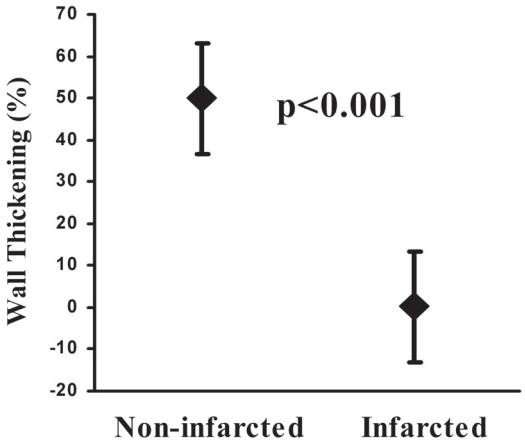

Figure 4. Regional wall thickening was significantly reduced in infarcted compared to non-infarcted myocardium.

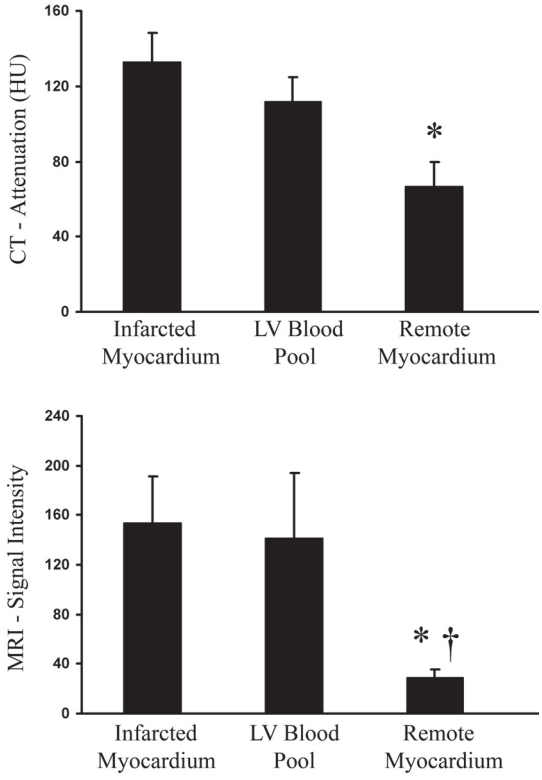

Figure 5. Mean Computerized Tomography (CT) attenuation value (HU) for infarcted myo-cardium is significantly higher compared with non-infarcted myocardium. Mean MR signal intensity value (AU) of infarcted myocardium is significantly higher compared to non-infarcted myocardium. * $p < 0.001$ compared to infarcted myocardium. † $p< 0.001$ compared to left ventricular blood pool.

but reversible injured myocardium with good correlation with in-vivo DE-MRI and ex-vivo TTC pathology. More studies are needed to demonstrate if DE-MSCT can also show myocardial infarction or scar at a longer time of follow-up after myocardial infarction.

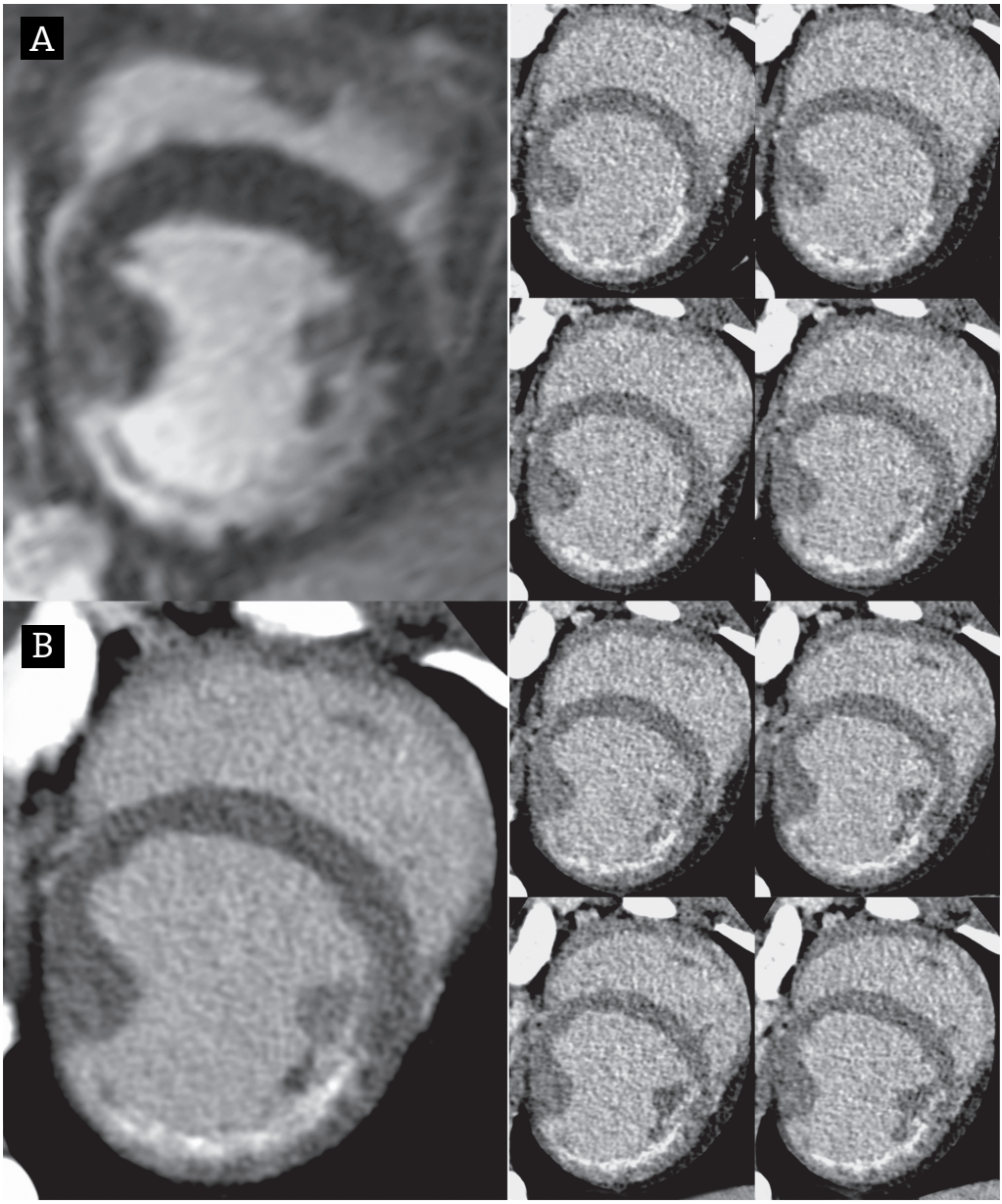

Figure 6. DE-MSCT provides higher spatial resolution images than DE-MRI. Image **A** represents an 8- mm-thick DE-MRI image, and image B represents the similar slice reconstructed from 8 different 1-mm-thick DE-MSCT images. Images on the right represent the eight reconstructed 1-mm-thick slices that together form image **B**. Abbreviations as in Fig. 1.

An advantage of MSCT is that it offers high spatial resolution imaging, allowing reconstruction of thin slices and thereby reducing possible partial volume artifacts. High-resolution DE-MSCT imaging also allowed the transmural differentiation of viable and nonviable myocardium. A major disadvantage of MSCT is the limited soft tissue contrast that is obtained. Tissue con-trast is related to the radiation dose that is applied and the amount of iodinated contrast material administered. For DE-MSCT imaging, we used the radiation dose that is used for MSCT coronary angiography (15/21 mSv for men/women). We administered 1gI/kg of iodine contrast to the pigs, equivalent to approximately 200 ml of iodine contrast to a patient of 70 kg, which is considered a normal dose of contrast during a conventional angiography procedure (25). Technical developments are desirable that reduce radiation exposure and limit the amount of iodinated contrast material needed. Recent developments include tube-current modulation which reduces radiation exposure by nearly a one-half by applying radiation only in the mid- to end-diastolic phase of the cardiac cycle (26).

DE-MRI

DE-MRI is an established non-invasive imaging modality that can assess reperfused and non-reperfused myocardial infarction (4). It is safe and patient friendly and can be repeated multiple times to evaluate therapy without causing harm to the patient. No heart rate control is necessary. Excellent soft tissue contrast is obtained with gadolinium chelates that have T1 shortening characteristics. Further improvement in tissue contrast is obtained by applying a non-selective inversion pulse before data-acquisition, allowing suppression of signal of remote myocardium (27). We observed a relative signal intensity between hyperenhanced and remote myocardium of 554 ± 156%. A disadvantage of MRI is the limited through-plane resolution resulting in a slice thickness of 4 to 8 mm (**Fig. 6)**. In the present study, differences in infarct size between post-mortem TTC pathology, DE-MSCT, and DE-MRI might have been caused by dissimilarity in slice thickness offered by these different modalities. DE-MSCT allowed reconstruction of a slice thickness of 1 mm, whereas DE-MRI was performed with a slice thickness of 8 mm, and TTC pathology, the standard of reference, was analyzed on a two-dimensional digital photograph. The accuracy and reproducibility of infarct size measurements with DE-MSCT and DE-MRI might further improve by using a semi-automated quantification software (17).

Conclusions

Delayed enhancement MRI is a well established non-invasive imaging modality that allows assessment of myocardial infarct size and has been shown to provide prognostic information in patients who suffered acute myocardial infarction. We

demonstrated that DE-MSCT can assess acute reperfused myocardial infarction in good agreement with in-vivo DE-MRI and post-mortem TTC pathology. Ongoing technical improvements of the CT scanner have resulted in high diagnostic performance to detect significant coronary stenosis in selected groups of patients without arrhythmia and a heart rate below 70 beats/min (6,7). Together with the assessment of infarct size, this new CT-technology might emerge as a clinical valuable tool to comprehensively evaluate post-infarction patients.

Acknowledgements

The authors thank Wendy Kerver for her help in the logistics of this study.

References

1. Baks T, van Geuns RJ, Biagini E, et al. Recovery of left ventricular function after primary angioplasty for acute myocardial infarction. Eur Heart J 2005;26:1070-7.
2. Miller TD, Christian TF, Hopfenspirger MR, Hodge DO, Gersh BJ, Gibbons RJ. Infarct size after acute myocardial infarction measured by quantitative tomographic 99mTc sestamibi imaging predicts subsequent mortality. Circulation 1995;92:334-41.
3. Judd RM, Lugo-Olivieri CH, Arai M, et al. Physiological basis of myocardial contrast enhancement in fast magnetic resonance images of 2-day-old reperfused canine infarcts. Circulation 1995;92:1902-10.
4. Kim RJ, Fieno DS, Parrish TB, et al. Relationship of MRI delayed contrast enhancement to irreversible injury, infarct age, and contractile function. Circulation 1999;100:1992-2002.
5. Gerber BL, Rochitte CE, Melin JA, et al. Microvascular obstruction and left ventricular remodeling early after acute myocardial infarction. Circulation 2000;101:2734-41.
6. Raff GL, Gallagher MJ, O'Neill WW, Goldstein JA. Diagnostic accuracy of noninvasive coronary angiography using 64-slice spiral computed tomography. J Am Coll Cardiol 2005;46:552-7.
7. Mollet NR, Cademartiri F, van Mieghem CA, et al. High-resolution spiral computed tomography coronary angiography in patients referred for diagnostic conventional coronary angiography. Circulation 2005;112:2318-23.
8. Mahnken AH, Koos R, Katoh M, et al. Assessment of myocardial viability in reperfused acute myocardial infarction using 16-slice computed tomography in comparison to magnetic resonance imaging. J Am Coll Cardiol 2005;45:2042-7.
9. Gosalia A, Haramati LB, Sheth MP, Spindola-Franco H. CT detection of acute myocardial infarction. AJR Am J Roentgenol 2004;182:1563-6.

10. Buecker A, Katoh M, Krombach GA, et al. A feasibility study of contrast enhancement of acute myocardial infarction in multislice computed tomography: comparison with magnetic resonance imaging and gross morphology in pigs. Invest Radiol 2005;40:700-4.
11. Hoffmann U, Millea R, Enzweiler C, et al. Acute myocardial infarction: contrast-enhanced multidetector row CT in a porcine model. Radiology 2004;231:697-701.
12. Flohr T, Stierstorfer K, Raupach R, Ulzheimer S, Bruder H. Performance evaluation of a 64-slice CT system with z-flying focal spot. Rofo 2004;176:1803-10.
13. Gupta A, Lee VS, Chung YC, Babb JS, Simonetti OP. Myocardial infarction: optimization of inversion times at delayed contrast-enhanced MR imaging. Radiology 2004;233:921-6.
14. Mahrholdt H, Wagner A, Judd RM, Sechtem U. Assessment of myocardial viability by cardiovascular magnetic resonance imaging. Eur Heart J 2002;23:602-19.
15. Higgins CB, Siemers PT, Newell JD, Schmidt W. Role of iodinated contrast material in the evaluation of myocardial infarction by computerized transmission tomography. Invest Radiol 1980;15: S176-82.
16. Rehwald WG, Fieno DS, Chen EL, Kim RJ, Judd RM. Myocardial magnetic resonance imaging contrast agent concentrations after reversible and irreversible ischemic injury. Circulation 2002;105:224-9.
17. Amado LC, Gerber BL, Gupta SN, et al. Accurate and objective infarct sizing by contrast-enhanced magnetic resonance imaging in a canine myocardial infarction model. J Am Coll Cardiol 2004;44:2383-9.
18. Weinmann HJ, Brasch RC, Press WR, Wesbey GE. Characteristics of gadolinium-DTPA complex: a potential NMR contrast agent. AJR Am J Roentgenol 1984;142:619-24.
19. Gray WR, Buja LM, Hagler HK, Parkey RW, Willerson JT. Computed tomography for localization and sizing of experimental acute myocardial infarcts. Circulation 1978;58:497-504.
20. Lardo AC, Cordeiro MA, Silva C, et al. Contrast-enhanced multidetector computed tomography viability imaging after myocardial infarction: characterization of myocyte death, microvascular obstruction, and chronic scar. Circulation 2006;113:394-404.
21. Baks T, van Geuns RJ, Biagini E, et al. Effects of primary angioplasty for acute myocardial infarction on early and late infarct size and left ventricular wall characteristics. J Am Coll Cardiol 2006;47:40-4.
22. Gerber BL, Garot J, Bluemke DA, Wu KC, Lima JA. Accuracy of contrast-enhanced magnetic resonance imaging in predicting improvement of regional myocardial function in patients after acute myocardial infarction. Circulation 2002;106:1083-9.
23. Beek AM, Kuhl HP, Bondarenko O, et al. Delayed contrast-enhanced magnetic resonance imaging for the prediction of regional functional improvement after acute myocardial infarction. J Am Coll Cardiol 2003;42:895-901.
24 Hombach V, Grebe O, Merkle N, et al. Sequelae of acute myocardial infarction regarding cardiac structure and function and their prognostic significance as assessed by magnetic resonance imaging. Eur Heart J 2005;26:549-57.
25. 7.1, Dawson P, Administration of contrast media. In: Dawson P and Claus, editors. Contrast media in practice. Springer-Verlag 1999

26. Jakobs TF, Becker CR, Ohnesorge B, et al. Multislice helical CT of the heart with retrospective ECG gating: reduction of radiation exposure by ECG-controlled tube current modulation. Eur Radiol 2002;12:1081-6.
27. Simonetti OP, Kim RJ, Fieno DS, et al. An improved MR imaging technique for the visualization of myocardial infarction. Radiology 2001;218:215-23.

Assessment of Acute Reperfused Myocardial Infarction with 64-slice Delayed Enhancement Computed Tomography

Timo Baks; Filippo Cademartiri; A. Moelker; Willem J. van der Giessen; Gabriel P. Krestin; Dirk J. Duncker; Pim J. de Feyter

Am J Roentgenology accepted

15

1, 2, 3, 4, 5, 6, 7, 8, 9 ,10, 11, 12, 13, 14,

Abstract

Objective

To evaluate the ability of delayed enhancement 64-slice Computed Tomography to assess myocardial infarct size in a porcine model of acute reperfused myocardial infarction. Computed Tomography allows non-invasive assessment of coronary artery stenosis but evaluation of myocardial viability in the subacute phase of acute myocardial infarction has not been validated yet. We performed delayed enhancement imaging in six domestic swine 5 days after reperfused acute myocardial infarction and assessed the relation between delayed enhancement patterns in-vivo and the extent of viable and non-viable myocardium at post mortem histochemistry. Delayed enhancement imaging was performed 15 minutes after administration of 80 ml of iodinated contrast agent using a 64-slice clinical CT scanner with an effective temporal resolution of 165 ms. We observed a good correlation between infarct size in vivo and infarct size at histochemistry (R^2=0.92).

Conclusion

Delayed enhancement imaging with 64-slice Computed Tomography allows accurate assessment of reperfused acute myocardial infarct size.

Introduction

Multislice Computed Tomography (MSCT) is now used for the evaluation of coronary artery disease and allows the detection of coronary artery stenosis with high diagnostic accuracy (1, 2). The diagnostic value of MSCT for the assessment of myocardial viability in the subacute phase of acute myocardial infarction is currently unclear. Previous studies showed that MSCT imaging performed during the first-pass of an iodinated contrast agent resulted in low tissue contrast between infarcted and non-infarcted myocardium and total infarct size appeared to be underestimated (3, 4). Using a delayed enhancement imaging protocol as applied in Magnetic Resonance Imaging (MRI) might be an alternative approach. Excellent tissue contrast with MRI is obtained 10-30 minutes after administration of gadolinium-derivates since this type of contrast agent accumulates in the infarcted tissue. Interestingly, the pharmacokinetic behavior of gadolinium-chelates and iodinated contrast agents is relatively similar (5). Therefore, we performed delayed enhancement MSCT imaging in a porcine model of reperfused acute myocardial infarction to investigate if reperfused infarct size can be assessed accurately with delayed enhancement MSCT.

Material and Methods

Animal model

Six Yorkshire-landrace pigs (2-3 months old, 22 kg) underwent coronary angiography followed by balloon occlusion of the left circumflex coronary artery. Reperfusion was obtained by deflating the balloon after 2 hours of ischemia. The study complied with the regulations of the animal care committee of the Erasmus MC and the "Guide for the Care and Use of Laboratory Animals" (NIH publication 1996). Animals were sedated (ketamine 20 mg/kg intramuscular and midazolam 1 mg/kg intramuscular), anaesthetized (thiopental, 12 mg/kg intravenously), intubated and mechanically ventilated (mixture of oxygen and nitrogen 1:2). Anaesthesia was maintained with fentanyl (12.5 microgram/kilogram/hour).

Computed Tomography

Five days after induction of myocardial infarction, all swine were anaesthetized as described above and underwent MSCT imaging. Mean heart rate decreased from approximately 80 to 45±9 beats per minute after administration of Zatebradine (10 mg/kg intravenously). A 64-slice clinical CT scanner was used for imaging (Sensation 64®, Siemens, Forchheim, Germany) with the following characteristics: number of detector rows 32x2 (oversampling in the z-axis obtained with flying focal spot),

number of slices per rotation 64, individual detector width 0.6 mm, gantry rotation time 330 ms, effective temporal resolution 165 ms. Delayed enhancement imaging was performed 15 minutes after administration of 80 ml of iodinated contrast agent through an ear vein (Iomeprol 400mgI/ml, Iomeron®, Bracco, Italy). The following scan parameters were used: kV 120, effective mAs 900, feed/rotation 3.84 mm and scan direction cranio-caudal. The estimated radiation dose if used for a human protocol was 15/21 milliSievert for male/female. Delayed enhancement MSCT datasets were reconstructed at −300ms, −350ms, and −400 ms before the next R wave (end-diastolic phase of the cardiac cycle). From the dataset with optimal image quality, images with a slice thickness of 1 mm and an increment of 0.5 mm were reconstructed in the short-axis view using a dedicated software platform with multiplanar capabilities (Leonardo, Siemens, Forchheim, Germany).

Data analysis

One day after MSCT-imaging, all animals were sacrificed and the hearts excised. The myocardium of the left ventricle was cut in 8 mm consecutive slices in the short axis view with a commercially available meatslicer. To obtain a viability staining, the slices were embedded in a solution of 1% Triphenyltetrazolium chloride (TTC) and 0.2 mol/L Sorensen's buffer (pH 7.4) at 37°C for 15 minutes, followed by fixation in 4% formalin. The slices were then photographed with a digital camera. The digitalized TTC-stained slices were loaded in a separate workstation with a commercially available analysis package (SigmaScan® Pro 5.0). TTC negative borders and endocardial and epicardial borders of the left ventricle were traced manually in all consecutive slices. Infarct size was defined as the TTC negative area as a percentage of total left ventricular slice area.

Reconstructed MSCT images were exported and transferred to a separate workstation with dedicated software (Cine Tool, GE Medical Systems, USA). The region with delayed enhancement was selected manually on these images. Infarct size per slice was calculated by dividing the delayed enhanced area by the total slice area. CT attenuation values (expressed in Hounsfield Units, HU) were measured by drawing three 10 mm^2 regions of interest in delayed enhanced myocardium, remote myocardium and the left ventricular cavity in a short axis slice located at the center of the infarction of each pig (3).

Statistical Analysis

Data are presented as mean ± standard deviation. Univariate linear regression analysis and Bland-Altman analysis were used to evaluate the relationship between infarct size measured with MSCT and infarct size measured with post-mortem histochemistry. One-way-ANOVA with repeated measurements was used for the comparison of CT attenuation values of delayed enhanced myocardium, remote myocardium and the left

ventricular cavity. Post-hoc Bonferroni correction was applied to adjust for multiple comparisons. Significance was accepted at p of ≤ 0.05 (two-tailed).

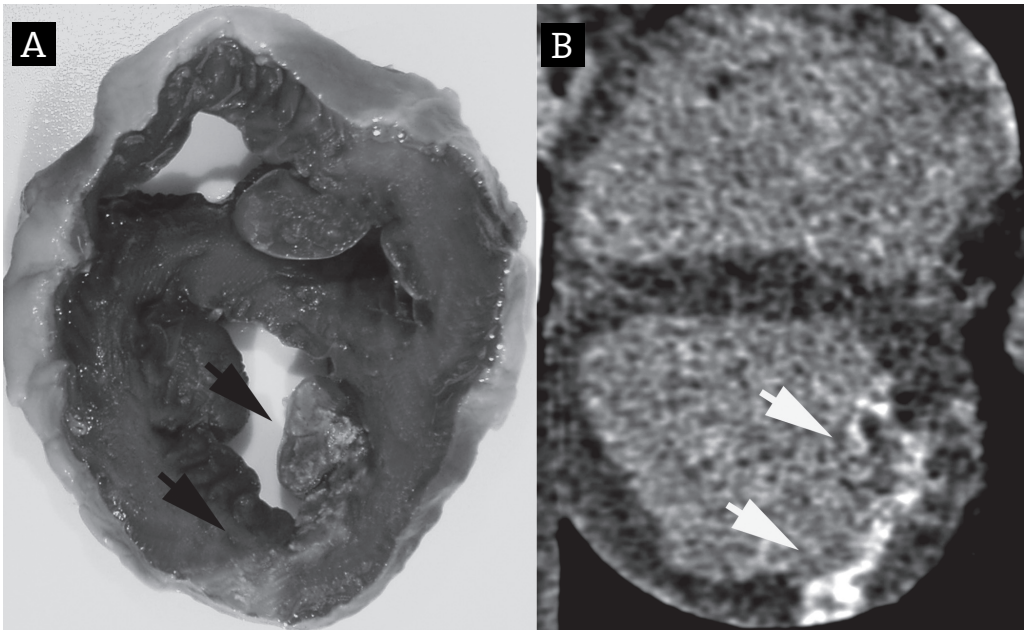

Figure 1. Subendocardial myocardial infarction in midventricular short axis view is demonstrated by (**A**) post mortem histochemistry (black arrows) and (**B**) delayed enhancement MSCT (white arrows). *

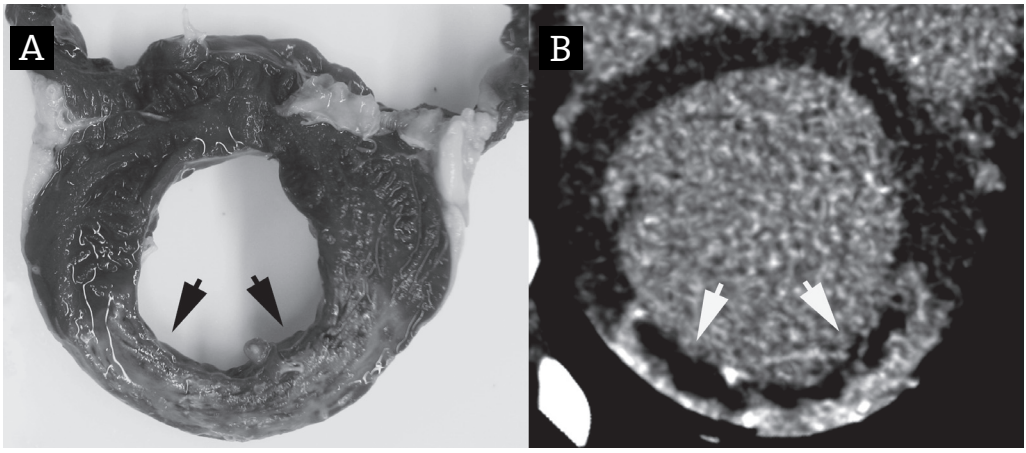

Figure 2. Transmural myocardial infarction in short axis view is demonstrated by (**A**) histochemistry (black arrows) and (**B**) delayed enhancement MSCT (white arrows). *

A

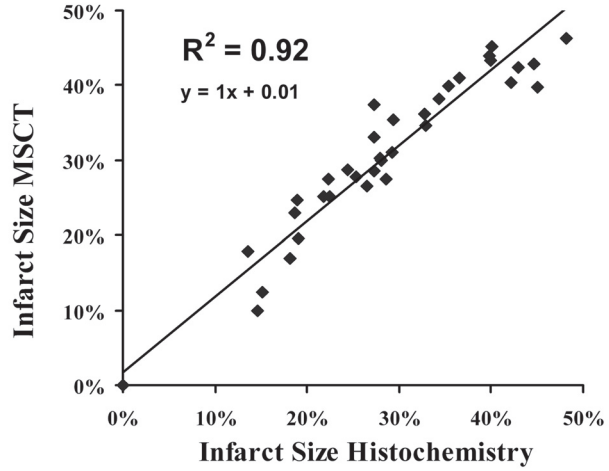

B

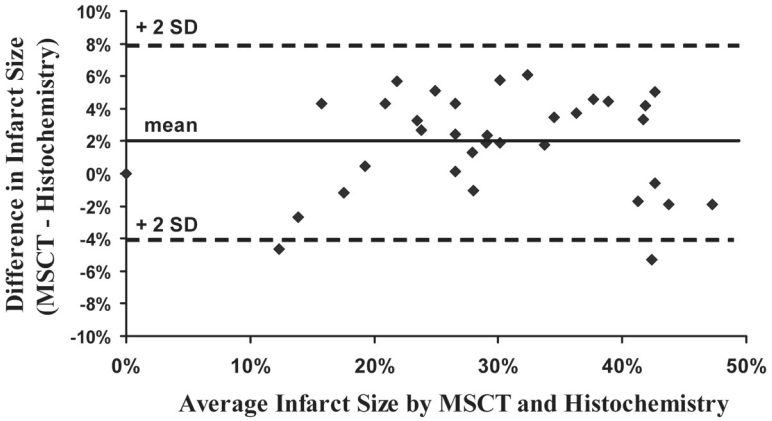

Figure 3a/b. Linear regression analysis (**A**) and Bland-Altman analysis (**B**) demonstrate the reliability of MSCT versus histochemistry to assess acute reperfused myocardial infarct size per slice.

Results

All MSCT data sets were of good image quality. Delayed enhancement was observed in the lateral wall of the left ventricle corresponding to the perfusion territory of the circumflex coronary artery (**Figures 1** and **2**).

No delayed enhancement was seen in remote myocardium. Of 42 available histochemistry slices, 4 slices had to be excluded due to post mortem shrinkage making the measurements of infarct area and slice area impossible. TTC negative

areas (infarcted myocardium) were observed in the lateral wall of the left ventricle while no TTC negative areas were observed in remote myocardium (**Figure. 1** and **2**).

Mean infarct size was 28±13% on MSCT images and 26±12% on histochemistry images. Infarct size measured with MSCT correlated well with infarct size measured on histochemistry (R^2=0.92; p<0.001) (**Figure 3**).

Discussion

MSCT technology has developed rapidly during the last decade with a marked increase in temporal and spatial resolution. Non-invasive evaluation of coronary artery disease is now feasible and several studies reported a good diagnostic accuracy for the detection of coronary artery stenosis. Evaluation of myocardial viability in the subacute phase of acute myocardial infarction has also been studied with MSCT, but limited data are available. For example, Hoffman et al. (3) performed 4-slice CT coronary angiography within 5 hours of acute non-reperfused myocardial infarction in swine and demonstrated a good correlation between the size of perfusion defects and the size of infarction estimated from post mortem histochemistry. Mahnken et al. (6) performed 16-slice CT coronary angiography followed by delayed enhancement CT and MRI in patients within 14 days of reperfused acute myocardial infarction. Infarct size measured on delayed enhancement CT and delayed enhancement MRI was comparable but infarct size measured on perfusion images remained underestimated.

In the present study, we used an experimental model of reperfused acute myocardial infarction since early aggressive reperfusion treatment is currently the preferred treatment in the clinical setting of acute myocardial infarction. Delayed enhancement imaging was performed since contrast agents used for MSCT (iodinated contrast material) and MRI (gadolinium-derivates) accumulate in the infarcted myocardium 10-30 minutes after intravenous administration while these contrast agents are being washed out of remote myocardium (7, 8). We did not perform perfusion imaging since MRI studies of reperfused myocardial infarction demonstrated that total infarct size remains underestimated with perfusion imaging. During the first pass of a contrast agent, infarcted myocardium with an intact microvasculature enhances normally while infarcted myocardium with microvascular obstruction appears as a perfusion defect (9). In conclusion, we demonstrated that infarct size can be assessed accurately with delayed enhancement 64-slice CT if performed 5 days after reperfused myocardial infarction.

Limitations

A well known concern of MSCT imaging is the use of iodinated contrast agents and the radiation exposure to the patient. Our results encourage further research that should aim at the optimization of protocols using less radiation and less iodinated contrast material and at the optimal timing of delayed enhancement imaging after contrast administration. Furthermore, image quality is heart rate dependent and might be impaired with heart rates above 70 beats per minutes (10).

Clinical Perspective

Measurement of infarct size in patients with acute myocardial infarction is clinically relevant since infarct size predicts left ventricular function and geometry and hence long-term clinical outcome (11, 12). Information on infarct size provided by MSCT would enhance the diagnostic armamentarium of the physician who lacks access to cardiac MRI or encounters patients that have contraindications for MRI.

Acknowledgements

The authors would like to thank Wendy Kerver for her help in the logistics of this study.

References

1. Nieman K, Cademartiri F, Lemos PA, Raaijmakers R, Pattynama PM, de Feyter PJ. Reliable noninvasive coronary angiography with fast submillimeter multislice spiral computed tomography. Circulation 2002;106(16):2051-4.
2. Leschka S, Alkadhi H, Plass A, Desbiolles L, Grunenfelder J, Marincek B, et al. Accuracy of MSCT coronary angiography with 64-slice technology: first experience. Eur Heart J 2005.
3. Hoffmann U, Millea R, Enzweiler C, Ferencik M, Gulick S, Titus J, et al. Acute myocardial infarction: contrast-enhanced multi-detector row CT in a porcine model. Radiology 2004;231(3):697-701.
4. Gosalia A, Haramati LB, Sheth MP, Spindola-Franco H. CT detection of acute myocardial infarction. AJR Am J Roentgenol 2004;182(6):1563-6.
5. Weinmann HJ, Brasch RC, Press WR, Wesbey GE. Characteristics of gadolinium-DTPA complex: a potential NMR contrast agent. AJR Am J Roentgenol 1984;142(3):619-24.
6. Mahnken AH, Koos R, Katoh M, Wildberger JE, Spuentrup E, Buecker A, et al. Assessment of myocardial viability in reperfused acute myocardial infarction using 16-slice computed tomography in comparison to magnetic resonance imaging. J Am Coll Cardiol 2005;45(12):2042-7.

7. Rehwald WG, Fieno DS, Chen EL, Kim RJ, Judd RM. Myocardial magnetic resonance imaging contrast agent concentrations after reversible and irreversible ischemic injury. Circulation 2002;105(2):224-9.
8. Higgins CB, Sovak M, Schmidt W, Siemers PT. Differential accumulation of radiopaque contrast material in acute myocardial infarction. Am J Cardiol 1979;43(1):47-51.
9. Gerber BL, Rochitte CE, Melin JA, McVeigh ER, Bluemke DA, Wu KC, et al. Microvascular obstruction and left ventricular remodeling early after acute myocardial infarction. Circulation 2000;101(23):2734-41.
10. Raff GL, Gallagher MJ, O'Neill WW, Goldstein JA. Diagnostic accuracy of noninvasive coronary angiography using 64-slice spiral computed tomography. J Am Coll Cardiol 2005;46(3):552-7.
11. Miller TD, Christian TF, Hopfenspirger MR, Hodge DO, Gersh BJ, Gibbons RJ. Infarct size after acute myocardial infarction measured by quantitative tomographic 99mTc sestamibi imaging predicts subsequent mortality. Circulation 1995;92(3):334-41.
12. Baks T, van Geuns RJ, Biagini E, Wielopolski P, Mollet NR, Cademartiri F, et al. Recovery of left ventricular function after primary angioplasty for acute myocardial infarction. Eur Heart J 2005;26(11):1070-7.

Part 5

Summary and Conclusions

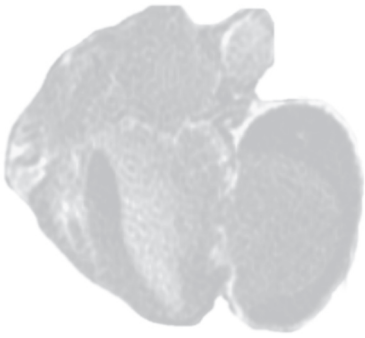

Summary and Conclusions

MRI is a versatile non-invasive imaging modality that can be applied in patients and in experimental models of ischemic heart disease. MRI allows refined assessment of regional and global left ventricular function and volumes, offers detailed information on myocardial perfusion and permits precise assessment of acute and chronic myocardial infarct size. In this thesis, the unique imaging capabilities of MRI are used in the setting of acute and chronic ischemic heart disease. We use MRI to monitor novel treatment strategies, to study pathophysiological mechanisms of ischemic heart disease and to evaluate the utility of MRI in the clinical setting. Furthermore, MRI based assessment of infarct size serves as an in-vivo standard of reference for MSCT, that is proposed as an alternative imaging modality to assess myocardial viability. In this thesis, we perform MRI and MSCT in experimental models of acute ischemic heart disease and in patients with acute and chronic ischemic heart disease.

Experimental Application of Magnetic Resonance Imaging

The advantage of using an experimental model of ischemic heart disease is the well controlled environment allowing the time to optimize experimental and imaging protocols. The versatility of MRI allows imaging of small rodent models with dedicated coils while larger mammals can be imaged with clinically available equipment. We used a porcine model of acute myocardial infarction and were able to obtain an excellent image quality in the majority of cases. Instrumented breath holds and gating to the electrocardiogram were applied to minimize the influence of cardiac and respiratory motion on data collection. Relatively small surface coils placed in proximity to the porcine heart gave excellent signal to noise images with high spatial resolution.

We performed MRI in a porcine model of reperfused acute myocardial infarction and studied the relation between infarct size and left ventricular diastolic function at 5 days after reperfusion. This study was started since infarct size is known to be a major determinant of left ventricular systolic (dys)function and remodeling in patients with a recent acute myocardial infarction (AMI), but the impact on left ventricular diastolic function is less well understood. Furthermore, infarct size and diastolic and systolic function and volumes are all predictors of cardiac mortality. Using cine-MRI, we calculated volume-time curves and diastolic function was expressed as peak filling

rate corrected for end-diastolic volume. Infarct size was assessed as the hyperenhanced region on standardized delayed-enhancement images. Our results show that acute myocardial infarct size is a major determinant of the extent of left ventricular diastolic dysfunction in the subacute phase of reperfused AMI. This relation was subsequently studied in patients who received successful primary percutaneous intervention with drug-eluting stent implantation for AMI with ST-segment elevation. A similar MRI protocol was applied. Infarct size appeared to be better related to the extent of diastolic dysfunction in the swine model than in patients. Finally, we explored the value of infarct size, ejection fraction and diastolic function at 5 days after reperfused AMI to predict left ventricular function and remodeling at 5 months. We found that acute infarct size was a better predictor than either ejection fraction or the extent of diastolic dysfunction at 5 days for left ventricular function and remodeling at 5 months. These findings might be explained by the presence of confounding variables in patients such as the presence of stunned myocardium and co-morbidities that influence the systolic and diastolic properties of the left ventricle. In our controlled experimental model, we were able to exclude multiple variables like the influence of co-morbidities as pre-existing hypertension (*Chapter 3*).

The capabilities of MRI to assess left ventricular function and infarct size were then used to monitor novel treatment strategies for left ventricular dysfunction in the setting of acute ischemic heart disease. Tissue regeneration after myocardial infarction via stem cell transplantation has shown potential as a therapy to prevent left ventricular remodeling and heart failure after acute myocardial infarction. First, we assessed the effects of intracoronary injection of human umbilical cord blood derived cultured unrestricted somatic stem cells (USSC) on regional and global left ventricular function, left ventricular geometry as well as infarct size. Using this study protocol, we observed that intracoronary application of unrestricted somatic stem cells did not attenuate LV remodeling and did not improve global and regional left ventricular function compared to a control group. In addition, USSC resulted in a larger infarct size at 4 weeks follow-up, which was accompanied by increases in inflammatory cells and calcifications in the infarct zone compared to swine who received medium in stead of stem cells. A different route of administration, for example transendomyocardial injection, might have led to different results (*Chapter 4*).

Second, we performed intracoronary injections of unselected bone marrow derived cells and selected bone marrow derived mononuclear cells in a porcine model of acute myocardial infarction. These cell types were used since several clinical trials showed encouraging results, although other clinical trials failed to repeat these positive findings. The effect of both cell-types on regional and global left ventricular function, left ven-

tricular geometry as well as infarct size was evaluated. We demonstrated that an intracoronary injection of either unselected bone marrow cells or mononuclear bone marrow cells one week after MI did not improve regional or global left ventricular function and did not reverse the enlargement of the left ventricle induced by the myocardial infarction. However, most interestingly, unselected bone marrow cells and mononuclear bone marrow cells did reduce infarct size four weeks after injection (*Chapter 5*).

MRI has been proposed as an imaging modality that can track iron labelled stem cells non-invasively in acute myocardial infarction. Direct evaluation of stem cell engraftment in post-ischemic or necrotic myocardium could attribute much to our understanding of the biological mechanisms that play a role in this complex process. However, no detailed studies are available that evaluated the MR characteristics of subacute and chronic infarctions without the application of stem-cells. We hypothesize that signal voids produced by ironoxide-labeled cells mimic the signal voids caused by hemoglobin degradation products as found in reperfused myocardial infarcts. Therefore, we applied clinically used MR pulse sequences in a porcine model of 1 week old and 5 weeks old reperfused myocardial infarction. We then compared the MR findings with histology of the infarct tissue. We indeed observed that reliable tracking of ironoxide-labeled cells in reperfused myocardial infarcts is hampered by signal voids produced by hemoglobin degradation products. We conclude that non-invasive tracking of iron-labeled cells by MRI in reperfused myocardial infarctions is hampered by MR characteristics of reperfused myocardial infarctions itself *(Chapter 6*).

Clinical Application of Magnetic Resonance Imaging

The superb imaging characteristics of MRI are used to study patients with acute and chronic heart disease. MRI is a safe and patient friendly imaging modality (although many patients disagree with the latter) so the effect of therapeutic interventions can be studied repeatedly without causing harm to the patient.

We performed MRI in patients with first ST-segment elevation AMI to study left ventricular remodeling and volumes and function. All patients were treated with state-of-the-art reperfusion therapy consisting of early successful implantation of a drug-eluting stent for first acute myocardial infarction (AMI). We assessed the presence of microvascular obstruction, the transmural extent of infarction and the total amount of irreversible damage (infarct size) that occurred to the left ventricular myocardium during prolonged ischemia. Also, we evaluated left ventricular volumes and function at 5 days and 5 months after AMI. We observed an inverse relation

between the transmural extent of delayed enhancement at 5 days and segmental wall thickening at 5 months after AMI. Also, we demonstrated that dysfunctional segments (segmental wall thickening less than 45%) without microvascular obstruction exhibited an increased end-diastolic wall thickness compared to remote myocardium. These segments without microvascular obstruction showed a significant improvement in wall thickening. Segments with microvascular obstruction despite a stented coronary artery demonstrated wall thinning at 5 months and showed no significant improvement in wall thickening at follow-up. Furthermore, we demonstrated an overall increase in mean ejection fraction of 7%. Improvement in regional and global left ventricular function might be caused by functional recovery of stunned (reversibly injured post-ischemic) myocardium.

Using MRI, the presence of stunned myocardium can be assessed indirectly by assessing the regional transmural extent of infarction. Dysfunctional myocardium with a subendocardial infarction constituting less than 25% of myocardial wall thickness exhibits more than 75% of dysfunctional but viable myocardium.

Interestingly, total infarct size at 5 days after AMI was a good predictor of ejection fraction, end-systolic and end-diastolic volume at 5 months. Infarct size assessed with delayed enhancement imaging appeared to be a better prognosticator than the extent of microvascular obstruction assessed with perfusion imaging. Remarkably, although epicardial coronary blood flow was restored in all patients within 6 hours of onset of symptoms, microvascular obstruction was identified with perfusion imaging at 5 days post AMI in 87% of patients. Finally, we also performed delayed enhancement imaging in patients 5 months after reperfused AMI. We demonstrated that infarct size decreased relatively to the same extent in small and large infarctions with a mean decrease of 31% (*Chapter 7 and 8*).

MRI also allows transmural differentiation of necrotic and viable myocardium in the setting of chronic ischemic heart disease. We used MRI to study the effect of drug-eluting stent implantation for a chronic total occlusion of a native coronary artery (CTO) on left ventricular volumes and function. We also evaluated the diagnostic value of MRI to predict improvement in regional and global left ventricular function after revascularization. Chronic total coronary occlusions (CTO) are observed in 35% to 50% of patients with significant coronary disease undergoing diagnostic angiography. Percutaneous coronary intervention (PCI) for CTO is increasingly used as treatment strategy and accounts for 10 to 15% of all angioplasties. However, the effect of PCI on myocardial contractility and left ventricular volumes of the individual patient with CTO is incompletely understood. Therefore, we performed MRI in patients with

a CTO planned for elective revascularization.We demonstrated the beneficial effect of successful drug-eluting stent implantation for CTO on end-systolic and end-diastolic volumes and segmental wall thickening. The extent of the left ventricle that was dysfunctional but viable before revascularization was related to improvement in end-systolic volume index and ejection fraction. Segmental wall thickening improved significantly in segments with <25% transmural extent of infarction, tended to improve in segments with 25-75% transmural extent of infarction whereas segments with >75% transmural extent of infarction did not improve (*Chapter 9*).

MR imaging is used in multiple studies to assess left ventricular function since MRI has proven to be an accurate and reproducible imaging modality for the quantitative analysis of the left ventricular function. Predominantly, manual segmentation of the left ventricle is performed in studies since automatic segmentation might be hampered by unsharp endocardial and epicardial boundaries. Moreover, large variations in image quality and large variations in shape of the left ventricle pose an even greater challenge for such an image processing task. We studied the accuracy and reproducibility of a novel automatic boundary detection algorithm of the left ventricle. We demonstrated that, using the 3 dimensional data available in a MRI dataset, the automatically derived endocardial and epicardial volumes compared favorable to the volumes obtained from manual analysis (*Chapter 10*).

We evaluated the relative merits of myocardial contrast echocardiography and magnetic resonance imaging to predict myocardial functional improvement after percutaneous coronary intervention. Using MRI, myocardial perfusion can be assessed and the high spatial resolution allows the transmural differentiation of necrotic and viable myocardium. Contrast enhanced echocardiography allows assessment of the no reflow phenomenon but cannot assess total infarct size. The major benefit of contrast echocardiography is the wide clinical availability and the availability as a bed side technique. We observed that both MRI and echocardiography can predict left ventricular function in patients who suffered acute myocardial infarction (*Chapter 11*).

Combining state-of-the-art MRI and MSCT imaging provide clinically relevant information that may guide therapeutic decision making. We demonstrate a case-report of a patient with a postinfarction pseudoaneurysm of the left ventricle. CMR provides detailed information on left ventricular function, the location and extent of the pseudoaneurysm and the extent of myocardial viability. MSCT provides a 3 dimensional data set that can be reconstructed to give an overview of the often complicated geometry of the left ventricle and pseudoaneurysm. MSCT also provides information on coronary artery stenosis (*Chapter 12*).

Contrast enhanced MRI can be used to assess iatrogenic myocardial infarction. We demonstrate a scar in the septum of a patient with hypertrophic obstructive cardiomyopathy treated with an alcohol ablation procedure to reduce the outflow tract obstruction (*Chapter 13)*.

Innovation in Viability Imaging

In recent years, Multislice Computed Tomography (MSCT) technology has made great strides and non-invasive assessment of coronary artery stenosis is now feasible with high diagnostic accuracy using a 64-slice scanner. Delayed enhancement MSCT has been proposed as an alternative non-invasive imaging modality for the detection of myocardial infarction. However, different imaging protocols have been proposed at different time points after myocardial infarction and the diagnostic accuracy is currently unclear. We performed MSCT and MRI in a porcine model of reperfused acute myocardial infarction at a mean of 5 days after infarction. Infarct size assessed with DE-MSCT correlated well with infarct size measured on TTC pathology slices. Also, infarct size assessed with DE-MRI correlated well with infarct size measured on TTC pathology slices. Accordingly, infarct size assessed with DE-MSCT correlated well with infarct size assessed with DE-MRI. Bland Altman analyses demonstrated a good agreement for the assessment of infarct size between DE-MSCT, DE-MRI and TTC pathology (*Chapter 14 and 15*).

Samenvatting en Conclusies

Magnetische Resonantie Imaging is een veelzijdige beeldvormende techniek die kan worden toegepast op patiënten en experimentele modellen van ischemische hartziekten. Met MRI kan de lokale wandbeweging worden bestudeerd maar ook de gehele hartfunctie. Ook de mate van perfusie van de hartspier kan worden vastgesteld alsmede het bepalen van de grootte van een acuut of chronisch myocard infarct. In dit proefschrift gebruiken we deze unieke kwaliteiten van MRI om het acute en chronische myocard infarct te bestuderen. MRI wordt gebruikt om het effect van nieuwe therapieën te monitoren, om de pathofysiologie van ischemische hartziekten te bestuderen en om de rol van MRI in de klinische omgeving te bepalen. Ook word MRI gebruikt om andere beeldvormende technieken verder te ontwikkelen. De mogelijkheid om met Multislice Computed Tomography (MSCT) de infarct grootte te meten wordt onderzocht. In dit proefschrift passen we MRI en MSCT toe in experimentele modellen van ischemische hartziekten en in klinische patiënten.

Experimentele toepassing van Magnetic Resonance Imaging

Het voordeel van het gebruiken van een experimenteel model is de goed gecontroleerde omstandigheden die het mogelijk maken om de experimentele -en MRI protocollen te optimaliseren. Met MRI kunnen kleine proefdieren worden bestudeerd met speciaal ontwikkelde spoelen, terwijl grotere proefdieren worden gescand met spoelen die ook gebruikt worden voor patiënten. In dit proefschrift hebben we een varkensmodel gebruikt van acuut myocard infarct. We waren is staat om een zeer goed beeldkwaliteit te verkrijgen in de meeste varkens. De storende invloed van ademhaling en hartslag werden geminimaliseerd door het gebruik van ademstilstanden en een elektrocardiogram. De spoelen die het signaal ontvangen werden dicht bij het hart geplaatst waardoor een goede signaal ruis verhouding werd bereikt.

MRI werd verricht in een varkens model van een acuut myocard infarct met reperfusie. We bestudeerden de relatie tussen infarct grootte en linker ventrikel diastolische functie op 5 dagen na infarct reperfusie. De invloed van infarct grootte op de systolische (dys)functie en linker ventrikel remodulering is bekend, maar de impact van infarct grootte op de diastolische functie is minder bekend. Infarct grootte, diastolische en systolische functie en volumina zijn allen voorspellers van cardiale mortaliteit. In

deze studie hebben we cine-MRI verricht om volume-tijd curves te berekenen en de diastolische functie werd vervolgens uitgedrukt in peak filling rate gecorrigeerd voor eind diastolisch volume. Infarct grootte werd gemeten op gestandaardiseerde delayed enhancement afbeeldingen. Deze studie liet zien dat infarct grootte een belangrijke factor is die de linker ventrikel diastolische functie bepaalt. Deze relatie hebben we ook in patiënten onderzocht die werden behandeld met een drug-eluting stent voor een acuut myocard infarct. Eenzelfde MRI protocol werd gebruikt. Infarct grootte bleek beter gerelateerd te zijn met de diastolische functie in het varkensmodel dan in patiënten. Tenslotte bleek dat infarct grootte gemeten op 5 dagen na infarct beter de linker ventrikel functie op 5 maanden voorspelde dan diastolische functie of systolische functie op 5 dagen na het infarct. Deze resultaten zouden verklaard kunnen worden door de factoren in patiënten die de diastolische en systolische eigenschappen van de linker ventrikel beïnvloeden. In het varkensmodel zijn de meeste van deze factoren ge-excludeerd of geminimaliseerd (*Hoofdstuk 3*).

MRI kan gebruikt worden om het effect van nieuwe therapieën voor ischemische hartziekten te monitoren. Recent onderzoek laat zien dat stamcel transplantatie na acuut myocard infarct kan leidden tot weefsel regeneratie en mogelijk functie herstel. We onderzochten het effect van een intracoronaire injectie van gecultiveerde somatische stamcellen (USSC) verkregen uit humaan navelstreng bloed in een varkensmodel van acuut gereperfundeerd myocard infarct. We bestudeerden het effect op hartfunctie, linker kamer geometrie en infarct grootte. Deze studie bracht naar voren dat er geen verbetering was in hartfunctie en linker ventrikel geometrie. De infarct grootte bleek zelfs groter te zijn in met USSC behandelde dieren vergeleken met controle dieren. Bij histologie werd een toename van inflammatiecellen gevonden en calcificaties. Wellicht dat de intracoronaire toedieningsroute een deel van deze waargenomen verschijnselen kan verklaren (*Hoofdstuk 4*).

In een tweede studie naar het effect van stamcel therapie voor acuut ischemische hartziekten, werden intracoronaire injecties verricht van ongeselecteerde beenmerg-cellen en geselecteerde mononucleaire beenmergcellen in een varkens-model van acuut myocard infarct. Deze celtypes hebben in diverse klinische trials veelbelovende resultaten laten zien, alhoewel andere klinische trials deze resultaten niet konden herhalen. De huidige studie laat zien dat beide celtypes de hartfunctie niet wisten te verbeteren en dat er geen positief effect was op de linker ventrikel remodulering. Een zeer interessante observatie was echter dat infarct grootte afname significant groter was in de varkens behandeld met ruw beenmerg en de mononucleaire cellen vergeleken met de controle varkens (*Hoofdstuk 5*).

In een aantal studies is MRI voorgesteld als een middel om met ijzer gelabelde cellen te volgen in bijvoorbeeld een acuut myocard infarct. Directe evaluatie van het gedrag van getransplanteerde cellen zou veel bijdragen aan ons inzicht in de biologische mechanismen die een rol spelen in dit complexe proces van stamcel transplantatie. Er zijn echter geen studies verricht naar de MRI karakteristieken van een acuut myocard infarct zonder getransplanteerde stamcellen. De signaal verstrooiing veroorzaakt door met ijzergelabelde cellen zou kunnen lijken op de signaal verstrooiing veroorzaakt door hemoglobine degradatie produkten die worden gevonden in acute myocardinfarcten. In deze studie pasten we klinisch gebruikte MRI technieken toe in een varkens model van acuut gereperfundeerd myocard infarct. We scanden de varkens 5 dagen en 5 weken na reperfusie en vergeleken de MRI afbeeldingen met histologische secties. Deze studie liet zien dat de signaal verstrooiing veroorzaakt door hemoglobine degradatie produkten een betrouwbaar vervolgen van met ijzer gelabelde cellen inderdaad niet toe staat (*Hoofdstuk 6*).

Klinische Toepassing van Magnetic Resonance Imaging

De veelzijdige toepassingsmogelijkheden van MRI worden in dit deel van de thesis gebruikt om patiënten met acute en chronische hartziekten te bestuderen. MRI is een afbeeldende techniek die veilig is voor de patiënt en het effect van een therapie kan goed bestudeerd worden aangezien patiënten vele malen gescand kunnen worden zonder dat de patiënten daarvan schade ondervinden.

MRI werd verricht in patiënten met een eerste acuut myocard infarct met ST-segment stijging om linker ventrikel functie en remodulering te bestuderen. Alle patiënten in de studie werden behandeld met een drug-eluting stent die werd geplaatst binnen 6 uur na het ontstaan van de klachten. Met MRI werd de aan –of afwezigheid van microvasculaire obstructie vastgesteld, de transmurale uitbreiding van het infarct en de totale infarct grootte. Tevens werden de volumina en functie van de linker ventrikel gemeten op 5 dagen en 5 maanden na reperfusie. Deze studie toonde aan dat een inverse relatie bestaat tussen de transmuraliteit van een infarct op 5 dagen en de wandverdikking op 5 maanden na reperfusie. Ook bleek dat in dysfunctionele segmenten (wandverdikking minder dan 45%) zonder microvasculaire obstructie de wanddikte eind-diastolisch verhoogd was ten opzichte van gezond myocard. Deze segmenten zonder microvasculaire obstructie toonden een significante verbetering in wandverdikking gedurende follow-up. Segmenten met microvasculaire obstructie ondanks een gestente coronair arterie toonden wandverdunning na 5 maanden en vertoonden geen significante toename in wandverdikking. De patiënten in deze

studie vertoonden een toename in ejectie fractie van 7%. De toename in regionale en globale hartfunctie zal waarschijnlijk veroorzaakt worden door het functioneel herstel van zogenaamd stunned myocardium. Met MRI kan indirect de hoeveelheid stunned myocard worden vastgesteld door de transmuraliteit van het infarct vast te stellen. Bijvoorbeeld: disfunctioneel myocard met een subendocardiaal infarct van minder dan 25% transmuraliteit van de wand heeft meer dan 75% van de wand aan viable (stunned) myocard. Deze studie toonde ook aan dat infarct grootte gemeten op 5 dagen een goede voorspeller was van ejectie fractie, eind-systolisch volume en eind-diastolisch volume op 5 maanden na reperfusie. Infarct grootte bleek een betere voorspeller te zijn dan de totale grootte van microvasculaire obstructie. Ondanks dat de epicardiale coronaire bloodtoevoer was hersteld in alle patiënten werd toch in 87% van de patiënten microvasculaire obstructie gezien 5 dagen na reperfusie. Tenslotte werd waargenomen dat totale infarct grootte met 31 % afnam tussen 5 dagen en 5 maanden na infarct (*Hoofdstuk 7 en 8*).

MRI kan ook worden toegepast om myocard viabiliteit te onderzoeken in patiënten met chronische ischemische hartziekten. In deze thesis werd MRI gebruikt om het effect te bestuderen van het plaatsen van een drug-eluting stent voor een chronische totale occlusie (CTO) van een natieve coronair op de linker ventrikel functie en volumina. Ook werd de diagnostische waarde bepaalt van MRI om de verbetering in ventrikel functie te voorspellen. Chronische totale coronaire occlusies worden gezien in 35 tot 50% van de patiënten die een diagnostische angiogram ondergaan. Het effect van een percutane coronaire interventie van een CTO op de linker ventrikel functie is echter onbekend. Deze studie toonde het positieve effect aan van percutane behandeling in patiënten met een CTO die tenminste 6 weken bestond. Het percentage van de linker ventrikel dat disfunctioneel maar viable was voor de recanalisatie was gerelateerd aan de mate van verbetering van zowel het eind-systolische volume als de ejectie fractie. Regionale wandverdikking verbeterde significant in segmenten met een transmuraliteit van infarcering van minder dan 25%, terwijl segmenten met een transmuraliteit van meer dan 75% functioneel niet verbeterden (*Hoofdstuk 9*).

Met MRI kan nauwkeurig de linker ventrikel functie worden vastgesteld en daarom wordt MRI nu in veel studies gebruikt. Meestal wordt een manuele segmentatie van de linker ventrikel afbeeldingen verricht, omdat beeldkwaliteit en de vorm van de linker ventrikel de automatische segmentatie moeilijk maken. In dit hoofdstuk bestuderen we de waarde van een nieuw algoritme waarmee automatisch de contouren van de linkerventrikel kunnen worden bepaald. We laten zien dat dit algoritme, dat de 3 dimensionele informatie gebruikt die aanwezig is in een MRI data-set, een significant toegevoegde waarde heeft (*Hoofdstuk 10*).

Contrast echocardiografie is een nieuwe techniek waarbij microbubbels kunnen worden gevisualiseerd in het myocard. In dit hoofdstuk werden MRI en contrast echocardiografie verricht in patiënten met een gereperfundeerd myocardinfarct teneinde eventuele functionele verbetering te voorspellen. Het voordeel van contrast echocardiografie is de makkelijke beschikbaarheid, maar het nadeel is dat je niet de totale infarct grootte kan beoordelen. In deze groep patiënten toonden we aan dat zowel MRI als contrast echocardiografie de ventrikulaire functie kan voorspellen na infarct (*Hoofdstuk 11*).

De combinatie van MRI met MSCT kan complementaire informatie geven waardevol voor de therapiekeuze. In deze casus van een patiënt met een post-infarct pseudo-aneurysma werd MRI verricht om hartfunctie en myocard viabiliteit aan te tonen. MSCT leverde 3 dimensionele informatie over de anatomie van de coronairen en de grootte en positie van het pseudoaneursysma (*Hoofstuk 12*).

Met MRI kan ook een iatrogeen infarct worden aangetoond zoals gedemonstreerd in deze casus van patient met hypertrofische obstructieve cardiomyopathie die een septum infarct werd aangedaan om de obstructie te verminderen (*Hoofdstuk 13*).

Innovatie in het afbeelden van Myocard Viabiliteit

De laatste jaren zijn de ontwikkelingen met de Multislice CT scanner snel gegaan en in geselecteerde patiënten populaties is het nu mogelijk om de coronairen niet-invasief af te beelden. MSCT is ook gebruikt om myocard infarcten af te beelden maar verschillende scanprotocollen en verschillende tijdstippen van scannen na een infarct maken de waarde van MSCT voor het vaststellen van myocardviabiliteit onduidelijk. Voor deze thesis hebben we MSCT en MRI verricht in een varkensmodel van acute myocard infarct 5 dagen na reperfusie. MSCT en MRI scans van infarct grootte werden vergeleken met ex-vivo pathologie kleuringen. Het blijkt dat zowel MRI (zoals eerder aangetoond) als ook MSCT (nieuw) zeer nauwkeurig de infarctgrootte kunnen vaststellen in-vivo (*Hoofdstuk 14 en 15*).

List of Publications

1. **Timo Baks;** Robert-Jan van Geuns; Elena Biagini; Piotr Wielopolski; Nico R. Mollet; Filippo Cademartiri; Willem J. van der Giessen; Gabriel P. Krestin; Dirk J. Duncker; Patrick W. Serruys; Pim J. de Feyter
   Recovery of left ventricular function after primary angioplasty for acute myocardial infarction
   Eur Heart J. 2005;26:1070-7
2. **Timo Baks;** Robert-Jan van Geuns; Elena Biagini; Piotr Wielopolski; Nico R. Mollet; Filippo Cademartiri; Willem J. van der Giessen; Gabriel P. Krestin; Patrick W. Serruys; Dirk J. Duncker; Pim J. de Feyter
   Effects of Primary Angioplasty for Acute Myocardial Infarction on Early and Late Infarct Size and Left Ventricular Wall Characteristics
   J Am Coll Cardiol 2006;47:40-4
3. **Timo Baks**; Robert-Jan van Geuns; Dirk J. Duncker; Filippo Cademartiri; Nico R. Mollet; Gabriel P. Krestin; Patrick W. Serruys; Pim J. de Feyter
   Prediction of Left Ventricular Function after Drug-eluting Stent Implantation for Chronic Total Coronary Occlusions
   J Am Coll Cardiol 2006;47:721-5
4. **Timo Baks;** Filippo Cademartiri; Amber Moelker; Robert-jan van Geuns; Gabriel P. Krestin; Dirk J. Duncker; Pim J. de Feyter
   MSCT and MRI for the assessment of Reperfused Acute Myocardial Infarction
   J Am Coll Cardiol. 2006 Jul 4;48(1):144-5
5. **Timo Baks**; Filippo Cademartiri; A. Moelker; Willem J. van der Giessen; Gabriel P. Krestin; Dirk J. Duncker; Pim J. de Feyter
   Assessment of Acute Reperfused Myocardial Infarction with 64-slice Delayed Enhancement Computed Tomography
   Am J Roentgenology accepted
6. **Timo Baks**; Filippo Cademartiri; H. Spierenburg; Pim J. de Feyter
   Chronic Pseudoaneurysm of the Left Ventricle
   Int J Cardiovasc Imaging 2005 Nov 30;1-3
7. Robert-jan van Geuns; **Timo Baks**; Ed Gronenschild; Jean-Paul Aben; P.A. Wielopolski; Filippo Cademartiri; P J de Feyter
   Automatic Quantitative Left Ventricular Analysis of Cine Magnetic Resonance Images using Three-Dimensional Information for Contour Detection
   Radiology. 2006 Jul;240(1):215-21

8. Elena Biagini, Robert J. van Geuns, **Timo Baks**, Eric Boersma, Vittoria Rizzello, Tjebbe W. Galema, Pim de Feyter, Folkert J. Ten Cate
   Comparison between contrast echocardiography and magnetic resonance imaging to predict improvement of myocardial function after primary coronary intervention.
   Am J Cardiol. 2006 Feb 1;97(3):361-6
9. Mollet N.R., Cademartiri, F., Van Mieghem, C.A.G., Runza, G.P., McFadden, E.P., **Baks, T**., Serruys, P.W., Krestin, G.P., De Feyter, P.J.
   High-resolution Spiral CT Coronary Angiography in Patients Referred for Diagnostic Conventional Coronary Angiography
   Circulation 2005;112:2318-23.
10. Mollet NR, Cademartiri F, Runza G, Belgrano M, **Baks T**, Meijboom WB, de Feyter PJ.
    Four-dimensional evaluation of a giant pseudo-aneurysm by multislice computed tomography.
    Int J Cardiovasc Imaging. 2005 Dec;21(6):667-8.
11. Cademartiri F., Mollet, N.R., Lemos, P.A., McFadden, P.A., Marano, R., **Baks, T.**, Stijnen, T., De Feyter, P.J., Krestin, G.P.
    Standard Versus User-Interactive Assessment of Significant Coronary Stenoses With Multislice Computed Tomography Coronary Angiography
    American Journal of Cardiology 2004;94:1590-3
12. Cademartiri F, Mollet N, Lemos PA, Pugliese F, **Baks T**, McFadden EP, Krestin GP, de Feyter PJ.
    Usefulness of multislice computed tomographic coronary angiography to assess in-stent restenosis.
    American Journal of Cardiology 2005;96:799-802.
13. van den Bos EJ, **Baks T**, Moelker AD, Kerver W, van Geuns RJ, van der Giessen WJ, Duncker DJ, Wielopolski PA.
    Magnetic resonance imaging of haemorrhage within reperfused myocardial infarcts: possible interference with iron oxide-labelled cell tracking?
    Eur Heart J. 2006;27:1620-6
14. Pugliese F, Mollet NR, Runza G, van Mieghem C, Meijboom WB, Malagutti P, **Baks T**, Krestin GP, deFeyter PJ, Cademartiri F.
    Diagnostic accuracy of non-invasive 64-slice CT coronary angiography in patients with stable angina pectoris.
    Eur Radiol. 2006;16:575-82.
15. Mollet NR, Cademartiri F, Runza G, Belgrano M, **Baks T**, Meijboom WB, de Feyter PJ.
    Four-dimensional evaluation of a giant pseudo-aneurysm by multislice computed tomography.
    Int J Cardiovasc Imaging. 2005;21:667-8.

16. Georgios Sianos; Michail I. Papafaklis; Eleni C. Vourvouri; Jurgen T. Ligthart; **Timo Baks**; Folkert J. Ten Cate; Patrick W. Serruys
    Hypertrophic obstructive cardiomyopathy: septal ablation with overlapping sirolimus-eluting and covered stents after failed alcoholization and concomitant coronary artery disease
    Circulation in press
17. Amber D. Moelker, **Timo Baks**, Dimitry Spitskovsky, Piotr A. Wielopolski, Heleen M.M. van Beusekom, Robert-Jan van Geuns, Stephan Wnendt, Dirk J. Duncker, Wim J. van der Giessen
    Intracoronary Delivery of Umbilical Cord Blood Derived Unrestricted Somatic Stem Cells is Not Suitable to Improve LV Function after Myocardial Infarction in Swine
    submitted
18. Amber D. Moelker; **Timo Baks**, Wendy Kerver; Heleen M.M. van Beusekom; Piotr A. Wielopolski, I. Peters, Dirk J. Duncker, Willem J. van der Giessen Reduction in infarct size, but not functional improvement after bone marrow cell administration in a porcine model of reperfused myocardial infarction
    Submitted
19. **Timo Baks;** Robert-Jan van Geuns; Sharon Kirschbaum; Amber Moelker; Willem J. van der Giessen; Dirk J. Duncker; Pim J. de Feyter
    Infarct Size and Diastolic Function in Acute Reperfused Myocardial Infarction and the Impact on Left Ventricular Remodeling
    submitted

Book Chapter

1. **Baks T**., van Geuns RJ., de Feyter P.J.
   Cardiovascular magnetic resonance imaging for the assessment of coronary arteries and myocardial viability.
   In: The Paris Course on Revascularization chapter 15, pgs 203-213
   Groupe Composer. ISBN 2913628168 2004

Abstracts

Radiological Society of Northern America 2004

1. **Timo Baks**, Robert-jan van Geuns, Elena Biagini, P. Wielopolski, G. Krestin, Pim de Feyter *oral presentation*: Prediction of recovery of stunned myocardium after primary angioplasty for acute myocardium infarction by magnetic resonance imaging
2. **Timo Baks**, Filippo Cademartiri, Mohammed Ouhlous, Nico Bruining, Ronald Hamers, Pim J. de Feyter *poster presentation:* Coronary Artery Plaque Imaging: a Human Ex-Vivo Model with state-of-the-art MRI and CT

American College of Cardiology 2005

3. **Timo Baks**, Robert-Jan van Geuns, Elena Biagini, Piotr Wielopolski, Nico R. Mollet, Filippo Cademartiri, Gabriel P. Krestin, Dirk J. Duncker, Patrick W. Serruys, Pim J. de Feyter *poster presentation:* Recovery of Left Ventricular Function after Primary Angioplasty for Acute Myocardial Infarction
4. **Timo Baks**, Robert-Jan van Geuns, Elena Biagini, Piotr Wielopolski, Nico R. Mollet, Filippo Cademartiri, Gabriel P. Krestin, J. Duncker, Pim J. de Feyter *poster presentation:* Effects of Primary Angioplasty for Acute Myocardial Infarction on Early and Late Infarct Size and Left Ventricular Wall Characteristics

European Society of Cardiology 2005

5. **Timo Baks**; Robert-Jan van Geuns; Dirk J. Duncker; Filippo Cademartiri; Gabriel P. Krestin; Patrick W. Serruys; Pim J. de Feyter *poster presentation:* Prediction of Left Ventricular Function after Drug-eluting Stent Implantation for Chronic Total Coronary Occlusions

American Heart Association 2005

6. **Timo Baks**; Robert-Jan van Geuns; Dirk J. Duncker; Filippo Cademartiri; Gabriel P. Krestin; Patrick W. Serruys; Pim J. de Feyter *oral presentation:* Prediction of Left Ventricular Function after Drug-eluting Stent Implantation for Chronic Total Coronary Occlusions

Nederlandse Vereniging van Cardiologie najaarscongres 2005

7. **Timo Baks**, Robert-jan van Geuns, Elena Biagini, P. Wielopolski, G. Krestin, Pim de Feyter *oral presentation*: Prediction of recovery of stunned myocardium after primary angioplasty for acute myocardium infarction by magnetic resonance imaging
   Best scientific presentation award

Radiological Society of Northern America 2005

8. **Timo Baks**; Amber Moelker; Willem van der Giessen; Dirk J. Duncker; Pim J. de Feyter; Filippo Cademartiri *oral presentation*: Delayed Enhancement in Acute Myocardial Infarction: 64-slice CT versus 1.5 Tesla MRI with pathology correlation
9. **Timo Baks**, Robert-Jan van Geuns, Elena Biagini, Piotr Wielopolski, Nico R. Mollet, Filippo Cademartiri, Gabriel P. Krestin, J. Duncker, Pim J. de Feyter *oral presentation:* Effects of Primary Angioplasty for Acute Myocardial Infarction on Early and Late Infarct Size and Left Ventricular Wall Characteristics

Society of Cardiomagnetic Resonance Imaging 2006

10. **Timo Baks**; Robert-Jan van Geuns; Dirk J. Duncker; Filippo Cademartiri; Gabriel P. Krestin; Patrick W. Serruys; Pim J. de Feyter *poster presentation:* Prediction of Left Ventricular Function after Drug-eluting Stent Implantation for Chronic Total Coronary Occlusions

Curriculum Vitae

Timo Baks was born on the 7th of January 1977 in 's-Gravenzande, the Netherlands. After finishing high school in 1995 at the Zandevelt College in 's-Gravenzande, he studied Medicine at the Erasmus University in Rotterdam. During his study he was involved in a Public Health Project of the International Federation of Medical Student Association (IFMSA) in Kampala, Uganda with a visit to the project site in 1998. He started his clinical training in 2000 and as part of his training he spent 3 months at the Surgery department of the Queens Elisabeth Hospital in Blantyre, Malawi. In 2002, he worked for a year as a house officer at the department of Internal Medicine, Cardiology and Pulmonology at the Albert Schweitzer Hospital of Dordrecht where he became interested in Cardiology. In April 2003, he was employed as a research fellow at the department of Cardiology and Radiology and became involved in non-invasive cardiac imaging with Magnetic Resonance Imaging and Computed Tomography under supervision of Prof. P.J. de Feyter and Prof. G.P. Krestin which resulted in this thesis. Currently, he is involved in the cardiology training with 3 years of residency at the Albert Schweitzer Hospital of Dordrecht and 3 years residency at the Thoraxcenter in Rotterdam.

DANKWOORD

Een terugblik op mijn onderszoeksjaren, een unieke kans op reflectie:

Prof. de Feyter, beste Pim, wil ik bedanken voor de geboden kans om onderzoek te doen in het Thoraxcentrum. Tijdens mijn "sollicitatie gesprek" vroeg ik: "wanneer zou ik kunnen beginnen?" "Wanneer je maar wilt", luidde het antwoord. Die vrijheid maakte het eerste jaar soms lastig. Daarna heb ik ervan genoten. Een nieuw manuscript was altijd terug binnen twee dagen. Veel heb ik geleerd van je schrijfstijl: een door mij geschreven pagina werd vaak tot enkele treffende woorden gededuceerd. Ook heb je altijd treffende of relativerende opmerkingen paraat waarvan ik er toch tenminste een zal noemen: in een discussie over atherosclerose; "De natuur is niet hoekig, heb jij je ooit gestoten aan je vrouw in bed?"

Prof. Krestin, beste Gabriël, bedankt voor de mogelijkheden die u heeft gecreëerd op de afdeling radiologie. Magneettijd is een schaars goed in de onderzoekswereld, maar dankzij uw beleid heb ik daar nooit gebrek aan gehad. Cardiac imaging; friend or foe? De goede samenwerking tussen cardiologie en radiologie heeft het zeker tot een Friend gemaakt.

Aan mijn co-promoter, **Robert-jan van Geuns**, heb ik veel te danken. Jouw intellectuele bijdrage aan dit proefschrift is geweldig en je praktische begeleiding was onmisbaar. Tevens wil ik je bedanken voor al die uren debatteren over MRI-zaken waarbij Miami Beach en andere lokaties ter wereld overigens prima voldeden. Computer-technisch heb ik je een zware tijd gegeven en tijdens het scannen zijn we het zelden eens. Toch staan in deze thesis veel mooie ideeën die we samen ten uitvoer hebben gebracht.

Prof. Duncker, beste Dirk, je enthousiasme over werkelijk alle soorten onderwerpen is zeer enthousiasmerend. Uren hebben we gesproken over stunning, hibernation, relaxatie tijden en de "domme clinicus"... Een bezoek aan de 23ste leverde mij altijd een schat aan ideeën en kennis op. Tevens verlengde het mijn manuscript met tenminste 500 woorden en 4 figuren.

Ik wil ook de overige leden van de commissie bedanken, te weten **Professor van der Giessen**, **Professor Poldermans**, **Professor van der Wall** en **Professor van Rossum**.

Een aantal bijzondere personen ben ik tegengekomen tijdens deze jaren en die wil ik hieronder noemen. **Elena Biagini**, altijd de drukte zelve, leerde mij de charme kennen

van de Italiaanse gebarentaal. Het scannen heb ik onder andere geleerd van en met **Jochem vd Berg**, altijd de rust zelve. Een aantal buitenlandse bezoeken waren leerzaam en gezellig. **Eric Boersma** wil ik bedanken voor het statistisch advies dat bijna altijd binnen een dag werd gegeven. **Piotr Wielopolski**, who invented physics and speaks all languages unfortunately lacks the words to explain the MRI principles to a starting researcher. However, I had a nice time at the MRI-suite and thanks for your presence. **Prof. Serruys** vroeg mij: "als jij je literatuur zo goed kent, wie heeft er dan als eerste ooit een CTO gerecanaliseerd", een aarzeling van mijn kant; "dat was ik" luidde het vanzelfsprekende antwoord. Een zeer inspirerend persoon. **Annet Louw,** charmant, wil ik bedanken voor het bewaken van de deadlines die ik van nature meestal zie als ze voorbij zijn. Een speciaal woord van dank gaat uit naar **Dirk Verver**, het resultaat van mijn jaren arbeid heb jij vormgegeven in het proefschrift dat u nu in handen heeft. Soms wat warrig van nature, maar het resultaat is prachtig, bedankt!

Ook wil ik alle leden van de imaging-groep bedanken: **Nico**, de Bourgondiër, zeker twee jaar kamergenoot, altijd gezellig, hulpvaardig, mooie verhalen ("gisteren gegeten in 3 sterren"): bedankt voor je hulp in praktische en research-technische zaken. **Filippo**, een briljant persoon, heeft mij laten zien wat hard werken is. Succes in Italië! **Annick**, kamergenoot, die me de taxi uitzet in chicago, runt simultaan vele projecten. **Bob**, overhemd uit zijn broek, gaat helaas kiten en niet windsurfen. **Eleni**, bon chance avec les petits! **Cecile**, kamergenote, stelde ik de vraag: "wil je vrijwilliger zijn voor een MRI-scan van het hart?" Was ik de eerste die wist dat je in verwachting was. Vergeef me mijn domme baby-vragen! **Carlos**, met het mooie Vlaamse accent, je betrokkenheid bij zowel klinisch als research werk respecteer ik enorm. **Sharon**, met de zo nu en dan schorre stem, jij had een paar jaar eerder moeten komen. Je energieke aanwezigheid in de "MRI-groep" maakt het scannen leuk en doet het onderzoek voortspoeden.

Van de experimentele cardiologie wil ik oa. **Amber**, **Wendy** en **Ewout** bedanken. Beste **Amber**, ik heb mijn eerste catheterisatie verricht onder jou deskundige begeleiding: na 2,2 seconden in de LCx... Ik wil je ook bedanken voor al die last minute varkens die ik zonodig wilde scannen. **Wendy**, bedankt voor het geven van wat broodnodige stress vlak voor het trouwen, alles was toch nog op tijd geregeld. Beste **Ewout**, jaargenoot, tegelijkertijd afgestudeerd, bijna tegelijkertijd onze proefschrift verdediging en nu collega`s in de kliniek. Succes met dit traject! Verder uiteraard dank aan **Rob**, **Daphne** en **Oana**.

Windguru thanks.cz!!

Marja, **Marijke**, **Denise**, **Marjolein**, **Wendy** en **Titia**; bedankt voor de talloze keren dat ik "even tussendoor" iets heb kunnen vragen of regelen. Bedankt voor jullie hulp tijdens allerlei praktische regelzaken. Alle laboranten en medeonderzoekers die gebruik maken van de MRI wil ik bedanken voor de geboden flexibiliteit die je als onderzoeker zo nodig hebt. Ook wil ik alle patiënten bedanken die uren hebben gespendeerd in de comfortabele omgeving van de MRI tunnel.

Een ander proefschrift zou ik kunnen schrijven over herenweekendjes, zeilescapades, De Partij en befaamde surfsessies, maar aangezien de inhoud zeker niet verdedigbaar zou zijn laat ik dat op dit moment. Mijn paranimfen, **Bas** en **Maarten**, die ik ken vanaf het eerste uur van de geneeskunde wil ik zeer bedanken. Geflankeerd door deze heren werd ik uit een kroeg gegooid in Groningen...tijdens mijn verdediging hoop ik op meer steun. Mooie tijden hebben we gehad en mooie tijden gaan er volgen.

Mijn **ouders**, **BBC Wildlife Photographers**, wil ik bedanken voor alle mogelijkheden die ze me geboden hebben, voor het fantastische 2005 waarin ik in het zomerhuis dit boekje heb weten te schrijven en bovenal voor hun ondernemende levensvisie.

Else, bloedmooi, enthousiast, geduldig en altijd gezellig: De aantrekkingskracht van jou op mij is niet in simpele Tesla's uit te drukken. Bedankt voor de mooie tijd die wij samen hebben en de vele mooie plannen die in ontwikkeling zijn!

COLOR SECTION

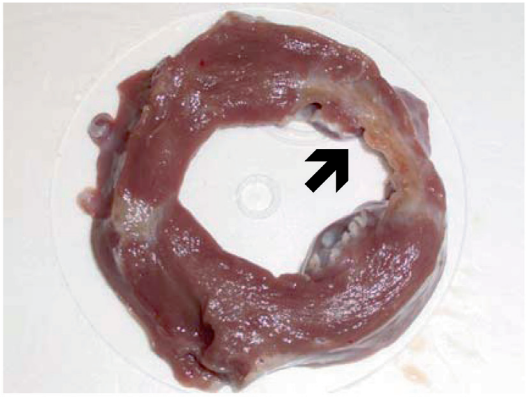

Chapter 4, Figure 1.

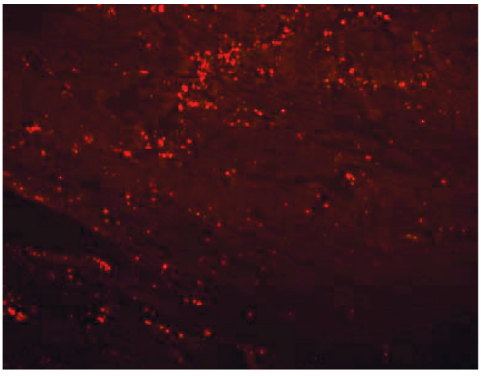

Chapter 4, Figure 2.

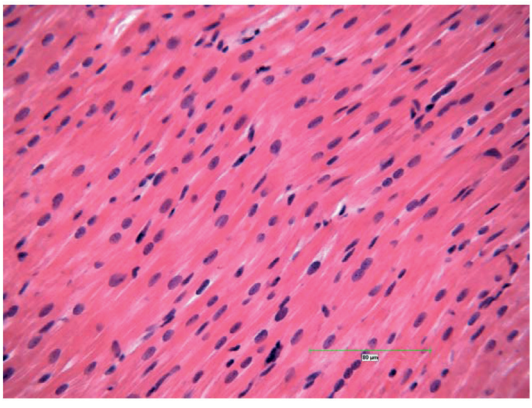

Chapter 4, Figure 3.

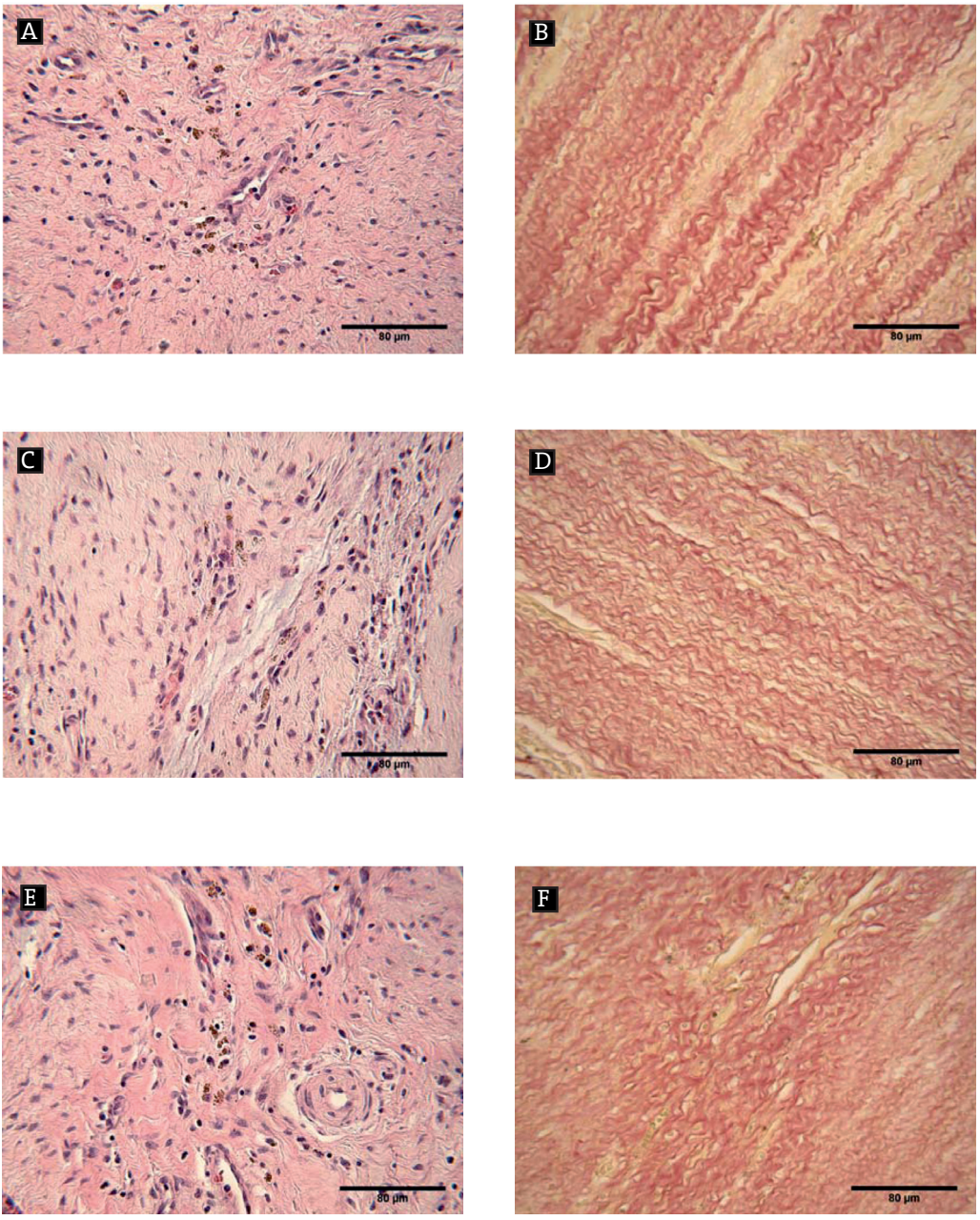

Chapter 4, Figure 7.

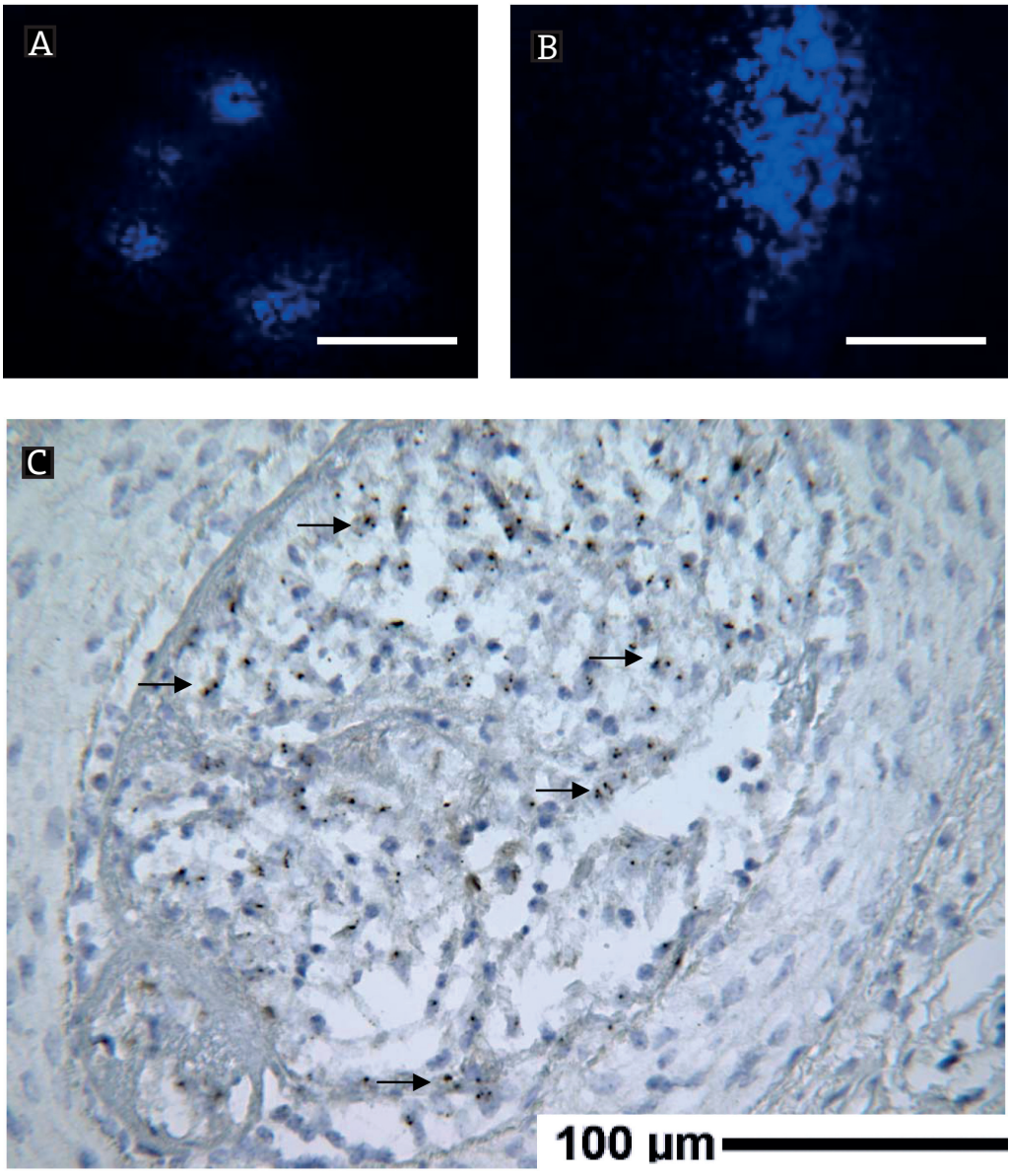

Chapter 5, Figure 1.

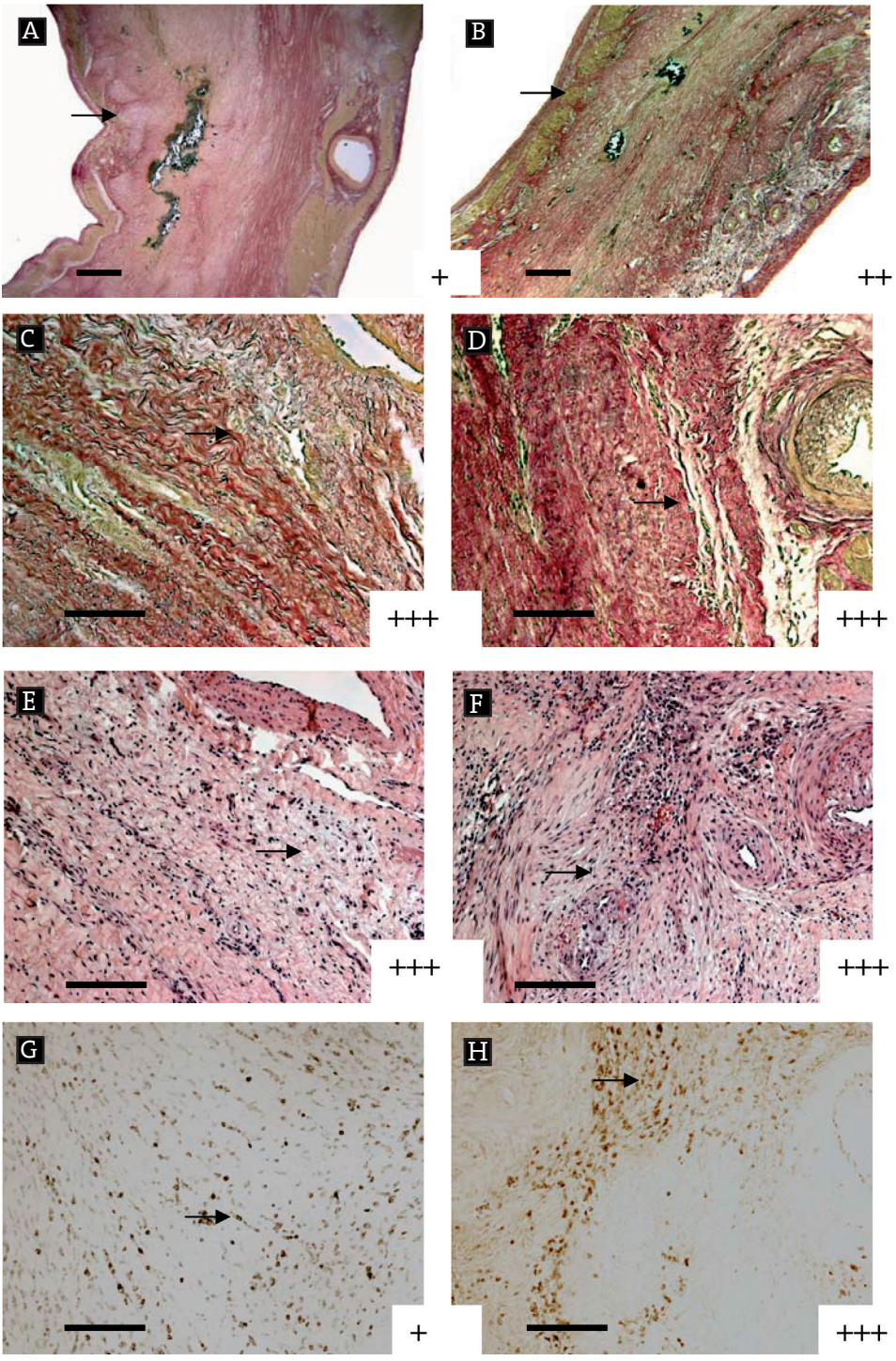

Chapter 5, Figure 4.

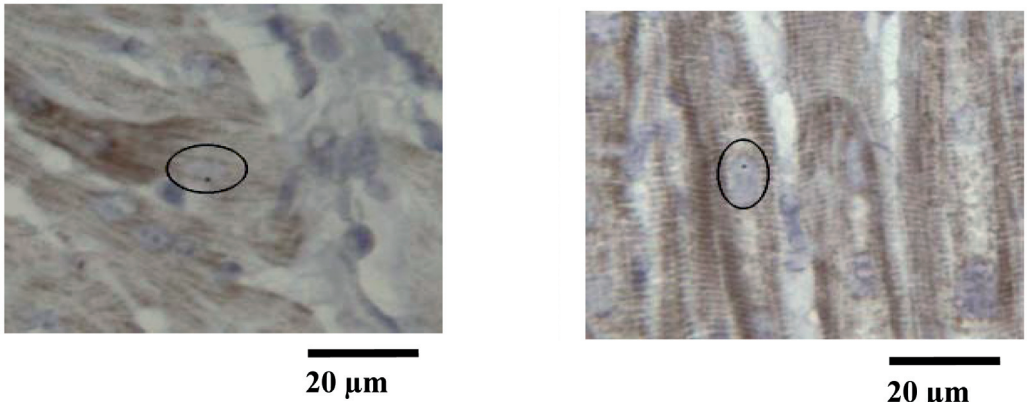

Chapter 5, Figure 5.

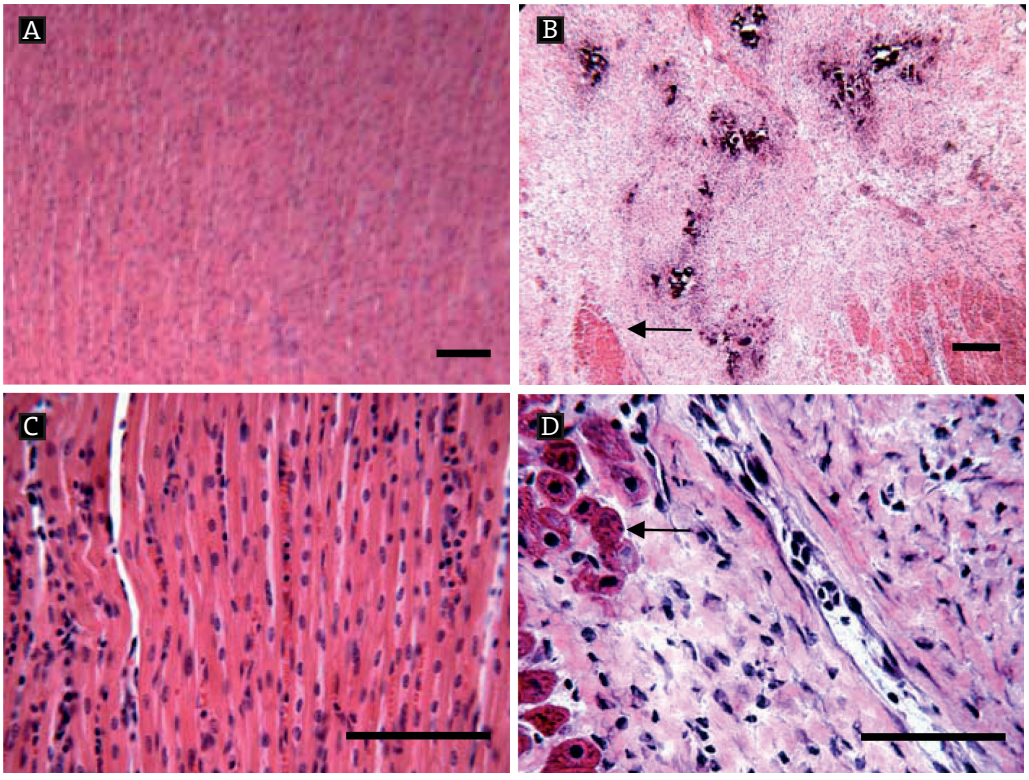

Chapter 5, Figure 6.

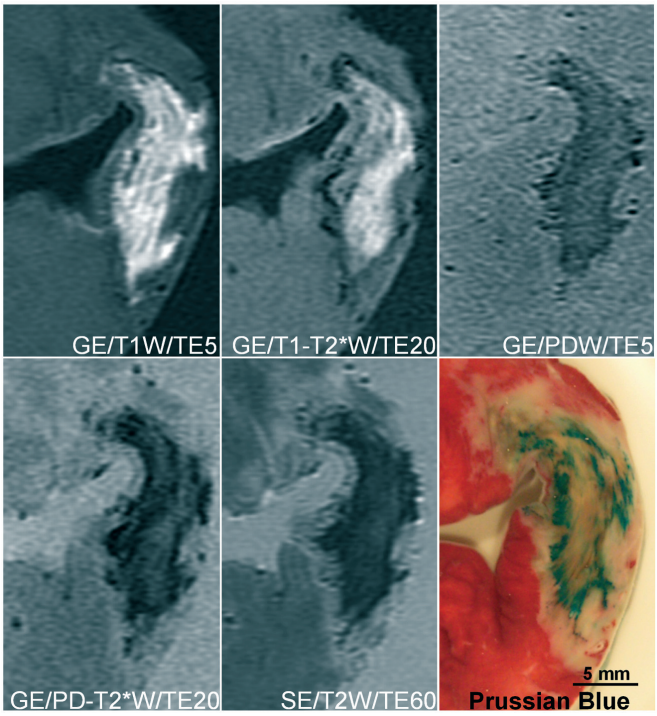

Chapter 6, Figure 3.

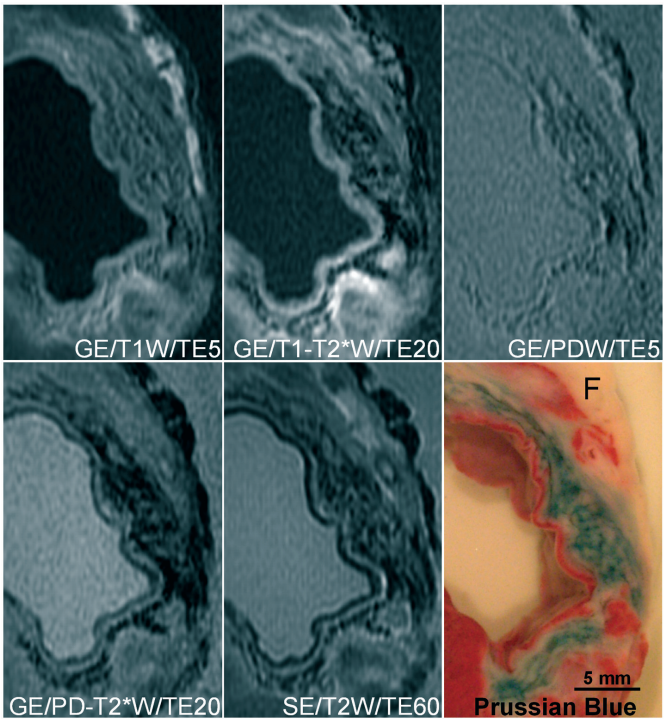

Chapter 6, Figure 4.

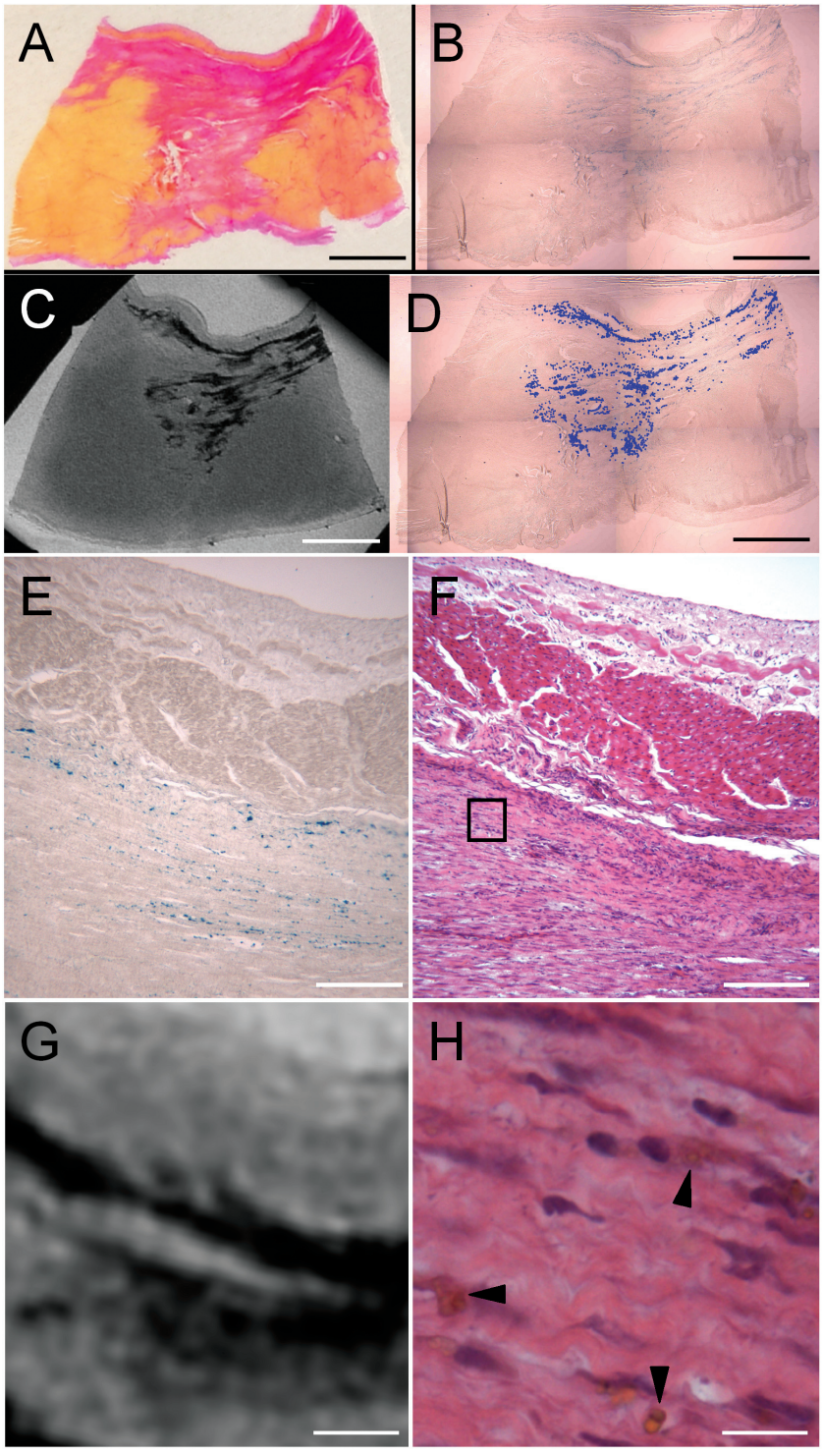

Chapter 6, Figure 5.

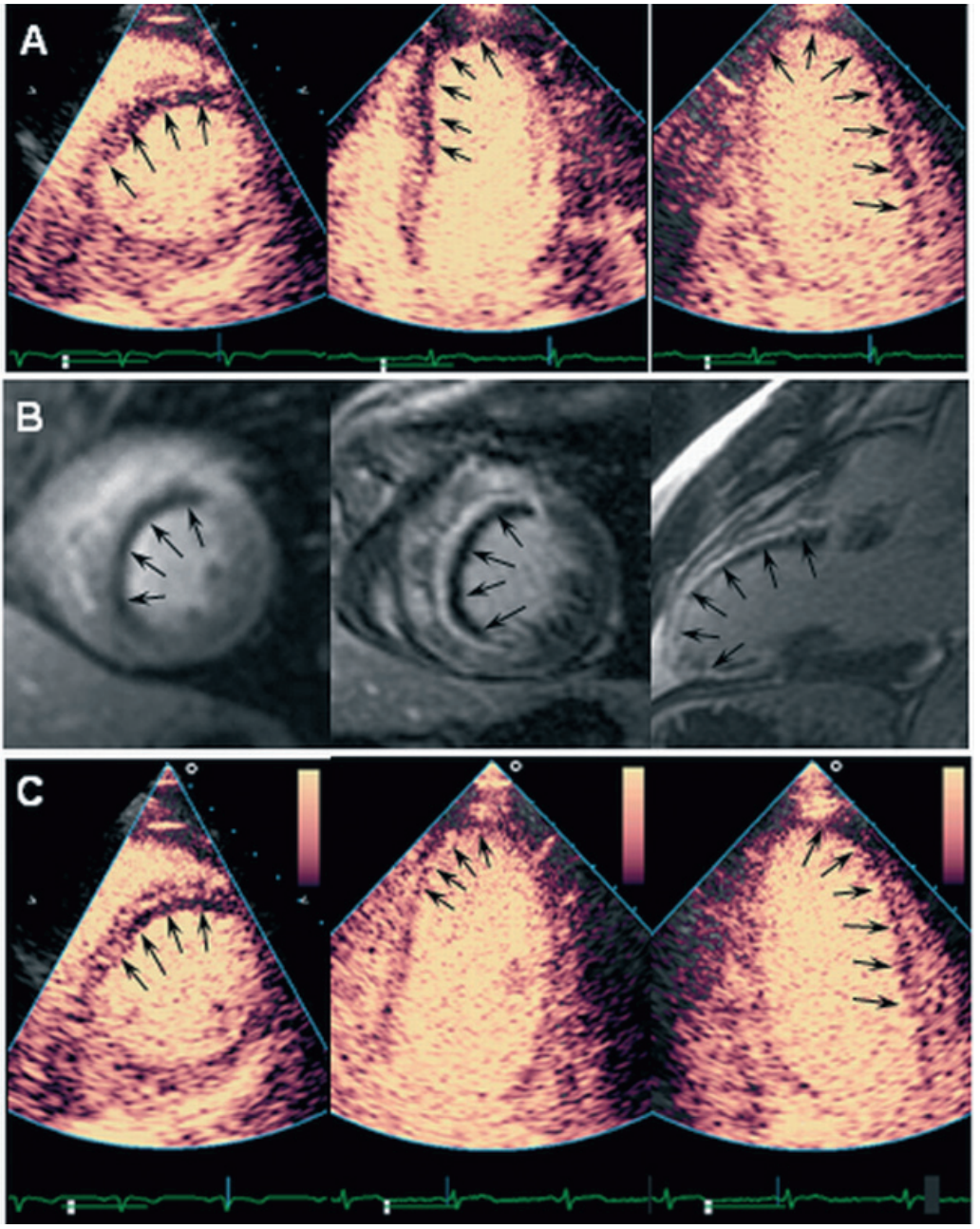

Chapter 11, Figure 2.

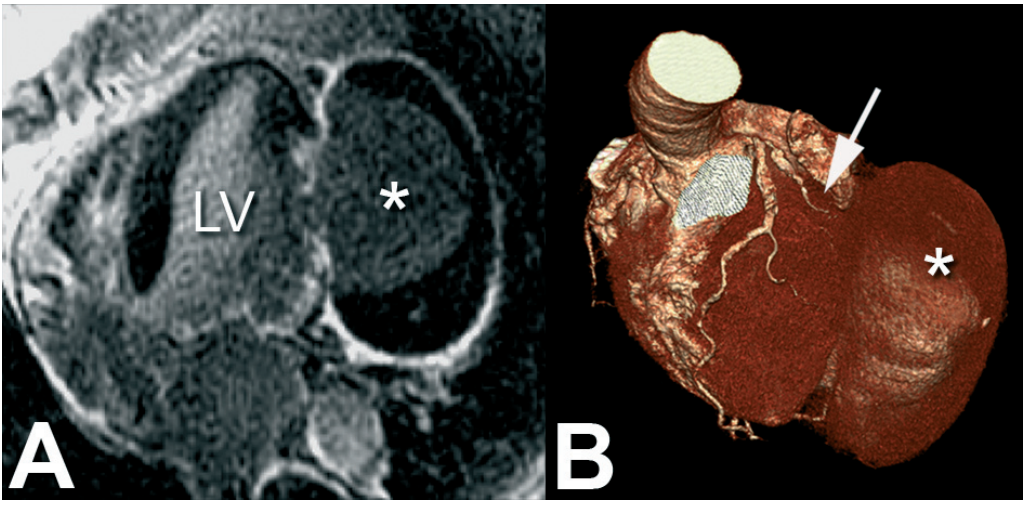

Chapter 12, Figure 1.

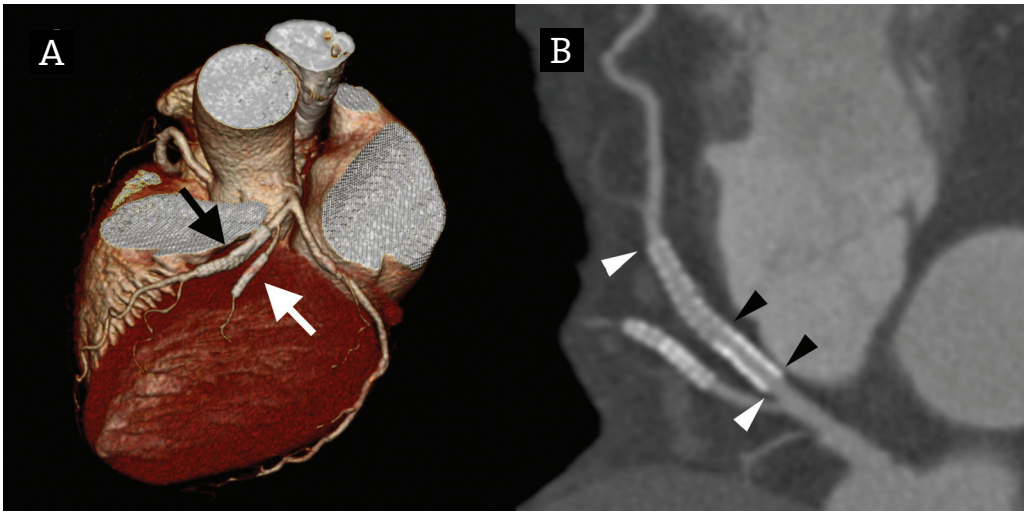

Chapter 13, Figure 2.

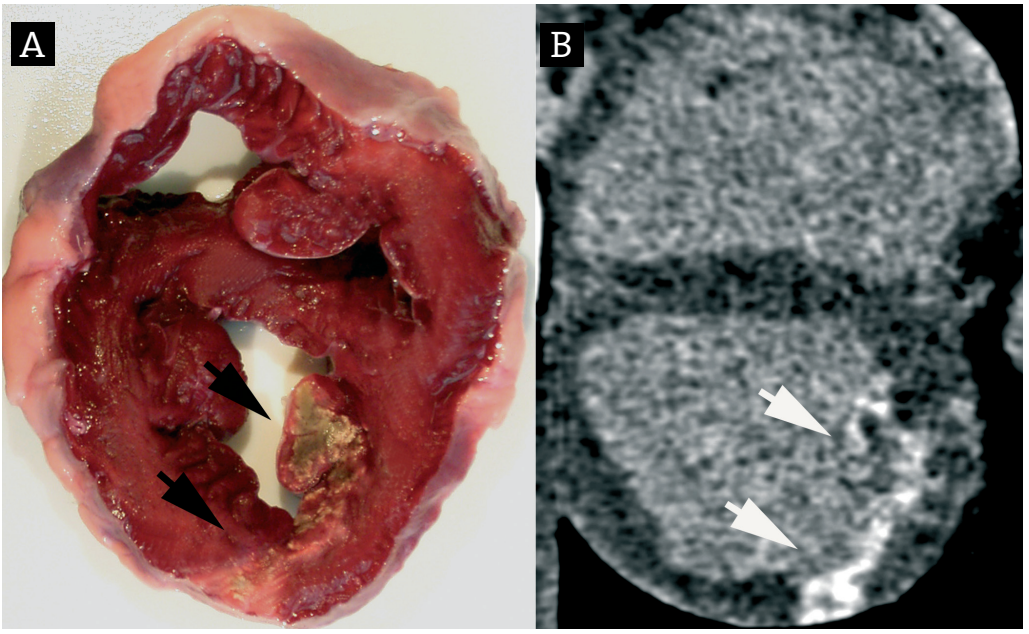

Chapter 15, Figure 1.

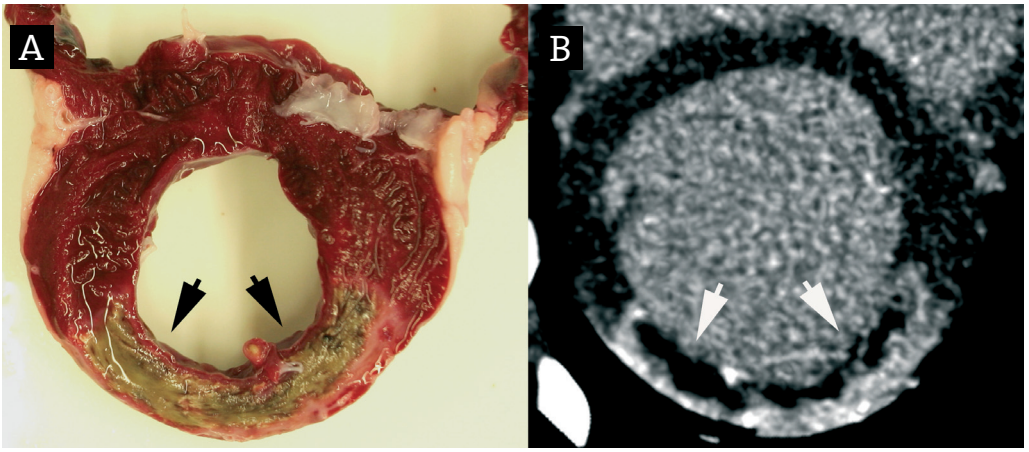

Chapter 15, Figure 2.